WILEY-VCH

Edited by Aiguo Wu and Wenzhi Ren

TiO_2 Nanoparticles

Applications in Nanobiotechnology and Nanomedicine

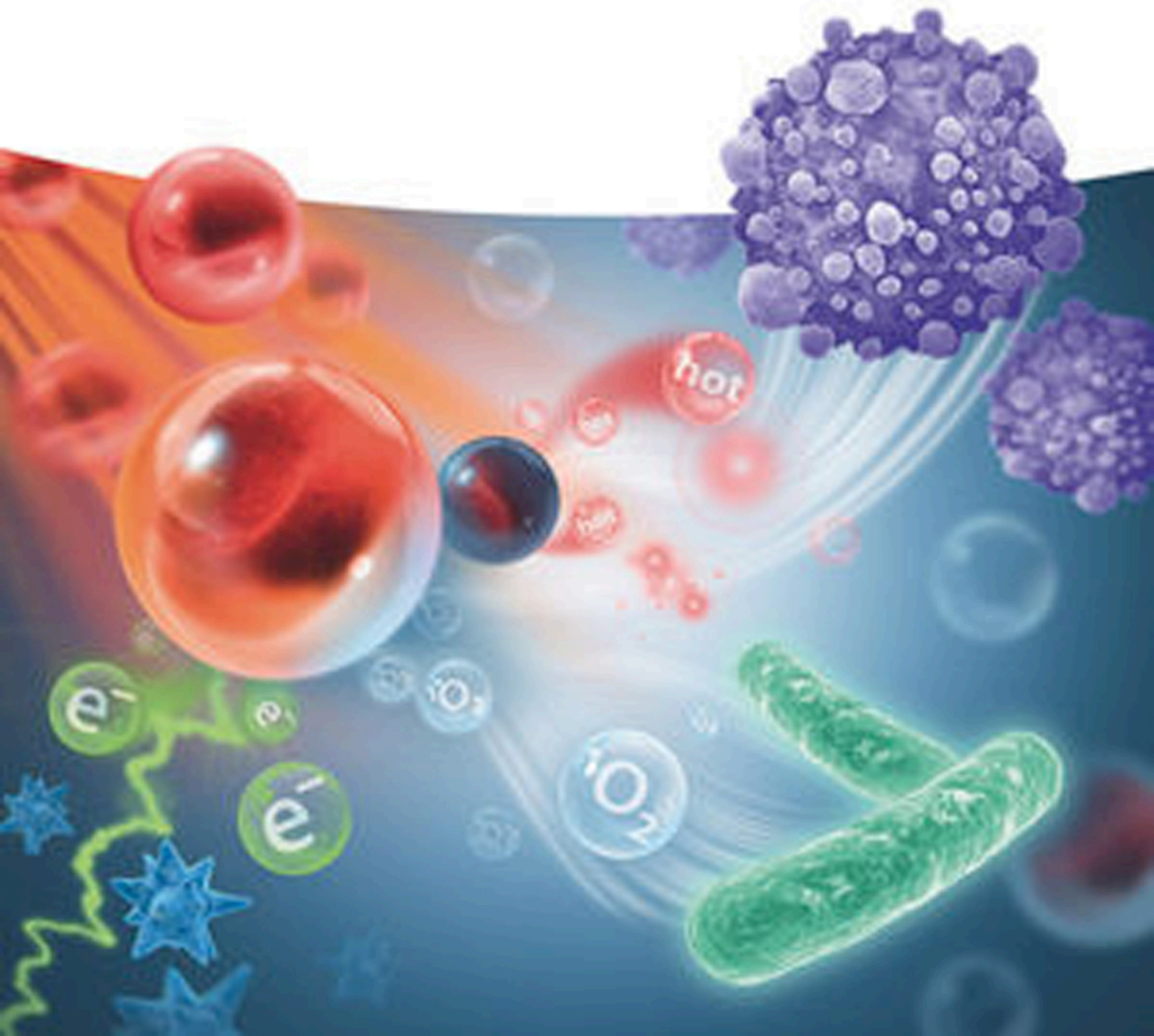

TiO_2 Nanoparticles

TiO_2 Nanoparticles

Applications in Nanobiotechnology and Nanomedicine

Edited by Aiguo Wu and Wenzhi Ren

WILEY-VCH

Editors

Prof. Aiguo Wu
Cixi Institute of Biomedical Engineering
Ningbo Institute of Materials
Technology and Engineering
Chinese Academy of Sciences
No. 1219 Zhongguan West Road
315201 Ningbo, Zhejiang
China

Dr. Wenzhi Ren
Cixi Institute of Biomedical Engineering
Ningbo Institute of Materials
Technology and Engineering
Chinese Academy of Sciences
No. 1219 Zhongguan West Road
315201 Ningbo
China

Cover:
Streaming blood cells: Shutterstock ID 2008770 / Sebastian Kaulitzki
Microscopic view of pancreatic cancer Cells: Stocktrek Images/Getty Images 506837559
Bacteria illustration: Eraxion/ iStockphoto 8493122

All books published by **Wiley-VCH** are carefully produced. Nevertheless, authors, editors, and publisher do not warrant the information contained in these books, including this book, to be free of errors. Readers are advised to keep in mind that statements, data, illustrations, procedural details or other items may inadvertently be inaccurate.

Library of Congress Card No.: applied for

British Library Cataloguing-in-Publication Data
A catalogue record for this book is available from the British Library.

Bibliographic information published by the Deutsche Nationalbibliothek
The Deutsche Nationalbibliothek lists this publication in the Deutsche Nationalbibliografie; detailed bibliographic data are available on the Internet at <http://dnb.d-nb.de>.

© 2020 Wiley-VCH Verlag GmbH & Co. KGaA, Boschstr. 12, 69469 Weinheim, Germany

All rights reserved (including those of translation into other languages). No part of this book may be reproduced in any form – by photoprinting, microfilm, or any other means – nor transmitted or translated into a machine language without written permission from the publishers. Registered names, trademarks, etc. used in this book, even when not specifically marked as such, are not to be considered unprotected by law.

Print ISBN: 978-3-527-34724-7
ePDF ISBN: 978-3-527-82545-5
ePub ISBN: 978-3-527-82544-8
oBook ISBN: 978-3-527-82543-1

Cover Design Formgeber, Mannheim, Germany

Typesetting SPi Global, Chennai, India
Printing and Binding

Printed on acid-free paper

10 9 8 7 6 5 4 3 2 1

Contents

Preface *ix*

1 TiO_2 Nanoparticles: Properties and Applications *1*
Ozioma U. Akakuru, Zubair M. Iqbal, and Aiguo Wu
1.1 Introduction *1*
1.2 Properties of TiO_2 Nanoparticles *2*
1.2.1 Crystal Properties *2*
1.2.2 Optical Properties *3*
1.2.3 Electrochemical Properties *5*
1.3 Synthesis of TiO_2 Nanoparticles *6*
1.3.1 The Hydrothermal Method *6*
1.3.2 Sol–Gel Method *8*
1.3.3 Solvothermal Method *10*
1.3.4 Chemical and Physical Vapor Deposition Method *11*
1.3.5 Thermal Decomposition Method *12*
1.3.6 Oxidation Method *13*
1.4 Applications of TiO_2 Nanoparticles *14*
1.4.1 Nanobiotechnology *14*
1.4.2 Nanomedicine *17*
1.4.3 Wastewater Treatment *21*
1.4.4 Air Treatment *26*
1.4.5 Energy Devices *29*
1.4.6 Water Splitting for Hydrogen Production *30*
1.4.7 Food and Cosmetics *34*
1.4.8 Soil Remediation *35*
1.4.9 Pesticides Removal *36*
1.4.10 Paint and Paper Productions *40*
1.5 Conclusion *41*
Acknowledgments *42*
References *42*

2 Toxicity of TiO_2 Nanoparticles *67*
Gohar I. Dar, Madiha Saeed, and Aiguo Wu
2.1 Introduction *67*
2.2 Modes of Exposure, Biodistribution, Clearance, and Fate of TiO_2 NPs *70*
2.2.1 Inhalation *70*
2.2.2 Oral Route *71*
2.2.3 Injection *72*
2.2.4 Dermal Route *73*
2.3 Cell Death Pathways Induced by TiO_2 NPs *74*
2.3.1 Apoptosis *74*
2.3.2 Autophagy *76*
2.3.3 Crosstalk Between Apoptosis and Autophagy *76*
2.3.4 Necrosis *77*
2.4 Toxicity of TiO_2 *77*
2.4.1 Cellular Uptake *78*
2.4.2 Oxidative Stress Effectuates by TiO_2 *78*
2.4.3 Genotoxicity *79*
2.4.4 Reproductive and Developmental Toxicity *81*
2.4.5 Carcinogenicity *81*
2.4.6 Immunotoxicity of TiO_2 NPs *83*
2.4.7 Neurotoxicity of TiO_2 NPs *83*
2.4.8 Acute Toxicity of TiO_2 *84*
2.4.9 Sub-acute Toxicity of TiO_2 *86*
2.4.10 Sub-chronic Toxicity of TiO_2 NPs *87*
2.5 Alternative Perspective *88*
2.6 Conclusion *89*
Acknowledgments *89*
References *89*

3 Antibacterial Applications of TiO_2 Nanoparticles *105*
Chen Xu, Jianjun Zheng, and Aiguo Wu
3.1 Introduction *105*
3.2 Antibacterial Effect of TiO_2 Nanoparticle *107*
3.3 Ion-Doped TiO_2 Nanoparticles and Their Antibacterial Effect *113*
3.4 Antibacterial Agent-Doped TiO_2 Nanoparticles and Their Antibacterial Effect *120*
3.4.1 Ag-Doped TiO_2 Nanoparticles *120*
3.4.2 Zn-Doped TiO_2 Nanoparticles *123*
3.4.3 Cu-Doped TiO_2 Nanoparticles *123*
3.5 Antibacterial Applications of TiO_2-Based Nanoparticles *124*
3.5.1 Medical Application *124*
3.5.2 Environmental Application *125*
3.5.3 Food Safety Application *126*
3.6 Conclusion and Outlook *126*
Acknowledgments *126*
References *127*

4 Surface-Enhanced Raman Spectrum of TiO_2 Nanoparticle for Biosensing (TiO_2 Nanoparticle Served as SERS Sensing Substrate) *133*
Jie Lin and Aiguo Wu
4.1 Introduction *133*
4.2 SERS Effect of Nanomaterial Substrate *135*
4.2.1 Mechanism of Non-metal SERS Platforms *135*
4.2.2 Advantages for TiO_2 SERS Substrate *136*
4.2.3 SERS Mechanism of TiO_2 SERS Substrate *137*
4.2.4 Novel Methods to Improve TiO_2 SERS Enhancement *139*
4.3 TiO_2 SERS Substrate Applied in Biosensing *144*
4.3.1 Cell Capture on TiO_2 Nanorod Arrays *144*
4.3.2 Cell Capture Performance of TiO_2 Coatings *147*
4.4 Conclusions and Future Perspectives *150*
Acknowledgments *151*
References *151*

5 Cancer Theranostics of White TiO_2 Nanomaterials *153*
Yang Gao, Sijia Sun, Zhibin Yin, Yanhong Liu, Aiguo Wu, and Leyong Zeng
5.1 Introduction *153*
5.2 TiO_2 as Inorganic Photosensitizer for Photodynamic Therapy *154*
5.2.1 Photodynamic Therapy Principle *154*
5.2.2 Ultraviolet Light Responsive Photodynamic Therapy *155*
5.2.3 980 nm Near-Infrared Light Responsive Photodynamic Therapy *156*
5.2.4 808 nm Near-Infrared Light Responsive Photodynamic Therapy *158*
5.2.5 Organic/Inorganic Dual-Mode Photodynamic Therapy *161*
5.3 TiO_2 as Sonosensitizer for Sonodynamic Therapy *162*
5.3.1 Sonodynamic Therapy Principle *162*
5.3.2 Sonodynamic Therapy *162*
5.3.3 High Intensity-Focused Ultrasound Therapy *166*
5.4 TiO_2 as Multifunctional Nanoprobes for Visualized Theranostics *167*
5.4.1 Magnetic Resonance Imaging and Phototherapy *167*
5.4.2 Fluorescent Imaging and Phototherapy *168*
5.4.3 Multi-mode Imaging and Phototherapy *169*
5.4.4 Drug Delivery and Synergistic Therapy *170*
5.5 Conclusions and Future Perspectives *172*
Acknowledgments *173*
References *173*

6 Cancer Theranostics of Black TiO_2 Nanoparticles *185*
Ting Dai, Wenzhi Ren, and Aiguo Wu
6.1 Introduction *185*
6.1.1 Limitations of White TiO_2 Nanoparticles in Cancer Treatment *185*
6.1.2 Advantages of Black TiO_2 Nanoparticles in Cancer Treatment *186*
6.2 Preparations and Properties of Black TiO_2 Nanomaterials *187*
6.2.1 Hydrogenation Reduction Method *187*

6.2.2 Hydrogen Plasma Method *187*
6.2.3 Chemical Reduction Method *188*
6.2.4 Properties of Black TiO_2 Nanomaterials *188*
6.3 Black TiO_2 for Phototherapy *189*
6.3.1 Black TiO_2 for Photothermal Therapy *190*
6.3.2 Black TiO_2 for Photodynamic Therapy *194*
6.3.3 Black TiO_2 for Synergistic Photothermal and Photodynamic Therapy *194*
6.4 Black TiO_2 for Imaging-Guided Phototherapy *195*
6.5 Black TiO_2 for Synergistic Chemo-phototherapy *199*
6.6 Black TiO_{2-x} for Synergistic of Sonodynamic–Photothermal Therapy *202*
6.7 Overview and Further Perspective *205*
Acknowledgments *207*
References *207*

7 Neurodegenerative Disease Diagnostics and Therapy of TiO_2-Based Nanoparticles *217*
Xiang Gao, Jieling Qin, Zhenqi Jiang, Juan Li, and Aiguo Wu
7.1 Introduction *217*
7.2 The Symptoms of Neurodegenerative Disease *219*
7.3 Traditional Diagnosis and Treatment for NDs *220*
7.3.1 Current Methods for the Diagnosis of NDs *220*
7.3.2 Current Medicine for the Treatment of NDs *220*
7.4 Nanoparticles in the Diagnosis and Treatment of NDs *221*
7.4.1 The Diagnosis of ND Using NPs *221*
7.4.2 The Treatment of ND Using NPs as Drug Delivery *222*
7.5 The Diagnosis of NDs Using TiO_2 *222*
7.6 The Therapy of NDs Using TiO_2 *225*
7.6.1 The Therapy of NDs Using TiO_2 as Drug Delivery Platform *225*
7.6.2 The Therapy of NDs Using TiO_2 as Light-Responsive Material *226*
7.7 The Dilemma Situation of TiO_2 in the NDs *226*
7.8 Conclusion *228*
Acknowledgments *228*
References *228*

Index *237*

Preface

The authors of this book have studied nanoprobe-based diagnosis and therapy of diseases over ten years. According to the concept of functional modification of nanomaterials, they have carried out a series of research on the design, construction, and performance regulation of TiO_2 nanoprobes in theranostics of cancers. For example, they prepared Janus structure of TiO_2–Fe_3O_4 nanoprobes for magnetic resonance imaging (MRI)-visualized photodynamic therapy (PDT) of breast cancer, developed TiO_2–upconversion nanoprobes for near-infrared-triggered PDT/chemotherapy of breast cancer, and explored novel black TiO_2 nanoprobes for photothermal therapy (PTT) of breast cancer and MRI-visualized PTT of pancreatic cancer stem cells, acting as substrate of surface-enhanced Raman spectroscopy (SERS) for the detection of drug-resistant cancer cells. Based on their study of TiO_2 nanoprobes in the past ten years, and reference to the related works of peers, the authors decide to write this book on the application of TiO_2 nanoparticles in nanobiotechnology, and nanomedicine. This book not only summarizes the research progress of TiO_2 but also points out the existent problems in TiO_2 biomedical applications and the potential development directions in future.

This book includes seven chapters. Chapter 1 briefly introduces the properties, preparation methods, and applications of TiO_2 nanoparticles in nanomedicine and nanobiotechnology. The properties of TiO_2 nanoparticles are the intrinsic reason for their applications. Understanding the preparation methods will help people to improve the performances of TiO_2 nanoparticles. Chapter 2 summarizes the pathway, distribution, clearance, ultimate fate of TiO_2 products *in vivo*, and the dose-dependent potential toxicity, as well as the interactions between TiO_2 and cells, which will help people to improve material design and reduce their toxicity. Chapter 3 reviews the latest research progress of TiO_2-based antimicrobial application, including how to improve the photocatalytic activity of TiO_2 by non-metal doping such as nitrogen and carbon, as well as metal doping with nickel and neodymium, which achieves visible light-triggered high efficiency of antimicrobial activity. Chapter 4 introduces the application of TiO_2 as SERS substrate in biosensors and focuses on the SERS enhancement mechanism of TiO_2 nanoparticles. Chapter 5 mainly reviews white TiO_2 nanoparticles and their nanocomposites with novel structures and properties in cancer theranostics, such as ultraviolet or near-infrared light-stimulated PDT, ultrasound-triggered sonodynamic therapy (SDT), and drug delivery. Chapter 6

summarizes the properties, preparation, and research progress of black TiO_2 nanoparticles in cancer theranostics, including black TiO_2 with the functions of PTT, PDT, SDT, drug carriers, and photothermal and photoacoustic imaging. Chapter 7 reviews the application of TiO_2 nanoparticles in neurodegenerative diseases.

The authors hope that the publication of this book will help readers to fully understand the preparation, performance regulation, latest research progress in the field of nanomedicine, and the problems hindering the further application of TiO_2 nanoparticles. In this regard, it will encourage readers to focus on and solve these problems in future, promote the clinical application of TiO_2 in nanomedicine, and provide more efficient safe treatments for patients. Finally, the editors of this book would like to thank all the authors in each chapter for their hard work in discussion and writing this book, and they appreciate the support of talent policies and the funding of various scientific and technological projects. They also thank the authors of the references whose figures are reused in this book.

September 20, 2019

Aiguo Wu
Cixi Institute of Biomedical Engineering
CAS Key Laboratory of Magnetic
Materials and Devices
& Key Laboratory of Additive Manufacturing
Materials of Zhejiang Province
Ningbo Institute of Materials
Technology and Engineering
Chinese Academy of Sciences
Ningbo 315201, P.R. China

1

TiO_2 Nanoparticles: Properties and Applications

Ozioma U. Akakuru[1], Zubair M. Iqbal[1,2], and Aiguo Wu[1]*

[1] Cixi Institute of Biomedical Engineering, CAS Key Laboratory of Magnetic Materials and Devices, & Key Laboratory of Additive Manufacturing Materials of Zhejiang Province, Ningbo Institute of Materials Technology and Engineering, Chinese Academy of Sciences, No. 1219 Zhongguan West Road, Ningbo 315201, P.R. China
[2] School of Materials Science and Engineering, Zhejiang Sci-Tech University, No.2 Road of Xiasha, Hangzhou, 310018, P.R. China

CHAPTER MENU

Introduction, 1
Properties of TiO_2 Nanoparticles, 2
Synthesis of TiO_2 Nanoparticles, 6
Applications of TiO_2 Nanoparticles, 14
Conclusion, 41

1.1 Introduction

The important discovery of ultraviolet (UV) light-mediated water splitting on titanium dioxide (TiO_2) surface by Fujishima and Honda [1] has promoted immense research on other applications of TiO_2 nanoparticles, particularly in nanobiotechnology and nanomedicine [2]. Undoubtedly, the past few decades have witnessed an exponential growth in nanoscience and nanotechnology research activities [3–5]. Nanoparticles have gained immense interest for both academic and industrial applications owing to the fact that the use of these nanoparticles with other materials has improved scientific discoveries and breakthroughs [6]. These advances have been aided by the fact that new chemical and physical properties of materials emerge on reduction of their sizes to the nanometer range and varying their shapes [7]. It has been reported that the specific surface area and the ratio of the surface to the volume of nanomaterials dramatically increase as their sizes decrease [8]. Interestingly, high surface area, a consequence of small particle size, is of benefit to TiO_2 nanoparticles, as the surface area-dependent interaction/reaction of TiO_2 nanoparticles devices and those of the contact media basically occurs at the surfaces or interfaces [7].

*Corresponding author: zubair@nimte.ac.cn, zubair@zstu.edu.cn

TiO_2 Nanoparticles: Applications in Nanobiotechnology and Nanomedicine,
First Edition. Edited by Aiguo Wu and Wenzhi Ren.
© 2020 Wiley-VCH Verlag GmbH & Co. KGaA. Published 2020 by Wiley-VCH Verlag GmbH & Co. KGaA.

Interestingly, TiO_2 nanoparticles have been extensively studied owing to their low production costs, mechanical and chemical stabilities, thin film transparency, bio- and chemical inertness, hydrophilicity, high light conversion efficiency, and corrosion resistance [9, 10]. Based on these exceptional properties, TiO_2 nanoparticles have vast array of applications that include nanomedicine, nanobiotechnology, solar and electrochemical cells, wastewater treatment, food, soil remediation, gas sensing, cosmetics, plastics, paint and paper productions, hydrogen fuel generation, antiseptics and antibacterial compositions, self-cleaning devices, and printing inks [10, 11]. Extensive research has been recently conducted on the nanomedical application of TiO_2 nanoparticles in the domains of cancer therapy and imaging. These recent progresses in nanomedicine do not only depend on the TiO_2 nanoparticles themselves but also on their functionalization with other inorganic or organic compounds [12]. Specifically, TiO_2 nanoparticles combined with magnetic nanoparticles have been used as magnetic resonance imaging (MRI) contrast agents and inorganic photosensitizers for photodynamic therapy [13], nanocarriers in chemotherapy [12], and in the recently discovered hydrogenated black TiO_2 nanoparticles as efficient cancer photothermal therapeutic agents [14]. Their cancer therapeutic efficacy has been linked to their good biocompatibility, low cytotoxicity, and unique photocatalytic properties [15].

Some researchers recently opined that there are many other new applications for TiO_2 that are either under way or presently in pilot production [16]. These new applications may be uncovered sooner than expected, due to the US FDA approval of TiO_2 to be freely incorporated into numerous domestic products (dental pastes, non-parenteral medicines, tablets, and oral capsules), thereby dramatically increasing the production and availability of TiO_2 for various applications [17]. This chapter will therefore discuss the properties, synthesis, and applications of TiO_2 nanoparticles with respect to nanobiotechnology and nanomedicine.

1.2 Properties of TiO_2 Nanoparticles

The fascinating properties of TiO_2 nanoparticles have dramatically enhanced their applications in various aspects [18, 19]. For instance, their high light-conversion efficiencies have been exploited for the fabrication of energy devices [20]. Their chemical stability, thin film transparency, and low production costs are responsible for their utility as photocatalysts for various environmental remediation strategies such as wastewater treatment, air pollution, and soil viability improvement [9]. Recently, TiO_2 nanoparticles were applied for cancer photothermal therapy (PTT), exploiting their non-radiative recombination ability [14]. In the following subsections, specific properties of TiO_2 nanoparticles will be discussed in more detail.

1.2.1 Crystal Properties

Nanocrystalline TiO_2 exists in three major polymorphic forms, which include rutile, anatase, and brookite, based on the conditions of fabrication and post

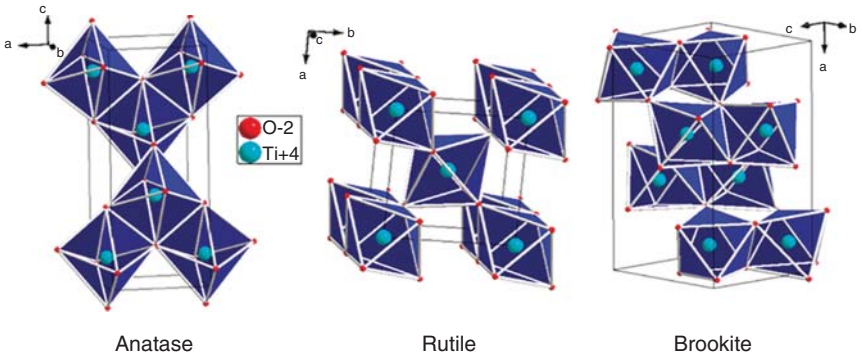

Figure 1.1 The crystal structures of anatase, rutile, brookite TiO_2 phases. Source: Adapted with permission from Dambournet et al. 2010 [27]. Copyright American Chemical Society.

fabrication heat treatment [21]. The fourth polymorphic form TiO_2(B) is quite uncommon [22]. Aside these four polymorphs, some researchers have reported the successful synthesis of two high-pressure phases from that of rutile: the TiO_2(II) that has the PbO_2-like structure [23] and the TiO_2(H) that structure looks more like a hollandite [24].

Both the anatase and rutile phases possess tetragonal crystal structures even though they do not belong to the same phase groups, while brookite has an orthorhombic structure and the uncommon TiO_2(B) phase is monoclinic [22, 25, 26]. As shown in Figure 1.1, the distortion of anatase phase octahedral structure is slightly larger than that of rutile [27]. It has been reported that even though the rutile phase is less stable than the anatase phase at 0 K, corresponding energy difference between these phases is rather small (about 2–10 kJ/mol). With respect to solar cell application, anatase phase TiO_2 is chosen over other phases as a result of its low density, high electron mobility, and low dielectric constant [22]. It is also attractive that in an anatase crystal, the reactivity of its (101) facets is much lower than that of its (001) facets [28].

As a consequence of the anatase phase low density, it easily undergoes transition to the rutile phase at high temperatures (usually around 450–1200 °C) [29]. This observed transformation is not only temperature dependent but is also affected by some other factors such as dopant concentration, initial phase, and particle size [30]. It has also been observed that both the brookite and anatase phases usually transform to the rutile phase at pre-determined particle sizes, wherein the rutile phase gains higher stability against the anatase phase at particles sizes that are greater than 14 nm [31]. Additionally, it has been reported that whenever the rutile phase is formed, it grows quicker in comparison to the anatase phase [22]. The crystal properties of TiO_2 are summarized in Table 1.1.

1.2.2 Optical Properties

The extensive use of TiO_2 nanoparticles in optical devices are attributed to their excellent mechanical durability, high transparency in the visible region, and chemical stability in aqueous medium [18]. Several other structural parameters

Table 1.1 The crystal properties of TiO_2 [20–22].

Properties	Anatase	Rutile	Brookite
Crystal structure	Tetragonal	Tetragonal	Orthorhombic
Density (g/cm^2)	3.894	4.250	4.120
Space group	$I4_1/amd$	$P4_2/mnm$	Pbca
Molecule (cell)	2	2	4
Lattice constant (Å)	$a = 3.784$ $b = 9.515$	$a = 4.594$ $b = 2.959$	$a = 9.184$ $b = 5.447$ $c = 5.154$
Ti—O bond length (Å)	1.937(4) 1.965(2)	1.949(4) 1.980(2)	1.87–2.04
O—Ti—O bond angle	77.7° 92.6°	81.2° 90.0°	77.0°–105.0°
Volume/molecule ($Å^3$)	34.061	31.216	32.172

such as phase composition, band gap, crystalline quality, size distribution, morphology, porosity, and particle size have been reported to influence the optical activities of TiO_2 nanoparticles [32]. Remarkably, decreasing the particle size of TiO_2 nanoparticles from 200 nm to smaller materials of about 10 nm or less changes the optical properties of these nanoparticles from opaque to transparent in the visible region of the light spectrum and subsequently to intriguing UV light blockers [33].

In pure TiO_2, the anatase phase shows superior catalytic ability and electron mobility than either the rutile or brookite phases, a property that is beneficial for photovoltaic and photocatalytic applications [20, 34]. The increased photoreactivity of the anatase phase has been linked to its low oxygen adsorption capacity, increased hydroxylation degree, and slightly higher Fermi level [20]. On the other hand, the rutile phase exhibits high refractive index and high optical absorptivity, which are responsible for its application in optical communication devices such as modulators, switches, and isolators [34].

On exposure of TiO_2 nanoparticles to UV light, the electrons in their valence bands (VB) gain energy and as such undergo excitation to corresponding conduction bands (CBs), thus generating holes (h^+) on those VBs (Figure 1.2). At this instance, the excited electrons (e^-) are purely in 3d states, and due to dissimilar parity, the probability for e^- transition is reduced, with attendant decrease in the e^-/h^+ recombination [22]. In this respect, the anatase phase is regarded as the active photocatalytic component that is also attributable to its chemical properties and the generation of charge carriers (e^- and h^+) that arise from its ability to absorb UV light, which is in correspondence with its band gap [35]. The rutile phase is generally regarded as a poor photocatalyst, due to the fact that the bulk recombination of h^+ and e^- takes place, whereby only the h^+ that are quite near to the surface are withheld and subsequently undergo surface transfer by the upward band bending [36]. These h^+ subsequently interact with the

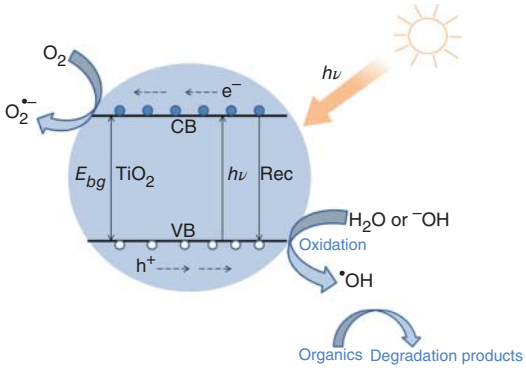

Figure 1.2 Illustration of the general mechanism of TiO_2 in solar photocatalysis process.

molecules of H_2O, thereby forming hydroxyl radicals ($OH^{\bullet}$) that in synergy with the h^+ effectively oxidize the organic compounds in their vicinity on the surface of the particles [35]. Also, the e^- in the CB interact with air molecular oxygen following a reduction reaction process, thereby producing superoxide radical anions ($O_2^{\bullet -}$) [36].

It is worthy of note that the charge couple (e^-/h^+) redox potential of an ideal photocatalyst is expected to fall within the domain of its band gap [37]. Additionally, the reduction activity of photoelectrons is determined by existence of energy level on the bottom of the CB of the photocatalyst, while the oxidation activity of photogenerated h^+ is a function of the energy level on top of the photocatalyst VB [22]. Based on these properties, TiO_2 nanoparticles are considered as near-ideal photocatalysts as their h^+ are redox selective and strongly oxidized, dramatically increasing more research into nano-sized TiO_2-based photocatalysts [37].

1.2.3 Electrochemical Properties

The chemical and physical properties of nano-TiO_2 are altered by their inherent electronic structure, size, shape, surface properties, and organization [38]. The electronic properties of TiO_2 nanoparticles have been reported as huge contributors to their particle- and crystal-size distributions [33]. TiO_2 in its pure form is a wide band gap n-type semiconductor that possesses indirect energy band gaps of the rutile, anatase, and brookite phases of 3.02, 3.2, and 2.96 eV, respectively [29, 39, 40]. It has also been reported that rutile Fermi level is lower than the anatase by ~0.1 eV [20]. Additionally, anatase has a smaller electron effective mass than rutile, resulting to an increase in mobility for the charge carriers in anatase, a characteristic that is highly favorable for optoelectronic devices production [20]. The TiO_2 CB consists of 3d orbitals of titanium, whereas its VB has 2p oxygen orbitals that form hybrids alongside 3d titanium orbitals [22].

The lattice oxygen sites in TiO_2 are very important with respect to the observed superhydrophilicity of TiO_2 nanoparticles, originating from the chemical conformation changes of their surfaces [41]. This is because some amounts of the trapped h^+ on the lattice sites of oxygen might interact with the TiO_2 specifically, thereby weakening the oxygen ions and lattice titanium bonds. As a consequence, H_2O molecules can interrupt these bonds resulting in the generation of new -OH

groups. These singly linked -OH groups are thermodynamically unstable and possess high surface energy, which leads to the generation of TiO_2 surface with superhydrophilicity [36, 41].

One of the observed disadvantages for the use of TiO_2 nanoparticles in photoelectrochemical devices is the large density of states that are involved in e^-/h^+ recombination and electron transfer reactions at the electrolyte–oxide interface, if located in the band gap [42]. On the other hand, this is an advantage for the adsorption of redox-active compounds on the surfaces of TiO_2 nanoparticles that is of special interest in dental implant applications [43]. For instance, serum proteins such as fibrinogen are reportedly chemisorbed by an electron transfer process on the surface of TiO_2 nanoparticles [42]. It was demonstrated that the electronic behavior of the TiO_2 nanoparticles affects the thrombogenicity of the fibrinogen due to the semiconducting property of fibrinogen, which is crucial in the blood coagulation pathway. It then follows that an alteration in the Fermi energy placement and/or band size of the TiO_2 nanoparticles could trigger a change in the adsorption and subsequent decomposition of the protein, since the band structure of the fibrinogen fits into that of the TiO_2 nanoparticles [42].

1.3 Synthesis of TiO_2 Nanoparticles

Numerous types of TiO_2 nanoparticles have been synthesized in the form of nanotubes, nanofibers, nanosheets, nanorods, and interconnected architectures [36, 44, 45]. The regularly employed synthesis methods are the hydrothermal, sol–gel, solvothermal, vapor deposition, oxidation, and the thermal decomposition methods. Other methods that have been used for the successful synthesis of various forms of TiO_2 nanoparticles include but not limited to sol, electrodeposition, sonochemical and microwave-assisted, and micelle and inverse micellar methods. For instance, in the micellar synthetic strategy, TiO_2 nanoparticles were prepared via the tetraisopropyl titanate hydrolysis in the presence of sodium bis (2-ethylhexyl) sulfosuccinate reverse micelles to obtain nanoparticles whose average size ranged from 20 to 200 nm [21]. Based on the micellar water pool, various TiO_2 phases were produced, wherein large pools afforded anatase and small pools afforded the amorphous nanoparticles. In the following subsections, some commonly used strategies for synthesizing TiO_2 nanoparticles are discussed in more detail.

1.3.1 The Hydrothermal Method

The hydrothermal synthetic method is usually conducted in steel pressure vessels, i.e. autoclaves with the Teflon liners under regulated pressure and temperature. This temperature can be increased from the boiling point of water up to saturation vapor pressure, but the pressure produced is also dependent on the amount of added solution [7]. Hydrothermal method has therefore been utilized by many researchers for the synthesis of TiO_2 nanoparticles [46–48]. In this regard, Dawson et al. synthesized TiO_2 nanoparticles by the hydrothermal method, wherein

they subjected various compositions and particle sizes of TiO_2 mixed powders to hydrothermal reaction in the presence of NaOH [49]. At 140 °C, trititanate nanotubes easily formed from the anatase phase of the starting material and at 170 °C, trititanate belts and plates formed from the rutile phase component. Increasing the reaction time to seven days exclusively converted all the TiO_2 to trititanate nanoplates and belts, without the formation of nanotubes. Hitherto, there is no clear description of the structure of TiO_2 nanotubes but researchers have assumed the existence of hydrogen titanate where the tubes are separated by hydrogen ions [2].

In a related experiment, pure rutile nanotubes with average diameters less than 20 nm were synthesized from rutile–anatase TiO_2 particles using the hydrothermal method in NaOH water–ethanol solution [50]. It was observed that the structure and morphology of the products depended on the type of alcohol, as well as the alcohol–water ratio. This was explained by the variation in optoelectronic behaviors of the rutile nanotubes and raw TiO_2. The hydrothermal method was also used to synthesize titanate nanotubes for the degradation of Acid Red 18 [51]. These researchers further calcined the nanotubes at various temperatures (400–700 °C) and observed that the nanotubes calcined at 600 °C were most active toward the Acid Red 18 decomposition. It was reported that the mechanism for the formation of TiO_2 nanotubes involved multilayered nanosheet wrapping, rather than the wrapping or scrolling of single-layered nanosheets, which is usually accompanied by the crystallization of successive layers [52]. Nano-sized TiO_2 has also been synthesized from commercial TiO_2 on a fluorine-doped tin oxide (FTO) substrate as shown in Figure 1.3a [53]. The reaction was carried out for 24 hours at 135 °C in a solution of NaOH, resulting in TiO_2 nanotubes with average diameter of 10–12 nm (Figure 1.3b,c).

In another study, nano-TiO_2 were obtained from titanium (IV) alkoxide in an acidified water–ethanol solution [47]. The dropwise addition of titanium tetraisopropoxide (TTIP) into the water–ethanol solution at pH 0.7, followed by a four hour reaction at 240 °C, yielded the TiO_2 nanoparticles dominated by the anatase phase. It was observed that tuning the solvent system and the Ti precursor was able to control the size of the as-synthesized nanoparticles to about 7–25 nm. Nanowires of TiO_2 have also been obtained by the hydrothermal method using white TiO_2 powders in 10–15 M NaOH at temperatures of about 150–200 °C without stirring in an autoclave for 24–72 hours [54]. Zhang and Gao treated $TiCl_4$ solution with an acid or organic salt for 12 hours at 33–423 °C to obtain TiO_2 nanorods [55]. They also reported that a change in the surfactant or the solvent composition could affect the morphology of the synthesized nanorods. The hydrothermal method was also employed by Chong et al. to synthesized TiO_2 nanofibers with average thickness of 40–100 nm [56]. The hydrothermal synthetic method was conducted in the presence of NaOH and an ion-exchange post-synthesis in a solution of HCl. Specifically, the researchers reacted 3 g anatase TiO_2 in 10 M NaOH (80 ml), followed by autoclaving for 48 hours at 180 °C in a poly-tetrafluoroethylene container. They obtained a sodium titanate nanofiber precipitate that underwent H^+ exchange and calcination for three hours at 700 °C to obtain the TiO_2 nanofibers.

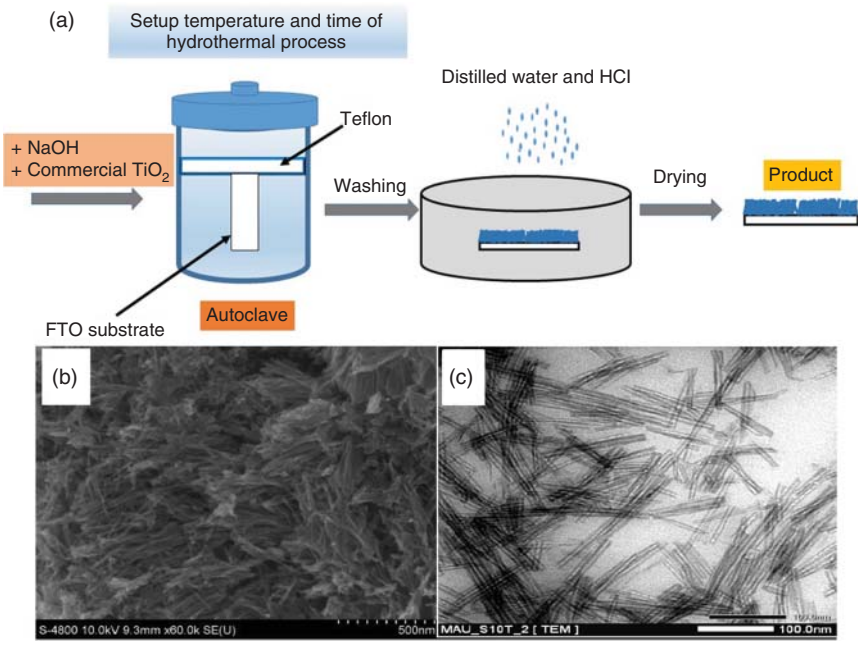

Figure 1.3 (a) Illustration of the synthesis process of TiO_2 nanotubes on an FTO substrate via the hydrothermal method, (b) field emission scanning electron microscopy (FESEM), and (c) transmission electron microscopy (TEM) images of the synthesized TiO_2 nanotubes. Source: Reprinted with permission from Viet et al. 2016 [53]. Copyright AIMS Press.

1.3.2 Sol–Gel Method

The sol–gel synthetic strategy is generally employed to synthesize crystalline or amorphous structures of organic or inorganic materials that offers the advantage of obtaining better purity and homogeneity of the synthesized nanoparticles at low temperatures [45]. Utilizing the sol–gel strategy, nano-TiO_2 were synthesized following hydrolysis of a TiO_2 precursor as shown in Figure 1.4 [57]. This usually proceeds by acid-mediated titanium (IV) alkoxide hydrolysis, which is followed by a condensation reaction [7]. The formation of the chains of Ti–O–Ti has been reportedly encouraged by slow hydrolysis rates, high amount of titanium (IV) alkoxide, and small amount of water [58, 59]. On the other hand, it is possible to obtain different shapes and sizes of anatase TiO_2 nanoparticles with high crystallinity by the tetramethylammonium hydroxide-mediated titanium (IV) alkoxide polycondensation [58]. Typically, the titanium (IV) alkoxide could be complemented with NaOH and an alcohol at 2 °C and heated for 13 days at 50–60 °C or six hours at an elevated temperature (90–100 °C). For the purpose of improving the crystal nature of the as-synthesized nanoparticle, a secondary heat treatment (175 and 200 °C) in an autoclave can be performed [7]. Furthermore, for the avoidance of agglomeration during the crystallization process of the nanoparticles, a prolonged heat treatment can be performed at temperatures below 100 °C [58].

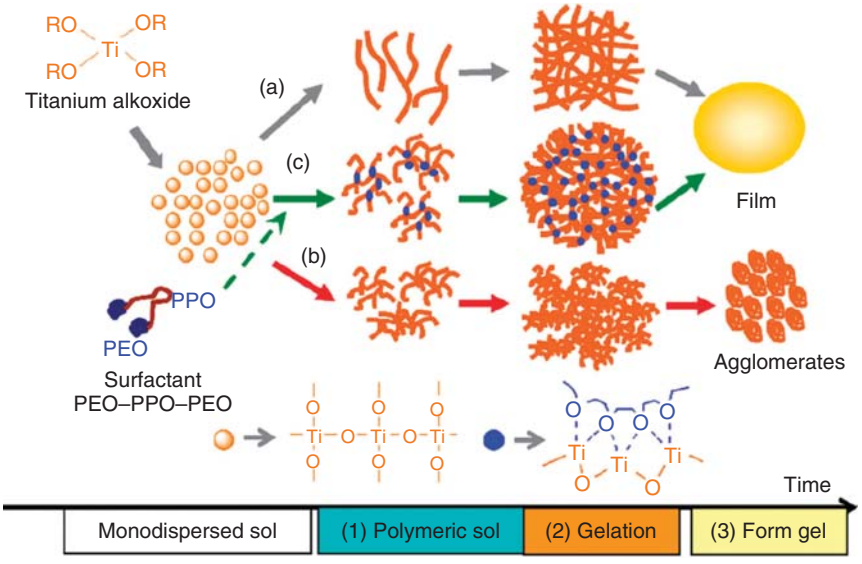

Figure 1.4 Illustrating the sol–gel synthetic mechanism in the presence of an (a) acid, (b) base, and (c) P123-templated, basic condition in dimethylformamide. Source: Adapted with permission from Cao et al. 2011 [57]. Copyright The Royal Society of Chemistry.

Although the sol–gel method has been regarded as a conventionally accepted method for the synthesis of TiO_2 nanoparticles, several disadvantages of this method has inevitably caused researchers to explore other synthesis strategies. Among these disadvantages is the fact that the calcination process obviously causes the grain growth and low specific surface area and induces phase transformations [60]. Additionally, comparatively poor crystallinity and particle size uniformity often characterize the synthesized nanoparticles [32]. These drawbacks notwithstanding, some researchers have successfully applied this strategy for the synthesis of TiO_2 nanoparticles for practical applications. For instance, TiO_2 nanorods were successfully prepared by sol–gel synthetic strategy by dipping porous anodic alumina membrane (denoted as AAM) template in a boiled sol of TiO_2, accompanied with the usual procedures of drying and heating [61]. These researchers observed that tuning the calcination temperature could control the nanorod crystal phases, demonstrated by the formation of anatase and rutile nanorods at low and high calcination temperatures, respectively. In another study, TiO_2–zinc phthalocyanine nanoparticles were obtained by the sol–gel strategy and applied as photosensitizers for cancer photodynamic therapy [62]. Additionally, the hydrolysis and condensation of titanium butoxide with gamma amine butyric acid and mineral acids as the precursors yielded amine-, phosphate-, and sulfate-functionalized TiO_2 nanoparticles in a typical sol–gel synthetic method [63]. These functionalized nanoparticles demonstrated good potential as copper complex drug carriers for cancer chemotherapy.

Utilizing the electrophoretic deposition of the colloidal suspensions of TiO_2 into AAM pores, Lin et al. obtained ordered arrays of TiO_2 nanowires [64]. They employed platinum anode and the AAM with a gold substrate fastened

to copper as the cathode. Making use of a voltage of about 2–5 V, a TiO_2 sol was successfully deposited into the AAM pores. A 5% NaOH dissolution of the AAM template yielded the TiO_2 nanowires, and it was observed that an AAM with long pores was desirable for the preparation of nanowires in favor of nanotubes. In a related study, nanotubes of TiO_2 were synthesized with an AAM template and other organic compounds [65]. Typically, the AAM was dipped into a solution of TTIP and later removed and kept in vacuum to allow the TTIP volume to pull through the template. Then, water vapor hydrolysis in the presence of HCl (24 hours), air drying at ambient temperature, calcination for two hours at 673 K and dissolution of the AAM in 6 M NaOH were conducted to obtain pure TiO_2 nanotubes. In another study, TiO_2 nanotubes were synthesized with a dilute TiF_4 coating of the AAM membranes at time periods of 12–48 hours at 60 °C [66]. The AAM membranes were then removed after the observed formation of the nanotubes. In another experiment by Sugimoto et al., TTIP was mixed with triethanolamine (TEOA) in a sol–gel synthetic strategy, followed by aging for one day at 100 °C and three days at 140 °C [67]. These researchers employed amines (TEOA, diethylenetriamine, ethylenediamine, trimethylamine, and triethylamine) as surfactants and shape controllers for the TiO_2 nanoparticles and observed a morphology change at above pH values of 11 and 9.5 in the presence of TEOA and the other amines, respectively. This control over shape was attributed to the adsorption of the amine shape controllers on the crystal planes of the TiO_2 nanoparticles. Mahshid et al. prepared biphase TiO_2 nanoparticles by the sol–gel method that yielded crystallite sizes between 27 and 107 nm [68]. Hussain et al. also synthesized novel nano-TiO_2 whose size ranged from 10 to 20 nm by the sol–gel technique [69].

In another study, Chong et al. synthesized TiO_2 nanoparticles by the sol–gel method [70]. They hydrolyzed titanium IV butoxide precursor with ethanol, followed by a condensation reaction. Through this first step, it was possible to control the homogeneity and microstructures of the eventually formed TiO_2 crystals. Control of the hydrolysis extent is very crucial in obtaining nano-sized TiO_2. For this purpose, these researchers carried out the hydrolysis in two stages, where the ethanol addition to the titanium IV butoxide precursor was utilized to target the partially hydrolyzed state. This partially hydrolyzed state ensures an improved molecular homogeneity and non-hydrolyzable Ti ligands for enhanced growth of the TiO_2 [71]. The control of the hydrolysis reaction extent was achieved by an acid-mediated hydrolysis with nitric acid, owing to the low range of ethanol functionality in the titanium IV butoxide precursor hydrolysis.

1.3.3 Solvothermal Method

The solvothermal synthetic strategy is closely related to the hydrothermal technique but for the use of non-aqueous solvents in the former [58]. Due to the use of a wide range of organic solvents of appreciably high boiling points in the former, the working temperatures can be elevated way much higher than is attainable in the later [7]. Moreover, the solvothermal method offers intriguing advantages including an improved tuning of morphology, particle size, crystallinity of the

synthesized nanoparticles, and temperature and pressure controls of the solvents used for the synthesis [72]. Additionally, this method provides a versatile route to the synthesis of TiO_2 nanoparticles with improved dispersity and narrow size distribution [7].

The solvothermal synthetic strategy was used for the preparation of TiO_2 nanorods and nanoparticles with or without surfactant mediation [58, 73]. In the light of this, anhydrous toluene was employed at 250 °C for 20 hours to dissolve TTIP, using oleic acid as a surfactant [74]. In a controlled hydrolyzation reaction, redispersible TiO_2 nanorods and nanoparticles were synthesized with $Ti(OC_4H_9)_4$ in the presence of linoleic acid. This reaction was carried out with a catalyst (triethylamine) to aid the inorganic Ti–O–Ti condensation in order to obtain the crystals with consistent morphology [73].

1.3.4 Chemical and Physical Vapor Deposition Method

Vapor deposition can be referred to as the condensation of materials in the vapor phase to solid phase [58]. In the absence of a chemical reaction in the vacuum chamber, the process is termed physical vapor deposition (PVD), otherwise it is termed chemical vapor deposition (CVD) [75]. In a typical CVD process, the deposition reaction is driven by thermal energy that heats the gases present in the coating compartment [7]. Employing TTIP pyrolysis in an atmosphere of oxygen/helium utilizing a liquid precursor, TiO_2 nanoparticles with average sizes below 10 nm were successfully synthesized [76].

Nevertheless, other CVD approaches exist, which include diffusion flame pyrolysis, ultrasonic spray pyrolysis, ultrasonic-assisted hydrolysis, electrostatic spray hydrolysis, laser-induced pyrolysis, and plasma-enhanced CVD (PECVD) [58]. In a typical PECVD, the amorphous TiO_2 nanoparticles are placed on the cold compartments of the reactor at temperatures less than 90 °C as shown in Figure 1.5a [77]. The obtained nanoparticles from PECVD after annealing same at high temperatures usually possess high surface areas (Figure 1.5b,c) [78].

In another experiment employing catalyst- and template-free metal organic CVD (MOCVD), Wu and Yu successfully grew TiO_2 nanorods on fused silica substrates [79]. Typically, O_2/N_2 flow was used to convey titanium acetylacetonate that was vaporizing in the low-temperature region of the furnace (200–230 °C) to the high-temperature region (500–700 °C), resulting in the growth of the TiO_2 nanorods on the substrates directly. The morphology and phase of the nanorods were demonstrated to be tunable with the reaction conditions. To illustrate this, at a pressure of 5 Torr, single-crystalline anatase and rutile nanorods were obtained at 560 and 630 °C, respectively, while at 3.6 Torr, anatase nanowalls comprising of well-aligned nanorods were obtained at 535 °C. The MOCVD method has also been applied using a WC–Co substrate and a TTIP precursor for the successful synthesis of TiO_2 nanorods as reported in a study by Pradhan et al. [80].

Primary PVD methods include ion plating, sputtering, laser surface alloying, thermal deposition, and laser vaporization [7]. The PVD method or thermal deposition has been employed for the synthesis of TiO_2 nanowires [81]. In a typical experiment conducted in a tube furnace, a titanium source (pure

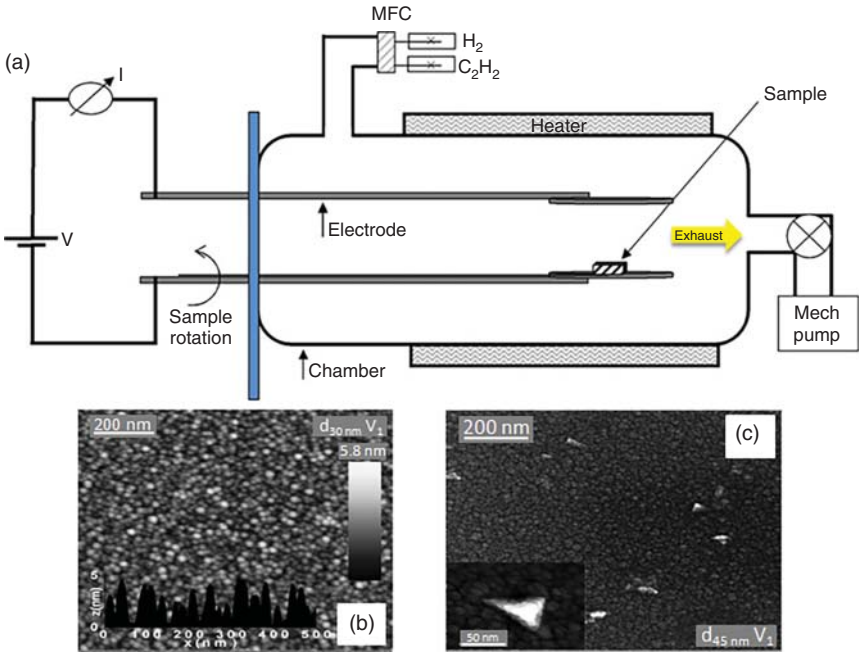

Figure 1.5 (a) Schematic diagram of a typical PECVD. Source: Baghgar et al. 2009 [77]. Reproduced with permission of Institute of Physics. (b) Atomic force. Source: Adapted with permission from Borras et al. 2009 [78]. Copyright American Chemical Society. (c) Scanning electron microscopy (SEM) images of TiO_2 grown by PECVD.

Ti metal) was loaded on a quartz boat, and under an argon atmosphere, the temperature was raised to 850 °C. This was followed by pumping down of the furnace chamber to about 300 Torr with the argon flow rate of 100 sccm for three hours, to obtain fine TiO_2 nanowires. In an alternative route, Wu et al. employed Au as a catalyst and deposited a nanopowder layer of Ti on the substrate, prior to the growth of the TiO_2 nanowires [82].

1.3.5 Thermal Decomposition Method

The thermal decomposition method has been employed in the past decade by various researchers for the synthesis of TiO_2 nanoparticles [83–85]. For instance, the thermal degradation of TTIP vapor at 300 °C, yielded TiO_2 nanoparticles in a study by Moravec et al. [84]. They saturated the carrier gas (dry, particle free, and deoxidized nitrogen) with the TTIP vapor in a saturator that was externally heated. It was observed that the formation of fine TiO_2 nanoparticles was initiated by the heterogeneous decomposition of the TTIP. In another experiment, TiO_2 nanoparticles were obtained by thermal decomposition of titanium (IV) *n*-butoxide in 1,4-butanediol. The reaction was also conducted in an autoclave at 300 °C for two hours at 25 °C. The obtained nanoparticles were further calcined for two hours at 500 °C in a box furnace and were obtained as crystals of anatase TiO_2 nanoparticles with average diameter of 15 nm.

Furthermore, TiO_2 nanoparticles with improved photocatalytic ability were successfully synthesized using the thermal decomposition method by treating the precursor titanyl sulfate with peroxo compounds such as hydrogen peroxide, urea hydrogen peroxide, and ammonium persulfate [86]. Annealing temperatures of 600, 850, and 700 °C were utilized in air at 60 minutes for the hydrogen peroxide, urea hydrogen peroxide, and ammonium persulfate peroxo-containing phases, respectively, to obtain the anatase phase TiO_2 nanoparticles. In a different study, Im et al. synthesized 10 nm-TiO_2 nanoparticles by thermally decomposing metal–organic frameworks (denoted as MIL-125 and MIL-125-NH_2) that contain titanium, for six hours at 350 °C in air [85]. They observed a random aggregation of the nanoparticles within the crystalline particles of the metal–organic framework precursors. These nanoparticles showed capacity for effective decomposition of 4-chlorophenol by photocatalysis.

1.3.6 Oxidation Method

This method involves the direct oxidation of the element titanium by the use of oxidants or anodic reactions to produce the nanoparticles [58]. For instance, using a voltage of 10–20 V and 0.5% hydrogen fluoride, Varghese et al. successfully prepared well-aligned TiO_2 nanotubes [87]. Annealing the anodized plate of titanium at 500 °C for six hours in the presence of oxygen was necessary in obtaining the nanotubes. It was observed that the diameter and length of the nanotubes could be controlled by tuning the applied voltage.

The hydrogen peroxide-induced oxidation of the element titanium was reported to be effective for the synthesis of TiO_2 nanotubes by placing the titanium metal in 50 ml hydrogen peroxide solution (30 wt%) for 72 hours at 353 K [88]. In the oxidative synthesis of TiO_2 nanoparticles, the phase of the products were controlled by adding specific inorganic salts in the preparation process, particularly during the dissolution precipitation [89]. For instance, NaCl is usually added for the generation of rutile phase, and NaF or Na_2SO_4 are required to obtain the anatase phase TiO_2 nanoparticles [90]. Acetone has also been employed as an oxygen source at 850 °C for 90 minutes to obtain well-aligned and highly dense TiO_2 nanorod arrays [91].

Furthermore, TiO_2 nanoparticles can be synthesized by either the wet or dry processes. In the dry process, the vapor phase oxidation of $TiCl_4$ is conducted, which leads to formation of amorphous TiO_2 nanoparticles as shown in Eq. (1.1). This is usually followed by annealing of the synthesized amorphous TiO_2 nanoparticles at different temperatures to obtain desired crystalline phases of anatase or rutile [21].

$$TiCl_4(g) + O_2(g) \rightarrow TiO_2(s) + 2Cl_2(g) \tag{1.1}$$

In the wet process, homogenous products and nanocomposites with complex shapes can be obtained, and there is also the possibility of controlling the stoichiometry. However, the presence of carbon (an impurity in this case), long processing times, and expensive precursors are the major drawbacks of this process [22].

1.4 Applications of TiO_2 Nanoparticles

Due to their fascinating properties, TiO_2 nanoparticles have found vast array of applications such as in nanobiotechnology [92], nanomedicine [14], energy devices [93], soil remediation [94], food [95], healthcare and cosmetic products [96], wastewater treatment [97], and paint [98], paper [99], and plastics productions [100]. Some of these general applications of TiO_2 nanoparticles will be briefly discussed in the following subsections.

1.4.1 Nanobiotechnology

Owing to the increasing difficulty in treating multidrug resistant strains (*Pseudomonas aeruginosa*), there is an urgent need to fabricate new class of antibacterial agents with totally different mode of action and structure from conventional agents [19]. Additionally, multidrug resistant strains have been linked to complications in present-day medicine [101]. These strains have also been identified worldwide as major nosocomial pathogens [102]. The last decade has witnessed various failures in the treatment of animal and human bacterial diseases that have been generally attributed to the strong resistance of bacterial pathogens to conventional drugs [103, 104]. This is mainly due to the ability of these bacterial pathogens to rapidly adapt to new environmental terrains such as antimicrobial molecules presence, consequently increasing the bacterial resistance following the use of antimicrobials [105]. In recent years, a good number of nanoparticles have demonstrated encouraging biological activities, particularly toward bacterial treatment [106]. Among these nanoparticles, nano-TiO_2 has gained attention based on its hydrolysis and oxidative properties [92]. It has also been observed that the biocidal action of nano-TiO_2 is partly a consequence of charge carrier (electron-hole) modulation at the external surface interface of the nanoparticles, giving rise to appreciable antimicrobial capabilities by optimizing the inorganic–organic interfacial contact and inorganic phase dispersions [107–110]. Additionally, nano-TiO_2 has been tipped to outperform metal-based systems and other chemicals such as H_2O_2, NO, and other small molecules due to the intrinsically environmental friendliness and non-contact antimicrobial action of TiO_2–polymer nanocomposites [111, 112]. As such, no release of toxic nanoparticles to the surrounding media (with adverse health effects) occurs in order to obtain the disinfection efficacies [113, 114].

Nano-TiO_2 has also been used for the disinfection of a broad microorganism spectrum [92, 115], but hitherto, the mechanism by which these nanoparticles induce microbial death is poorly understood [116]. Rather, most studies have focused on the alteration of enzyme activities that depend on coenzyme-A [117], hydroxyl radicals-induced DNA damage [118], and the popular oxidative attack by nano-TiO_2 on the inner and outer cell membranes of microorganisms [119, 120]. As regards antibacterial coatings, high density of nano-TiO_2 on the surface enhances the generation of reactive oxygen species (ROS) with resultant increase in antibacterial efficacy [121]. Notwithstanding, several other antimicrobial applications based on the generation of ROS as a mechanism of action

have been documented [115, 122]. These include disinfectants or biocides such as potassium permanganate, ozone, hydrogen peroxide, pancreatic acid, etc. [123]. Some researchers have incorporated these biocides into the nanocomposites of polymers, thereby generating vast antimicrobial materials with wide range of applications such as in biomedicine, packaging, etc. [116, 124–128]. Unfortunately, kinetic and thermodynamic barriers reduce the dispersal of such inorganic (often hydrophilic) nanoparticles (NPs) in the matrices of hydrophobic polymers, thereby posing serious challenges to the development of such materials [116]. However, other approaches that are seemingly more targeted can be considered in order to enhance the generation of ROS, such as the photodynamic inactivation (PDI). A typical PDI entails the excitation of photosensitizer dyes to the long-lived triplet states that then undergo some reactions involving energy transfers to either produce singlet oxygen or the hydroxyl radicals [129, 130]. PDI has therefore been applied with photosensitizers in solution or heterogeneous dyes, wherein the dyes are conjugated to polymer films or other solid supports [131, 132]. For instance, PDI was exploited using the common photosensitizer (methylene blue) that was excited at 660 nm (red light) and potentiated with an inorganic nontoxic salt (potassium iodide) [133]. This gave rise to an increase in the killing of Gram-positive and Gram-negative bacteria by 2-logs. However, a recent report has demonstrated that the antimicrobial photocatalysis of TiO_2 nanoparticles could be potentiated with sodium iodide with a resultant 3-log increase in antimicrobial efficacy [134].

In the light of these, an investigation into the inhibition effectiveness of TiO_2 nanoparticles in combination with active antibiotics of the cell wall (cefotaxime and cefazidime) against *P. aeruginosa* (a multidrug resistant strain) was carried out [19]. The *P. aeruginosa* was isolated from endo-tracheal tract, sputum, pus, and bronchoalveolar lavage. It was observed that upon exposure to UV light for one hour, the TiO_2 nanoparticles demonstrated antimicrobial effect on the nosocomial pathogen at nanoparticle concentrations of 350 mg/ml and higher. Additionally, a 6-log increase in minimum inhibitory concentration values was generated for the cefotaxime against cefazidime.

In a related study, the photocatalytic effect of low-dose UV light-activated TiO_2 nanoparticles on the genome/proteome-wide expression of *P. aeruginosa* was investigated two minutes post treatment [116]. They analyzed and quantified the radical species released from *P. aeruginosa* biofilms and estimated the contribution of such radicals in the damage and ultimate death of cells. It was observed that the photocatalytic action of the TiO_2 nanoparticles triggered a decline in the expression of a large collection of genes/proteins responsible for growth and signaling functions in parallel with the subsequent impacts on coenzyme-independent respiration, cell wall structure, and ion homeostasis. It was also observed that the nano-TiO_2-mediated biocidal action or those of other photoactive nanoparticles were counteracted by the cells as the cells triggered numerous regulatory responses with no significant metabolic function loss within the time scale of the experiment. They also established clear-cut indications of nano-TiO_2 selective catalysis in distinct cell-critical systems. These researchers therefore proposed the combination of biological and chemical methods to tackle the present limitations in understanding the link

between microorganism transport and metabolic properties, and nano-TiO_2 photo-induced biocidal efficacy. This would also benefit the proper definition of the nature of photocatalyzed reactions, the cells that take part in the response, and the degree at which nano-TiO_2 biocidal action could be reversed.

The antimicrobial effect of TiO_2 nanoparticles on another drug-resistant nosocomial pathogen (methicillin-resistant *Staphylococcus aureus*, denoted as MRSA) was demonstrated in a study by Jesline et al. [106]. The MRSA was described as a major nosocomial pathogen linked to an array of infections such as the catheter-related and surgical site infections, bacteremia, soft tissue and skin infection, and pneumonia. They attributed the main contributory factor for pathogen resistance of antibiotics to the formation of biofilms. Additionally, the strong resistance to drugs by MRSA was described by their formation of extracellular polymeric substances consisting of nucleic acids, lipids, and polysaccharides. Importantly, a sessile bacteria that is embedded in an extracellular polymeric substance is capable of withstanding the immune responses from the host and as such becomes less accessible by antibiotics as such drugs experience difficulties in penetrating the biofilm. These researchers monitored the production of biofilms by the MRSA using the culture plate method and thus reported that UV-mediated treatment with TiO_2 nanoparticles significantly suppressed the production of these biofilms. An earlier report also explains that the ability of TiO_2 nanoparticles to decompose organic compounds lies on their constant release of superoxide ions and hydroxyl radicals that is efficient for inhibiting MRSA growth [135]. Furthermore, Chorianopoulos et al. investigated the photocatalytic effect of TiO_2 nanoparticles on the production of biofilms by the *Listeria monocytogenes* bacteria [136]. In that study, various TiO_2 nanoparticles were deposited on stainless steel and glass surfaces in a doctor-blade strategy. These surfaces were irradiated with UV light after the formation of the biofilms. They observed a fast log reduction of the biofilm attributable to the presence of the UV-activated nanoparticles, compared with the control test.

It has also been demonstrated that the addition of an inorganic salt (potassium iodide) significantly increased the photocatalytic effect of TiO_2 nanoparticles on fungi and Gram-positive and Gram-negative bacteria by approximately six logs [115]. The antimicrobial effect was dependent on the intensity of the applied UV light, and the concentrations of the potassium iodide and TiO_2 nanoparticles. They established that the most effective potassium iodide concentration for the enhanced antimicrobial effect was 100 mM. They observed that in the reaction mixture, there was a generation of long-lived antimicrobial species that may probably be iodine and hypoiodite, but more killing was produced by short-lived antibacterial reactive species. Strategically, the iodide quenched the fluorescent probes for singlet oxygen and the hydroxyl radicals. The TiO_2–UV–potassium iodide produced a tri-iodide (whose peak was observed at 350 nm and formed blue compound with starch) but was intensively decreased when the MRSA cells were present.

Nano-TiO_2 has also been used to kill a broad spectrum of bacteria including *Escherichia coli*, *S. aureus*, *Bacteroides fragilis, P. aeruginosa*, and *Enterococcus hirae*, in a study on orthopedic implants infections [137]. In the clinic, the

metal pins used for the application of external fixation devices or skeletal tractions to manage orthopedic fractures are highly susceptible to pin site infections [138]. These fractures most times are associated with bone and wound infections [139]. The high adaptability of bacteria enabling their colonization on damaged tissue cells or "inert" biomaterials surfaces remain the most critical complication in the external fixation strategy for the management of pin tract infection [140]. Notably, the stability of pin–bone interfaces is reduced by the pin tract infection, while an unstable pin–bone-fixator construct may cause half-pin loosening and pin site infections [137]. The colonization of external fixators with bacteria such as *Staphylococcus epidermidis* and *S. aureus* was reported in an earlier study by Collinge et al. [141]. In developed countries, antibiotics are routinely administered to ameliorate these infections, while other common practices include surgical debridement, stabilization, and irrigation, when indicated [138]. Due to the widespread use of antibiotics and the buildup of drug resistance in bacteria, the need to develop alternative means for sterilization cannot be overemphasized. Moreover, the conventional sterilization strategy of wiping is not effective at the long run, time and staff intensive, and cannot be standardized, coupled with the challenges associated with using aggressive chemicals for such practice [142]. For this reason, Tsuang et al. demonstrated that the coating of an orthopedic implant with TiO_2 nanoparticles could reduce bacteria-related colonization of such implants and the associated infections [137]. They observed that almost all the tested bacteria were killed following 50 minutes of UV irradiation of the TiO_2 nanoparticles. Additionally, a decrease in the formation of bacterial colonies on top of the nano-TiO_2-coated metal plates. It was also established that the photokilling of the bacteria followed a two-step decay kinetics, wherein a relatively lower rate was followed by a higher one. However, this was contrary to earlier photokilling kinetic reports that were described by pseudo-first-order reactions [143, 144].

1.4.2 Nanomedicine

Exploiting the optical properties of TiO_2 nanoparticles, some researchers have applied same for *in vitro* and *in vivo* cancer PTT [14, 15]. A recent strategic research demonstrated the use of hydrogenated TiO_2 nanoparticles in cancer PTT, wherein the photothermal ability of the nanoparticles was attributed to their dramatically improved non-radiative recombination [14]. They employed black TiO_2 nanoparticles for the PTT of cancer cells owing to the limitations of white TiO_2 nanoparticles as regards the mutagenicity and shallow penetration of UV light. The hydrogenated TiO_2 nanoparticles were coated with polyethylene glycol (PEG) and were observed to possess good biocompatibility and low toxicity, low cost and simple preparation strategy, and excellent near-infrared (NIR) effect. A better cancer PTT ability triggered by NIR of the hydrogenated TiO_2 nanoparticles was observed as against photodynamic therapy (PDT) of TiO_2 nanoparticles induced by UV light.

In a related study, an NIR-triggered multifunctional nanoplatform comprised of black TiO_2 nanoparticles was successfully and rationally constructed for an effective cancer theranostics [15]. These PEGylated nanoparticles demonstrated

fascinating hemo/histocompatibility, wide absorption range, and high stability and dispersity in aqueous solution. Irradiated by a single NIR laser, these novel multifunctional nanoparticles showed high PDT/PTT synergistic cancer therapeutic efficacy under photoacoustic/infrared thermal imaging. Notably, the obstacles associated with the use of high laser power density, UV light, multi-component nanocomposites, and combination cancer therapy were circumvented by the use of these synthesized novel multifunctional theranostic nanoparticles. Furthermore, these novel multifunctional nanoparticles demonstrated negligible side effects to main tissues and blood in three months of investigation.

The potential of nano-sized TiO_2 as photosensitizers for PDT have indeed been extensively investigated in the last few decades [2, 13, 62]. To this end, photosensitizers based on TiO_2 nanoparticles for cancer PDT were prepared by incorporating zinc phthalocyanine (ZnPc) into the porous networks of the TiO_2 nanoparticles as reported in a study by Lopez et al. [62]. These photosensitizers demonstrated negligible cytotoxicity following the 3-(4,5-dimethylthiazol-2-yl)-2,5-diphenyltetrazolium bromide (MTT) assay on four mammalian cell lines and parasites, namely, human hepatocellular liver carcinoma cells, human-derived fibroblasts, human acute monocytic leukemia cell line, and the African green monkey epithelial cells. The mechanism for cell necrosis following the PDT was determined by the preferential localization of the photosensitizers in target organelles such as lysosomes or mitochondria. Without an external impetus, TiO_2 nanoparticles are excited by UV wavelengths in the region of 320–400 nm, which are harmful to the human body due to the fact that hemoglobin, melanin, and proteins are also excited in this UV range [2]. Taking cognizance of this, Lopez et al. demonstrated that incorporating the ZnPc increases the useful wavelength of the TiO_2 nanoparticles to the visible region, wherein an intercomponent electron transfer is achieved in the molecular semiconductor–semiconductor oxide of the couple [62].

Similarly, ZnPc-integrated TiO_2 nanoparticles have also been synthesized for *in vitro* cancer PDT [145]. It was observed that the toxicity of ZnPc was reduced by the TiO_2 nanoparticles, while the ZnPc–TiO_2 nanoparticles demonstrated good PDT potential when tested differently with human healthy lung cell lines (WI38), hepatocellular carcinoma (HepG2), and colorectal adenocarcinoma tumor (HT29). The ZnPc–TiO_2 nanoparticles were further labeled with ^{131}I radionuclide and it was observed that the ^{131}I–ZnPc–TiO_2 nanoparticles demonstrated good potential for nuclear imaging. Recently, Yurt et al. synthesized Subphthalocyanine (SubPc)-integrated TiO_2 nanoparticles that were also labelled with the ^{131}I radionuclide (denoted as^{131}I–SubPc–TiO_2) [146]. When treated differently with WI38, HepG2, and HT29, these nanoparticles also demonstrated good potential as nuclear imaging and PDT agents.

Upconversion TiO_2 nanoparticles have also been synthesized and applied in the PDT of cancer [147–149]. The upconversion nanoparticles (UCNPs) of $NaYF_4$:Yb^{3+} and Tm^{3+}@$NaGdF_4$:Yb^{3+} were used for the synthesis of UCNP@TiO_2 nanoparticles for the NIR-induced photoactivation of the TiO_2 nanoparticles. The UCNP@TiO_2 nanoparticles generated ROS-induced apoptosis of tumor cells by reducing the mitochondrial membrane potential,

subsequently releasing cytochrome C for the activation of caspase-3. To mitigate the multidrug resistance of breast cancer cells, UCNPs of $NaYF_4$:Yb/Tm-TiO_2 as inorganic photosensitizers loaded with an anticancer drug doxorubicin (DOX) were successfully synthesized and applied for the NIR-induced PDT of breast cancer [149]. By exploiting the upconversion luminescence ability of the $NaYF_4$:Yb/Tm that converts NIR radiation to UV light, the TiO_2 could then generate sufficient ROS for effective PDT with observed low photo-damage and deep penetration. The cellular uptake of these nanoprobes was enhanced by their folic acid functionalization, enabling the accelerated release of DOX in the drug resistant MCF-7/ADR and MCF-7 cells.

Recently, TiO_2 nanoparticles were grafted into and outside UCNP@mesoporous silica (UCNP@$mSiO_2$) nanovehicle [148]. Furthermore, a UV-cleavable derivative linker of *o*-nitrobenzene (TC linker) was employed as a "gate" for the encapsulation of DOX inside the $mSiO_2$. It was reported that upon NIR irradiation, the emitted UV light excited the TiO_2 to afford ROS, caused the photodegradation of the TC linker and also enhanced DOX release for a synergistic PDT and chemotherapy.

Furthermore, TiO_2 nanoparticles have also been applied as drug carriers for cancer chemotherapy. In this regard, the surfaces of TiO_2 nanoparticles were functionalized by phosphate, sulfate, and amine groups in a sol–gel synthetic strategy with titanium butoxide [63]. These functionalized TiO_2 nanoparticles were further loaded with copper complexes to obtain potential drug delivery systems with average sizes of 4–10 nm. Interestingly, the morphology of the functionalized TiO_2 nanoparticles and the structures of the copper complexes remained unchanged after the drug loading. Additionally, cell viability tests using these nanoparticles showed not less than a 90% survival for all the cell lines tested. In another study, the porosity of TiO_2 nanowhiskers (Ws) were exploited for the loading of the anticancer drug daunorubicin (DNR) [150]. These TiO_2 Ws demonstrated good biocompatibility and enhanced photocatalytic ability. On irradiation with UV light, efficient PDT was observed on hepatic carcinoma cells (SMMC-7721) as there was an increase in the intracellular concentration of the DNR that obviously increased its anti-tumor efficacy as shown in Figure 1.6. Moreover, the excellent drug delivery capacity of the TiO_2Ws has been linked to their large surface area and reactivity [2].

Nanoparticles of TiO_2 have also been investigated for their application in sonodynamic cancer therapy as a result of the deep penetration capacity of ultrasound radiation enabling the targeting of deep-seated tumors and other diseases [151]. Prior to the emergence of TiO_2-based sonosensitizers for sonodynamic therapy, most sonosensitizers used for generating ROS on ultrasonic activation were organic compounds such as 5-aminolevulinic acid, phthalocyanines, porphyrin, etc. [152, 153]. To investigate the utility of TiO_2 nanoparticles for sonodynamic therapy, Shen et al. synthesized TiO_2-encapsulated Fe_3O_4 nanoparticles, denoted as TiO_2@Fe_3O_4 [151]. The TiO_2 nanoparticles were employed as both sonosensitizers and as carriers for the loading of DOX. It was observed that the core–shell TiO_2@Fe_3O_4 nanoparticles demonstrated a pH-dependent loading of DOX and its subsequent release to MCF-7 and subline of the ubiquitous keratin-forming tumor (KB) cells. Additionally, ROS were efficiently generated by the

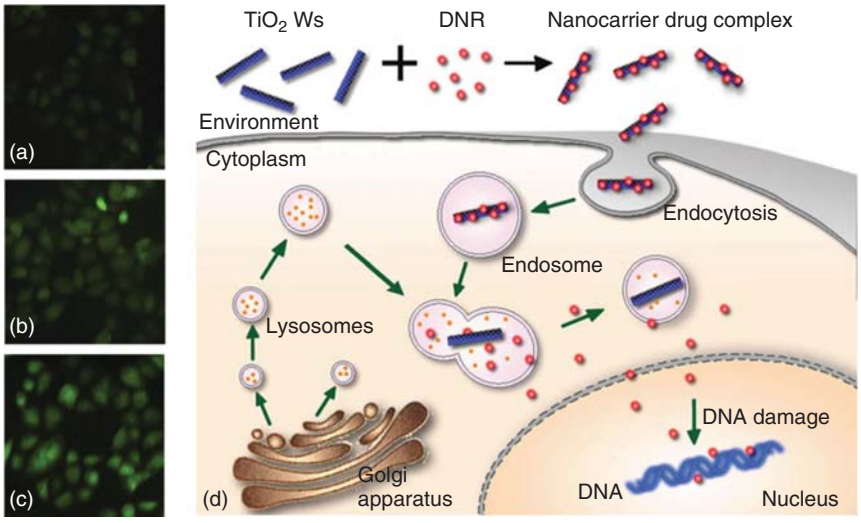

Figure 1.6 Fluorescence microscopic images of the SMMC-7721 cancer cells that were treated with DNR (a), DNR–TiO_2 nanoparticles (b), and DNR–TiO_2Ws (c). (d) Illustration of the possible mechanism for the cellular uptake of TiO_2Ws in the SMMC-7721 cancer cells. Source: Adapted with permission from Li et al. 2009 [150]. Copyright Elsevier Limited.

TiO_2@Fe_3O_4 nanoparticles upon ultrasound irradiation. Owing to the enhanced accumulation of the core–shell nanoparticles in the tumor region and the long-time retention effect, a combinational sonodynamic and chemotherapeutic outcome was observed, with minimal side effects. To illustrate this, they reported that the combination therapy showed an 88.36% inhibitory effect as against 38.91% and 28.36% for sonodynamic therapy and chemotherapy, respectively.

In another study, TiO_2–PEG nanoparticles were successfully synthesized and also applied as sonosensitizers in a combination of photodynamic (PD) and sonodynamic therapies [154]. Upon irradiation of the nanoparticles with 5.0 mW/cm^2 laser, the nanoparticles demonstrated an effective reduction in the viability and membrane integrity of human glioblastoma cells U251. The generation of singlet oxygen alongside other ROS after sonoactivation was utilized for sonodynamic therapy using core–shell TiO_2–polyallylamine micelle nanoparticles in a study by Harada et al. [155]. Their findings are very important and capable of revolutionizing imaging-guided sonodynamic therapy for diseases such as the neoplastic maladies.

In combination with other macromolecules and nanomaterials, nano-sized TiO_2 has been used for the synergistic theranostics of certain diseases [13, 151, 156, 157]. To this end, Zeng et al. synthesized TiO_2–Fe_3O_4 nanocomposites and applied same for the theranostics of neoplastic disease [13]. The TiO_2 nanoparticles in the nanocomposites served as excellent photosensitizers for PDT, while the Fe_3O_4 provided contrast enhancement for MRI. In another experiment, TiO_2 nanoparticles were used in combination with another photosensitizer chlorine e6 to obtain a synergistically enhanced PDT, contrary to those obtained from the individual photosensitizers [156].

Undoubtedly, medical implants have dramatically revolutionized orthopedic surgeries, particularly the endoprosthetics. However, the liberal application of cardiovascular stents and orthopedic implants have been hindered by autoimmune reactions [2]. To this end, Ti and its alloys, especially TiO_2-based nanoparticles have been reported as effective surface coatings for orthopedic implants to mitigate these reactions [158]. Additionally, there are suggestions that TiO_2-based nanoparticles provide safe tissue-recognition scaffolds in endoprosthetic surgeries [159]. To elaborate this, TiO_2 nanotubes were synthesized and used to ameliorate acetabulum hip joint or tibia-tarsal joint fractures in prosthetic articular surgery [160]. The utility of TiO_2 nanotubes in enhancing osteoblast adhesion *in vitro*, strong bone adhesion *in vivo*, and bone mineralization has also been documented [161]. In a pull-out testing after a four-week implantation of TiO_2 nanotubes in rabbit tibias, it was demonstrated that up to a ninefold increase in bone-bonding strength was obtained against the use of TiO_2 grit-blasted surfaces.

1.4.3 Wastewater Treatment

Drinkable and clean water that is free of carcinogenic substances, harmful bacteria, and toxic chemicals is crucial for human health [97]. According to the 2018 World Water Development Report of the United Nations, the past decade has witnessed a 1% yearly rise in global water demand, and it is expected that in 2050, the demand for clean water will increase by about one-third of its present state [162]. Importantly, the high demand for clean water is also increased as a result of its crucial role in industrial processes such as in the production of electronic devices, pharmaceuticals, paints, foods, and other beverages [163–166]. To meet this ever-increasing demand for quality water supply, numerous efforts are made to reclaim wastewaters both from households and industries. Advances in nanotechnology and nanoengineering have demonstrated good promise in achieving marked improvements in the quality of water, aided by nanosorbents [167], nanocatalysts [168], nanoparticle-enhanced filtration [169], and bioactive nanomaterials [170]. Owing to the fact that remarkable changes in the physical and chemical properties and enhancements in the surface-to-volume ratios (increase in surface reactivity) of materials are obtained when they are prepared in nanoscales (1–100 nm), nanotechnology-based materials that reduce the amounts of toxic substances to low levels could appreciably contribute to achieving good standards for water quality and decrease adverse health challenges [171–173]. Various photocatalytic nanomaterials have been investigated in the past decade for their water treatment abilities. These include the nanorods and nanoparticles of zinc oxide [174, 175], nanocubes of silver chloride [176, 177], quantum dots and nanoparticles of bismuth vanadate [178], and cadmium sulfide [179, 180].

In recent times, environmental purification with TiO_2 nanoparticles as a photocatalyst has attracted great attention due to their chemical stability, low pollutant loading, low toxicity, self-cleaning ability, hydrophilicity, and availability at low cost [97]. Specifically, wastewater treatment with TiO_2 nanoparticles has been demonstrated as an effective technique for degrading organic contaminants by

photocatalysis [181]. The pH of the solution has been reported as a crucial parameter in the photocatalytic degradation reactions that take place on the surfaces of the nanoparticles, as it controls the surface charge properties and size of the aggregates formed by the photocatalyst [44, 181]. In this regard, Nasikhudin et al. evaluated the efficacy of TiO_2 nanoparticles for the photodegradation of methylene blue at different pH conditions [44]. They reported that the TiO_2 nanoparticles have the anatase structure with average size of 27 nm. On exposure to UV light, 97% of the methylene blue dye was photodegraded in three hours, while a 15% photodegradation was observed without UV illumination at same time. They attributed the 15% degradation to mere adsorption of methylene blue by the TiO_2, rather than photocatalytic degradation. They also observed that the specific degradation of the methylene blue in acidic (pH 4.1), neutral (pH 7.0), and basic media (pH 9.7) were 40%, 90%, and 97%, respectively, suggesting that a better photodegradation of the organic pollutant occurs in alkaline medium. This was attributed to the abundant hydroxyl groups in basic medium that can react directly with a hole in the TiO_2 nanoparticles, thereby generating -OH radicals.

The effects of varying the precursors and conditions in the sol–gel synthesis of on the photocatalytic activity of TiO_2 nanoparticles for the removal of an organic pollutant was investigated in a study by Behnajady et al. [182]. Particularly, these researchers varied the solvent percent, reflux time and temperature, sol drying method, calcination temperature, and water percent. The organic pollutant (C.I. Acid Red 27) was used as a model textile industry contaminant whose photodegradation was monitored under the irradiation with a UV-C light. These researchers established that the photo-induced degradation of the C.I. Acid Red 27 by the TiO_2 nanoparticles was a function of solvent type, precursor type, and other conditions of the synthesis process. In comparison to the commercial TiO_2 P25, the TiO_2 nanoparticles that were synthesized with titanium (IV) isopropoxide as precursor, methanol as the reflux solvent for three hours at 80 °C, coupled with appropriate thermal drying of the sol, and calcination at 450 °C demonstrated approximately same photocatalytic activity.

Several constraints have limited the utility of nano-TiO_2 for large-scale water treatment: (i) its large band gap (3.2 eV for the anatase phase) limiting its light absorption at the UV region, wherein a small range (3–5%) of the solar spectrum can be used for the activation of the nanoparticles, (ii) the quick e^-/h^+ recombination that occur during the TiO_2 photocatalysis, and (iii) the occurrence of TiO_2 nanoparticles in slurry form during the treatment process, making it particularly difficult to recover and recycle the nanoparticles [183].

Interestingly, recent studies have also shown that embedding an Fe_3O_4 core can improve the magnetic separation of TiO_2 nanoparticles due to the fact that the Fe_3O_4 itself is superparamagnetic at particle sizes less than 20 nm [97, 184–186]. It is worthy of note that this strategy has been employed in numerous studies for the treatment of water and wastewater [187–190]. For instance, Chen and coworkers synthesized Fe_3O_4@TiO_2 nanospheres and tested same for the photodegradation of Rhodamine B (RhB). The nanospheres demonstrated high crystallinity degree and excellent magnetic properties that enabled the recovery of the nanospheres by magnetization. Following UV irradiation of the nanospheres, the intensity of the absorption maximum of RhB at 552 nm decreased with time.

They observed that the UV-induced degradation of the RhB was initially fast and later became slow. Additionally, the Fe_3O_4@TiO_2 nanospheres could not degrade RhB in the dark, confirming that the degradation process was photo-induced. The degradation of RhB was also observed to be very slow in the absence of the photocatalyst. Taken together, the 95% degradation of the RhB dye in 60 minutes recorded with the nanospheres was superior to the 55% degradation recorded with a commercial photocatalyst (P25), thus confirming the excellent synergy between the Fe_3O_4 and TiO_2nanoparticles.

Other researchers have also proposed other strategies to improve the photocatalytic ability of TiO_2 nanoparticles including surface sensitization, inclusion of an inert support, incorporation of metal ion or noble metals, transition and non-metals doping, and synthesizing nanocomposites of other nanomaterials with TiO_2 nanoparticles [183, 191]. For instance, Li et al. reported that TiO_2 nanoparticles can be doped with SiO_2 or alumina to improve its photocatalytic performance, surface area, and/or thermal stability [192]. Nano-TiO_2 can also be anchored onto carbon-based materials including carbon nanotubes (CNTs) [193–195], graphene [196–198], and carbon nanofibers [199], to obtain nanohybrids with improved photocatalytic abilities for wastewater treatment. Carbon-based materials offer suitable anchors for TiO_2 due to their fascinating chemical resistance [200], mechanical [201], thermal [202], electrical [203–205], and optical properties [206, 207], coupled with the fabrication of structures with optimized pore and surface properties [208–210], giving rise to fast charge transfer on the TiO_2/carbon hybrid composites [211, 212]. Carbon-based TiO_2 nanoparticles are not only used for the treatment of wastewater but have also been applied for the production of hydrogen by the photocatalytic water splitting [213–215], antibiotic photocatalyst [216], and photodegradation of biological pollutants [217, 218]. In particular, CNTs and graphene show potential for contributing to the enhancement of the photo-induced activities of TiO_2 nanoparticles, owing to their large surface area, decrease of electron/hole recombination, tuning band gap for visible light catalysis, and excellent active sites [219].

Some mechanisms have been proposed for the photocatalytic behavior of TiO_2/CNTs: first, the nanotubes may behave as photosensitizers by facilitating electron transfers to the surfaces of the TiO_2 nanoparticles, which might be responsible for effectively extending the photocatalytic activity of the TiO_2 to the visible light region [220, 221]. Second, the CNTs can assume the role of an effective electron sink, which is typical of p-type semiconductors [222], and also create a form of Schottky barrier (a space-charge region) at the interface of the TiO_2/CNTs. Irrespective of the fact that TiO_2 exhibits the behavior of typical n-type semiconductors, CNTs cause the movement of photo-induced electrons in the TiO_2 to freely migrate toward the direction of the CNTs, which may possess a lower Fermi level that can be likened to that of a metal [219]. Additionally, some other researchers have proposed a range of hypothesis for the TiO_2/CNTs photocatalytic mechanism [218, 223]. Application of TiO_2/nanocarbon composites in advanced oxidation processes for wastewater treatment may show good self-purification effects in comparison with ozonation and UV light irradiation. On an industrial scale, the nanocomposites are

expected to demonstrate effective wastewater treatment in advanced oxidation technologies due to the ability of the nanocarbon materials to form tight support to immobilize the TiO_2 nanoparticles, thereby inhibiting the nanoparticles loss as the fluid stream flows [224, 225].

In a study by Matsunaga and Inagaki, carbon-coated TiO_2 nanoparticles were synthesized and applied for the photodegradation of methylene blue [226]. Specifically, they mix the powders of anatase TiO_2 and poly(vinyl alcohol) in a 90/10 mass ratio and heated same at various temperatures (500, 600, 700, 800, 900, and 1000 °C) for one hour. They measured the carbon contents in the nanoparticles following combustion of same in air at 800 °C. They observed that the anatase phase of the TiO_2 remained stable up to 700 °C after carbon coating with a slight improvement in crystallinity, while carbon content was 5% by mass. Heat treatment above 800 °C commenced the phase transformation from the anatase to rutile phase with carbon content of 3.6% by mass. A complete phase transformation to the rutile phase was observed at 900 °C heat treatment. At this temperature, the rutile phase was observed to react with the coated carbon, giving rise to a reduced TiO_2 phase identified as Ti_9O_{17} following the X-ray diffraction analysis. The heat treatment up to 1000 °C was dominated by the Ti_9O_{17} with a small carbon content of 1.4 wt%. The methylene blue photodegradation at room temperature and concentration of 1.4×10^5 mol/l under 1 mW/cm^2 UV irradiation was best observed with the carbon-coated TiO_2 nanoparticles after 800 °C heat treatment. They also observed a reduction in the photodegradation rate constant for the methylene blue at temperatures higher than 800 °C, attributed to the dominance of the reduced TiO_2 phase (Ti_9O_{17}). In another study, chitosan–TiO_2 nanocomposite fibers were synthesized and applied for the degradation of organic contaminants in wastewater [227]. Various TiO_2 loadings (1, 5, 10,15, and 20 wt%) were used to understand the effect of varying the concentration of TiO_2 on the photocatalytic property of the nanocomposite fibers. The researchers separately kept each chitosan–TiO_2 nanocomposite fibers formulation in each salt solution of $CuSO_4$, $NiSO_4$, $AgNO_3$, and $CoNO_3$ and observed that the metal ions of the salts (Cu^{2+}, Ni^+, Ag^+, and Co^{2+} ions) were loaded onto the nanocomposite fibers. This led to the reduction of these ions to their corresponding zero-valent metal nanoparticles (ZV-MNPs) such as Cu^0, Ni^0, Ag^0, and Co^0, following a $NaBH_4$ treatment. The ZV-MNPs-templated chitosan–TiO_2 fibers were then applied for the photo-induced degradation of some organic dyestuffs (methyl orange, methylene blue, acridine orange, and congo red) and nitrophenols including 2-nitrophenol, 3-nitrophenol, 4-nitrophenol, and 2,6-dinitrophenol. Among all the tested ZV-MNPs-templated chitosan–TiO_2 fibers, Cu^0 ZV-MNP with 15 wt% TiO_2 demonstrated the highest photocatalytic efficiency for the degradation of the organic dyes and nitrophenols. Moreover, the Cu^0 ZV-MNP-templated fibers could easily be recovered from solution after the photodegradation process by a simple pull-out of the fiber from the medium.

Furthermore, chitosan–TiO_2 nanoparticles were modified with tungstophosphoric acid (TPA) and investigated for their photobleaching activity on an organic dyestuff malachite green in a study by Rengifo-Herrera et al. [228]. Various TPA/TiO_2 to chitosan ratios (10%, 20%, 30%, and 40% w/w) were

employed in the study to determine the effect of varying the ratios on the photobleaching capacity of the photocatalysts. They observed an effective dispersion of the TPA/TiO_2 nanoparticles through the films of the chitosan by scanning electron microscopy that was coupled with energy dispersive X-ray spectroscopy. Additionally, weak interactions between the TPA/TiO_2 nanoparticles and the functional groups on the chitosan by Fourier transform infrared spectroscopy. With respect to the photobleaching of malachite green, the chitosan-TPA/TiO_2 nanoparticles with 30% w/w ratio demonstrated the highest photocatalytic activity upon exposure to UV-A and visible light. The photocatalytic effect observed with this formulation (30% w/w ratio) was higher than that recorded for chitosan films with same amount of the commercial Evonik P25. Particularly, the 30% w/w ratio formulation exhibited an excellent photobleaching performance at irradiation wavelengths above 450 nm that was accompanied by a slight fading of the color of malachite green at wavelengths above 590 nm. After five reuse cycles, the 30% w/w ratio formulation also demonstrated impressive stability and malachite green photobleaching. Notably, as a result of *N*-demethylation oxidative reactions, a hypsochromic shift was observed for the wavelength of maximum absorption for the malachite green. These researchers therefore established that the TPA–modified chitosan–TiO_2 nanoparticles could induce a solid–gas interface photobleaching of malachite green by an oxidative path, following photosensitized and photocatalytic routes.

As rapid industrialization in various countries has expanded the application of numerous synthetic dyestuffs in industrial processes to meet the ever-increasing consumer product demand. Wastewater containing industrial dye stuffs has been reported to be highly refractory due to its high concentration of organic compounds and salts, making it less biodegradable in the environment [229, 230]. In order to save the natural environment and reduce the bioaccumulation of these synthetic dyestuffs, the direct discharge of industrial wastewater to local water treatment plants or environmental waterways should be discouraged [231, 232]. Rather, the on-site pre-treatment of these industrial effluents to ensure that most of the toxic parent synthetic azo-compounds and their intermediates or derivatives are appreciably reduced before discharging same to waterways or local water treatment plants [233]. It has been pointed out in a study by Chong et al. that the main challenges for the application of photocatalytic nanoparticles in advanced industrial dye treatment are to improve the separation and ultimately recover the used photocatalysts as to prevent same from entering the environment [70]. To this end, these researchers synthesized a functional form of TiO_2–zeolite nanocomposites by a modified sol–gel method with titanium IV butoxide as the precursor and applied the nanocomposites for the enhanced treatment of industrial dye-contaminated water and the recovery of the nanocomposites after treatment. They observed that the nanocomposites-enhanced removal of the industrial dye (reactive black 5 dye) followed a pseudo-first-order reaction with a rate constant of 0.042 per minute at low concentration of the dye. This indicated that the TiO_2–zeolite nanocomposites followed an adsorption-oriented industrial dye removal by photocatalytic degradation that could benefit the removal of untreated and trace dye stuffs at the treatment stage of industrial dye wastewater.

Furthermore, it was reported that sustainable and effective treatment of the wastewater from hospitals is often challenging to environmental and wastewater engineers worldwide [234, 235]. This is because such wastewater usually contains pharmaceutical, radioactive, and chemical substances, alongside numerous pathogenic microorganisms [236, 237]. The dominance of pharmaceutical and radioactive compounds in the environment that resulted in the contamination of drinking, surface, and ground waters has been documented in the literature [238–240]. In this regard, the assessment of TiO_2 nanofibers for the treatment and biodegradability enhancement of a pharmaceutical compound (carbamazepine) in a hospital wastewater mimic was conducted in a study by Chong and Jin [56]. The hospital wastewater mimic was prepared by dissolving 5000 µg/l of the carbamazepine in municipal wastewater obtained from a water treatment facility in South Australia, while the TiO_2 nanofibers were synthesized by the hydrothermal method in NaOH, followed by an ion exchange post-synthesis in HCl. They observed that the TiO_2 nanofibers removed 78% of the carbamazepine, 23% phosphate, and 40% chemical oxygen demand (COD) within four hours. Additionally, a shift in the molecular weight of the organic fractions in the synthetic hospital wastewater from >10–1000 to <10 kDa demonstrated that the photocatalytic treatment with the TiO_2 nanofibers could appreciably enhance the biodegradability of the organic compound. Moreover, the nanofibers-mediated photodegradation profile of the carbamazepine at high concentrations in the hospital wastewater mimic was better described by the Langmuir–Hinshelwood kinetics model.

1.4.4 Air Treatment

On the other hand, air pollutants such as the nitrates and sulfur dioxide have potentials for generating persistent negative effects on human and animal health. As it is with water treatment, TiO_2 nanoparticles are the most extensively studied photocatalysts for improved air purification. The photocatalysis of TiO_2 nanoparticles stands tall as one of the various efficient advanced oxidation processes for the decomposition of microbiologically and chemically stable volatile organic compounds (VOCs). Unfortunately, advances in the photocatalysis of these nanoparticles have been significantly hindered by their relatively low surface area and poor adsorption properties for organic compounds [241]. A group of researchers reported an enhancement of the removal of NO using TiO_2 nanoparticles that were coated with carbon [226]. For this purpose, they dissolved 0.03 g of the nanoparticles in acetone under a supersonic vibration. The dissolved nanoparticles were then spread on a filter paper and exposed to an NO-containing air bubbled in a distilled water column with an NO concentration of 0.6 ppm and flow rate of 3 l/min at room temperature. The nanoparticles were illuminated with UV light for 60 minutes and another 30 minutes without illumination for 10 repeated cycles. Two UV lamps with power of 19 W and 158 mm away from the nanoparticles were used for the illumination through quartz glasses whose thickness were 5 mm. Then, the NO concentration in the

gas and that of the reaction product (NO_2) were measured by chemiluminescence at one minute interval. They observed a decrease in the NO concentration in the effluent gas within one minute of UV irradiation. Turning off the UV lamp resulted in a return of the NO concentration to its initial concentration, also within one minute. Additionally, high decomposition of NO, i.e. high photoactivity, was recorded with the carbon-coated TiO_2 nanoparticles calcined at 500 and 600 °C as against those calcined at temperatures between 700 and 1000 °C. This was attributed to the high abundance of anatase TiO_2 obtained at calcination temperatures of 500 and 600 °C, whereas the rutile phase was prominent above those temperatures, i.e. between 700 and 1000 °C. Moreover, a larger decomposition fraction value was observed in the first cycle, followed by a near-constant decomposition from the second cycle onward.

For the purpose of exploiting the high photocatalytic ability of TiO_2 nanoparticles, numerous reactor designs have been developed and tested, including honeycomb [242], carberry type [243], fluidized bed [244], and the multi-tubular type [245]. Most of these reactors employ immobilized TiO_2 on the surfaces of aluminum [243, 246], glass [247, 248], concrete [249], or carbon [250–252]. The first substrate, i.e. aluminum, is one of the most commonly used supporting materials that is mainly attributed to its ability to withstand high temperatures during the calcination process, and its high transparency. Additionally, its design ease, strength, and low price have been reported as factors that have increased the choice of aluminum substrates over others, irrespective of its seldom deactivation effect on the catalyst [253]. The deactivation effect has been attributed to its migration from the support to the catalyst with subsequent Al_2O_3 and $Al(OH)_3$ coexistence [241]. Furthermore, the application of aluminum substrate for most photocatalytic processes with TiO_2 nanoparticles has been suppressed by its sodium content, which is detrimental to TiO_2 photocatalytic property in situations whereby high temperatures are required to treat the deposited film [254, 255]. This drawback can be addressed by introducing amorphous SiO_2 layer barrier between the carrier and the TiO_2 film [256, 257] or employing the mixed film of TiO_2/SiO_2 [258, 259].

In this regard, Šuligoj et al. immobilized TiO_2 nanoparticles on porous SiO_2 substrate and investigated its air-cleaning effect [241]. These researchers used titania in aqueous solutions from two different sources: a TiO_2 sol that was prepared at low temperature at the University of Nova Gorica and a TiO_2 suspension obtained from a producer of TiO_2 at Slovenia, Cinkarna Celje. They also employed two different mesoporous SiO_2 types: SBA-15 that had an ordered arrangement of hexagonal pores and KIL-2 that had a disordered mesoporosity between the particles. These researchers then monitored the adsorption properties, photocatalytic activities, and structural characteristics of the catalysts that were deposited as thin films on aluminum plates. They observed higher air-cleaning and adsorption activities with the TiO_2 produced at Slovenia, Cinkarna Celje. They attributed this to the higher amount of Ti–OH groups on its surface in comparison with the TiO_2 sol prepared at the University of Nova Gorica. Moreover, the introduction of the mesoporous SiO_2 increased the adsorption and photocatalytic activities for both sources of the TiO_2 with the SBA-15 showing enhanced effect than the KIL-2.

In another study, nano-TiO_2 were conjugated with a metal–organic framework, NH_2-UiO-66 and applied for the purification of VOCs [260]. The TiO_2@NH_2-UiO-66 was synthesized by employing the hard–soft acid–base strategy with tunable TiO_2 size and content. It was observed that the TiO_2@NH_2-UiO-66 nanocomposites increased the separation of electrons and holes generated by UV illumination following an appreciable extension of optical absorption in comparison to bare TiO_2. This was also attributed to the intriguing interface contact between the NH_2-UiO-66 and TiO_2. Moreover, an effective diffusion of the VOCs into the pores of the outer NH_2-UiO-66 was enabled by their abundant 3D cavities that were interconnected. This was responsible for the observed high concentration microenvironment of the VOCs around the embedded TiO_2. A significantly enhanced photocatalysis and deactivation resistance in the course of the gaseous styrene photo-induced degradation under visible light irradiation was also observed. This was ascribed to the synergism between the NH_2-UiO-66 and TiO_2. Whereas the photodegradation efficiency for the removal of styrene achieved with bare TiO_2 was 32.5% in 600 minutes, up to a 99% removal ratio and efficient mineralization of the styrene to CO_2 was obtained with the TiO_2@NH_2-UiO-66 nanocomposites that possess 5 wt% TiO_2.

Since the promotion of an air-cleaning TiO_2-based paint (KNOxOUT) by Pacific Paints (Boysen) Philippines, Inc., which has the capacity of cleaning nitrogen oxides (NOx) from automobile emissions [261], research into the utility of TiO_2 nanoparticles for air purification has increased tremendously. Nitrogen oxides are known respiratory irritants and ground-state ozone precursors. For instance, Le et al. recently investigated the air-cleaning ability of a silver nanoparticles-coated air filter with TiO_2 nanoparticles [262]. The nano-TiO_2 with average size of 16–20 nm were prepared by the sol–gel synthetic strategy and placed on a porous quartz tube with a diameter of 74 mm, length of 418 mm, and deposit density of about 16.4 mg/cm^2. The formation of the photocatalytic filter tube by this deposition process was mediated by a poly(methylmethacrylate) layer. Additionally, they synthesized silver nanoparticles with average size of about 20 nm by the aqueous molecular solution method and coated same on a polypropylene pre-filter. They observed that a high VOCs, fungi, and bacteria degradation was obtained with four photocatalytic filter tubes, four UVA lamps operating at 36 W, an electrostatic air filter, and an air cleaner whose capacity was 250 m^3/h. Interestingly, this air-cleaning equipment demonstrated more than 99% killing of the microorganisms after passing air through it. Furthermore, the degradation of various VOCs differed with time. They observed a 43% oxidation of benzene in 150 minutes, and the removal of 80% acetone, 91.6% butanol, and 70.1% diethyl ether in 100, 55, and 120 minutes, respectively, using a 10 m^3 box. These researchers also tested the air-cleaning equipment in practical (real-life) condition at E Hospital, Hanoi, Vietnam. In an intensive care room, 69% and 63% bacteria and fungi, respectively, were killed in six hours using a 125 m^3 box.

Similarly, the sol–gel method was used by Haider et al. to prepare TiO_2 nanoparticles and also investigated same for air purification [263]. They employed a titanium trichloride precursor and calcinations at two temperatures (500 and 900 °C). At 500 °C, the nanoparticles were observed to have the

anatase structure, while a rutile structure was observed for the nanoparticles at 900 °C. Moreover, increasing the calcination temperature consequently increase crystallinity of the product. The indoor and outdoor air-cleaning abilities of the nanoparticles were investigated using glass substrates coated with the nanoparticles. The TiO_2 nanoparticles-coated films exhibited good permeability, optical activity, and a low water contact angle. The aforementioned properties are characteristic of materials applicable as self-cleaning agents. These researchers therefore inferred that the synthesized TiO_2 nanoparticles could be used as surface coating in microbiological sensitive areas such as hospitals and food factories to mitigate air pollution. Notwithstanding the various studies on the utility of TiO_2 nanoparticles for air cleaning, some researchers have reported that the mechanism for this application is still unclear [261, 264].

1.4.5 Energy Devices

The ever-increasing growth in nanoscience and nanotechnology research has showcased new chemical and physical properties of TiO_2 nanoparticles, thereby providing new avenues for developing nano-sized solar cells composed of TiO_2 [38]. In this regard, TiO_2 nanoparticles have been recently synthesized in various forms, wherein their surface areas are maximized to facilitate the interface reaction between the interacting media and the TiO_2 nanoparticles in photovoltaic devices [93]. Surface modification has proven to affect the interfacial energy offset and transport, charge separation, and the recombination processes of TiO_2 nanoparticles [7, 265]. Among the various TiO_2 nanoparticle forms, nanowhiskers have been reported to be the most suitable for the fabrication of solar cells and windscreens due to their enhanced charge transportation [2]. In order to enhance the effective collection of electrons that are injected into the TiO_2 nanoparticles, high electron mobility of the nanoparticles are greatly desired [38].

As a consequence of the exposed surface area and high surface reactivity of TiO_2, it undergoes physical and chemical transformations by its interaction with some environmental factors (sunlight, natural organic matter, ionic species, etc.) in practical applications [93]. This behavior has been attributed to aggregation process where e.g. either the hydroxyl groups on the TiO_2 surface interacts with various components in aqueous medium or pH variation during the photocatalytic process generates particle aggregation [266]. Therefore, an in-depth knowledge of the transformations of TiO_2 nanoparticles in aqueous irradiated suspensions is essential in understanding their photocatalytic behaviors. A general overview of the photocatalytic applications of TiO_2 nanoparticles is presented in Figure 1.7.

It has been reported that the major setback for the use of TiO_2 nanoparticles in semiconductor-based sensing devices is their relative humidity sensitivity, making the response of such sensors in environments with variable humidity to be unreliable [265]. The presence of the hydroxyl groups on the surfaces of these nanoparticles have been attributed to be responsible for these sensitivity variations [266]. The surface chemistry of TiO_2 nanoparticles is rather complex and highly dependent on the preparation route and the crystalline state of the

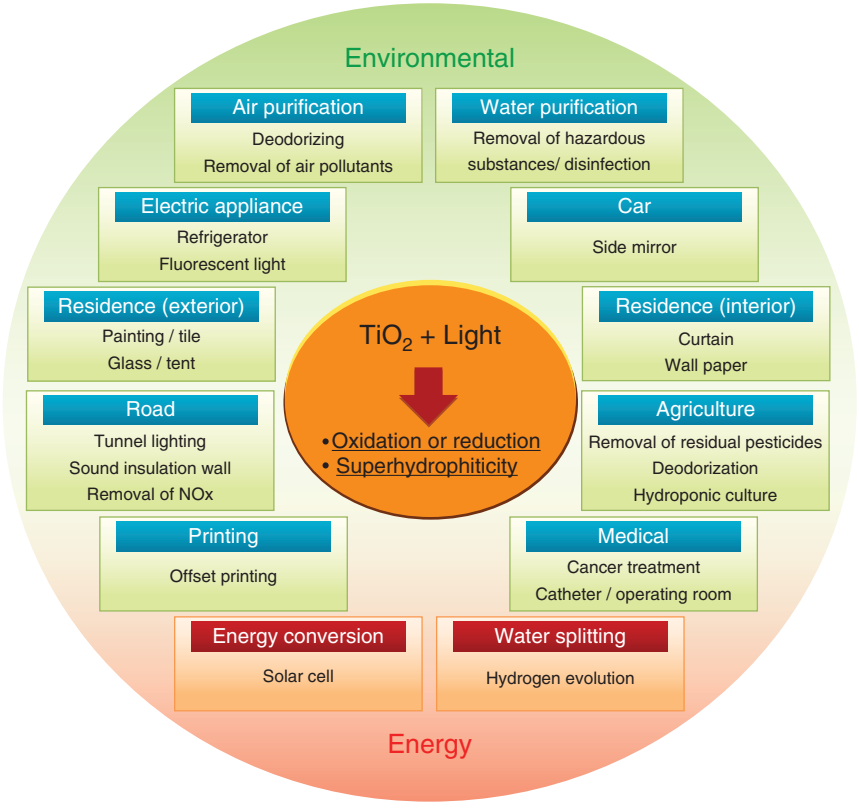

Figure 1.7 Illustration of the general photocatalytic applications of TiO_2 nanoparticles. Source: Adapted with permission from Nakata and Fujishima 2012 [36]. Copyright Elsevier Limited.

nanoparticles [267]. For the purpose of reducing the impact of these hydroxyl groups, surface modification of the TiO_2 nanoparticles were carried out by grafting with hexamethyldisilazane, thereby reducing the density of the hydroxyl groups and the cross-sensitivity of the sensor to humidity [265].

1.4.6 Water Splitting for Hydrogen Production

Chemical fuel production by the conversion of solar energy is regarded as a crucial strategy for ameliorating the present-day world energy challenges [268, 269]. Right from the early discovery of water splitting on an electrode of TiO_2 in 1972 [1], photocatalysis has attracted much interest as a promising technique for the production of environmentally friendly, clean, and low-cost hydrogen (H_2), using the solar energy [270, 271]. For an effective water splitting, titania has proven superior to other oxide semiconductor photocatalysts due to its chemical and biological inertness, environmental friendliness, long-term stability against chemical and photo-corrosion, availability, and cost effectiveness [272–275]. Owing to the fact that bare TiO_2 demonstrates relatively poor photocatalytic behavior, photocatalytic production of H_2 on TiO_2 highly depends on the

amount and nature of cocatalysts [276, 277]. This is due to the fact that TiO_2 is mainly active under UV illumination to overcome the anatase phase band gap (3.2 eV) [278] and exhibits fast e^-/h^+ recombination owing to its high trap states density [279, 280]. It then follows that appropriate band gap engineering is necessary in order to utilize TiO_2 as a semiconductor photocatalyst for enhanced H_2 production by water splitting. Earlier on, some cations such as Ag, Al, Mn, Cr, Fe, V, Sb, Nd, and Ru were employed as dopants for the effective introduction of states into the band gap of TiO_2 [281]. However, Asahi et al. reported that various issues such as enhanced centers for carrier recombination, the importance of a low-cost facility for ion-implantation, and thermal instability present obvious challenges to this technique [282]. These researchers rather suggested that nitrogen doping into the TiO_2 provides an improved avenue for band gap engineering than cationic or anionic doping. Notwithstanding, a later experimental and theoretical study raised some reservations about the suitability of the n-doping technique as the most efficient doping strategy [283]. Moreover, the reported photocatalysis of the n-doped TiO_2 for the photo-induced reduction of water to produce H_2 is relatively low [284].

In order to enhance H_2 production by water splitting with TiO_2 nanoparticles, a group of researchers added platinum (Pt) as a cocatalyst to the nanoparticles and observed an enhanced evolution of H_2 in the presence of some sacrificial reagents [37]. Unfortunately, the scarce nature and high cost of the noble metal Pt poses a challenge on the scalability of this strategy. Park et al. reported the successful synthesis of carbon-doped TiO_2 nanotubes for effective H_2 evolution [275]. The nanotubes were vertically grown and demonstrated high aspect ratios that enabled the photocleavage of water molecules in the presence of white light irradiation. They observed that the synthesized nanotube arrays also demonstrated far much higher water splitting efficiency and photocurrent density on exposure to visible light with wavelength of more than 420 nm in comparison with bare TiO_2 nanotubes. Additionally, the carbon-doped TiO_2 nanotube arrays outperformed the commercial photocatalyst (P-25) with more than 20 times higher photocurrent under visible light irradiation.

In another experiment, Chen et al. demonstrated a conceptually different strategy for the enhancement of solar absorption and its consequent utility for water splitting by black TiO_2 nanocrystals following the introduction of disorder in the nanophase surface layers by hydrogenation [89]. The TiO_2 nanocrystals were prepared with a TTIP precursor in the presence of ethanol, deionized water, an organic template Pluronic F127, and hydrochloric acid. This yielded the nanocrystals that were further calcined for six hours at 500 °C for the purpose of removing the Pluronic F127 and enhance the TiO_2 crystallization. For the purpose of introducing the disorders into the nanophase of the TiO_2, these researchers generated a porous TiO_2 nanocrystals network that was <10 nm and hydrogenated the material. The disorder-engineered nanocrystals demonstrated a shift in the absorption onset from UV to NIR region after the hydrogenation process that was accompanied by a remarkable color change. They also reported that the disorder-engineered nanocrystals showed marked photocatalytic activities such as organic compounds photo-oxidation in water and the evolution of H_2 using sacrificial donor in the presence of solar light.

Particularly, 0.2 mmol H_2 was generated by 0.02 g of the disorder-engineered black nanocrystals in one hour of solar irradiation, i.e. 10 mmol/h for every gram of the black TiO_2 photocatalyst. Notably, the production rate for H_2 reported by these researchers was higher than those of many semiconductor photocatalysts by a magnitude of about 2 orders [271, 285].

In a related experiment by Wang et al., H_2 treatment was demonstrated as an effective and facile technique to enhance the photocatalytic activity of TiO_2 nanowires for H_2 evolution by water splitting, following photoelectrochemical means [286]. These researchers annealed pristine rutile TiO_2 nanowires at different temperatures ranging from 200 to 500 °C in a H_2 atmosphere to successfully synthesize the H_2-treated rutile TiO_2 nanowires, denoted as H : TiO_2 nanowires. They observed that the H : TiO_2 nanowires demonstrated significantly improved photocurrent all through the potential window in comparison with pristine TiO_2 nanowires. More importantly, low photocurrent saturation potentials of −0.6 V versus Ag/AgCl (0.4 V versus reversible hydrogen electrode [RHE]) were obtained with the H : TiO_2 nanowires that show that these nanowires could efficiently separate and transport charges. Additionally, a photocurrent density of about 1.97 mA/cm^2 was achieved with the optimized H : TiO_2 nanowires in 1 M NaOH at −0.6 V versus Ag/AgCl in an imitated solar light illumination from a 150 W Xenon lamp, operating at 100 mW/cm^2, and coupled with a 1.5 G AM filter. The photocurrent density obtained for the H : TiO_2 nanowires corresponds to about 1.63% solar-to-H_2 efficiency. These researchers further established that a solar-to-H_2 efficiency of about 1.1% (best value for TiO_2-based photoanode) could be obtained for the H : TiO_2 nanowires. They achieved this by an integration of the spectrum of incident photon-to-current conversion efficiency (IPCE) of the nanowires with a standard 1.5 G AM solar spectrum, so as to eliminate the discrepancy between solar light and the xenon lamp irradiance. Theoretically, rutile TiO_2 (optical band gap = 3.0 eV) was predicted to afford about 2.25% photoconversion efficiency at the maximum with a 100 mW/cm^2 and 1.5 G irradiation, but the reported efficiency and photocurrent densities for TiO_2-based photoanodes still fall below this theoretical prediction [287]. The enhancement of the photocurrent for the H : TiO_2 nanowires was ascribed to an improvement in the photocatalytic activity of TiO_2 nanoparticles in the UV range as ascertained by IPCE analyses. Furthermore, the H_2 treatment increased the TiO_2 nanowire donor density by a magnitude of 3 orders, through the creation of high oxygen vacancies density that serve as effective electron donors. These researchers also obtained similar photocurrent enhancements with H_2 treated anatase TiO_2 nanotubes.

Differently, mesoporous TiO_2 nanoparticles with regular mesopore and interpenetrated systems have gained recent research interest based on their intriguing properties such as environmental benignity, tunable mesostructures and pore sizes, low cost, excellent optical and electronic properties, high specific surface areas, and good chemical stability [288–290]. Irrespective of their potentials for photoelectrochemical water splitting and application in photovoltaic cells, numerous research have focused on enhancing their photocatalytic activities by enhancing their abilities to absorb solar light, charge separation, and transport [291–293]. Additionally, several strategies such as

band gap engineering, controlling heterojunctions, optimizing exposed facets, and maximizing crystallinity have been employed for the design of performance mesoporous TiO_2 materials with improved performance [294–298]. In this regard, Zhou et al. demonstrated the simple synthesis of mesoporous black TiO_2 nanomaterials with ordered mesostructures, high crystalline anatase walls, and high surface areas [299]. The mesoporous black TiO_2 nanomaterials were synthesized by an evaporation-mediated self-assembly in combination with an encircling process with ethylenediamine. They elaborated the fact that employing a high surface area and thermally stable mesoporous TiO_2 precursor for the hydrogenation is very crucial for the fabrication of the ordered mesoporous nanomaterials. This facilitates the diffusion of H_2 gas into the TiO_2, interaction of H_2 gas with TiO_2 structures, maintains the ordered mesoporous structures, inhibits phase transformation (anatase to rutile), and crystal formation in the hydrogenation process at 500 °C. They observed that the ordered mesoporous nanomaterials possess large pore size of about 9.6 nm, high surface area of about 124 m^2/g, and large pore volume of 0.24 cm^3/g. Notably, an extension of photoactivity (from UV to visible and NIR regions) was observed for the ordered mesoporous nanomaterials. Moreover, the ordered mesoporous nanomaterials demonstrated a substantially high photocatalytic H_2 generation rate (136.2 μmol/h) approximately two times higher than the observed rate for pristine ordered mesoporous TiO_2.

Furthermore, it has been reported that the addition of a layered structure of molybdenum disulfide (MoS_2) could enhance the production of H_2 by photocatalysis with TiO_2 [300]. This may have been guided by the progress made so far on H_2 evolution with MoS_2 as an electrocatalyst [301–304]. However, the potential of MoS_2 as a cocatalyst for the evolution of H_2 by photocatalysis has only gained sporadic attention, irrespective of the high activities demonstrated by this cocatalyst in heterogeneous catalysis for H_2 production [305–307]. In a bid to exploit the potential of MoS_2 to combine with TiO_2 nanocrystals and enhance H_2 production, Xiang et al. investigated the synergistic effect of the cocatalysts MoS_2 and graphene on the photocatalytic activity of TiO_2. Graphene has also been reported in other studies as a promising cocatalyst for the evolution of H_2 by photocatalysis due to its intriguing electron mobility and specific surface area [308–311]. Leveraging the intriguing properties of graphene and MoS_2 as cocatalysts, their composite nanomaterial with TiO_2 nanocrystals were prepared following a facile two-step hydrothermal strategy employing tetrabutylorthotitanate as the precursor for TiO_2 and thiourea, graphene oxide, and sodium molybdate as precursors for the graphene/MoS_2hybrid. The TiO_2/graphene/MoS_2 nanocomposite exhibited a quantum efficiency of 9.7% under a UV irradiation of 365 nm. Additionally, a high rate for the production of H_2 (165.3 μmol/h) was obtained with the nanocomposite when the composition of the graphene/MoS_2 cocatalyst was 0.5 wt% and the graphene composition in this cocatalyst was 5.0 wt%. The high photocatalytic activity observed with the nanocomposite arose from the synergistic effect of the graphene and MoS_2 in the hybrid cocatalyst, serving as source of sites for adsorption and an electron collector, respectively.

1.4.7 Food and Cosmetics

Indeed, advances in nanoscience and nanotechnology have markedly provided benefits to various fields, including the food and cosmetic industries [312]. As such, some nanomaterials, particularly TiO_2 nanoparticles have been widely applied in food processing, packaging, nutrition, and healthcare products [313–315]. For instance, the application of TiO_2 nanoparticles in food packaging was investigated by using same as a material for the disinfection of *L. monocytogenes* biofilm-contaminated packaging surfaces [136]. It was observed that the nanoparticles decreased the formation of the biofilms by 3 log CFU/cm^2 following UV irradiation for 90 minutes.

In a related experiment, TiO_2 nanoparticles were coated on a food packaging film (low density polyethylene) and their capacity to inactivate *E. coli* was investigated under fluorescent and UV lights [316]. Under UV light, the antimicrobial effect of the nanoparticles was higher than that which was observed under fluorescent light and depended on the concentration of the nanoparticles and exposure time. Recently, Xie and Hung embedded TiO_2 nanoparticles in the biodegradable film of cellulose acetate and irradiated same with a 1.3 mW/cm^2 intensity UV light for two hours [95]. They observed that the nanoparticle-embedded film demonstrated a 1.69 log CFU/ml decrease in the growth of *E. coli*, suggesting the potential use of this film as an antibacterial food packaging material. Additionally, nano-sized TiO_2 has long been used as a food flavor enhancer and colorant in diary and confectionary products, seeds, beverages, toothpastes, and some medications [317–319].

On the other hand, TiO_2 nanoparticles are extensively used as inorganic UV absorbers in sunscreen products, enabling the application of an optically transparent film on the human skin [315, 320]. The addition of TiO_2 nanoparticles in sunscreen products has been reported to prevent skin irritation and the disruption of the endocrine system [321]. Various researchers have also quantified the amounts of these nanoparticles as useful components of sunscreen products [96, 320–322]. In the light of this, Lewicka et al. determined the elemental composition, shape, dimension, surface area, and crystal phase of TiO_2 nanoparticles in commercial sunscreen products [320]. They observed that the products contained mainly rutile nanocrystals with near-spherical or needle-like shapes and average size of about 25 nm. Similarly, Lu et al. observed anatase and rutile TiO_2 nanoparticles (~24 nm) with spherical and needle-like shapes, respectively, in commercial sunscreen samples [321]. Weir et al. also determined the presence of TiO_2 nanoparticles in various brands of commercial personal care products [96]. They reported that about 10% of TiO_2 nanoparticles by weight was found in sunscreens, while shaving creams, deodorants, and shampoos contained about 0.1 μg/mg.

In another study, Jaroenworaluck et al. synthesized silica-coated TiO_2 nanoparticles and characterized same for application in sunscreen products [315]. They observed that the non-crystalline nano-sized silica coating enhanced the UV absorption capacity of the TiO_2 nanoparticles, thereby suggesting their potential utility in enhancing the efficacy of sunscreen products.

1.4.8 Soil Remediation

The application of TiO_2 nanoparticles in agriculture is relatively new and as such requires more exploration following the gains that have already been made from the use of these nanoparticles for pesticide degradation, residue detection, and plant protection [323]. There are various interesting reports on the remediation of contaminated soil with nano-TiO_2, especially for the UV-mediated degradation of soil organic pollutants [5, 324]. Notably, environmental weathering processes including biodegradation, dissolution, and volatilization generally remove the more bioavailable and lighter hydrocarbons, while the recalcitrant and less bioavailable heavy hydrocarbons (HHCs) are left behind. Common biodegradation strategies such as slurry bioreactors and land farming have been employed to remove these HHCs from the soil [325–327]. However, these strategies are characterized by slow degradation with about two- to six-month timeframes of remediation [94]. This has been attributed to the recalcitrant structures and low biodegradabilities of the HHCs. Additionally, in some instances, depending on the nature of soil and the conditions therein, good standards for soil cleanup may not be obtained using bioremediation as a single technology. Therefore, an integration of bioremediation with advanced oxidation processes could afford less expensive and scalable enhancement of HHCs bioavailability with a consequent increase in processing capacities and treatment rates [328–330].

Nano-TiO_2 and its derivatives have also been investigated for their abilities to clean up other organic pollutants by the photocatalytic oxidation process as demonstrated in the photodegradation of diphenylarsinic acid (DPAA) using TiO_2 nanoparticles [331]. DPAA is usually formed from the leakages of arsenic weapons and pose adverse health effects to humans. Unfortunately, strategies for their remediation are still scarce. These researchers firstly studied the DPAA degradation pathway and identified arsenate as the final product. For the purpose of optimizing operational parameters for the effective removal of the DPAA including TiO_2 nanoparticles dosage, light intensity, irradiation time, and soil–water ratio, the researchers advantageously conducted 9 experiments following an orthogonal array experimental design $L_9(3)^4$, as against the conventional 81 experiments required in a one-factor-at-a-time design. They therefore reported that the optimal conditions for the treatment of 4 g contaminated soil with 20 mg/kg DPAA was 5% TiO_2 nanoparticles, light intensity of 40 mW/cm^2, irradiation time of three hours, and a soil–water ratio of 1 : 10. They observed that the aforementioned parameters yielded an 82.7% removal efficiency of the DPAA. The researchers further validated this method in nine different soil samples but changed the irradiation time to 1.5 hours and obtained removal efficiencies of 57.0–78.6%. Additionally, they observed that the removal efficiencies negatively correlated with pH, phosphorus content, electrical conductivity, and organic matter content. Furthermore, the generation of hydroxyl radicals by the TiO_2 nanoparticles as monitored by electron spin resonance (ESR) were found to be affected by the soil properties.

Wang et al. also applied the photocatalysis of TiO_2 nanoparticles in combination with nonthermal discharge plasma for the removal of *p*-nitrophenol from contaminated soil [332]. Nitrophenols are biorefractory and toxic organic

compounds that are extensively used as intermediates and raw materials for the production of pharmaceuticals, pigments, wood preservatives, dyes, rubber chemicals, pesticides, and explosives [333]. Notably, three of these nitrophenols (2,4-dinitrophenol, 2-nitrophenol, and 4-nitrophenol) had earlier been listed as priority pollutants in the US Environmental Protection Agency (USEPA) list [334]. In the study conducted on the removal of *p*-nitrophenol, Wang et al. envisaged that the photocatalysis of the TiO_2 nanoparticles could be driven by pulsed discharge plasma [332]. They reported that up to 88% of the *p*-nitrophenol was successfully removed in 10 minutes by employing this process. Enhancing the pulsed discharge voltage was also found to increase the removal efficiency of the pollutant. These researchers monitored the mineralization of the pollutant and the formation of intermediates by UV–vis spectroscopic analysis, denitrification, COx selectivity analysis, and total organic carbon. Following these techniques, they identified some intermediates, mainly benzoquinone, benzo[d][1, 2, 3]-trioxole, hydroquinone, phenol, acetic acid, NO^{2-}, NO^{3-}, formic acid, oxalic acid, and catechol. The generation of these major intermediates demonstrated the enhanced effect of the TiO_2 catalytic pulsed discharge plasma system. When compared with the plasma system alone, it was observed that the enhancements in pollutant mineralization and degradation were achieved with the generation of increased amounts of active species such as H_2O_2 and O_3 in the TiO_2 catalytic pulsed discharge plasma system.

1.4.9 Pesticides Removal

Among the organic contaminants, pesticides (insecticides, fungicides, and herbicides), i.e. formulations with wide structural variety and usually applied to targets in the field or household to achieve intended efficacy to certain fungal diseases, weeds and pests, form a large portion of these pollutants [22]. Although pesticides are used in agriculture mainly to boost crop yield, excessive usage of same may lead to adverse effects to humans and the environment at large [323]. Moreover, repeated and indiscriminate applications of pesticides causes an accumulation of pesticide residues in the area of application and biota [335]. There are numerous reports on pesticide contamination of air, land, and aquatic environments and as such pose serious treats to humans, non-target plant species, terrestrial organisms, and aquatic life [331, 336, 337]. As a consequence, tangible efforts have been made in developing appropriate strategies for the removal of these noxious chemicals and possibly destroy the bio-recalcitrant organic pollutants [335]. For this purpose, photocatalysis with semiconductors has gained meaningful research interest as a favorable strategy to remedy the problems associated with pesticide residue accumulation in the environment [338, 339]. For the past decade, TiO_2 nanoparticles have been widely investigated as photocatalytic semiconductors for the efficient degradation of pesticides [339]. Numerous research have also been conducted in order to modify TiO_2 nanoparticles for enhanced photodegradation outcomes [335, 340–342]. Following a UV light-induced photocatalytic process and TiO_2 nanoparticles, various pesticides have been reportedly degraded [343, 344].

Specifically, unmodified and modified TiO_2 nanoparticles have been used to degrade some pesticides such as imidacloprid [5], methamidophos [336], chlorfenapyr [337], atrazine [345], chlorotoluron [346], cinosulfuron [347], Diuron [324], chlorpyrifos [344], etc. For instance, Ahmari et al. demonstrated that the UV irradiation of TiO_2 nanoparticles was capable of eliminating imidacloprid in less than two hours [5]. Imidacloprid, an organic pesticide composed of nitramide, dihydroimidazole, and pyridinium attacks the central nervous system of insects, even though it poses less toxicity to humans. In order to irradiate the imidacloprid suspension and the TiO_2 nanoparticles, a UV lamp placed in a reactor was used. The reactor also comprised of a coaxial cylinder whose inner cylinder uniformly rotated at constant speed. These researchers operated the reactor in two modes; batch and continuous. In the continuous mode, the nano-TiO_2 was adequately deposited on a textile base due to the passage of the pesticide suspension through the reactor. Changes in the concentration of the pesticide was determined by UV–vis spectroscopy. They observed that the exposure of the pollutant to the nano-TiO_2 photocatalyst was increased as a consequence of the reactor design strategy with an inner rotating cylinder. This obviously caused an increase in the rate of mass transfer. Additionally, they observed that the efficiency of the irradiation increased as a result of small gap between the cylinders, thus allowing the contact between the light source and a small suspension volume.

This reactor design was also employed in another study for the removal of linear alkyl benzene sulfonate (LAS) from solution using TiO_2 nanoparticles [348]. LAS is a widely used nonionic surfactant for the production of detergents. The pollutant suspension and the TiO_2 nanoparticles were incorporated into the reactor and the changes in pollutant concentration were determined by UV–vis spectroscopy. It was reported that at high LAS concentrations, UV irradiation of the TiO_2 nanoparticles outperformed activated nano-TiO_2, whereas at low concentrations of LAS, the time required to attain pollutant elimination was markedly reduced. In another experiment, Affam and Chaudhuri investigated the degradation of three pesticides including chlorpyrifos, chlorothalonil, and cypermethrin with TiO_2 nanoparticles that was irradiated with a UVA light source at 365 nm [344]. They further determined the degradation enhancement and biodegradability index, i.e. the ratio of biological oxygen demand (BOD_5) to chemical oxygen demand (COD), following the addition of hydrogen peroxide. After 300 minutes of UVA irradiation of the TiO_2 nanoparticles (1.5 g/l) at pH 6, the removal of total oxygen demand (TOC) and COD were 8.45% and 25.95%, respectively. Following the UVA irradiation of the TiO_2 nanoparticles (1.5 g/l) in the presence of hydrogen peroxide (100 mg/l) at pH 6 for 300 minutes, the TOC and COD removal were 21.54 and 53.62, respectively. This was accompanied with an increase in biodegradability index up to 0.26. Mineralization was also observed, which was evidenced by an increase in nitrate-nitrogen from 0.70 to 13.80 mg/l and a corresponding decrease in ammonia-nitrogen from 22.00 to 7.80 mg/l in 300 minutes. They also observed that the pesticides degradation followed the pseudo-first-order kinetics with rate constants of 0.0008 and 0.0025 per minute for the removal of TOC and COD, respectively.

Žabar et al. also studied the photodegradation of imidacloprid and thiamethoxam using a photoreactor equipped with six polychromatic fluorescent lamps and glass slides immobilized with TiO_2 [349]. They observed the photodegradation of the pesticides within two hours of UV irradiation. The degradation processes were also described to follow the first-order kinetics. Additionally, the imidacloprid and thiamethoxam degradation was monitored by high performance liquid chromatography, and the mineralization efficiency was determined by measuring the total organic carbon. However, the mineralization rate was low with values of $19.1\% \pm 0.2$ and $14.4\% \pm 2.9\%$ for imidacloprid and thiamethoxam, respectively, showing that various transformation products were rather formed. These researchers further analyzed the accruing transformation products, which led to the first ever discovery of the compound clothianidin. In another study, Zhang et al. investigated the photodegradation of 4,4′-biphenol with TiO_2 nanoparticles in the presence of cyclodextrins. For the purpose of inducing the photodegradation by UV irradiation, a metal halide lamp operating at 250 W and a wavelength of 365 nm was used as the light source. They further investigated the inclusion complex of the cyclodextrins with the 4,4′-biphenol, and the adsorption of 4,4′-biphenol on the TiO_2 surface in the presence and absence of the cyclodextrins. They observed that the photocatalytic reaction was dominated by the inclusion complex behaviors of cyclodextrins with the 4,4′-biphenol. However, a large inclusion constant of 5600 per molar of 4,4′-biphenol with β-cyclodextrin accompanied with an increase in the adsorption on the TiO_2 surface resulted in an enhanced photodegradation. Conversely, an opposite effect was observed with α-cyclodextrin that was attributed to a small inclusion constant of 355 per molar.

The mechanism, degradation performance, and technical feasibility of aqueous imidacloprid were investigated in a different study by Malato et al. [350]. They utilized two photocatalytic systems on a pilot scale, since it is possible to employ natural UV light. For this purpose, homogeneous and heterogeneous photocatalysis using photo-Fenton reaction and TiO_2, respectively, were studied. The utility of equivalent field conditions and pilot scale enabled proper comparison of the toxicity and mineralization extents, and the transformation products obtained from the mineralization processes of both systems. It was observed that <2.0 mg/l (95%) mineralization was attained after 450 minutes with the TiO_2 and 250 minutes with photo-Fenton reaction. This demonstrated that the total organic carbon disappears slower (~2.4 times) with the TiO_2 than the photo-Fenton reaction. In a related study, Agüera et al. oxidized imidacloprid in water at a concentration of 50 mg/l using TiO_2 in conjunction with formulating agents [351]. The oxidized solutions were analyzed complementarily with liquid chromatography (LC)-atmospheric pressure chemical ionization (APCI)-mass spectroscopy (MS) and GC-Ion Trap-MS employing either chemical ionization (CI) or electron ionization (EI) as the ionization modes. The complementary analysis provided an avenue for adequate evaluation and confirmation of the pesticide decay and the existence of accruing degradation products. Whereas the LC-APCI-MS technique provided adequate monitoring of the imidacloprid and a degradation product (6-chloronicotinic acid) in the course of the degradation, the Gas chromatography–mass spectroscopy (GC–MS) technique enabled the

detection of five other degradation products. Unequivocally, three of these five degradation products were identified. Furthermore, other complementary analytical techniques including ion chromatography and total organic carbon were employed to evaluate the degree of mineralization. They observed that after irradiating the TiO_2 with UV light for 450 minutes, both the pesticide and its degradation products were not detected. Interestingly, a near-total mineralization was recorded after the irradiation for 700 minutes.

Higarashi and Jardim reported that Diuron in 4 cm of contaminated top soil was degraded by TiO_2 nanoparticles in a UV radiation intensity-dependent degradation rate [324]. Herbicides such as Diuron belong to a class of pesticides with wide application in agriculture. Owing to their high vapor pressure and lipid affinity, and low biodegradability, these haloaromatic pesticides are generally considered as persistent chemicals. Unfortunately, if they are accidentally or uncontrollably disposed in the soil, they stand a high chance of posing adverse health risks to humans. These researchers spiked soil samples with Diuron concentrations of 10, 50, and 100 mg/kg, loaded the soil samples with various TiO_2 concentrations (0%, 0.1%, 0.5%, 1%, and 2% w/w), and then exposed them to solar light (average intensity = 2 mW/cm at 365 nm, 47 W and 22 S). They observed that both the TiO_2 and Diuron concentrations negligibly affected the photodegradation kinetics that was largely dependent on the intensity of the radiation. These researchers further evaluated the effects of water and $Ca(OH)_2$ on the photo-induced degradation process. They also reported that the addition of water increased the degradation rate of the Diuron. On the other hand, pH increase following the addition of $Ca(OH)_2$ had no effect of the degradation rates. Additionally, the photocatalytic degradation of the pesticide obtained by combining the solar light with TiO_2 was demonstrated to be efficient.

Furthermore, the photocatalytic degradation of melathion by WO_3-modified TiO_2 nanoparticles was investigated in a study by Ramos-Delgado et al. [340]. The TiO_2 nanoparticles were synthesized by the sol–gel synthetic technique using tetrabutylorthotitanate and ammonium *p*-tungstate at a pH of 3. The TiO_2 nanoparticles were then modified with two different WO_3 percentages, i.e. 2 and 5 wt% in the presence of 2-butanol and an aging time of 48 hours. Structural analysis of the WO_3/TiO_2 photocatalysts demonstrated the dispersion of the WO_3 on the TiO_2 surface with particle sizes of 19.4 and 25.6 nm for the 2% and 5% WO_3 percentages, respectively. They also reported the 2% WO_3/TiO_2 photocatalytic formulation showed the best degradation effect, evidenced by the 76% total organic carbon reduction after 300 minutes of UV irradiation. Meanwhile, this was compared with those of bare TiO_2 and 5% WO_3/TiO_2 photocatalytic formulation that exhibited 47% and 28% mineralization, respectively. The researchers therefore established a long-term stability of the 2% WO_3/TiO_2 photocatalytic formulation following numerous successive cycles obtained in ascertaining the efficacy of the formulation after repeated use.

In a related study, nano-TiO_2 also prepared by the sol–gel synthetic technique was sulfate-modified and investigated for the degradation of methyl orange [338]. In that study, tetraisopropylorthotitanate was used as the starting material and the synthesized TiO_2 nanoparticles were promoted with different weight percentages (2.0, 2.5, 3.0, and 3.5 wt%) of sulfate, following an incipient wetness

impregnation strategy. They observed the mesoporous nature of the synthesized TiO_2 nanoparticles and established the fact that sulfate modification of the nanoparticles could reduce phase transformation and enhance the thermal stability of the nano-TiO_2. Additionally, the sulfate modification was found to decrease the crystal size and enhance the surface area of the TiO_2 nanoparticles. With respect to the degradation of the organic dyestuff, the researchers observed that the degradation efficiency obtained using the 2.5 wt% sulfate loading (61%) was about two times more than that achieved with unmodified nano-TiO_2 (33%). Moreover, the degradation profile was best described by a first-order kinetics.

1.4.10 Paint and Paper Productions

Owing to its light-scattering ability, TiO_2 stands as the most widely used white pigment in the paint and paper industries [98]. The utility of TiO_2 in the paint industry dates back to the late 1920s when the anatase phase was more dominant. In the 1940s, industrialists commenced the use of the rutile phase but with no surface treatments [352]. Today, the surface-treated rutile phase forms have practically replaced the earlier forms.

It has been demonstrated that an aged paint leachate contained appreciable amounts of TiO_2 nanoparticles [353]. The leachate was employed to investigate the phytotoxicity of TiO_2 nanoparticles to lettuce leaves by foliar exposure. Although no acute phytotoxicity was observed, TiO_2 nanoparticles were internalized in the leaves and all types of tissues of the lettuce plant, thus showcasing these nanoparticles as active components of paints. Furthermore, Kaegi et al. reported that TiO_2 nanoparticles are components of both new and aged facade paints [354]. They used a centrifugation-based sample preparation technique to recover about 20–300 nm of the nanoparticles, also emphasizing their utility in paint production. Elsewhere, the environmental fate of TiO_2 nanoparticles was investigated by comparing the impacts of pristine TiO_2 nanoparticles and those released from a TiO_2 nanoparticles-containing paint [355]. By shaking an aged paint powder in water, 580 μg/l of TiO_2 nanoparticles (average diameter of 200–300 nm) were obtained, demonstrating the actual incorporation of these nanoparticles in paint production.

In the papermaking industry, fillers are normally used to enhance the optical properties, printing quality, writability, environmental friendliness, sheet formation, and dimensional stability of papers [356]. This has increased the general interest of papermaking industries to enhance the filler contents of papers [357]. Notwithstanding, it is also very important to overcome the major drawbacks associated with the use of mineral fillers, which includes the reduction of fiber-to-fiber bonding. Obviously, the fiber-to-fiber bonding reduction induces a subsequent decrease in the strength properties of the paper and additional challenges such as dusting, white waters circulation, and retention [358]. These fillers such as TiO_2 nanoparticles, calcium carbonate, talc, and kaolin are usually mixed with the pure fiber pulp to produce the paper sheets [359]. Importantly, TiO_2 nanoparticles have been employed as fillers largely due to their fascinating refractive index, insolubility in acidic and alkaline solutions, and high

degree of whiteness [360]. To this end, Tao et al. prepared novel $CaCO_3$@TiO_2 core–shell nanoparticles and applied same as fillers in paper production [356]. They employed carbonization as a process to obtain $CaCO_3$ and the relatively cheap inorganic titanium sulfate as a precursor for the TiO_2 nanoparticles. It was observed that the $CaCO_3$@TiO_2 showed higher UV absorption capacity than either components. Additionally, the $CaCO_3$@TiO_2 filler-containing paper demonstrated a 3% improved whiteness (73.80%) than pure fiber paper (70.35%) but comparable with that of TiO_2 nanoparticle-incorporated paper (73.16%).

In a related study, Adel et al. also prepared uncoated and chitosan-coated $CaCO_3$@TiO_2 core–shell nanoparticles as fillers and coats, respectively, in paint production [99]. They also observed that the $CaCO_3$@TiO_2 nanoparticles demonstrated improved photo-stabilization of the paper after exposure to UV light. Moreover, an enhanced thermal stability of the paper was achieved by incorporating the chitosan-coated core–shell nanoparticles. This corroborates earlier reports on the improvements of TiO_2 thermal stability [227], mechanical property [361], and biodegradability following incorporation with chitosan [362]. Undoubtedly, these improvements can be attributed to the widely reported fascinating biodegradability of chitosan [227, 363, 364]. In another experiment, novel antifungal nanocomposites synthesized by incorporating chitosan and TiO_2 nanoparticles into carboxymethyl cellulose polymeric membrane were tested for their capacity to preserve the carboxymethyl cellulose in paper-art-works [365]. They investigated the antifungal activity of the nanocomposites on two commonly found fungi species in library materials: *Aspergillus niger* and *Aspergillus flavus*. They observed that the yellow color and adherence of the carboxymethyl cellulose adhesive of the paper was preserved due to the presence of the TiO_2 and chitosan nanoparticles.

1.5 Conclusion

Indeed, TiO_2 nanoparticles have been demonstrated to possess low production cost, thin film transparency, chemical and mechanical stability, bio- and chemical inertness, high light conversion efficiency, hydrophilicity, and corrosion resistance. Taking advantage of some specific properties such as their exceptional photocatalytic ability, biocompatibility, low toxicity, and production costs, these nanoparticles have been successfully applied in nanomedicine and nanobiotechnology. Interestingly, these nanoparticles can be synthesized by a wide range of methods including hydrothermal, sol–gel, thermal decomposition, vapor deposition, micelle and inverse micellar, oxidation, sonochemical, microwave-assisted, and electrodeposition methods. The vast array of synthetic methods for these nanoparticles has dramatically increased their utility in various other aspects including wastewater treatment, soil remediation, energy devices, food, cosmetics, paints, paper, antiseptics, and printing inks. Taken together, we envisage the emergence of new applications for these nanoparticles, compensating the ever-increasing research into the exploitation of their fascinating properties.

Acknowledgments

The authors would like to thank the continuous support by National Key R&D Program of China (2018YFC0910601, 2019YFA0405603), Natural Science Foundation of China (31971292, U1432114 to Aiguo Wu and 8161101589, 81950410638 to M. Zubair Iqbal), Zhejiang Province Financial Supporting (2017C03042, LY18H180011), and the Science & Technology Bureau of Ningbo City (2015B11002,2017C110022). Furthermore, the authors also acknowledge Shanghai Synchrotron Radiation Facility at Line BL15U (No. h15sr0021) for X-ray fluorescence imaging and National Synchrotron Radiation Laboratory in Hefei for soft X-ray imaging (No. 2016-HLS-PT-002193). Ozioma Udochukwu Akakuru also appreciates the Chinese Academy of Sciences (CAS) and The World Academy of Sciences (TWAS) for the award of the CAS-TWAS President's Fellowship (2017A8017422001) for PhD studies.

References

1 Fujishima, A. and Honda, K. (1972). Electrochemical photolysis of water at a semiconductor electrode. *Nature* 238: 37–38.
2 Rehman, F.U., Zhao, C., Jiang, H., and Wang, X. (2016). Biomedical applications of nano-titania in theranostics and photodynamic therapy. *Biomaterials Science* 4: 40–54.
3 Alivisatos, A.P. (1996). Semiconductor clusters, nanocrystals, and quantum dots. *Science* 271: 933.
4 Barnard, A.S., Erdin, S., Lin, Y. et al. (2006). Modeling the structure and electronic properties of TiO_2 nanoparticles. *Physical Review B* 73: 205405.
5 Ahmari, H., Heris, S.Z., and Khayyat, M.H. (2018). The effect of titanium dioxide nanoparticles and UV irradiation on photocatalytic degradation of Imidaclopride. *Environmental Technology* 39: 536–547.
6 Shehap, A.M. and Akil, D.S. (2016). Structural and optical properties of TiO_2 nanoparticles/PVA for different composites thin films. *International Journal of Nanoelectronics and Materials* 9: 17–36.
7 Chen, X. and Mao, S.S. (2007). Titanium dioxide nanomaterials: synthesis, properties, modifications, and applications. *Chemical Reviews* 107: 2891–2959.
8 Choi, H.C., Jung, Y.M., and Kim, S.B. (2005). Size effects in the Raman spectra of TiO_2 nanoparticles. *Vibrational Spectroscopy* 37: 33–38.
9 Li, Y., Zhang, S., Yu, Q., and Yin, W. (2007). The effects of activated carbon supports on the structure and properties of TiO_2 nanoparticles prepared by a sol–gel method. *Applied Surface Science* 253: 9254–9258.
10 Camps, I., Borlaf, M., Colomer, M.T. et al. (2017). Structure-property relationships for Eu doped TiO_2 thin films grown by a laser assisted technique from colloidal sols. *RSC Advances* 7: 37643–37653.
11 Trujillo-Navarrete, B., del Pilar Haro-Vázquez, M., Félix-Navarro, R.M. et al. (2017). Effect of Nd^{3+} doping on structure, microstructure, lattice distortion

and electronic properties of TiO_2 nanoparticles. *Journal of Rare Earths* 35: 259–270.

12 Çeşmeli, S. and Biray Avci, C. (2018). Application of titanium dioxide (TiO_2) nanoparticles in cancer therapies. *Journal of Drug Targeting* 27: 762–766.

13 Zeng, L., Ren, W., Xiang, L. et al. (2013). Multifunctional Fe_3O_4–TiO_2 nanocomposites for magnetic resonance imaging and potential photodynamic therapy. *Nanoscale* 5: 2107–2113.

14 Ren, W., Yan, Y., Zeng, L. et al. (2015). A near infrared light triggered hydrogenated black TiO_2 for cancer photothermal therapy. *Advanced Healthcare Materials* 4: 1526–1536.

15 Mou, J., Lin, T., Huang, F. et al. (2016). Black titania-based theranostic nanoplatform for single NIR laser induced dual-modal imaging-guided PTT/PDT. *Biomaterials* 84: 13–24.

16 Gomes, S.I.L., Roca, C.P., von der Kammer, F. et al. (2018). Mechanisms of (photo)toxicity of TiO_2 nanomaterials (NM103, NM104, NM105): using high-throughput gene expression in *Enchytraeus crypticus*. *Nanoscale* 10: 21960–21970.

17 Skocaj, M., Filipic, M., Petkovic, J., and Novak, S. (2011). Titanium dioxide in our everyday life; is it safe? *Radiology and Oncology* 45: 227–247.

18 Govindasamy, G., Murugasen, P., and Sagadevan, S. (2016). Investigations on the synthesis, optical and electrical properties of TiO_2 thin films by chemical bath deposition (CBD) method. *Materials Research* 19: 413–419.

19 Arora, B., Murar, M., and Dhumale, V. (2015). Antimicrobial potential of TiO_2 nanoparticles against MDR *Pseudomonas aeruginosa*. *Journal of Experimental Nanoscience* 10: 819–827.

20 Mo, S.-D. and Ching, W.Y. (1995). Electronic and optical properties of three phases of titanium dioxide: rutile, anatase, and brookite. *Physical Review B* 51: 13023–13032.

21 Hoang, V.V., Zung, H., and Trong, N.H.B. (2007). Structural properties of amorphous TiO_2 nanoparticles. *The European Physical Journal D* 44: 515–524.

22 Gupta, S.M. and Tripathi, M. (2011). A review of TiO_2 nanoparticles. *Chinese Science Bulletin* 56: 1639.

23 Simons, P.Y. and Dachille, F. (1967). The structure of TiO_2II, a high-pressure phase of TiO_2. *Acta Crystallographica* 23: 334–336.

24 Latroche, M., Brohan, L., Marchand, R., and Tournoux, M. (1989). New hollandite oxides: TiO_2(H) and $K_{0.06}TiO_2$. *Journal of Solid State Chemistry* 81: 78–82.

25 Kingon, A.I., Maria, J.-P., and Streiffer, S.K. (2000). Alternative dielectrics to silicon dioxide for memory and logic devices. *Nature* 406: 1032–1038.

26 Li, W., Ni, C., Lin, H. et al. (2004). Size dependence of thermal stability of TiO_2 nanoparticles. *Journal of Applied Physics* 96: 6663–6668.

27 Dambournet, D., Belharouak, I., and Amine, K. (2010). Tailored preparation methods of TiO_2 anatase, rutile, brookite: mechanism of formation and electrochemical properties. *Chemistry of Materials* 22: 1173–1179.

28 Selloni, A. (2008). Anatase shows its reactive side. *Nature Materials* 7: 613.

29 Tripathi, A.K., Singh, M.K., Mathpal, M.C. et al. (2013). Study of structural transformation in TiO_2 nanoparticles and its optical properties. *Journal of Alloys and Compounds* 549: 114–120.

30 Arbiol, J., Cerdà, J., Dezanneau, G. et al. (2002). Effects of Nb doping on the TiO_2 anatase-to-rutile phase transition. *Journal of Applied Physics* 92: 853–861.

31 Zhang, Q., Gao, L., and Guo, J. (2000). Effects of calcination on the photocatalytic properties of nanosized TiO_2 powders prepared by $TiCl_4$ hydrolysis. *Applied Catalysis B* 26: 207–215.

32 Christy, P.D., Jothi, N.S.N., Melikechi, N., and Sagayaraj, P. (2009). Synthesis, structural and optical properties of well dispersed anatase TiO_2 nanoparticles by non-hydrothermal method. *Crystal Research and Technology* 44: 484–488.

33 Auvinen, S., Alatalo, M., Haario, H. et al. (2011). Size and shape dependence of the electronic and spectral properties in TiO_2 nanoparticles. *The Journal of Physical Chemistry C* 115: 8484–8493.

34 Shaikh, S.F., Mane, R.S., Min, B.K. et al. (2016). D-sorbitol-induced phase control of TiO_2 nanoparticles and its application for dye-sensitized solar cells. *Scientific Reports* 6: 20103.

35 Fujishima, A., Zhang, X., and Tryk, D.A. (2008). TiO_2 photocatalysis and related surface phenomena. *Surface Science Reports* 63: 515–582.

36 Nakata, K. and Fujishima, A. (2012). TiO_2 photocatalysis: design and applications. *Journal of Photochemistry and Photobiology C* 13: 169–189.

37 Carp, O., Huisman, C.L., and Reller, A. (2004). Photoinduced reactivity of titanium dioxide. *Progress in Solid State Chemistry* 32: 33–177.

38 Bai, Y., Mora-Seró, I., De Angelis, F. et al. (2014). Titanium dioxide nanomaterials for photovoltaic applications. *Chemical Reviews* 114: 10095–10130.

39 Gogos, A., Knauer, K., and Bucheli, T.D. (2012). Nanomaterials in plant protection and fertilization: current state, foreseen applications, and research priorities. *Journal of Agricultural and Food Chemistry* 60: 9781–9792.

40 Kumar, S.G. and Devi, L.G. (2011). Review on modified TiO_2 photocatalysis under UV/visible light: selected results and related mechanisms on interfacial charge carrier transfer dynamics. *The Journal of Physical Chemistry A* 115: 13211–13241.

41 Ikeda, K., Sakai, H., Baba, R. et al. (1997). Photocatalytic reactions involving radical chain reactions using microelectrodes. *The Journal of Physical Chemistry B* 101: 2617–2620.

42 Löberg, J., Perez Holmberg, J., Mattisson, I. et al. (2013). Electronic properties of TiO_2 nanoparticles films and the effect on apatite-forming ability. *International Journal of Dentistry* 2013: 139615.

43 Park, J.Y. and Davies, J.E. (2000). Red blood cell and platelet interactions with titanium implant surfaces. *Clinical Oral Implants Research* 11: 530–539.

44 Nasikhudin, E.P., Diantoro, M., Kusumaatmaja, A., and Triyana, K. (2018). Study on photocatalytic properties of TiO_2 nanoparticle in various pH condition. *Journal of Physics: Conference Series* 1011: 012069.

45 Tański, T., Matysiak, W., and Krzemiński, Ł. (2017). Analysis of optical properties of TiO_2 nanoparticles and PAN/TiO_2 composite nanofibers. *Materials and Manufacturing Processes* 32: 1218–1224.

46 Feng, X., Zhai, J., and Jiang, L. (2005). The fabrication and switchable superhydrophobicity of TiO_2 nanorod films. *Angewandte Chemie International Edition* 44: 5115–5118.

47 Chae, S.Y., Park, M.K., Lee, S.K. et al. (2003). Preparation of size-controlled TiO_2 nanoparticles and derivation of optically transparent photocatalytic films. *Chemistry of Materials* 15: 3326–3331.

48 Yang, Z., Choi, D., Kerisit, S. et al. (2009). Nanostructures and lithium electrochemical reactivity of lithium titanites and titanium oxides: a review. *Journal of Power Sources* 192: 588–598.

49 Dawson, G., Chen, W., Zhang, T. et al. (2010). A study on the effect of starting material phase on the production of trititanate nanotubes. *Solid State Sciences* 12: 2170–2176.

50 Yan, J., Feng, S., Lu, H. et al. (2010). Alcohol induced liquid-phase synthesis of rutile titania nanotubes. *Materials Science and Engineering B* 172: 114–120.

51 Mozia, S. (2010). Application of temperature modified titanate nanotubes for removal of an azo dye from water in a hybrid photocatalysis-MD process. *Catalysis Today* 156: 198–207.

52 Bavykin, D.V., Parmon, V.N., Lapkin, A.A., and Walsh, F.C. (2004). The effect of hydrothermal conditions on the mesoporous structure of TiO_2 nanotubes. *Journal of Materials Chemistry* 14: 3370–3377.

53 Viet, P.V., Hieu, L.V., and Thi, C.M. (2016). The directed preparation of TiO_2 nanotubes film on FTO substrate via hydrothermal method for gas sensing application. *AIMS Materials Science* 3: 460–469.

54 Zhang, Y.X., Li, G.H., Jin, Y.X. et al. (2002). Hydrothermal synthesis and photoluminescence of TiO_2 nanowires. *Chemical Physics Letters* 365: 300–304.

55 Zhang, Q. and Gao, L. (2003). Preparation of oxide nanocrystals with tunable morphologies by the moderate hydrothermal method: insights from rutile TiO_2. *Langmuir* 19: 967–971.

56 Chong, M.N. and Jin, B. (2012). Photocatalytic treatment of high concentration carbamazepine in synthetic hospital wastewater. *Journal of Hazardous Materials* 199–200: 135–142.

57 Cao, X., Jing, W., Xing, W. et al. (2011). Fabrication of a visible-light response mesoporous TiO_2 membrane with superior water permeability via a weak alkaline sol–gel process. *Chemical Communications* 47: 3457–3459.

58 Chen, X. (2009). Titanium dioxide nanomaterials and their energy applications. *Chinese Journal of Catalysis* 30: 839–851.

59 Bessekhouad, Y., Robert, D., and Weber, J.V. (2003). Synthesis of photocatalytic TiO_2 nanoparticles: optimization of the preparation conditions. *Journal of Photochemistry and Photobiology A* 157: 47–53.

60 Wang, C., Deng, Z.-X., Zhang, G. et al. (2002). Synthesis of nanocrystalline TiO_2 in alcohols. *Powder Technology* 125: 39–44.

61 Miao, L., Tanemura, S., Toh, S. et al. (2004). Heating-sol–gel template process for the growth of TiO_2 nanorods with rutile and anatase structure. *Applied Surface Science* 238: 175–179.

62 Lopez, T., Ortiz, E., Alvarez, M. et al. (2010). Study of the stabilization of zinc phthalocyanine in sol–gel TiO_2 for photodynamic therapy applications. *Nanomedicine: Nanotechnology, Biology, and Medicine* 6: 777–785.

63 López, T., Ortiz, E., Guevara, P. et al. (2014). Physicochemical characterization of functionalized-nanostructured-titania as a carrier of copper complexes for cancer treatment. *Materials Chemistry and Physics* 146: 37–49.

64 Lin, Y., Wu, G.S., Yuan, X.Y. et al. (2003). Fabrication and optical properties of TiO_2 nanowire arrays made by sol gel electrophoresis deposition into anodic alumina membranes. *Journal of Physics* 15: 2917–2922.

65 Lee, S., Jeon, C., and Park, Y. (2004). Fabrication of TiO_2 tubules by template synthesis and hydrolysis with water vapor. *Chemistry of Materials* 16: 4292–4295.

66 Liu, S.M., Gan, L.M., Liu, L.H. et al. (2002). Synthesis of single-crystalline TiO_2 nanotubes. *Chemistry of Materials* 14: 1391–1397.

67 Sugimoto, T., Zhou, X., and Muramatsu, A. (2003). Synthesis of uniform anatase TiO_2 nanoparticles by gel–sol method. 3. Formation process and size control. *Journal of Colloid and Interface Science* 259: 43–52.

68 Mahshid, S., Askari, M., Sasani Ghamsari, M. et al. (2009). Mixed-phase TiO_2 nanoparticles preparation using sol–gel method. *Journal of Alloys and Compounds* 478: 586–589.

69 Hussain, M., Ceccarelli, R., Marchisio, D.L. et al. (2010). Synthesis, characterization, and photocatalytic application of novel TiO_2 nanoparticles. *Chemical Engineering Journal* 157: 45–51.

70 Chong, M.N., Tneu, Z.Y., Poh, P.E. et al. (2015). Synthesis, characterisation and application of TiO_2–zeolite nanocomposites for the advanced treatment of industrial dye wastewater. *Journal of the Taiwan Institute of Chemical Engineers* 50: 288–296.

71 Chong, M.N. and Jin, B. (2012). Sol–gel synthesis of inorganic mesostructured composite photocatalyst for water purification: an insight into the synthesis fundamentals, reaction, and binding mechanisms. *Synthesis and Reactivity in Inorganic, Metal-Organic, and Nano-Metal Chemistry* 42: 68–75.

72 Ranga Rao, A. and Dutta, V. (2007). Low-temperature synthesis of TiO_2 nanoparticles and preparation of TiO_2 thin films by spray deposition. *Solar Energy Materials and Solar Cells* 91: 1075–1080.

73 Li, X.L., Peng, Q., Yi, J.X. et al. (2006). Near monodisperse TiO_2 nanoparticles and nanorods. *Chemistry (Weinheim an der Bergstrasse, Germany)* 12: 2383–2391.

74 Kim, C.-S., Moon, B.K., Park, J.-H. et al. (2003). Solvothermal synthesis of nanocrystalline TiO_2 in toluene with surfactant. *Journal of Crystal Growth* 257: 309–315.

75 Ayllón, J.A., Figueras, A., Garelik, S. et al. (1999). Preparation of TiO_2 powder using titanium tetraisopropoxide decomposition in a plasma enhanced

chemical vapor deposition (PECVD) reactor. *Journal of Materials Science Letters* 18: 1319–1321.

76 Seifried, S., Winterer, M., and Hahn, H. (2000). Nanocrystalline titania films and particles by chemical vapor synthesis. *Chemical Vapor Deposition* 6: 239–244.

77 Baghgar, M., Abdi, Y., and Arzi, E. (2009). Fabrication of low-pressure field ionization gas sensor using bent carbon nanotubes. *Journal of Physics D* 42: 135502.

78 Borras, A., Sanchez-Valencia, J.R., Widmer, R. et al. (2009). Growth of crystalline TiO_2 by plasma enhanced chemical vapor deposition. *Crystal Growth and Design* 9: 2868–2876.

79 Wu, J.-J. and Yu, C.-C. (2004). Aligned TiO_2 nanorods and nanowalls. *The Journal of Physical Chemistry B* 108: 3377–3379.

80 Pradhan, S.K., Reucroft, P.J., Yang, F., and Dozier, A. (2003). Growth of TiO_2 nanorods by metalorganic chemical vapor deposition. *Journal of Crystal Growth* 256: 83–88.

81 Xiang, B., Zhang, Y., Wang, Z. et al. (2005). Field-emission properties of TiO_2 nanowire arrays. *Journal of Physics D* 38: 1152–1155.

82 Wu, J.-M., Shih, H.C., and Wu, W.-T. (2005). Electron field emission from single crystalline TiO_2 nanowires prepared by thermal evaporation. *Chemical Physics Letters* 413: 490–494.

83 Ritala, M., Leskela, M., Niinisto, L., and Haussalo, P. (1993). Titanium isopropoxide as a precursor in atomic layer epitaxy of titanium dioxide thin films. *Chemistry of Materials* 5: 1174–1181.

84 Moravec, P., Smolík, J., and Levdansky, V.V. (2001). Preparation of TiO_2 fine particles by thermal decomposition of titanium tetraisopropoxide vapor. *Journal of Materials Science Letters* 20: 2033–2037.

85 Im, J.H., Kang, E., Yang, S.J. et al. (2014). Simple preparation of anatase titanium dioxide nanoparticles by heating titanium–organic frameworks. *Bulletin of the Korean Chemical Society* 35: 2477–2480.

86 Savinkina, E.V., Obolenskaya, L.N., Kuzmicheva, G.M. et al. (2018). Effects of peroxo precursors and annealing temperature on properties and photocatalytic activity of nanoscale titania. *Journal of Materials Research* 33: 1422–1432.

87 Varghese, O.K., Gong, D., Paulose, M. et al. (2011). Crystallization and high-temperature structural stability of titanium oxide nanotube arrays. *Journal of Materials Research* 18: 156–165.

88 Kim, H., Noh, K., Choi, C. et al. (2011). Extreme superomniphobicity of multiwalled 8 nm TiO_2 nanotubes. *Langmuir* 27: 10191–10196.

89 Chen, X., Liu, L., Yu, P.Y., and Mao, S.S. (2011). Increasing solar absorption for photocatalysis with black hydrogenated titanium dioxide nanocrystals. *Science* 331: 746.

90 Wu, J.M., Zhang, T.W., Zeng, Y.W. et al. (2005). Large-scale preparation of ordered titania nanorods with enhanced photocatalytic activity. *Langmuir* 21: 6995–7002.

91 Peng, X. and Chen, A. (2004). Aligned TiO_2 nanorod arrays synthesized by oxidizing titanium with acetone. *Journal of Materials Chemistry* 14: 2542–2548.

92 Maness, P.C., Smolinski, S., Blake, D.M. et al. (1999). Bactericidal activity of photocatalytic TiO_2 reaction: toward an understanding of its killing mechanism. *Applied and Environmental Microbiology* 65: 4094–4098.

93 Carbajo, J., Tolosana-Moranchel, A., Casas, J.A. et al. (2018). Analysis of photoefficiency in TiO_2 aqueous suspensions: effect of titania hydrodynamic particle size and catalyst loading on their optical properties. *Applied Catalysis B* 221: 1–8.

94 Yang, Y., Javed, H., Zhang, D. et al. (2017). Merits and limitations of TiO_2-based photocatalytic pretreatment of soils impacted by crude oil for expediting bioremediation. *Frontiers of Chemical Science and Engineering* 11: 387–394.

95 Xie, J. and Hung, Y.-C. (2018). UV-A activated TiO_2 embedded biodegradable polymer film for antimicrobial food packaging application. *LWT* 96: 307–314.

96 Weir, A., Westerhoff, P., Fabricius, L. et al. (2012). Titanium dioxide nanoparticles in food and personal care products. *Environmental Science and Technology* 46: 2242–2250.

97 Ahmed, S.N. and Haider, W. (2018). Heterogeneous photocatalysis and its potential applications in water and wastewater treatment: a review. *Nanotechnology* 29: 342001.

98 Karlsson, M.C.F., Álvarez-Asencio, R., Bordes, R. et al. (2018). Characterization of paint formulated using secondary TiO_2 pigments recovered from waste paint. *Journal of Coatings Technology and Research* 16: 607–617.

99 Adel, A.M., Ahmed, N.M., Diab, M.A., and Selim, M.M. (2016). The influence of TiO_2/CC core/shell pigments on the properties of paper sheets. *Powder Technology* 291: 437–447.

100 Carneiro, J.O., Teixeira, V., Portinha, A. et al. (2007). Iron-doped photocatalytic TiO_2 sputtered coatings on plastics for self-cleaning applications. *Materials Science and Engineering B* 138: 144–150.

101 Obritsch, M.D., Fish, D.N., MacLaren, R., and Jung, R. (2005). Nosocomial infections due to multidrug-resistant *Pseudomonas aeruginosa*: epidemiology and treatment options. *Pharmacotherapy* 25: 1353–1364.

102 Mesaros, N., Nordmann, P., Plesiat, P. et al. (2007). *Pseudomonas aeruginosa*: resistance and therapeutic options at the turn of the new millennium. *Clinical Microbiology and Infection* 13: 560–578.

103 Gottlieb, T. and Nimmo, G.R. (2011). Antibiotic resistance is an emerging threat to public health: an urgent call to action at the Antimicrobial Resistance Summit 2011. *The Medical Journal of Australia* 194: 281–283.

104 Davies, J. and Davies, D. (2010). Origins and evolution of antibiotic resistance. *Microbiology and Molecular Biology Reviews* 74: 417–433.

105 Falagas, M.E. and Bliziotis, I.A. (2007). Pandrug-resistant Gram-negative bacteria: the dawn of the post-antibiotic era? *International Journal of Antimicrobial Agents* 29: 630–636.

106 Jesline, A., John, N.P., Narayanan, P.M. et al. (2015). Antimicrobial activity of zinc and titanium dioxide nanoparticles against biofilm-producing methicillin-resistant *Staphylococcus aureus*. *Applied Nanoscience* 5: 157–162.

107 Hamming, L.M., Qiao, R., Messersmith, P.B., and Brinson, L.C. (2009). Effects of dispersion and interfacial modification on the macroscale properties of TiO_2 polymer matrix nanocomposites. *Composites Science and Technology* 69: 1880–1886.

108 Kubacka, A., Ferrer, M., and Fernández-García, M. (2012). Kinetics of photocatalytic disinfection in TiO_2-containing polymer thin films: UV and visible light performances. *Applied Catalysis B* 121–122: 230–238.

109 Kubacka, A., Serrano, C., Ferrer, M. et al. (2007). High-performance dual-action polymer-TiO_2 nanocomposite films via melting processing. *Nano Letters* 7: 2529–2534.

110 Kubacka, A., Ferrer, M., Cerrada, M.L. et al. (2009). Boosting TiO_2-anatase antimicrobial activity: polymer-oxide thin films. *Applied Catalysis B* 89: 441–447.

111 Josset, S., Keller, N., Lett, M.-C. et al. (2008). Numeration methods for targeting photoactive materials in the UV-A photocatalytic removal of microorganisms. *Chemical Society Reviews* 37: 744–755.

112 Wiener, J., Quinn, J.P., Bradford, P.A. et al. (1999). Multiple antibiotic–resistant *Klebsiella* and *Escherichia coli* in nursing homes. *Journal of the American Medical Association* 281: 517–523.

113 AshaRani, P.V., Low Kah Mun, G., Hande, M.P., and Valiyaveettil, S. (2009). Cytotoxicity and genotoxicity of silver nanoparticles in human cells. *ACS Nano* 3: 279–290.

114 Llorens, A., Lloret, E., Picouet, P.A. et al. (2012). Metallic-based micro and nanocomposites in food contact materials and active food packaging. *Trends in Food Science and Technology* 24: 19–29.

115 Huang, Y.-Y., Choi, H., Kushida, Y. et al. (2016). Broad-spectrum antimicrobial effects of photocatalysis using titanium dioxide nanoparticles are strongly potentiated by addition of potassium iodide. *Antimicrobial Agents and Chemotherapy* 60: 5445.

116 Kubacka, A., Diez, M.S., Rojo, D. et al. (2014). Understanding the antimicrobial mechanism of TiO_2-based nanocomposite films in a pathogenic bacterium. *Scientific Reports* 4: 4134.

117 Matsunaga, T., Tomoda, R., Nakajima, T., and Wake, H. (1985). Photoelectrochemical sterilization of microbial cells by semiconductor powders. *FEMS Microbiology Letters* 29: 211–214.

118 Gogniat, G. and Dukan, S. (2007). TiO_2 photocatalysis causes DNA damage via Fenton reaction-generated hydroxyl radicals during the recovery period. *Applied and Environmental Microbiology* 73: 7740–7743.

119 Foster, H.A., Ditta, I.B., Varghese, S., and Steele, A. (2011). Photocatalytic disinfection using titanium dioxide: spectrum and mechanism of antimicrobial activity. *Applied Microbiology and Biotechnology* 90: 1847–1868.

120 Kiwi, J. and Nadtochenko, V. (2005). Evidence for the mechanism of photocatalytic degradation of the bacterial wall membrane at the TiO_2 interface by ATR-FTIR and laser kinetic spectroscopy. *Langmuir* 21: 4631–4641.

121 Amézaga-Madrid, P., Nevárez-Moorillón, G.V., Orrantia-Borunda, E., and Miki-Yoshida, M. (2002). Photoinduced bactericidal activity against *Pseudomonas aeruginosa* by TiO_2 based thin films. *FEMS Microbiology Letters* 211: 183–188.

122 Vatansever, F., de Melo, W.C.M.A., Avci, P. et al. (2013). Antimicrobial strategies centered around reactive oxygen species – bactericidal antibiotics, photodynamic therapy, and beyond. *FEMS Microbiology Reviews* 37: 955–989.

123 Maillard, J.-Y. (2002). Bacterial target sites for biocide action. *Journal of Applied Microbiology* 92: 16S–27S.

124 Rai, M., Yadav, A., and Gade, A. (2009). Silver nanoparticles as a new generation of antimicrobials. *Biotechnology Advances* 27: 76–83.

125 Noimark, S., Dunnill, C.W., Wilson, M., and Parkin, I.P. (2009). The role of surfaces in catheter-associated infections. *Chemical Society Reviews* 38: 3435–3448.

126 Appendini, P. and Hotchkiss, J.H. (2002). Review of antimicrobial food packaging. *Innovative Food Science & Emerging Technologies* 3: 113–126.

127 Duncan, T.V. (2011). Applications of nanotechnology in food packaging and food safety: barrier materials, antimicrobials and sensors. *Journal of Colloid and Interface Science* 363: 1–24.

128 Dunlop, P.S.M., Sheeran, C.P., Byrne, J.A. et al. (2010). Inactivation of clinically relevant pathogens by photocatalytic coatings. *Journal of Photochemistry and Photobiology A* 216: 303–310.

129 Yin, R., Agrawal, T., Khan, U. et al. (2015). Antimicrobial photodynamic inactivation in nanomedicine: small light strides against bad bugs. *Nanomedicine (London, England)* 10: 2379–2404.

130 Hamblin, M.R. and Hasan, T. (2004). Photodynamic therapy: a new antimicrobial approach to infectious disease? *Photochemical & Photobiological Sciences* 3: 436–450.

131 McCoy, C.P., O'Neil, E.J., Cowley, J.F. et al. (2014). Photodynamic antimicrobial polymers for infection control. *PLoS One* 9: e108500.

132 Bezman, S.A., Burtis, P.A., Izod, T.P.J., and Thayer, M.A. (1978). Photodynamic inactivation of *E. coli* by rose bengal immobilized on polystyrene beads. *Photochemistry and Photobiology* 28: 325–329.

133 Vecchio, D., Gupta, A., Huang, L. et al. (2015). Bacterial photodynamic inactivation mediated by methylene blue and red light is enhanced by synergistic effect of potassium iodide. *Antimicrobial Agents and Chemotherapy* 59: 5203–5212.

134 Wu, X., Huang, Y.-Y., Kushida, Y. et al. (2016). Broad-spectrum antimicrobial photocatalysis mediated by titanium dioxide and UVA is potentiated by addition of bromide ion via formation of hypobromite. *Free Radical Biology and Medicine* 95: 74–81.

135 Shah, M.S.A.S., Nag, M., Kalagara, T. et al. (2008). Silver on PEG-PU-TiO_2 polymer nanocomposite films: an excellent system for antibacterial applications. *Chemistry of Materials* 20: 2455–2460.

136 Chorianopoulos, N.G., Tsoukleris, D.S., Panagou, E.Z. et al. (2011). Use of titanium dioxide (TiO_2) photocatalysts as alternative means for *Listeria*

monocytogenes biofilm disinfection in food processing. *Food Microbiology* 28: 164–170.

137 Tsuang, Y.-H., Sun, J.-S., Huang, Y.-C. et al. (2008). Studies of photokilling of bacteria using titanium dioxide nanoparticles. *Artificial Organs* 32: 167–174.

138 Gosselin, R.A., Roberts, I., and Gillespie, W.J. (2004). Antibiotics for preventing infection in open limb fractures. *The Cochrane Database of Systematic Reviews* https://doi.org/10.1002/14651858.CD003764.pub2.

139 Lethaby, A., Temple, J., and Santy-Tomlinson, J. (2013). Pin site care for preventing infections associated with external bone fixators and pins. *The Cochrane Database of Systematic Reviews* https://doi.org/10.1002/14651858.CD004551.pub3.

140 Bosetti, M., Masse, A., Tobin, E., and Cannas, M. (2002). Silver coated materials for external fixation devices: *in vitro* biocompatibility and genotoxicity. *Biomaterials* 23: 887–892.

141 Collinge, C.A., Goll, G., Seligson, D., and Easley, K.J. (1994). Pin tract infections: silver vs uncoated pins. *Orthopedics* 17: 445–448.

142 Kühn, K.P., Chaberny, I.F., Massholder, K. et al. (2003). Disinfection of surfaces by photocatalytic oxidation with titanium dioxide and UVA light. *Chemosphere* 53: 71–77.

143 Watts, R.J., Kong, S., Orr, M.P. et al. (1995). Photocatalytic inactivation of coliform bacteria and viruses in secondary wastewater effluent. *Water Research* 29: 95–100.

144 Wei, C., Lin, W.Y., Zainal, Z. et al. (1994). Bactericidal activity of TiO_2 photocatalyst in aqueous media: toward a solar-assisted water disinfection system. *Environmental Science and Technology* 28: 934–938.

145 Yurt, F., Ince, M., Colak, S.G. et al. (2017). Investigation of *in vitro* PDT activities of zinc phthalocyanine immobilised TiO_2 nanoparticles. *International Journal of Pharmaceutics* 524: 467–474.

146 Yurt, F., Sarı, F.A., Ince, M. et al. (2018). Photodynamic therapy and nuclear imaging activities of SubPhthalocyanine integrated TiO_2 nanoparticles. *Journal of Photochemistry and Photobiology A* 367: 45–55.

147 Hou, Z., Zhang, Y., Deng, K. et al. (2015). UV-emitting upconversion-based TiO_2 photosensitizing nanoplatform: near-infrared light mediated *in vivo* photodynamic therapy via mitochondria-involved apoptosis pathway. *ACS Nano* 9: 2584–2599.

148 Tong, R., Lin, H., Chen, Y. et al. (2017). Near-infrared mediated chemo/photodynamic synergistic therapy with DOX-UCNPs@mSiO_2/TiO_2-TC nanocomposite. *Materials Science & Engineering C, Materials for Biological Applications* 78: 998–1005.

149 Zeng, L., Pan, Y., Tian, Y. et al. (2015). Doxorubicin-loaded $NaYF_4$:Yb/Tm-TiO_2 inorganic photosensitizers for NIR-triggered photodynamic therapy and enhanced chemotherapy in drug-resistant breast cancers. *Biomaterials* 57: 93–106.

150 Li, Q., Wang, X., Lu, X. et al. (2009). The incorporation of daunorubicin in cancer cells through the use of titanium dioxide whiskers. *Biomaterials* 30: 4708–4715.

151 Shen, S., Wu, L., Liu, J. et al. (2015). Core-shell structured Fe_3O_4@TiO_2-doxorubicin nanoparticles for targeted chemo-sonodynamic therapy of cancer. *International Journal of Pharmaceutics* 486: 380–388.

152 Yumita, N., Iwase, Y., Nishi, K. et al. (2012). Involvement of reactive oxygen species in sonodynamically induced apoptosis using a novel porphyrin derivative. *Theranostics* 2: 880–888.

153 Wang, P., Xiao, L., Wang, X. et al. (2010). Sonodynamic effects of protoporphyrin IX disodium salt on Ehrlich ascetic tumor cells. *Ultrasonics* 50: 634–638.

154 Yamaguchi, S., Kobayashi, H., Narita, T. et al. (2011). Sonodynamic therapy using water-dispersed TiO_2-polyethylene glycol compound on glioma cells: comparison of cytotoxic mechanism with photodynamic therapy. *Ultrasonics Sonochemistry* 18: 1197–1204.

155 Harada, A., Ono, M., Yuba, E., and Kono, K. (2013). Titanium dioxide nanoparticle-entrapped polyion complex micelles generate singlet oxygen in the cells by ultrasound irradiation for sonodynamic therapy. *Biomaterials Science* 1: 65–73.

156 Yoshikazu, T., Mao, Y., Norimichi, K., and Tsutomu, M. (2006). Anticancer effect of dye-sensitized TiO_2 nanocrystals by polychromatic visible light irradiation. *Chemistry Letters* 35: 496–497.

157 Saeed, M., Iqbal, M.Z., Ren, W. et al. (2019). Tunable fabrication of new theranostic Fe_3O_4-black TiO_2 nanocomposites: dual wavelength stimulated synergistic imaging-guided phototherapy in cancer. *Journal of Materials Chemistry B* 7: 210–223.

158 Feng, B., Weng, J., Yang, B.C. et al. (2003). Characterization of surface oxide films on titanium and adhesion of osteoblast. *Biomaterials* 24: 4663–4670.

159 Tautzenberger, A., Kovtun, A., and Ignatius, A. (2012). Nanoparticles and their potential for application in bone. *International Journal of Nanomedicine* 7: 4545–4557.

160 Sul, Y.T. (2010). Electrochemical growth behavior, surface properties, and enhanced in vivo bone response of TiO_2 nanotubes on microstructured surfaces of blasted, screw-shaped titanium implants. *International Journal of Nanomedicine* 5: 87–100.

161 Bjursten, L.M., Rasmusson, L., Oh, S. et al. (2010). Titanium dioxide nanotubes enhance bone bonding *in vivo*. *Journal of Biomedical Materials Research Part A* 92: 1218–1224.

162 UNESCO (2018). The United Nations World Water Development Report 2018: Nature-Based Solutions for Water.

163 Kirby, R.M., Bartram, J., and Carr, R. (2003). Water in food production and processing: quantity and quality concerns. *Food Control* 14: 283–299.

164 Compton, M., Willis, S., Rezaie, B., and Humes, K. (2018). Food processing industry energy and water consumption in the Pacific northwest. *Innovative Food Science & Emerging Technologies* 47: 371–383.

165 Valta, K., Kosanovic, T., Malamis, D. et al. (2015). Overview of water usage and wastewater management in the food and beverage industry. *Desalination and Water Treatment* 53: 3335–3347.

166 Ölmez, H. (2013). Water consumption, reuse and reduction strategies in food processing. In: *Sustainable Food Processing* (eds. B.K. Tiwari, T. Norton and N.M. Holden), 401–434. USA: John Wiley and Sons Ltd.
167 Khajeh, M., Laurent, S., and Dastafkan, K. (2013). Nanoadsorbents: classification, preparation, and applications (with emphasis on aqueous media). *Chemical Reviews* 113: 7728–7768.
168 Sadjadi, S. (2014). Nanocatalytic wastewater treatment system for the removal of toxic organic compounds. In: *Nanomaterials for Environmental Protection* (eds. B.I. Kharisov, O.V. Kharissova and D. HVR), 401–427. USA: John Wiley and Sons Ltd.
169 Papageorgiou, S.K., Katsaros, F.K., Favvas, E.P. et al. (2012). Alginate fibers as photocatalyst immobilizing agents applied in hybrid photocatalytic/ultrafiltration water treatment processes. *Water Research* 46: 1858–1872.
170 Veréb, G., Manczinger, L., Oszkó, A. et al. (2013). Highly efficient bacteria inactivation and phenol degradation by visible light irradiated iodine doped TiO_2. *Applied Catalysis B: Environmental* 129: 194–201.
171 Liu, Y., Li, J., Qiu, X., and Burda, C. (2006). Novel TiO_2 nanocatalysts for wastewater purification: tapping energy from the sun. *Water Science and Technology* 54: 47–54.
172 Likodimos, V., Han, C., Pelaez, M. et al. (2013). Anion-doped TiO_2 nanocatalysts for water purification under visible Light. *Industrial and Engineering Chemistry Research* 52: 13957–13964.
173 Anjum, M., Miandad, R., Waqas, M. et al. (2016). Remediation of wastewater using various nano-materials. *Arabian Journal of Chemistry* https://doi.org/10.1016/j.arabjc.2016.10.004.
174 Rodríguez, J., Paraguay-Delgado, F., López, A. et al. (2010). Synthesis and characterization of ZnO nanorod films for photocatalytic disinfection of contaminated water. *Thin Solid Films* 519: 729–735.
175 Rajendran, S., Khan, M.M., Gracia, F. et al. (2016). Ce^{3+}-ion-induced visible-light photocatalytic degradation and electrochemical activity of ZnO/CeO_2 nanocomposite. *Scientific Reports* 6: 31641.
176 Shu, J., Wang, Z., Xia, G. et al. (2014). One-pot synthesis of AgCl@Ag hybrid photocatalyst with high photocatalytic activity and photostability under visible light and sunlight irradiation. *Chemical Engineering Journal* 252: 374–381.
177 Yang, S.-F., Niu, C.-G., Huang, D.-W. et al. (2017). $SrTiO_3$ nanocubes decorated with Ag/AgCl nanoparticles as photocatalysts with enhanced visible-light photocatalytic activity towards the degradation of dyes, phenol and bisphenol A. *Environmental Science: Nano* 4: 585–595.
178 Das, T., Rocquefelte, X., Laskowski, R. et al. (2017). Investigation of the optical and excitonic properties of the visible light-driven photocatalytic $BiVO_4$ material. *Chemistry of Materials* 29: 3380–3386.
179 Yue, Z., Liu, A., Zhang, C. et al. (2017). Noble-metal-free hetero-structural CdS/Nb_2O_5/N-doped-graphene ternary photocatalytic system as visible-light-driven photocatalyst for hydrogen evolution. *Applied Catalysis B: Environmental* 201: 202–210.

180 Zhu, Y., Wang, Y., Chen, Z. et al. (2015). Visible light induced photocatalysis on CdS quantum dots decorated TiO_2 nanotube arrays. *Applied Catalysis A: General* 498: 159–166.

181 Carbajo, J., Bahamonde, A., and Faraldos, M. (2017). Photocatalyst performance in wastewater treatment applications: towards the role of TiO_2 properties. *Molecular Catalysis* 434: 167–174.

182 Behnajady, M.A., Eskandarloo, H., Modirshahla, N., and Shokri, M. (2011). Investigation of the effect of sol–gel synthesis variables on structural and photocatalytic properties of TiO_2 nanoparticles. *Desalination* 278: 10–17.

183 Kanakaraju, D. and Wong, S.P. (2018). Photocatalytic efficiency of TiO_2-biomass loaded mixture for wastewater treatment. *Journal of Chemistry* 2018: 14.

184 Yang, X., Chen, W., Huang, J. et al. (2015). Rapid degradation of methylene blue in a novel heterogeneous Fe_3O_4 @rGO@TiO_2-catalyzed photo-Fenton system. *Scientific Reports* 5: 10632.

185 Mascolo, M.C., Pei, Y., and Ring, T.A. (2013). Room temperature co-precipitation synthesis of magnetite nanoparticles in a large pH window with different bases. *Materials (Basel)* 6: 5549–5567.

186 Upadhyay, S., Parekh, K., and Pandey, B. (2016). Influence of crystallite size on the magnetic properties of Fe_3O_4 nanoparticles. *Journal of Alloys and Compounds* 678: 478–485.

187 Chen, Y., Yuan, T., Wang, F. et al. (2016). Magnetically separable Fe_3O_4@TiO_2 nanospheres: preparation and photocatalytic activity. *Journal of Materials Science* 27: 9983–9988.

188 Han, L., Li, Q., Chen, S. et al. (2017). A magnetically recoverable Fe_3O_4-NH_2-Pd sorbent for capture of mercury from coal derived fuel gas. *Scientific Reports* 7: 7448.

189 Bagbi, Y., Sarswat, A., Mohan, D. et al. (2017). Lead and chromium adsorption from water using L-cysteine functionalized magnetite (Fe_3O_4) nanoparticles. *Scientific Reports* 7: 7672.

190 Han, S., Yu, H., Yang, T. et al. (2017). Magnetic activated-ATP@Fe_3O_4 nanocomposite as an efficient Fenton-like heterogeneous catalyst for degradation of ethidium bromide. *Scientific Reports* 7: 6070.

191 Fagan, R., McCormack, D.E., Dionysiou, D.D., and Pillai, S.C. (2016). A review of solar and visible light active TiO_2 photocatalysis for treating bacteria, cyanotoxins and contaminants of emerging concern. *Materials Science in Semiconductor Processing* 42: 2–14.

192 Li, C.-C., Chang, S.-J., and Tai, M.-Y. (2010). Surface chemistry and dispersion property of TiO_2 nanoparticles. *Journal of the American Ceramic Society* 93: 4008–4010.

193 Cong, Y., Li, X., Qin, Y. et al. (2011). Carbon-doped TiO_2 coating on multiwalled carbon nanotubes with higher visible light photocatalytic activity. *Applied Catalysis B* 107: 128–134.

194 Jeon, S., Yun, J., Lee, Y.-S., and Kim, H.-I. (2012). Preparation of poly(vinyl alcohol)/poly(acrylic acid)/TiO_2/carbon nanotube composite nanofibers and their photobleaching properties. *Journal of Industrial and Engineering Chemistry* 18: 487–491.

195 Chen, J., Li, G., Huang, Y. et al. (2012). Optimization synthesis of carbon nanotubes-anatase TiO_2 composite photocatalyst by response surface methodology for photocatalytic degradation of gaseous styrene. *Applied Catalysis B* 123–124: 69–77.

196 Yang, M.-Q., Zhang, N., and Xu, Y.-J. (2013). Synthesis of fullerene–, carbon nanotube–, and graphene–TiO_2 nanocomposite photocatalysts for selective oxidation: a comparative study. *ACS Applied Materials & Interfaces* 5: 1156–1164.

197 Perera, S.D., Mariano, R.G., Vu, K. et al. (2012). Hydrothermal synthesis of graphene-TiO_2 nanotube composites with enhanced photocatalytic activity. *ACS Catalysis* 2: 949–956.

198 Williams, G., Seger, B., and Kamat, P.V. (2008). TiO_2-graphene nanocomposites. UV-assisted photocatalytic reduction of graphene oxide. *ACS Nano* 2: 1487–1491.

199 Baek, M.-H., Jung, W.-C., Yoon, J.-W. et al. (2013). Preparation, characterization and photocatalytic activity evaluation of micro- and mesoporous TiO_2/spherical activated carbon. *Journal of Industrial and Engineering Chemistry* 19: 469–477.

200 Politano, A. and Chiarello, G. (2013). Quenching of plasmons modes in air-exposed graphene-Ru contacts for plasmonic devices. *Applied Physics Letters* 102: 201608.

201 Ahmed, K., Nizami, S.S., and Raza, N.Z. (2013). Characteristics of natural rubber hybrid composites based on marble sludge/carbon black and marble sludge/rice husk derived silica. *Journal of Industrial and Engineering Chemistry* 19: 1169–1176.

202 Nardecchia, S., Carriazo, D., Ferrer, M.L. et al. (2013). Three dimensional macroporous architectures and aerogels built of carbon nanotubes and/or graphene: synthesis and applications. *Chemical Society Reviews* 42: 794–830.

203 Meng, L.-Y. and Park, S.-J. (2013). Influence of carbon nanofibers on electrochemical properties of carbon nanofibers/glass fibers composites. *Current Applied Physics* 13: 640–644.

204 Kim, K.-S. and Park, S.-J. (2012). Electrochemical performance of graphene/carbon electrode contained well-balanced micro- and mesopores by activation-free method. *Electrochimica Acta* 65: 50–56.

205 Kim, K.-S. and Park, S.-J. (2012). Synthesis and electrochemical performance of well-balanced mesopore/micropore contained carbons by activation-free method. *Electrochemistry Communications* 22: 89–92.

206 De Volder, M.F.L., Tawfick, S.H., Baughman, R.H., and Hart, A.J. (2013). Carbon nanotubes: present and future commercial applications. *Science* 339: 535–539.

207 Li, L., Wu, G., Yang, G. et al. (2013). Focusing on luminescent graphene quantum dots: current status and future perspectives. *Nanoscale* 5: 4015–4039.

208 Min, Y., He, G., Li, R. et al. (2013). Doping nitrogen anion enhanced photocatalytic activity on TiO_2 hybridized with graphene composite under solar light. *Separation and Purification Technology* 106: 97–104.

209 Lee, S.-Y. and Park, S.-J. (2011). Preparation and characterization of ordered porous carbons for increasing hydrogen storage behaviors. *Journal of Solid State Chemistry* 184: 2655–2660.

210 Kim, K.-S. and Park, S.-J. (2012). High electrochemical performance of carbon black-bonded carbon nanotubes for electrode materials. *Materials Research Bulletin* 47: 4146–4150.

211 Park, S.-J., Jung, Y., and Kim, S. (2012). Effect of fluorine–oxygen mixed gas treated graphite fibers on electrochemical behaviors of platinum–ruthenium nanoparticles toward methanol oxidation. *Journal of Fluorine Chemistry* 144: 124–129.

212 Kim, S., Cho, M.-H., Lee, J.-R., and Park, S.-J. (2006). Influence of plasma treatment of carbon blacks on electrochemical activity of Pt/carbon blacks catalysts for DMFCs. *Journal of Power Sources* 159: 46–48.

213 Yang, N., Liu, Y., Wen, H. et al. (2013). Photocatalytic properties of graphdiyne and graphene modified TiO_2: from theory to experiment. *ACS Nano* 7: 1504–1512.

214 Ng, Y.H., Ikeda, S., Matsumura, M., and Amal, R. (2012). A perspective on fabricating carbon-based nanomaterials by photocatalysis and their applications. *Energy & Environmental Science* 5: 9307–9318.

215 Chu, D., Yuan, X., Qin, G. et al. (2008). Efficient carbon-doped nanostructured TiO_2 (anatase) film for photoelectrochemical solar cells. *Journal of Nanoparticle Research* 10: 357–363.

216 Brunet, L., Lyon, D.Y., Hotze, E.M. et al. (2009). Comparative photoactivity and antibacterial properties of C_{60} fullerenes and titanium dioxide nanoparticles. *Environmental Science and Technology* 43: 4355–4360.

217 Sigmund, W., Yuh, J., Park, H. et al. (2006). Processing and structure relationships in electrospinning of ceramic fiber systems. *Journal of the American Ceramic Society* 89: 395–407.

218 Woan, K., Pyrgiotakis, G., and Sigmund, W. (2009). Photocatalytic carbon-nanotube–TiO_2 composites. *Advanced Materials* 21: 2233–2239.

219 Lee, S.-Y. and Park, S.-J. (2013). TiO_2 photocatalyst for water treatment applications. *Journal of Industrial and Engineering Chemistry* 19: 1761–1769.

220 Ou, Y., Lin, J., Fang, S., and Liao, D. (2006). MWNT–TiO_2:Ni composite catalyst: a new class of catalyst for photocatalytic H_2 evolution from water under visible light illumination. *Chemical Physics Letters* 429: 199–203.

221 Akhavan, O., Abdolahad, M., Abdi, Y., and Mohajerzadeh, S. (2009). Synthesis of titania/carbon nanotube heterojunction arrays for photoinactivation of *E. coli* in visible light irradiation. *Carbon* 47: 3280–3287.

222 Chen, Y., Crittenden, J.C., Hackney, S. et al. (2005). Preparation of a novel TiO_2-based p–n junction nanotube photocatalyst. *Environmental Science and Technology* 39: 1201–1208.

223 Luo, Y., Heng, Y., Dai, X. et al. (2009). Preparation and photocatalytic ability of highly defective carbon nanotubes. *Journal of Solid State Chemistry* 182: 2521–2525.

224 Ewa, K. and Sven, R. (2010). Photoreactors for wastewater treatment: a review. *Recent Patents on Engineering* 4: 242–266.

225 Mozia, S. (2010). Photocatalytic membrane reactors (PMRs) in water and wastewater treatment. A review. *Separation and Purification Technology* 73: 71–91.

226 Matsunaga, T. and Inagaki, M. (2006). Carbon-coated anatase for oxidation of methylene blue and NO. *Applied Catalysis B: Environmental* 64: 9–12.

227 Ali, F., Khan, S.B., Kamal, T. et al. (2018). Chitosan-titanium oxide fibers supported zero-valent nanoparticles: highly efficient and easily retrievable catalyst for the removal of organic pollutants. *Scientific Reports* 8: 6260.

228 Rengifo-Herrera, J.A., Marín-Silva, D.A., Mendoza-Portillo, E. et al. (2018). Chitosan films containing TiO_2 nanoparticles modified with tungstophosphoric acid for the photobleaching of malachite green in solid-gas interfaces upon different wavelengths. *Molecular Catalysis* 448: 1–9.

229 Alinsafi, A., Khemis, M., Pons, M.N. et al. (2005). Electro-coagulation of reactive textile dyes and textile wastewater. *Chemical Engineering and Processing* 44: 461–470.

230 Vimonses, V., Lei, S., Jin, B. et al. (2009). Adsorption of congo red by three Australian kaolins. *Applied Clay Science* 43: 465–472.

231 Sial, R.A., Chaudhary, M.F., Abbas, S.T. et al. (2006). Quality of effluents from Hattar Industrial Estate. *Journal of Zhejiang University Science B* 7: 974–980.

232 Phiri, O., Mumba, P., Moyo, B.H.Z., and Kadewa, W. (2005). Assessment of the impact of industrial effluents on water quality of receiving rivers in urban areas of Malawi. *International Journal of Environmental Science and Technology* 2: 237–244.

233 Ahmad, M., Bajahlan, A.S., and Hammad, W.S. (2008). Industrial effluent quality, pollution monitoring and environmental management. *Environmental Monitoring and Assessment* 147: 297–306.

234 Oyekale, A.S. and Oyekale, T.O. (2017). Healthcare waste management practices and safety indicators in Nigeria. *BMC Public Health* 17: 740.

235 Ali, M. and Kuroiwa, C. (2009). Status and challenges of hospital solid waste management: case studies from Thailand, Pakistan, and Mongolia. *Journal of Material Cycles and Waste Management* 11: 251–257.

236 Emmanuel, E., Perrodin, Y., Keck, G. et al. (2005). Ecotoxicological risk assessment of hospital wastewater: a proposed framework for raw effluents discharging into urban sewer network. *Journal of Hazardous Materials* 117: 1–11.

237 Verlicchi, P., Galletti, A., Petrovic, M., and Barceló, D. (2010). Hospital effluents as a source of emerging pollutants: an overview of micropollutants and sustainable treatment options. *Journal of Hydrology* 389: 416–428.

238 Putschew, A., Wischnack, S., and Jekel, M. (2000). Occurrence of triiodinated X-ray contrast agents in the aquatic environment. *Science of the Total Environment* 255: 129–134.

239 Sacher, F., Lange, F.T., Brauch, H.J., and Blankenhorn, I. (2001). Pharmaceuticals in groundwaters analytical methods and results of a monitoring program in Baden-Wurttemberg, Germany. *Journal of Chromatography A* 938: 199–210.

240 Anderson, P.D., D'Aco, V.J., Shanahan, P. et al. (2004). Screening analysis of human pharmaceutical compounds in U.S. surface waters. *Environmental Science and Technology* 38: 838–849.

241 Šuligoj, A., Štangar, U.L., and Tušar, N.N. (2014). Photocatalytic air-cleaning using TiO_2 nanoparticles in porous silica substrate. *Chemical Papers* 68: 1265–1272.

242 Taranto, J., Frochot, D., and Pichat, P. (2009). Photocatalytic air purification: comparative efficacy and pressure drop of a TiO_2-coated thin mesh and a honeycomb monolith at high air velocities using a 0.4 m^3 close-loop reactor. *Separation and Purification Technology* 67: 187–193.

243 Tasbihi, M., Kete, M., Raichur, A.M. et al. (2012). Photocatalytic degradation of gaseous toluene by using immobilized titania/silica on aluminum sheets. *Environmental Science and Pollution Research* 19: 3735–3742.

244 Prieto, O., Fermoso, J., and Irusta, R. (2007). Photocatalytic degradation of toluene in air using a fluidized bed photoreactor. *International Journal of Photoenergy* 2007: 8.

245 Adams, M., Skillen, N., McCullagh, C., and Robertson, P.K.J. (2013). Development of a doped titania immobilised thin film multi tubular photoreactor. *Applied Catalysis B* 130–131: 99–105.

246 Tasbihi, M., Štangar, U.L., Černigoj, U., and Kogej, K. (2009). Low-temperature synthesis and characterization of anatase TiO_2 powders from inorganic precursors. *Photochemical & Photobiological Sciences* 8: 719–725.

247 Zita, J., Krýsa, J., Černigoj, U. et al. (2011). Photocatalytic properties of different TiO_2 thin films of various porosity and titania loading. *Catalysis Today* 161: 29–34.

248 Arıer, Ü.Ö.A. and Tepehan, F.Z. (2011). Influence of heat treatment on the particle size of nanobrookite TiO_2 thin films produced by sol–gel method. *Surface and Coatings Technology* 206: 37–42.

249 Folli, A., Pade, C., Hansen, T.B. et al. (2012). TiO_2 photocatalysis in cementitious systems: insights into self-cleaning and depollution chemistry. *Cement and Concrete Research* 42: 539–548.

250 Fu, P., Luan, Y., and Dai, X. (2004). Preparation of activated carbon fibers supported TiO_2 photocatalyst and evaluation of its photocatalytic reactivity. *Journal of Molecular Catalysis A* 221: 81–88.

251 Ye, S.-Y., Li, M.-B., Song, X.-L. et al. (2011). Enhanced photocatalytic decomposition of gaseous ozone in cold storage environments using a TiO_2/ACF film. *Chemical Engineering Journal* 167: 28–34.

252 Ye, S.-Y., Tian, Q.-M., Song, X.-L., and Luo, S.-C. (2009). Photoelectrocatalytic degradation of ethylene by a combination of TiO_2 and activated carbon felts. *Journal of Photochemistry and Photobiology A* 208: 27–35.

253 Chen, S.-Z., Zhang, P.-Y., Zhu, W.-P. et al. (2006). Deactivation of TiO_2 photocatalytic films loaded on aluminium: XPS and AFM analyses. *Applied Surface Science* 252: 7532–7538.

254 Novotna, P., Krysa, J., Maixner, J. et al. (2010). Photocatalytic activity of sol–gel TiO_2 thin films deposited on soda lime glass and soda lime

glass precoated with a SiO_2 layer. *Surface and Coatings Technology* 204: 2570–2575.

255 Černigoj, U., Štangar, U.L., Trebše, P. et al. (2006). Photocatalytically active TiO_2 thin films produced by surfactant-assisted sol–gel processing. *Thin Solid Films* 495: 327–332.

256 Zita, J., Krýsa, J., and Mills, A. (2009). Correlation of oxidative and reductive dye bleaching on TiO_2 photocatalyst films. *Journal of Photochemistry and Photobiology A* 203: 119–124.

257 Štangar, U.L., Černigoj, U., Trebše, P. et al. (2006). Photocatalytic TiO_2 coatings: effect of substrate and template. *Monatshefte für Chemie / Chemical Monthly* 137: 647–655.

258 Novotná, P., Zita, J., Krýsa, J. et al. (2008). Two-component transparent TiO_2/SiO_2 and TiO_2/PDMS films as efficient photocatalysts for environmental cleaning. *Applied Catalysis B* 79: 179–185.

259 Çamurlu, H.E., Kesmez, Ö., Burunkaya, E. et al. (2012). Sol–gel thin films with anti-reflective and self-cleaning properties. *Chemical Papers* 66: 461–471.

260 Yao, P., Liu, H., Wang, D. et al. (2018). Enhanced visible-light photocatalytic activity to volatile organic compounds degradation and deactivation resistance mechanism of titania confined inside a metal-organic framework. *Journal of Colloid and Interface Science* 522: 174–182.

261 Burton, A. (2012). Titanium dioxide photocleans polluted air. *Environmental Health Perspectives* 120 https://doi.org/10.1289/ehp.120-a229.

262 Le, T.S., Dao, T.H., Nguyen, D.C. et al. (2015). Air purification equipment combining a filter coated by silver nanoparticles with a nano-TiO_2 photocatalyst for use in hospitals. *Advances in Natural Sciences* 6: 015016.

263 Haider, A., Al-Anbari, R., Kadhim, G., and Jameel, Z. (2018). Synthesis and photocatalytic activity for TiO_2 nanoparticles as air purification. *MATEC Web of Conferences* 162: 05006.

264 Shah, S.N.A., Shah, Z., Hussain, M., and Khan, M. (2017). Hazardous effects of titanium dioxide nanoparticles in ecosystem. *Bioinorganic Chemistry and Applications* 2017: 12.

265 Baraton, M.-I. and Merhari, L. (2004). Surface chemistry of TiO_2 nanoparticles: influence on electrical and gas sensing properties. *Journal of the European Ceramic Society* 24: 1399–1404.

266 Liu, X., Chen, G., Keller, A.A., and Su, C. (2013). Effects of dominant material properties on the stability and transport of TiO_2 nanoparticles and carbon nanotubes in aquatic environments: from synthesis to fate. *Environmental Science* 15: 169–189.

267 Juhasz, G. (2018). Electrochemical properties of anatase-type TiO_2 nanoparticles with different morphology. *ECS Transactions* 85: 3–10.

268 Hou, Y., Abrams, B.L., Vesborg, P.C. et al. (2011). Bioinspired molecular co-catalysts bonded to a silicon photocathode for solar hydrogen evolution. *Nature Materials* 10: 434–438.

269 Paracchino, A., Laporte, V., Sivula, K. et al. (2011). Highly active oxide photocathode for photoelectrochemical water reduction. *Nature Materials* 10: 456–461.

270 Maeda, K., Xiong, A., Yoshinaga, T. et al. (2010). Photocatalytic overall water splitting promoted by two different cocatalysts for hydrogen and oxygen evolution under visible light. *Angewandte Chemie International Edition* 49: 4096–4099.

271 Kudo, A. and Miseki, Y. (2009). Heterogeneous photocatalyst materials for water splitting. *Chemical Society Reviews* 38: 253–278.

272 Liu, S., Yu, J., and Jaroniec, M. (2011). Anatase TiO_2 with dominant high-energy {001} facets: synthesis, properties, and applications. *Chemistry of Materials* 23: 4085–4093.

273 Yu, J., Qi, L., and Jaroniec, M. (2010). Hydrogen production by photocatalytic water splitting over Pt/TiO_2 nanosheets with exposed (001) facets. *The Journal of Physical Chemistry C* 114: 13118–13125.

274 Ksibi, M., Rossignol, S., Tatibouët, J.-M., and Trapalis, C. (2008). Synthesis and solid characterization of nitrogen and sulfur-doped TiO_2 photocatalysts active under near visible light. *Materials Letters* 62: 4204–4206.

275 Park, J.H., Kim, S., and Bard, A.J. (2006). Novel carbon-doped TiO_2 nanotube arrays with high aspect ratios for efficient solar water splitting. *Nano Letters* 6: 24–28.

276 Yu, J. and Ran, J. (2011). Facile preparation and enhanced photocatalytic H_2-production activity of $Cu(OH)_2$ cluster modified TiO_2. *Energy & Environmental Science* 4: 1364–1371.

277 Murdoch, M., Waterhouse, G.I., Nadeem, M.A. et al. (2011). The effect of gold loading and particle size on photocatalytic hydrogen production from ethanol over Au/TiO_2 nanoparticles. *Nature Chemistry* 3: 489–492.

278 Zuo, F., Wang, L., Wu, T. et al. (2010). Self-doped Ti^{3+} enhanced photocatalyst for hydrogen production under visible light. *Journal of the American Chemical Society* 132: 11856–11857.

279 Li, Y. and Zhang, J.Z. (2010). Hydrogen generation from photoelectrochemical water splitting based on nanomaterials. *Laser & Photonics Reviews* 4: 517–528.

280 Walter, M.G., Warren, E.L., McKone, J.R. et al. (2010). Solar water splitting cells. *Chemical Reviews* 110: 6446–6473.

281 Justicia, I., Ordejón, P., Canto, G. et al. (2002). Designed self-doped titanium oxide thin films for efficient visible-light photocatalysis. *Advanced Materials* 14: 1399–1402.

282 Asahi, R., Morikawa, T., Ohwaki, T. et al. (2001). Visible-light photocatalysis in nitrogen-doped titanium oxides. *Science* 293: 269–271.

283 Thompson, T.L. and Yates, J.T. (2006). Surface science studies of the photoactivation of TiO_2 - new photochemical processes. *Chemical Reviews* 106: 4428–4453.

284 Kim, H.G., Hwang, D.W., and Lee, J.S. (2004). An undoped, single-phase oxide photocatalyst working under visible light. *Journal of the American Chemical Society* 126: 8912–8913.

285 Chen, X., Shen, S., Guo, L., and Mao, S.S. (2010). Semiconductor-based photocatalytic hydrogen generation. *Chemical Reviews* 110: 6503–6570.

286 Wang, G., Wang, H., Ling, Y. et al. (2011). Hydrogen-treated TiO_2 nanowire arrays for photoelectrochemical water splitting. *Nano Letters* 11: 3026–3033.

287 Murphy, A.B., Barnes, P.R.F., Randeniya, L.K. et al. (2006). Efficiency of solar water splitting using semiconductor electrodes. *International Journal of Hydrogen Energy* 31: 1999–2017.

288 Bian, Z., Tachikawa, T., Zhang, P. et al. (2014). Au/TiO_2 superstructure-based plasmonic photocatalysts exhibiting efficient charge separation and unprecedented activity. *Journal of the American Chemical Society* 136: 458–465.

289 Crossland, E.J., Noel, N., Sivaram, V. et al. (2013). Mesoporous TiO_2 single crystals delivering enhanced mobility and optoelectronic device performance. *Nature* 495: 215–219.

290 Crepaldi, E.L., GJAA, S.-I., Grosso, D. et al. (2003). Controlled formation of highly organized mesoporous titania thin films: from mesostructured hybrids to mesoporous nanoanatase TiO_2. *Journal of the American Chemical Society* 125: 9770–9786.

291 Vivero-Escoto, J.L., Chiang, Y.D., Wu, K., and Yamauchi, Y. (2012). Recent progress in mesoporous titania materials: adjusting morphology for innovative applications. *Science and Technology of Advanced Materials* 13: 013003.

292 Zhou, W. and Fu, H. (2013). Mesoporous TiO_2: preparation, doping, and as a composite for photocatalysis. *ChemCatChem* 5: 885–894.

293 Li, W., Wu, Z., Wang, J. et al. (2014). A perspective on mesoporous TiO_2 materials. *Chemistry of Materials* 26: 287–298.

294 Joo, J.B., Zhang, Q., Dahl, M. et al. (2012). Control of the nanoscale crystallinity in mesoporous TiO_2 shells for enhanced photocatalytic activity. *Energy & Environmental Science* 5: 6321–6327.

295 Zhou, W., Sun, F., Pan, K. et al. (2011). Well-ordered large-pore mesoporous anatase TiO_2 with remarkably high thermal stability and improved crystallinity: preparation, characterization, and photocatalytic performance. *Advanced Functional Materials* 21: 1922–1930.

296 Liu, G., Zhao, Y., Sun, C. et al. (2008). Synergistic effects of B/N doping on the visible-light photocatalytic activity of mesoporous TiO_2. *Angewandte Chemie International Edition* 47: 4516–4520.

297 Li, H., Bian, Z., Zhu, J. et al. (2007). Mesoporous Au/TiO_2 nanocomposites with enhanced photocatalytic activity. *Journal of the American Chemical Society* 129: 4538–4539.

298 Zhang, R., Tu, B., and Zhao, D. (2010). Synthesis of highly stable and crystalline mesoporous anatase by using a simple surfactant sulfuric acid carbonization method. *Chemistry A European Journal* 16: 9977–9981.

299 Zhou, W., Li, W., Wang, J.-Q. et al. (2014). Ordered mesoporous black TiO_2 as highly efficient hydrogen evolution photocatalyst. *Journal of the American Chemical Society* 136: 9280–9283.

300 Xiang, Q., Yu, J., and Jaroniec, M. (2012). Synergetic effect of MoS_2 and graphene as cocatalysts for enhanced photocatalytic H_2 production activity of TiO_2 nanoparticles. *Journal of the American Chemical Society* 134: 6575–6578.

301 Hinnemann, B., Moses, P.G., Bonde, J. et al. (2005). Biomimetic hydrogen evolution: MoS_2 nanoparticles as catalyst for hydrogen evolution. *Journal of the American Chemical Society* 127: 5308–5309.

302 Li, Y., Wang, H., Xie, L. et al. (2011). MoS_2 nanoparticles grown on graphene: an advanced catalyst for the hydrogen evolution reaction. *Journal of the American Chemical Society* 133: 7296–7299.

303 Karunadasa, H.I., Montalvo, E., Sun, Y. et al. (2012). A molecular MoS_2 edge site mimic for catalytic hydrogen generation. *Science* 335: 698–702.

304 Bonde, J., Moses, P.G., Jaramillo, T.F. et al. (2009). Hydrogen evolution on nano-particulate transition metal sulfides. *Faraday Discussions* 140: 219–231.

305 Jaramillo, T.F., Jorgensen, K.P., Bonde, J. et al. (2007). Identification of active edge sites for electrochemical H_2 evolution from MoS_2 nanocatalysts. *Science* 317: 100–102.

306 Kanda, S., Akita, T., Fujishima, M., and Tada, H. (2011). Facile synthesis and catalytic activity of MoS_2/TiO_2 by a photodeposition-based technique and its oxidized derivative MoO_3/TiO_2 with a unique photochromism. *Journal of Colloid and Interface Science* 354: 607–610.

307 Zong, X., Yan, H., Wu, G. et al. (2008). Enhancement of photocatalytic H_2 evolution on CdS by loading MoS_2 as cocatalyst under visible light irradiation. *Journal of the American Chemical Society* 130: 7176–7177.

308 Xiang, Q., Yu, J., and Jaroniec, M. (2011). Enhanced photocatalytic H_2-production activity of graphene-modified titania nanosheets. *Nanoscale* 3: 3670–3678.

309 Lightcap, I.V., Kosel, T.H., and Kamat, P.V. (2010). Anchoring semiconductor and metal nanoparticles on a two-dimensional catalyst mat. Storing and shuttling electrons with reduced graphene oxide. *Nano Letters* 10: 577–583.

310 Liang, Y., Li, Y., Wang, H. et al. (2011). Co_3O_4 nanocrystals on graphene as a synergistic catalyst for oxygen reduction reaction. *Nature Materials* 10: 780–786.

311 Li, Q., Guo, B., Yu, J. et al. (2011). Highly efficient visible-light-driven photocatalytic hydrogen production of CdS-cluster-decorated graphene nanosheets. *Journal of the American Chemical Society* 133: 10878–10884.

312 Chen, H., Zhao, R., Wang, B. et al. (2017). The effects of orally administered Ag, TiO_2 and SiO_2 nanoparticles on gut microbiota composition and colitis induction in mice. *NanoImpact* 8: 80–88.

313 Singh, P.K., Jairath, G., and Ahlawat, S.S. (2016). Nanotechnology: a future tool to improve quality and safety in meat industry. *Journal of Food Science and Technology* 53: 1739–1749.

314 Sadeghi, R., Rodriguez, R.J., Yao, Y., and Kokini, J.L. (2017). Advances in nanotechnology as they pertain to food and agriculture: benefits and risks. *Annual Review of Food Science and Technology* 8: 467–492.

315 Jaroenworaluck, A., Sunsaneeyametha, W., Kosachan, N., and Stevens, R. (2006). Characteristics of silica-coated TiO_2 and its UV absorption for sunscreen cosmetic applications. *Surface and Interface Analysis* 38: 473–477.

316 Othman, S.H., Abd Salam, N.R., Zainal, N. et al. (2014). Antimicrobial activity of TiO_2 nanoparticle-coated film for potential food packaging applications. *International Journal of Photoenergy* 2014: 6.

317 Manesh, R.R., Grassi, G., Bergami, E. et al. (2018). Co-exposure to titanium dioxide nanoparticles does not affect cadmium toxicity in radish seeds (*Raphanus sativus*). *Ecotoxicology and Environmental Safety* 148: 359–366.

318 Feizi, H., Rezvani Moghaddam, P., Shahtahmassebi, N., and Fotovat, A. (2012). Impact of bulk and nanosized titanium dioxide (TiO_2) on wheat seed germination and seedling growth. *Biological Trace Element Research* 146: 101–106.

319 Dudefoi, W., Moniz, K., Allen-Vercoe, E. et al. (2017). Impact of food grade and nano-TiO_2 particles on a human intestinal community. *Food and Chemical Toxicology* 106: 242–249.

320 Lewicka, Z.A., Benedetto, A.F., Benoit, D.N. et al. (2011). The structure, composition, and dimensions of TiO_2 and ZnO nanomaterials in commercial sunscreens. *Journal of Nanoparticle Research* 13: 3607.

321 Lu, P.-J., Huang, S.-C., Chen, Y.-P. et al. (2015). Analysis of titanium dioxide and zinc oxide nanoparticles in cosmetics. *Journal of Food and Drug Analysis* 23: 587–594.

322 Labille, J., Feng, J., Botta, C. et al. (2010). Aging of TiO_2 nanocomposites used in sunscreen. Dispersion and fate of the degradation products in aqueous environment. *Environmental Pollution* 158: 3482–3489.

323 Wang, Y., Sun, C., Zhao, X. et al. (2016). The application of nano-TiO_2 photo semiconductors in agriculture. *Nanoscale Research Letters* 11: 529.

324 Higarashi, M.M. and Jardim, W.F. (2002). Remediation of pesticide contaminated soil using TiO_2 mediated by solar light. *Catalysis Today* 76: 201–207.

325 Robles-González, I.V., Fava, F., and Poggi-Varaldo, H.M. (2008). A review on slurry bioreactors for bioremediation of soils and sediments. *Microbial Cell Factories* 7: 5.

326 Tomei, M.C. and Daugulis, A.J. (2013). Ex situ bioremediation of contaminated soils: an overview of conventional and innovative technologies. *Critical Reviews in Environmental Science and Technology* 43: 2107–2139.

327 Kuyukina, M.S., Ivshina, I.B., Ritchkova, M.I. et al. (2003). Bioremediation of crude oil-contaminated soil using slurry-phase biological treatment and land farming techniques. *Soil and Sediment Contamination* 12: 85–99.

328 Nogueira, A.A., Bassin, J.P., Cerqueira, A.C., and Dezotti, M. (2016). Integration of biofiltration and advanced oxidation processes for tertiary treatment of an oil refinery wastewater aiming at water reuse. *Environmental Science and Pollution Research International* 23: 9730–9741.

329 Kyriacou, A., Lasaridi, K.E., Kotsou, M. et al. (2005). Combined bioremediation and advanced oxidation of green table olive processing wastewater. *Process Biochemistry* 40: 1401–1408.

330 Rubalcaba, A., Suarez-Ojeda, M.E., Stuber, F. et al. (2007). Phenol wastewater remediation: advanced oxidation processes coupled to a biological treatment. *Water Science and Technology* 55: 221–227.

331 Wang, A.N., Teng, Y., Hu, X.F. et al. (2016). Diphenylarsinic acid contaminated soil remediation by titanium dioxide (P25) photocatalysis: degradation pathway, optimization of operating parameters and effects of soil properties. *The Science of the Total Environment* 541: 348–355.

332 Wang, T.C., Lu, N., Li, J., and Wu, Y. (2011). Plasma-TiO_2 catalytic method for high-efficiency remediation of *p*-nitrophenol contaminated soil in pulsed discharge. *Environmental Science and Technology* 45: 9301–9307.

333 Uberoi, V. and Bhattacharya, S.K. (1997). Toxicity and degradability of nitrophenols in anaerobic systems. *Water Environment Research* 69: 146–156.

334 Zhao, Q., Liu, X., Sun, M. et al. (2015). Natural kaolin derived stable SBA-15 as a support for Fe/BiOCl: a novel and efficient Fenton-like catalyst for the degradation of 2-nitrophenol. *RSC Advances* 5: 36948–36956.

335 Ahmed, S., Rasul, M.G., Brown, R., and Hashib, M.A. (2011). Influence of parameters on the heterogeneous photocatalytic degradation of pesticides and phenolic contaminants in wastewater: a short review. *Journal of Environmental Management* 92: 311–330.

336 Dai, K., Peng, T., Chen, H. et al. (2008). Photocatalytic degradation and mineralization of commercial methamidophos in aqueous titania suspension. *Environmental Science and Technology* 42: 1505–1510.

337 Cao, Y., Yi, L., Huang, L. et al. (2006). Mechanism and pathways of chlorfenapyr photocatalytic degradation in aqueous suspension of TiO_2. *Environmental Science and Technology* 40: 3373–3377.

338 Parida, K.M., Sahu, N., Biswal, N.R. et al. (2008). Preparation, characterization, and photocatalytic activity of sulfate-modified titania for degradation of methyl orange under visible light. *Journal of Colloid and Interface Science* 318: 231–237.

339 Guan, H., Chi, D., Yu, J., and Li, X. (2008). A novel photodegradable insecticide: preparation, characterization and properties evaluation of nano-imidacloprid. *Pesticide Biochemistry and Physiology* 92: 83–91.

340 Ramos-Delgado, N.A., Gracia-Pinilla, M.A., Maya-Treviño, L. et al. (2013). Solar photocatalytic activity of TiO_2 modified with WO_3 on the degradation of an organophosphorus pesticide. *Journal of Hazardous Materials* 263: 36–44.

341 Leghari, S.A.K., Sajjad, S., Chen, F., and Zhang, J. (2011). WO_3/TiO_2 composite with morphology change via hydrothermal template-free route as an efficient visible light photocatalyst. *Chemical Engineering Journal* 166: 906–915.

342 Attarchi, N., Montazer, M., and Toliyat, T. (2013). $Ag/TiO_2/\beta$-CD nano composite: preparation and photo catalytic properties for methylene blue degradation. *Applied Catalysis A: General* 467: 107–116.

343 Zhang, X., Wu, F., Wang, Z. et al. (2009). Photocatalytic degradation of 4,4′-biphenol in TiO_2 suspension in the presence of cyclodextrins: a trinity integrated mechanism. *Journal of Molecular Catalysis A* 301: 134–139.

344 Affam, A.C. and Chaudhuri, M. (2013). Degradation of pesticides chlorpyrifos, cypermethrin and chlorothalonil in aqueous solution by TiO_2 photocatalysis. *Journal of Environmental Management* 130: 160–165.

345 Konstantinou, I.K., Sakellarides, T.M., Sakkas, V.A., and Albanis, T.A. (2001). Photocatalytic degradation of selected s-triazine herbicides and organophosphorus insecticides over aqueous TiO_2 suspensions. *Environmental Science and Technology* 35: 398–405.

346 Parra, S., Olivero, J., and Pulgarin, C. (2002). Relationships between physicochemical properties and photoreactivity of four biorecalcitrant phenylurea herbicides in aqueous TiO_2 suspension. *Applied Catalysis B* 36: 75–85.

347 Vulliet, E., Emmelin, C., Chovelon, J.-M. et al. (2002). Photocatalytic degradation of sulfonylurea herbicides in aqueous TiO_2. *Applied Catalysis B* 38: 127–137.

348 Ahmari, H., Zeinali Heris, S., and Hassanzadeh Khayyat, M. (2016). Photo catalytic degradation of linear alkylbenzene sulfonic acid. *Research on Chemical Intermediates* 42: 6587–6606.

349 Žabar, R., Komel, T., Fabjan, J. et al. (2012). Photocatalytic degradation with immobilised TiO_2 of three selected neonicotinoid insecticides: imidacloprid, thiamethoxam and clothianidin. *Chemosphere* 89: 293–301.

350 Malato, S., Caceres, J., Aguera, A. et al. (2001). Degradation of imidacloprid in water by photo-Fenton and TiO_2 photocatalysis at a solar pilot plant: a comparative study. *Environmental Science and Technology* 35: 4359–4366.

351 Agüera, A., Almansa, E., Malato, S. et al. (1998). Evaluation of photocatalytic degradation of imidacloprid in industrial water by GC-MS and LC-MS. *Analusis* 26: 245–250.

352 Siddle, G.R. (1975). The prospects for titanium dioxide in the paint industry. *Pigment & Resin Technology* 4: 4–12.

353 Larue, C., Castillo-Michel, H., Sobanska, S. et al. (2014). Fate of pristine TiO_2 nanoparticles and aged paint-containing TiO_2 nanoparticles in lettuce crop after foliar exposure. *Journal of Hazardous Materials* 273: 17–26.

354 Kaegi, R., Ulrich, A., Sinnet, B. et al. (2008). Synthetic TiO_2 nanoparticle emission from exterior facades into the aquatic environment. *Environmental Pollution* 156: 233–239.

355 Al-Kattan, A., Wichser, A., Zuin, S. et al. (2014). Behavior of TiO_2 released from nano-TiO_2-containing paint and comparison to pristine nano-TiO_2. *Environmental Science and Technology* 48: 6710–6718.

356 Tao, H., He, Y., and Zhao, X. (2015). Preparation and characterization of calcium carbonate–titanium dioxide core–shell ($CaCO_3$@TiO_2) nanoparticles and application in the papermaking industry. *Powder Technology* 283: 308–314.

357 Shen, J., Song, Z., Qian, X., and Liu, W. (2009). Modification of papermaking grade fillers: a brief review. 4: 20.

358 Shen, J., Song, Z., Qian, X., and Yang, F. (2010). Carboxymethyl cellulose/alum modified precipitated calcium carbonate fillers: preparation and their use in papermaking. *Carbohydrate Polymers* 81: 545–553.

359 Zhang, Y., Liu, Y., Ge, C. et al. (2009). Evolution mechanism of alumina nanofilms on rutile TiO_2 starting from sodium metaaluminate and the pigmentary properties. *Powder Technology* 192: 171–177.

360 Lu, Z., Ren, M., Yin, H. et al. (2009). Preparation of nanosized anatase TiO_2-coated kaolin composites and their pigmentary properties. *Powder Technology* 196: 122–125.

361 Amin, K.A.M. and Panhuis, M.I. (2012). Reinforced materials based on chitosan, TiO_2 and Ag composites. *Polymers* 4: 590–599.

362 Kavitha, K., Prabhu, M., Rajendran, V. et al. (2013). Optimization of nano-titania and titania–chitosan nanocomposite to enhance biocompatibility. *Current Nanoscience* 9: 308–317.

363 Akakuru, O.U., Louis, H., Uwaoma, R. et al. (2019). Novel highly-swellable and pH-responsive slow release formulations of clotrimazole with chitosan-g-PEG/starch microparticles. *Reactive and Functional Polymers* 135: 32–43.

364 Akakuru, O.U., Louis, H., Akakuru, O.C., and Eno, E.A. (2019). Facile fabrication of pH-responsive and swellable slow release microparticles of chlorpheniramine maleate with chitosan-starch matrices and their crosslinks. *International Journal of Polymeric Materials and Polymeric Biomaterials*: 1–15. https://doi.org/10.1080/00914037.2018.1563084.

365 Ariafar, A.A., Afsharpour, M., and Samanian, K. (2018). Use of TiO_2/chitosan nanoparticles for enhancing the preservative effects of carboxymethyl cellulose in paper-art-works against biodeterioration. *International Biodeterioration & Biodegradation* 131: 67–77.

2

Toxicity of TiO_2 Nanoparticles

*Gohar I. Dar[1,2], Madiha Saeed[1,2], and Aiguo Wu[1]**

[1] *Cixi Institute of Biomedical Engineering, CAS Key Laboratory of Magnetic Materials and Devices, & Key Laboratory of Additive Manufacturing Materials of Zhejiang Province, Ningbo Institute of Materials Technology and Engineering, Chinese Academy of Sciences, 1219 Zhongguan West Road, Zhenhai District, Ningbo, 315201, P.R. China*
[2] *University of Chinese Academy of Sciences, No.19(A) Yuquan Road, Shijingshan District, Beijing, 100049, P.R. China*

CHAPTER MENU

Introduction, 67
Modes of Exposure, Biodistribution, Clearance, and Fate of TiO_2 NPs, 70
Cell Death Pathways Induced by TiO_2 NPs, 74
Toxicity of TiO_2, 77
Alternative Perspective, 88
Conclusion, 89

2.1 Introduction

Nanotechnology and nanomedicine are the complementary disciplines having marvelous applications in many areas aimed at the improvement of human life. The development of nanotechnology has resulted in massive production of nanoparticle (NP)-based products that ultimately lead to the rapid development in their applications in diverse areas of life. However, NPs having various interfaces are capable to interact with the biological entities and impair their structure and functions. NPs are able to undergo cellular and molecular interactions in a biological environment. Therefore, the toxicity of NPs is a complicated issue [1–11]. The understanding of the underlying key mechanism of toxicity is of paramount importance in resolving this issue.

Titanium is considered as one of the most abundant and bioavailable element. It is the second most abundant metal as well as the ninth ultimate abundant ingredient in the Earth's surface [12]. Metal oxide-based NPs, especially titanium dioxide (TiO_2) NPs, have been extensively explored for their biomedical applications, including therapeutics and theranostics [5, 13, 14]. Owing to its low toxicity, biocompatibility, long-term photostability, strong oxidizing properties, and ease of

*Corresponding author: aiguo@nimte.ac.cn

TiO_2 Nanoparticles: Applications in Nanobiotechnology and Nanomedicine,
First Edition. Edited by Aiguo Wu and Wenzhi Ren.
© 2020 Wiley-VCH Verlag GmbH & Co. KGaA. Published 2020 by Wiley-VCH Verlag GmbH & Co. KGaA.

availability, titanium has been immensely utilized [15]. The worldwide production of TiO_2 accounts for 70% of the volume of pigments. The diameter of about 200–300 nm is typically used in various applications; however, small-sized NPs in the range of 10–50 nm are also used in sunscreens, catalysts, etc., since the refractive index is higher at the nanoscale. It is believed to be one of the most commonly used materials in various commercial products, including food, drugs, cosmetics, sunscreens, varnishes, coatings, and paints [16–19]. The estimated annual production of nano-TiO_2 only in the United States is 3800–7800 tons [19].

The photocatalytic killing efficiency of TiO_2 for cancer cells was reported by A. Fujishima et al. [20, 21]. TiO_2 is capable of generating different cytotoxic reactive oxygen species (ROS) (i.e. $O_2^{\bullet -}$, $OH^{\bullet}$, H_2O_2) [22–24]. Chen et al. studied a black TiO_2 (hydrogenated) with a band gap shift of TiO_2 near to1.5 eV [25]. The absorption increment in the near-infrared (NIR) region was verily enhanced, which attained the researcher's interest in black TiO_2 (b-TiO_2) nanomaterials (NMs) [26]. In 2015, pioneers Ren et al. inquired the application of b-TiO_2 in biomedical field as a potential photothermal therapy (PTT) agent [27], and then it was used for synergistic photodynamic therapy (PDT) and PTT [28, 29]. mSiO_2-coated B-TiO_2 core–shell nanocomposites and mesoporous TiO_{2-x} have been reported for NIR-triggered drug release [30, 31]. The potential of TiO_2 NPs to invoke the ROS under irradiation has been employed for PDT and sonodynamic therapy (SDT) in cancer cells [32–35]. The SDT and PDT are efficient and controllable mechanisms to make restrictions in tumor growth and may lead to future promising route. According to researches NP-based therapeutic routes are confident to conquer the confines of traditional treatment methods. However, there are two sides of a coin – the generated ROS might induce oxidative stress and severe toxicity [36, 37]. The exposure of ultraviolet (UV) light also induces severe damage to healthy tissues [38, 39].

Indeed, nanotechnology has a remarkable impact on society. However, there are numerous societal concerns about NP exposure that may derail its promising applications. NPs are entered in the human body by various pathways, including respiratory, digestive, intravenous injection, and dermal pathways. During these pathways, NPs can easily interact with biological systems. NPs may accumulate in the body for a long period or eliminate, depending upon their physiological properties. Moreover, the unexpected invasion of NPs in biological systems may disturb homeostasis, impair signaling pathways, and induce cell death, since biological systems work in coordination.

The major exposure routes of NPs are inhalation, oral, injection, and dermal. The continuous exposure of NPs, especially through inhalation, may cause potential health risks. The long-term exposure of NPs without necessary precautions may result in severe side effects and even mortalities [40]. However, careful studies of nanotoxicology while avoiding premature conclusions are prerequisite to ensure the safety of consumers and workers [41] (Figure 2.1).

NMs properties, size, surface chemistry, and behavior of biomolecules are of paramount importance for their safe biomedical applications. It is imperative to understand various exposure pathways of TiO_2 NPs, their biological effects, long-term behavior, fate, and mechanism of excretion. Therefore, material toxicity and long-term implications should be thoroughly explored [5]. Moreover, it is essential to understand NPs interactions with biological entities and to evaluate the impact of toxicity for their safe implementation [7].

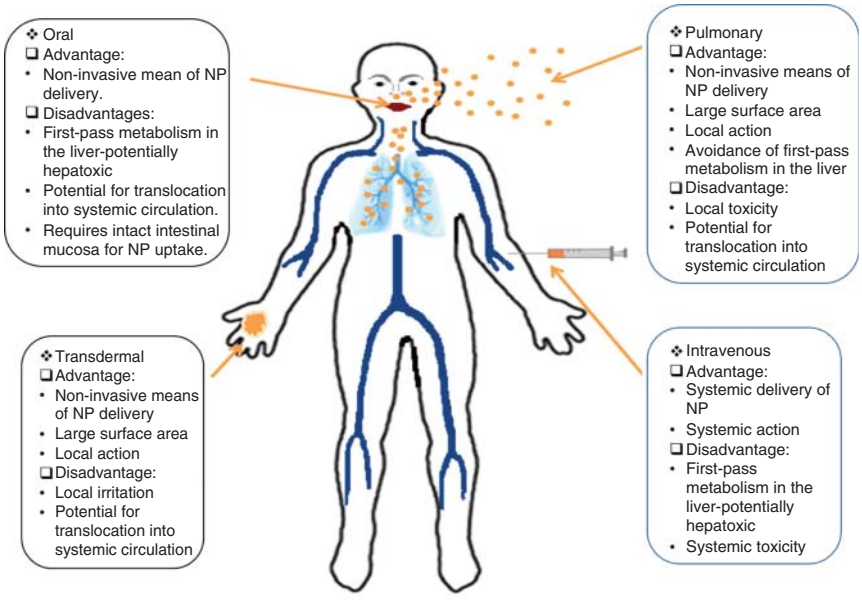
❖ Oral
❑ Advantage:
• Non-invasive mean of NP delivery.
❑ Disadvantages:
• First-pass metabolism in the liver-potentially hepatoxic
• Potential for translocation into systemic circulation.
• Requires intact intestinal mucosa for NP uptake.
❖ Pulmonary
❑ Advantage:
• Non-invasive means of NP delivery
• Large surface area
• Local action
• Avoidance of first-pass metabolism in the liver
❑ Disadvantage:
• Local toxicity
• Potential for translocation into systemic circulation
❖ Transdermal
❑ Advantage:
• Non-invasive means of NP delivery
• Large surface area
• Local action
❑ Disadvantage:
• Local irritation
• Potential for translocation into systemic circulation
❖ Intravenous
❑ Advantage:
• Systemic delivery of NP
• Systemic action
❑ Disadvantage:
• First-pass metabolism in the liver-potentially hepatoxic
• Systemic toxicity

Figure 2.1 Description of various pathways of nanoparticle exposures throughout the body with advantages and disadvantages indications. Source: Reproduced with the permission of Mu et al. [230].

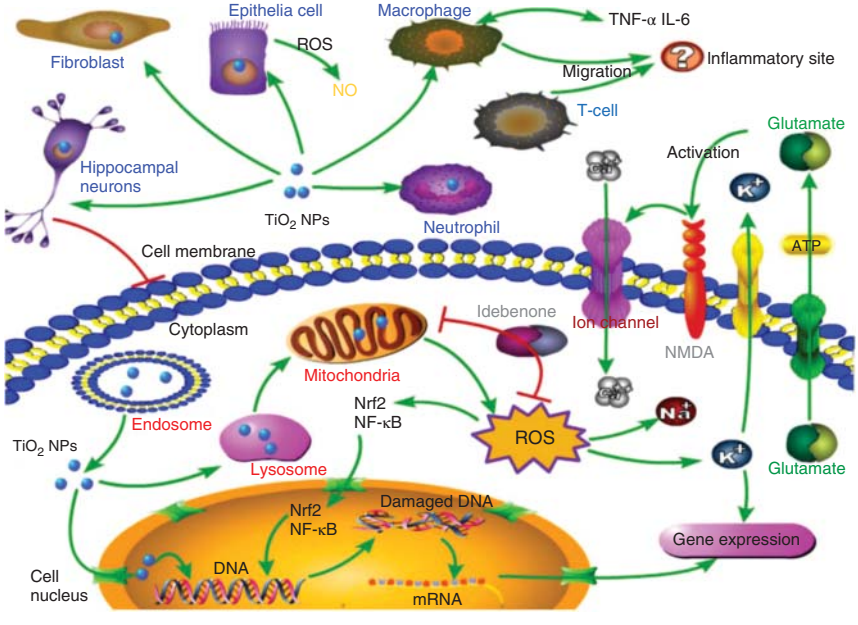

Figure 2.2 Graphical presentation of the toxicity effects in vertebrates and invertebrates through exposure of titanium dioxide nanoparticles. NMDA, *N*-methyl-D-aspartate. Source: Reproduced with the permission of Hu et al. [119].

Realizations of the immense potential of TiO_2 in various applications demand a thorough understanding of their interaction with cells and the ultimate mode of cell death as a product of this interaction. It is imperative to make judgments of the mechanisms of TiO_2-mediated toxicity. Herein, major modes of exposure, biodistribution, and clearance, as well as ultimate mechanisms of cell death under the exposure of TiO_2 NPs, are briefly discussed. Knowledge of the safe applications of TiO_2 NPs and their long-term fates is summarized. The potential toxicity of TiO_2 NPs and its implications are also discussed. The critical points that are highlighted must be considered for safe applications of TiO_2 (Figure 2.2).

2.2 Modes of Exposure, Biodistribution, Clearance, and Fate of TiO_2 NPs

NPs may adopt various routes to enter the human body, including inhalation, ingestion, intravenous injection, skin contact, etc. NPs are systematically distributed to distal organs and lymphatic system, where they interrupt to biological pathways before their clearance from the body. The activity and reactivity of NMs at nano–bio interface is determined by the rate of absorption, distribution, metabolism, and elimination (ADME). NMs are mainly distributed/accumulated in the liver, kidneys, spleen, central nervous system, bone marrow, lymph nodes, etc. [42]. Metal oxide-based NPs are found to be bio-reactive, which trigger various signaling pathways. Among other metal oxides, NPs of zinc oxide are comparatively more toxic, although TiO_2 NPs are also not bio inert [3].

2.2.1 Inhalation

Inhalation, in which lungs are mainly involved, is considered a promising systemic delivery route. NMs are inhaled and deposited in different pulmonary compartments of lungs, depending on their sizes. For instance, the smaller NMs are deeply penetrated into the lungs and may also translocate to other organs, including the brain. NMs are then cleared from different compartments, such as NMs in the gas-exchange region are cleared by alveolar macrophages (professional phagocytes or antigen-presenting cells) and subsequently drained into lymph nodes. Therefore, it is a slow clearance route, whereas NMs are rapidly cleared via the mucociliary escalator. Moreover, inhaled NMs may also translocate into pulmonary epithelial cells and bloodstream [42–44].

The physiochemical properties of NMs and their interactions with the biological interface can decide the magnitude of cellular and molecular responses. In rodents, both microparticles (μP) and nanoparticle adopt numerous transport routes within and out of the lungs, and μPs retain longer on the alveolar epithelium, while NPs can rapidly relocate into interstitial spaces. However, the other species may adopt different transport routes than the rodents [45]. The ultrafine TiO_2 NPs (20 nm) have been shown to stimulate the higher inflammatory response as compared with the comparatively larger particles (250 nm) in the lower respiratory tract of the lungs when exposed for 12 weeks. The higher

pulmonary effect is attributed to larger specific surface area, altered persistence, the increased retention, and interstitial access of ultrafine NPs. Therefore, the particle sizes and surfaces are reported to be more important than the mass of the retained particles [46].

Inhaled TiO_2 NPs (22 nm) appear in different compartments of lung tissue, capillaries, and on the luminal surface of the airways and alveoli. Subsequent translocation of NPs results in its accumulation in major organs of the body (the heart, liver, nervous system, etc.) [47]. The retention time of NPs in different compartments is also dependent on the exposure time and type of compartment in which NPs are trapped. Smaller-sized TiO_2 NPs are easily transported between different compartments/tissues and then translocated into the circulatory system [48]. The studies declare that deposited NPs in the alveoli of lungs can bypass the major clearance mechanisms within 24 hours of aerosol inhalation. The phagocytosed and free particles in alveoli and/or airways are cleared by the larynx [49]. After one hour of intratracheal instillation, about 4% of the delivered dose passes through the air–blood barrier and mainly retained in the carcass (4%). A small amount of TiO_2 NP translocates into the circulatory system, where they accumulate in almost all organs and tissues. From the absorbed/translocated TiO_2 NPs, about 5–20% passes through the gut epithelium and then undergoes to long-term clearance from the lungs via larynx. The persistent fraction of NPs in the lungs is mainly cleared by macrophage-mediated pathways [50].

The fate, as well as clearance of the inhaled NMs, is dependent on the lung compartment in which they are deposited in a size-dependent manner. Large-sized (1–10 μm) NMs are mainly penetrated in the conducting airways with ciliated epithelial cells, including trachea and bronchi, whereas small-sized (<100 nm) NMs are preferentially localized in alveoli. The clearance via mucociliary transport is considered as the fastest route, while the deposition into the bronchial pathways and lung periphery epithelium is a long-term and slow process. The deposited/accumulated NMs are then subsequently eliminated by translocation into the circulatory system and transportation to the draining lymph nodes and/or to the reticuloendothelial system (RES) [42, 49, 51, 52].

2.2.2 Oral Route

Oral route or ingestion is the most recommended path for drug administration as it extend the greatest degree of patient acquiescence [53]. Frequent consumptions of NMs impose toxicity in the gastrointestinal tract and various organs. NMs, including TiO_2, are capable to traverse the intestinal epithelial barrier and circulate into blood, resulting in accumulation in major organs over the long term [54]. Titanium is frequently ingested as an additive in various daily routine stuffs like in personal care, food, and in various consumer credentials. Food-grade TiO_2 (E171) is a major content of many products, such as sweets, candies, and chewing gums. Sunscreens and toothpaste are the main personal care products that contain up to 10% titanium by weight. Moreover, titanium is one of the major components in deodorants, shampoos, and shaving creams as well as in pharmaceutical products [53].

The biokinetic/biodistribution patterns significantly vary if the administration route is different. Most of the NPs are cleared by fecal route after oral administration of same TiO_2 NPs. It also results in its absorption (0.6%) in the intestinal membrane, a fraction of titanium (>0.001%) found in major organs after seven days. Therefore, NPs may subject to chronic exposure, due to its slow clearance, accumulation, and systemic circulation [55]. Size of particles play a main role in toxicity; therefore, TiO_2 NPs with size 25 and 80 nm are claimed to be more toxic than particles of 155 nm. NPs are absorbed by the gastrointestinal tract and transported to tissues and organs, where they gathered in the liver, spleen, kidneys, and lung tissues and may lead to nephrotoxicity and hepatic injury [56]. The extent of response and toxicity of NPs may also be affected by age. Young rats are found to be more susceptible to oral toxicity than adult rats. The liver and heart are more affected in young rats, while the liver and kidney are slightly affected in adult rats, suggesting that TiO_2 NPs may selectively target the liver even after oral exposure. NPs are mainly located in the mucosa of the stomach and small intestine, and the rate/extent of absorption from the gastrointestinal tract is found to be very low, Therefore, TiO_2 NPs may not be translocated into the circulatory system [57].

Inhaled or ingested NMs are excreted via mucociliary clearance pathways, in which they pass from the mouth to laryngopharynx, esophagus, which subsequently transports swallowed NMs into the stomach. NMs that are entrapped by hepatocytes are generally excreted to the intestines via bile and then may be translocated across the intestinal barrier or cleared from the body via feces [58]. Ingested NMs can be discharged as feces and urine via the gastrointestinal route. However, the fate of NMs is dependent on their physicochemical properties. Finally, NMs are released into the environment and may interact with living organisms [53]. It seems that the absorption of NPs across the gastrointestinal epithelium and systemic circulation greatly influence the fate of ingested NPs. The ingested NPs may interact with various biological pathways that cause potential toxicity.

2.2.3 Injection

The direct injection of NMs is considered as the rapid delivery route, such as intravenous, intratumor, and subcutaneous injections. TiO_2 (23.5 nm) can induce endothelial cell leakiness, which is even independent of apoptosis and oxidative stress and is attributed to intracellular signaling cascades. Moreover, injections of TiO_2 in mice results in leakiness of subcutaneous blood vessels [59]. Intracellular processing and uptake mechanism, including endocytosis initiate within four hours of NPs exposure/incubation and particles may release into the cytoplasm up to 48 hours [3]. Exposure of TiO_2 NPs may impair cell membrane, resulting in a disruption in cell adhesion, proliferation, and migration capabilities. It may also trigger signaling pathways, induce toxicity [9, 60] and immunogenicity [61], affect cytoskeleton structures [62, 63], and impair major organs, including the liver, kidney, lung, spleen, and brain [64], thus, impede its biomedical application.

Intravenously injected NMs are mainly cleared via the liver, kidneys, or RES. The distribution and fate of the NMs are dependent on the physicochemical properties. However, after subcutaneous and intratumor injection, the interstitial

lymphatic flow rate at the tumor site is also a contributing factor. Physicochemical properties, especially size, are one of the major parameters since small-sized NMs are absorbed into capillaries and rapidly cleared, whereas large-sized NMs are accumulated into major organs or drained into the lymphatic system [42]. Large-sized NPs are usually accumulated in the body for a long period and may clear by hepatic route. Results of a biokinetics study of relatively large-sized TiO_2 NPs (70 nm) showed that highest concentration of titanium is found in the liver (95.5%), 0.4% in the blood, and the detectable amount in almost all organs on day 1. NPs subsequently released via the liver, however, retained in tissues and organs till day 28 [65].

The negligible toxicity of black TiO_2 (b-TiO_2) NPs is reported in recent years, which suggest their biocompatibility nature and great potential in biomedical application [27, 29–31, 66–68]. No significant toxicity, inflammation, tissue damage, pulmonary fibrosis, or necrosis and no change in hepatic and kidney functions suggested nontoxicity nature of TiO_2 [27]. No significant changes in cell morphologies and no obvious cytotoxicity in the liver, epithelial, and brain capillary endothelial as well as in cancer cells intravenous injection suggest their biocompatibility [66]. b-TiO_2 are undertaken by the RES at 24 hours post intravenous injection [28, 66]. For b-TiO_2-based NPs, no obvious cytotoxicity and evident toxic effects against fibroblast and cancer cells are reported [29]. No inflammation, pulmonary fibrosis, and necrosis further suggested no liver and kidney dysfunction [30, 69]. Moreover, rapid excretion of polyethylene glycol (PEG)-coated TiO_2 via urine and feces after 48 hours of intravenous injection is indicative of great therapeutic biosafety [68]. *In vivo* long-term toxicity assessment of up to 90 days detected no obvious disorder and fluctuation in biochemistry parameters of the liver, kidney, brain, etc. Furthermore, the RES is suggested as a clearance mechanism [28].

The liver is mainly involved in the metabolism and clearance of NMs after intravenous administration; however, NMs are processed and eliminated in a size-dependent manner through three main mechanisms, such as a rapid renal clearance (if size <6 nm), a relatively slow hepatobiliary clearance (if size>6 nm), while persistent NPs are subsequently cleared via the mononuclear phagocyte system (MPS) that may take months to years [42, 58].

2.2.4 Dermal Route

The interactions between the skin and NMs, including cosmetic products and airborne NMs, are known as dermal interactions. Skin is consisting of different layers (such as stratum corneum, stratum spinosum, and stratum basale) that make the skin fairly impermeable and a protective barrier against external exposure [70]. TiO_2 NPs are a major component of commercially available sunscreens, owing to their unique properties, including UV scattering and reflecting capabilities. Although, it is generally believed that healthy and intact skin acts as an effective barrier that does not allow NPs to penetrate into stratum corneum. However, skin disrupting conditions (e.g. eczema) may be of serious toxicity concerns due to the increased NPs penetration [18, 71–75]. Therefore, special attention should be paid on safety evaluation before human use.

2.3 Cell Death Pathways Induced by TiO_2 NPs

2.3.1 Apoptosis

Cell death is mainly classified in at least three categories, such as apoptosis, necrosis, and autophagy. There are two main pathways extrinsic and intrinsic against molecular course that can lead to the apoptosis, such as the death receptor pathways and mitochondrial pathway. Various stimuli (e.g. heat, ROS, growth factors, etc.) can activate the intrinsic pathway, whereas the extrinsic apoptosis pathway may be connected to the intrinsic pathway through BH3-interacting domain death agonist (Bid). Upon destabilization of lysosomal membranes, the leakage of lysosomal hydrolases and cathepsins released into the cytosol activates mitochondrial apoptosis or non-apoptotic cell death pathways that allow cell death of apoptosis-resistant cells. Lysosomal membrane permeabilization (LMP) is a potentially lethal process in which the ectopic release of lysosomal proteases activates the additional hydrolases and caspases. The caspase pathway is indirectly activated by the proteolytic activation of Bid, which induce mitochondrial outer membrane permeabilization (MOMP). MOMP is a major checkpoint of both necrotic cell death and apoptotic that leads to caspase activation and release of cytochrome c. However, massive LMP may result in necrosis without caspase activation pathways [76–79]. Intrinsic apoptosis can be induced by a plethora of intracellular stress environments, such as DNA damage, oxidative stress, and many others. ROS act as the main stimulus to activate lysosomal destabilization. As a result, enhanced ROS generation precedes LMP and cell death. Several NMs are capable to stimulate signaling cascades by interacting with biological entities. It is believed that NMs can trigger extrinsic and intrinsic apoptotic pathways; however, NMs-induced intrinsic apoptotic pathways are mediated by increased ROS and oxidative stress. Redox properties of NMs promote the ROS generation, oxidative stress, and bio-related redox mechanisms [6, 60, 80–83].

Oxidative stress can be induced by the generation of ROS, which disturbs the various signaling pathways leading to the restrain of cell cycle, genotoxicity, and mitochondrial dysfunction in different cell lines. Therefore, oxidative stress and inflammatory responses are correlated with TiO_2 NP-induced toxicity [18, 54, 84]. TiO_2 NPs invokes the oxidative stress, DNA damage, and mitochondrial dysfunction are found to be mainly responsible for toxicity in inhalation models, but not frequently observed in intestinal models. However, cell exposure to TiO_2 NP may lead to an increase in intracellular ROS in intestinal epithelial cells. Furthermore, increased free calcium levels, structural disruption in cells, and changes in intracellular electrolytes are observed to be associated with the exposure of TiO_2 NPs [54]. The oxidative stress and pro-inflammatory responses are considered to be linked with size, surface, and concentration of internalized NPs [85, 86]. Exposure of TiO_2 NPs led to increased ROS production, reduced glutathione, induction of oxidative stress, and stimulation of inflammation-related genes. The increased ROS level triggers the activation of signaling pathways that induce caspase-dependent apoptotic death in the human bronchial epithelial cell line [87].

TiO_2 may induce toxicity by internalization of NPs and disturbing various cellular mechanisms. Physicochemical characteristics of NMs play a crucial role for their toxicity, including protein interactions, apoptosis, autophagy, genotoxicity, etc. [88]. TiO_2 NP can produce ROS in bronchial epithelial cells that undergo apoptotic cell death after being exposed with TiO_2 (15 nm) NP. NPs induce lipid peroxidation, destabilization of lysosomal membrane, which in turn release cathepsin B in order to activate caspase for apoptosis [89]. TiO_2 (24 nm) treated cells experience meaningful apoptosis, not dependent of the classical pathways (p53-Bax) [90]. TiO_2 (10–20 nm) induces oxidative stress, genotoxicity, lipid peroxidation, increment in hydrogen peroxide/nitric oxide production, and micronuclei formation in human bronchial epithelial cell line [91].

The decreased glutathione level and increased lipid peroxidation and ROS level, after exposure to TiO_2 NPs, may lead to cell death. ROS generation is the cause of initial mitochondria-mediated apoptosis and genotoxicity in the liver cells of human (HepG2 cells). Up-regulation of pro-apoptotic (Bax) and down-regulation of antiapoptotic (Bcl-2) is attributed to increased p53 expression as a result of TiO_2 exposure, which leads to cytochrome c release and ultimate formation of an apoptosome. Caspase-dependent pathways activation, such as caspase-9 and caspase-3, triggers the cascade of events and cell death [92]. Intragastric exposure of TiO_2 NPs for back to back (60 days) may result in their accumulation in the mouse hippocampus and ROS overproduction that leads to mitochondrial-mediated hippocampal apoptosis. TiO_2 NPs activate caspase-3 and caspase-9 and promote the Bax and cytochrome c while inhibiting Bcl-2 [93]. The expression of Bax, Bcl-2, cytochrome c, and p53 is altered by the exposure of TiO_2 NPs, suggesting the stimulation of intrinsic mitochondrial apoptosis pathway. TiO_2 NPs up-regulate the expression of caspase 9 without any significant change in the expression of caspase 8 and t-Bid in human bronchial epithelial cells [94]. TiO_2 NPs (<100 nm) stimulate ROS generation and oxidative stress in a concentration-dependent manner in mouse fibroblast cells [95].

TiO_2-induced pulmonary toxicity results in alveolar epithelial cell apoptosis. Activation of various signaling pathways, including cell cycle, complement cascades, and chemokines, as well as altered genes expression in an epithelial cell, was observed after being exposed with TiO_2 NPs (19–21 nm) [96]. In apoptosis-resistant transformed cells ($Bak^{-/-}Bax^{-/-}$), TiO_2 NPs (25 nm) induce lysosome-mediated cell death in a dose-dependent manner via apoptotic-independent (Bak/Bax independent) signaling pathway [97]. When exposed to UV irradiation, TiO_2 NPs (<100 nm) can induce caspase-dependent apoptotic cell death through ROS-mediated transcriptional upregulation of the death receptor and pre-apoptotic protein, like upregulation of the FAS (death receptor) and Bax activation (pre-apoptotic protein) in normal human cells [98].

The nature of the NMs and its interaction with cells/tissues/organ is crucial to activating a particular pathway; since the different molecular pathways are activated by the same type of NPs. NMs can trigger various cell death pathways, due to the extent of cellular insult, although it is difficult to declare a comprehensive mechanism for NMs-induced cell death due to conflicting data [84, 99].

2.3.2 Autophagy

Autophagy is critical factor to preserve the homeostasis and survival of cell under stressed circumstances, such as starvation, protein aggregate-induced stress, oxidative stress, and pathogen infection. It is a cytoprotective process to cope with stress that may lead to autophagic cell death in case of increased numbers of autophagosomes (in dying cells). Autophagy mechanism is defined as in which cytoplasmic materials, containing organelles and portions, are wrapped around a flat membrane cistern and form a double membrane vacuole (autophagosome) for degradation. The fusion of autophagosome with lysosomal and/or endosomal results in the formation of autolysosomes and amphisomes, respectively. Then the luminal contents of autophagosomes are digested and degraded by lysosomal hydrolases [100, 101].

It is generally believed that the increased ROS induces oxidative stress; however, it may also stimulate autophagy as a survival pathway, suggesting that ROS plays a vital role in regulating autophagic activity [100]. Autophagy is a fundamental cellular pathway that keeps cellular homeostasis. It is considered as a clearance/degradation mechanism for insoluble NPs, including TiO_2. In human primary keratinocytes, induction of autophagy is indicated as a pro-survival signal for the safe use of TiO_2 NPs. TiO_2-induced autophagy degrades toxic cytoplasmic content and maintains intracellular homeostasis [102, 103]. It is reported as a standard mechanism for rapid clearance of TiO_2 NPs (18 nm), which stimulate the cellular response in a dose-dependent manner without inducting ROS-mediated toxicity and oxidative stress (in human keratinocyte (HaCaT) cells) [104]. TiO_2 NPs (21 nm) can also induce autophagy in human brain-derived endothelial cells [105]. Rapamycin and its analogues activate the autophagy process by inhibiting its suppressor, mammalian target of rapamycin (mTOR). The AMP-activated kinase (AMPK) can sense altered intracellular AMP/adenosine triphosphate (ATP) ratio. Its activation stimulates autophagy while inhibiting mTOR. Therefore, regulation of autophagy is being carried out by various mTOR-dependent and mTOR-independent pathways [100]. After being exposed to TiO_2, autophagy acts as a protective and antioxidant system to relieve the toxic effects by triggering various signaling pathways, such as activation of AMPK and inhibition of mTOR. However, the solubility, surface reactivity, and chemical composition of NPs influence the cellular response and degrees of autophagy [103].

2.3.3 Crosstalk Between Apoptosis and Autophagy

The cell takes the "decision to die" after being exposed to lethal stimulus/inducer. Apoptosis is the default pathway that is initiated in reaction to most stimuli. However, the alternative pathway, autophagy activates as a cell death effector mechanism when apoptotic effectors are inhibited. Autophagy and apoptotic cell death are incompatible with each other when apoptosis inhibitors facilitate autophagy and apoptosis effectors inhibit autophagy [101].The well-regulated processes, i.e. apoptosis and autophagy, are crucial for maintaining homeostasis and development. The relation between the Beclin 1 (the autophagy protein) and

Bcl-2 (antiapoptotic protein) is a crucial point of convergence of the autophagic and apoptotic machinery [106]. Beclin 1 plays a major task in autophagy, also called "programmed cell survival." The "BH3-only members" of Bcl-2 family can promote apoptosis. In contrast to other BH3-only proteins, even an over-expressed Beclin 1 does not play a pro-apoptotic function. Caspase-mediated cleavage of Beclin 1 can stimulate crosstalk between apoptosis and autophagy. In apoptosis, the pro-autophagic activity of Beclin 1 can be inhibited by caspases. Caspase-3, 7, and 8 can cleave Beclin 1 in order to destroy its autophagic potential. Proapoptotic protein, Bax, induce apoptosis by promoting caspase-mediated cleavage of Beclin 1. However, Bcl-XL and non-cleavable Beclin 1 can restore autophagy. On the other hand, caspase-8 that acts as a death receptor–effector can also be cleaved by autophagy and evoked a feedback process. Therefore, apoptosis and autophagy might be activated by the same stimuli and share signaling pathways [107]. There are areas of crosstalk and interplay between apoptosis and autophagy, suggesting coordination between these pathways throughout homeostasis and development [100].

2.3.4 Necrosis

The massive LMP can cause necrosis [108] that are also reported as a mode of cell death after exposure of TiO_2 NPs; however, physiochemical properties, especially size, crystal structure, and exposure time might play the substantial job in order to decide the impact of toxicity and mode of cell death [84, 109, 110]. The overwhelming nanotoxicological studies make it difficult to distinguish between different cell deaths pathways [111]. It seems that lysosomes, dubbed "suicide bags," may conduct a crucial task in NMs-induced cellular reactions and may participate in apoptosis, autophagy, and in regulated necrosis.

2.4 Toxicity of TiO_2

Titanium dioxide is classified in three dominant crystallographic arrangements, i.e. brookite, rutile, and anatase, in which rutile have maximum stability and the last two structures are substantial in environment [112]. Every one of these forms has its own different attributions, environmental influences, and different applications. Besides this, in the company of light TiO_2 have adverse effect on microorganisms through output of ROS [113]. Anatase titanium NPs are employed in the production of some marketable products such as self-cleaning window coatings and sunscreens [114, 115]. Furthermore, commercial rutile titania and anatase exhibit the delivery of superoxide radical and release of H_2O_2 outside the cells of body and make an additional effect on mitochondria membrane that is called hyper-polarization [116]. For illustration, as TiO_2 are capable to take in large amount of UV radiation, the hydroxyl sort of species resigned in aqueous media may be referred to as the cause of essential harm to DNA, consequence of further environmental risks [117]. Hu et al. investigated the various metal oxide NPs *in vitro* cytotoxicity to the subjected organisms, and it was conformed that among

ZnO, Al_2O_3, SnO_2, CuO, Fe_2O_3, and TiO_2, the metal oxide titanium NPs exhibit lower results of toxicity with rising cation charge [118]. On the other hand, ZnO was referred as more extremely toxic among all other metal oxide NPs. Wang et al. investigated that titanium dioxide at nanoscale have great ability of oxidizing and production of free radicals [56]. Here we try to elaborate briefly about the toxicity of titanium NPs (TiO_2) with different aspects.

2.4.1 Cellular Uptake

The characteristics of NPs have great significance regarding toxicity, like their shape, solubility, aggregation, size, crystallinity, surface chemistry, charge, and surface area. These NP features can effectuate the subcellular localization, toxic effects, and cellular uptake [119]. Particularly, there are two ways of cellular uptake of NPs: one is active uptake and the other one is passive uptake, as active uptake is done by the process of endocytosis and the passive uptake is continued by free diffusion process. Geiser et al. investigated that, TiO_2 powders is employed in rats through inhalation, resultantly nano-sized NPs were not cleared but micron-sized particles were fascinatedly removed through alveolar macrophages. As phagocytes usually remove the particles larger than 500 nm [120] so the remaining smaller matter retained and caused adverse effect on tissues and make burden on other cells as well. Subsequently the inhalation liability and the free TiO_2 NPs were located in the cytoplasm of fibroblasts and endothelial cells [47]. Kocbek et al. investigated an *in vitro* study where the 25 nm TiO_2 NPs were uptaken by endocytosis in the human keratinocytes and also confirmed that the summation of NPs is in the amphisomes as well as in endosomes, supporting the endocytotic uptake mechanism [121]. Xia et al. examined the uptake of TiO_2 NPs that are fluorescence labeled and smaller in size <12 nm, and they are identified in the lung endothelial BEAS-2B cells, in the caveolar compartments, and in the late endosomal [122]. Further studies showed that the aggregated titanium NPs (TiO_2 NPs) that are less than 200 nm in size are qualified to access into the red blood cells, which have absence of phagocytic receptors, as long as other considerable size particles have capability to incline on surface of the cells [123].

2.4.2 Oxidative Stress Effectuates by TiO_2

In the case of TiO_2 NPs, the negative biological effects through oxidative stress has been chronic; by that proof it makes an increase in the production of oxidative output and ROS [87, 91, 124, 125]. Among various other adverse effects caused by the NPs, the oxidative stress is considered to be the main process for biological unfavorable effects. As oxidative stress is conveying by TiO_2 NPs in both cases with and without UV radiation. Uchino et al. reported that different sizes and crystalline morphologies have brought on the various measurements of hydroxyl radicals under UV irradiation, and these yield radicals associated to the cytotoxicity upon the ovary cells [126]. Dodd et al. further investigate that the TiO_2 NPs upon UV radiation produced the hydroxyl radicals, which are the dominant reason of the damaging results that respond to contribute carboxyl radicals [127].

In addition, studies showed that without photoactivation the TiO_2 nano-sized particles have also invoke the ROS and related biological unfavorable issues. Gurr et al. reported that the oxidative damage invoked in the human bronchial epithelial (BEAS-2B) cells is the result of combination of anatase and rutile TiO_2 NPs [128]. In another study, Petković et al. analogize the two different nano-sized pre-irradiated and non-irradiated anatase TiO_2 particles and their genotoxicity and cytotoxicity effects [128]. The result revealed that only TiO_2 particles has induced the oxidative damaging of DNA, and on the other hand non-irradiated NPs have only make slightly impact on DNA strand breakage, no aftereffect on cells survival. But after pre-irradiation both samples of NPs revealed same results of DNA breaks and oxidative damage as well as restrict the cell viability results. Kang et al. had confirmed the prompt of inflammation through the function of oxidative stress in TiO_2 NPs [129]. In summary, high concentrations of TiO_2 that induced large amount of oxidative stress can be commanding to cell damage-related reactions, although low level of oxidative stress may cause inflammation that might be energized through ROS activation of signaling tracks.

2.4.3 Genotoxicity

The views about the genotoxicity of TiO_2 NPs is argumentative and not so clear, early researches revealed that in standard assays there was no evidence of genotoxicity [130, 131]. But recently, researchers showed the results about genotoxicity of TiO_2 both in *in vitro* and *in vivo* studies. Some properties of NPs make some impact on genotoxicity of TiO_2 like those particles that are smaller in size showed more genotoxic effect than the larger particles in size instead of whatever their crystalline phase they have. Due to their smaller size, it's a bit easy for them to penetrate in nucleus and cytoplasm for accumulation inside [132]. Another effect agglomerations of TiO_2 NPs are being examined in various studies; whereas smaller sized almost 200 nm showed no invoke on genotoxicity, larger agglomerations showed some DNA damage results in various cell lines [126, 133, 134]. Due to photocatalytic characteristic of anatase TiO_2 NPs, they showed some more unfavorable effects than rutile TiO_2 particles [135]. In recent years, researchers use different test systems both *in vitro*, Ames test, DNA breaks, cell transformation, and micronucleus test, and *in vivo* studies on bone marrow cells of rat to examine the genotoxic effects of TiO_2. Gurr et al. examined different size of anatase TiO_2 NPs and rutile TiO_2 particles where anatase NPs having size about 20 nm showed some evidence of extension in micronuclei structure, while rutile and anatase of 200 nm size did not show any results [136]. In another study, high concentration of TiO_2 NPs is exposed to retinal pigment epithelial cells (RPE-19) and found that the particles were being observed in endoplasmic reticulum [137]. Jugan et al. reported in his work that both anatase and rutile TiO_2 NPs having spherical shape with the size of almost 12–140 nm showed the oxidative stress in A549 cells and invoke oxidative effect and single-strand interruption to DNA [136]. In this study it was also observed that TiO_2 NPs weaken the strength of cells in repairing the DNA through the inactivity of both sequences base excision repair (BER) and nucleotide excision repair (NER). Further studies revealed that TiO_2 NPs substantiate the genotoxicity and cytotoxicity effects in the human

amnion epithelial cells [138]. Other examinations revealed that increased in nitric oxide synthases (NOS) messenger RNA (mRNA) expression and extracellular ROS in NR8383 rat lung is being carried out due to TiO_2 NPs [139]. Bhattacharya et al. compared the effect of cytotoxicity and genotoxicity in the human bronchial epithelial (BEAS-2B) cells and human lung fibroblasts through employment of TiO_2 NPs and found that fibroblasts are more sensory [140]. In this examination, in the human lung fibroblasts, DNA adduct formation, and oxidative stress is being observed rather than DNA breakage by TiO_2 NPs. Trouiller et al. reported the micronuclei formation, signs of DNA double-strand interruption, and invoke of oxidative DNA damage in mice is being examined after oral exposure of TiO_2 by drinking water [141]. In this work authors observed also pro-inflammatory cytokines, and they claimed that for genotoxic effects the yield of inflammatory is accountable. Wang et al. used the comet assay, cytokinesis block micronucleus (CBMN) assay, human lymphoblastoid cells, and hypoxanthine-guanine phosphoribosyltransferase (*HPRT)* gene mutation assay for the finding of genotoxic effects caused by the TiO_2 NPs of 7–8 nm in size for different intervals up to 48 hours [142]. TiO_2 NPs invoke about fivefold increment (65 μg/ml) in tail moment and also increased 2.5-fold (130 μg/ml) in the binucleated cells. While Shi et al. observed in the examination on the BEAS 2B cells, they described that caspase 8/t-Bid pathway is not a cause of induced apoptosis through mitochondrial apoptosis [94]. These outcomes make the sense that effects of TiO_2 NPs are different for different cell lines. In another study conducted on human lymphocytes, it revealed that DNA breakage and invoke of MN configuration are also being carried out by the TiO_2 NPs [143]. The cells that were treated by TiO_2 NPs also showed the creation of ROS. Xue et al. observed the inhibitive characteristic of *N*-acetylcysteine (NAC) regarding the generation of ROS by exposing it to TiO_2 NPs. Falck et al. compared the coated and uncoated anatase and rutile TiO_2 NPs and showed that the uncoated NPs were more productive than SiO_2 coated TiO_2 NPs as regards the unsubstantial induction of micronuclei on BEAS 2B cells [144]. This work is further supported by Manoet al. by showing that rutile TiO_2 NPs revealed low activity in genotoxicity because of coating mechanism [145]. They examined the human acute monocytic leukemia (THP-1) cells and human pulmonary epithelial (NCI-H292) cells with PEG coated TiO_2 NPs and found that the induction stress and related cytotoxic effects were meaningfully decreased. Petkovic et al. studied the effects of genotoxicity with the employment of rutile TiO_2 NPs of <100 nm size (TiO_2-Ru) and anatase NPs of <25 nm size (TiO_2-An) in the human hepatoma HepG2 cells [146]. They revealed that the anatase TiO_2 NPs invoke the oxidized purines and DNA strand breaks. In another test conducted on Caco-2 cells, results revealed that anatase and rutile TiO_2 NPs make meaningful DNA damage and lactate dehydrogenase (LDH) leakage as compared with undiluted anatase TiO_2 exhibited by formamidopyrimidine [fapy]-DNA glycosylase (FPG)–comet assay [147]. Another factor per unit surface area also showed high cytotoxicity results of anatase and rutile TiO_2 NPs. For this purpose, researchers examined the WST-1 assay to reveal the significant mutual relation between cytotoxicity and anatase NPs surface area.

While some results in *in vivo* studies are contrasting in various cases, the investigators used the A549 cells against TiO_2 NPs of about 28 nm size with various

immersions up to 40 μg/ml for 24 h, and results showed no signals of ROS production [148]. In another study, Woodruff et al. revealed the results of uncoated TiO_2 NPs under the circumstances of Comet assays and Ames assays in the thymidine kinase heterozygote (TK6) cells, and no meaningful effects of genotoxicity was observed, and no DNA or oxidative DNA injury observed [149]. Linnainmaa et al. examined both TiO_2 NPs and fine particles (FPs) by employment of MN assays in the rat liver epithelial cells, and results revealed the negative response that there were no primary clastogenic potential [150]. Fisichella et al. showed that in their examination no adverse effects were detected on Caco-2 cells treated through TiO_2 NPs with core of rutile having concentration of 100 μg/ml for various interval up to 72 hours [151].

According to different results by different investigators, many contradictions are existing in the literature regarding to the genotoxicity effects by TiO_2 NPs. In some other studies, both *in vitro* and *in vivo*, various results showed positive response, and some of them reveals negative response, which were recorded by use of different cultured cells, various particle size distribution, and dispersion for illustration [152]. However, where there is some genotoxicity effect shown by the cells, most of them are closely connected with circulatory and respiratory system. Therefore, more research is required to justify the terms and conditions in which the genotoxicity effects of TiO_2 NPs will be examined [153, 154].

2.4.4 Reproductive and Developmental Toxicity

Whereas TiO_2 NPs may penetrate into placenta and fetal tissue through absorption, reproductive toxicity effects in human through exposure of TiO_2 NPs are not yet proven. On the other hand, when other species like abalone embryo and zebra fish are treated by TiO_2 NPs, and results revealed that it inhibit hatching, malformations, and induced impair reproduction [155, 156], although some contradiction is being observed in the case of zebra fish [157]. The research data is not sufficient to define the developmental toxicity effects in the mammals. Hougaard et al. investigated on mated C57BL/6BomTac mice through coated TiO_2 NPs by inhalation mechanism, and average changing is being recorded in the neurobehavioral site [158]. Yamashita et al. examined the pregnant mice intravenously with titanium and silica NPs having size of, respectively, 35 and 75 nm, and results showed some complex effects to pregnancy [159]. In the major organs, fetal brain, fetal liver, and in placenta, TiO_2 NPs were detected. In another work, Komatsu et al. worked on the testis leydig cells of mouse *in vitro* to check the cytotoxicity effects of carbon black and TiO_2 NPs, and results showed the TiO_2 NPs were more cytotoxic [160]. The leydig cells elevate the TiO_2 NPs and resultantly proliferation, and viability effects and gene expressions were observed. Limited research showed the results both *in vitro* and *in vivo*, and the reproductive toxicity was observed by TiO_2 NPs.

2.4.5 Carcinogenicity

There is no satisfactory understanding found about carcinogenicity mechanisms through metal induction. But in the cells, genetic and non-genetic influences

responded by TiO_2 NPs may exhibited the effects of carcinogenicity [161]. In the animal experiments, respiratory tract cancer was observed in subjected rats due to high absorption of TiO_2 NPs of about <100 nm in size with 10 mg/m^3 and TiO_2 FPs with 250 mg/m^3 with almost <2.5 μm size [162]. Heinrich et al. reported the carcinogenic effects caused by TiO_2 NPs of about 15–40 nm in size in rats and determined that NPs exhibited tumorigenic effects at immersion of nearly 10 mg/m^3 with interval of six months. Considering the equal concentrations of both TiO_2 NPs and TiO_2 FPs, the NPs showed more effects of carcinogenicity than FPs in rats. According to this distinction in results of carcinogenicity strength against TiO_2 NPs and TiO_2 FPs, risk evaluations and employment exposures to various diameters of both NPs and FPs should be mentioned [163]. Kuempel et al. determined the unfavorable effects of exposure employments of TiO_2 NPs to health through usage of lung dosimetry miniature [164]. In another study, hydrophilic TiO_2 NPs of about 25 nm size with various concentrations were employed on female rats through intratracheal instillation as interval of one week up to 30 weeks [165]. In order to examine the carcinogenicity and toxicological effects, Bernard et al. employed 5.0% of dietary coated TiO_2 NPs in fed diets of the rats for more than 100 weeks [166]. They didn't find any effects of either carcinogenicity or toxicity even for high dose (5.0%) of TiO_2 coated NPs.

In order to examine the skin cancer effects by TiO_2 NPs, Sagawa et al. conducted experiments on two-stage skin miniature by usage of silicon coated (35 nm) and non-coated TiO_2 NPs (20 nm) in the suspension of silicon oil and Pentalan 408 [167]. After the analysis, results showed that there were no effects of skin cancer monitored because of coated and non-coated NPs owing to no penetrations through skin. In another study, Newman et al. showed no skin carcinogenic effects were observed because TiO_2 were incapable of making an access to enter completely in dermal tissues [73]. Author suggested that further research is needed regarding to safety parameters to use TiO_2 NPs in skin burn conditions and in sunscreens. Pulmonary inquiries endure the carcinogenicity effects of TiO_2 particles through inhalation and intratracheal examinations. As long as dermal exposure revealed opposite results to pulmonary studies, TiO_2 NPs are non-carcinogenetic.

In epidemiological examinations, there were no evidence monitored about the correlation of raised in cancer risk of lungs against occupational exposure of TiO_2 NPs. Hence, more research didn't conduct investigation about the lung cancer risk and particle size of TiO_2 correlation, which raised the dispute about the evaluation of occupational carcinogenicity caused by TiO_2 NPs [141]. In other epidemiological studies without define particle size, no results were found in the support of TiO_2 NPs against lung cancer effects [168, 169]. As per focused studies of epidemiological, there were no relation being concluded of lung cancer symptoms/increased in cancer caused by TiO_2 NPs. Moreover, due to considerable agglomerations of NPs both *in vivo* and *in vitro*, there is a challenge to make safe evaluations of health hazards caused by fabricated NPs [170]. There is correlation existing between decrease in surface area that showed the agglomerations of TiO_2 NPs at an unvarying pH, and it was proven through experiment results [171]. Thus the unfavorable factor oxidative stress is caused by the influence of larger surface area against biological contexture [172]. Meanwhile, all TiO_2 NPs that

have marketable ability ensured their evaluation and managed properly their production and applications against different environment or conditions. At this particular point, risk assessments of TiO_2 NPs cannot be reliably defined due to less reliable data about dose reaction assay as well as on human exposure against TiO_2.

In many experiments conducted on animal models and on various cells, TiO_2 NPs and FPs showed the tumorigenesis, genotoxicity, and cytotoxicity effects [173]. As discussed earlier, mutations, DNA strand breakage, cell transformations, and chromosomal effectuations were included in various studies both *in vivo* and *in vitro*. The lack of balance in cellular redox was examined through oxidative stress in different types of cancer cells. The harmful effects of oxidative stress to cellular DNA can help to initialize the mutations. Further the mutations carried out in the DNA may lead to perform significant task in the growth of different cancer cells.

2.4.6 Immunotoxicity of TiO_2 NPs

The physiochemical characteristics of TiO_2 NPs allowed them to elevate immune cells like monocytes, leukocytes, macrophages, dendritic cells, and platelets. In the study of monoblastoid cell (U937), necrosis and apoptosis effects were invoked by the TiO_2 NPs in absorption comparable to that detected in plasma and blood [174]. Palomäki et al. investigated the silica-coated rutile TiO_2 and uncoated TiO_2 particles on the murine macrophages (RAW246.7) and murine dendritic cells (bm-DC). In their studies, results showed the enrich formulations of different proinflammatory cytokines invoked by TiO_2 NPs in corresponding cells [175]. Meanwhile, TiO_2 particles showed more toxicity in dendritic cells rather than macrophages. As TiO_2 NPs actuated the NLRP3 inflammasome, a sophisticated form of various proteins exist in the cytoplasm can dominant the IL 1β-secretion. There were separated illustration for long-term and short-term liability of neutrophils against anatase TiO_2 particles, as long as longer time viability exhibited the cytokine yielding and apoptosis inhabitation and short-term showed the altering of morphology that leads to move these cells. These assessments support that the TiO_2 NPs are neutrophil Agonist in *in vitro* studies. Moon et al. investigated the factors raised by TiO_2 in mice related to immune reaction, and results revealed the improved in expansion of subcutaneously breed B16F10 melanoma because of factors affecting immune such as macrophages, T-lymphocytes, killer cells, and B-cells [176].

2.4.7 Neurotoxicity of TiO_2 NPs

It was described in early studies that NPs passed through blood brain blockage and use olfactory track to reach in the nervous system [177–179]. In *in vitro* examination, brain microglia cell (BV2) showed the effects of oxidative stress against TiO_2 (Degussa P25) NPs, which further allied to inflammation, cell cycle, and apoptosis and in up and down inhibition of genes associated with energy metabolism [116, 124]. As long as TiO_2 (Degussa P25) showed contrast behavior, no toxicity effects were shown in N27 neurons as compared to BV2 cell, although TiO_2 Degussa P25 NPs exposure to complicated brain cell showed

neuron damaging in short period of time through ROS production. Liu et al. showed the apoptosis and oxidative stress effects against various dose rates by employment of TiO_2 NPs in the neuronal cell PC12 [180]. In another study, silicon coated rutile TiO_2 NPs were employed on mouse, and results showed these NPs have capability of developments of stem cells respecting to neurons [181]. These consequences revealed that TiO_2 NPs responded according to type of cell and intervene of oxidative stress. Scuri et al. conducted experiment on newborn rats through inhalation mechanism of TiO_2 NPs (12 mg/m^3), and results showed the up-regulations of lung neurotrophins articulation, leading to regulatory and sensitivity of neuronal cell growth that have association in asthma [182]. These outcomes were related to elaboration of moderate airway inflammation and airway hyperactivity.

2.4.8 Acute Toxicity of TiO_2

The studies about effects of TiO_2 NPs on humans is not explored widely. The value median lethal dose (LD_{50}) is actually used to determine the dosage outcome to death percentage (50%) of animals during experiments. Meanwhile, in 2002 Organization for Economic Co-operation and Development (OECD) officially ended this testing of acute toxicity rules (TG401), although there are other techniques and rules to examine the acute toxicity like dose–response method (TG425), up and down procedure (TG423), and fixed dose procedure (TG420).

In an inhalation examination, aerosols of TiO_2 NPs up to 50 mg/m^3 are employed on rats via inhalation mechanism for five days with interval of six hours a day [183]. Postmortem examination will be carried out either yet to 3 and 16 days after employment or as soon as after last liability. Lung inflammation is depending on dose to cause in the increment of neutrophil numbers and bronchoalveolar lavage fluid (BALF) cell, enzyme exertion, and overall contents of protein. The proper pathological measurements didn't exhibit the inhibition of systemic induction. In an examination conducted on mice to study inhalation through employment of TiO_2 NPs of size about 2–5 nm, results revealed the large number of alveolar macrophages and number of entire cells in the BALF [184]. Although mice regained its condition after three weeks of exposure, these results revealed the pulmonary inflammation caused by TiO_2 NPs. In another report against TiO_2 particles inhalation, microvascular unhealthy behavior in shoulder arteries were caused through TiO_2 NPs and FPs of size 21 nm and 1 μm [185]. TiO_2 NPs were more effective than FPs with respect to mass. The supplementary vascular condition consociated through particular matter (PM) liability of TiO_2 NPs of 100 nm in size and FPs 710 nm because of neurogenic actuation mechanisms [186]. Furthermore, after 24 hours of inhalation (TiO_2 NPs; 21 nm), low response of coronary arterioles against dilators were observed [187]. It is being observed that less lung burdens didn't make any special change in the BALF regulation against inflammation of lungs. These results are accepted and played a vital role between the cardiovascular complications and PM. Various cardiac complications like change in heart rate, blood clotting, and change in blood pressure can be aftereffect of PM exposure [188]. Liu et al. conducted intratracheal instillation experiment on rats by usage of body weight

(BW) 0.5–50 mg/kg dose of TiO_2 particles [189]. According to histopathological test concerned to lung tissues, the rats were effected by inflammatory lesions that was dependent on dose of TiO_2 NPs. Furthermore, TiO_2 NPs of size 21 nm and of 50 nm invoked less pulmonary toxicity effects than the TiO_2 particles of 5 nm in size. In another study, Kobayashi et al. examined the pulmonary reaction against different interval of 24 hours to 1 week through intra-tracheal instillation of TiO_2 NPs of 19 and 20 nm in size having concentration of 5 mg/ml. The more unfavorable pulmonary disorder effects were observed due to TiO_2 NPs had exposure of 24 hours than one-week exposure. Liu et al. studied the consequences on immune system due to intra-tracheal examination of TiO_2 NPs in the rats [190]. The results revealed the adverse effects on structure of cell and observed the disorder in the function of alveolar macrophages (AM) associated to immune system due to TiO_2 NPs exposure. These consequences were responsible for reduction in immune reaction against particular treatment of 5 and 200 nm TiO_2 NPs. The macrophage phagocytic capability was dependent on dose of TiO_2 NPs; capability was increased for low dose and decreased for high dose. Furthermore, the capability of chemotactic in macrophages were reduced after TiO_2 exposure as well as decreased the Fc receptors articulation on the surface of cell [191].

Warheit et al. investigated the dermal annoyance caused by anatase and rutile NPs (in H_2O) in rabbits and in mice (lymph node assay) for three days, and results showed no effects of skin irritations [152]. Another study results showed no prominent aftereffects of acute eye, vaginal mucous, and dermal irritation in mice caused by TiO_2 NPs exposure with interval of 1–48 hours [192]. In some other studies about toxicity of TiO_2 NPs (20 nm), after two weeks results showed provisory toxicity in Wistar skin of mice [193]. The reduction was observed in the balance of glutathione S-transferase (GST) and catalase activity. Moreover, increment was followed in the exertion of lipid peroxidation and in the lactate dehydrogenase, as well as increased in level of serum glutamic oxaloacetic transaminase creatinine, blood urea nitrogen, and in serum glutamic pyruvic transaminase were observed. Even so, no prominent effects were monitored through histopathological examinations at tissue status. Accordingly, consequences suggested that TiO_2 can induce the renal and hepatic toxicity through short-term dermal exposure in rats. Withal, in the operating skin, the hair follicles can be the spots from where the TiO_2 NPs were able to penetrate.

One-time oral activity of TiO_2 NPs of three different sizes 25, 80, and 155 nm in mice for two weeks were conducted to test the acute toxicity. After two-week exposure of TiO_2 NPs, results showed no significant acute toxicity. On the other hand, large coefficients of hepatic effects were observed in female mice through exposure of TiO_2 NPs of 80 and 25 nm in size. Post-exposure of particles revealed the hepatic renal harm effects through the alteration in pathology of the kidney and liver, as well as in serum biochemical measurements like blood urea nitrogen (BUN), alanine aminotransferase, LDH, and aspartate aminotransferase. Accordingly, systemic toxicity was not substantiating but biochemical alteration was revealed by various studies through oral liability. In nanomedicine, investigation can be done against the usage of TiO_2 NPs through the intraperitoneal examinations. In the study of intraperitoneal liability on

mice, anatase TiO_2 NPs of size 5 nm with high dose revealed severe effects like undo the level of lipid and blood sugar as well as involved in the injury of the kidney, myocardium, and liver [194]. Moreover, tracer functions of the kidney were fall down like BUN and uric acid; tracer functions of the liver like leucine, total protein, albumin levels, pseudo cholinesterase, alanine aminotransferase (ALT), and acid peptide were prominently increased because of TiO_2 NPs high dose. The glucose, lipoprotein cholesterol, and triglycerides content were raised prominently. Furthermore, the intraperitoneal injection of TiO_2 NPs in mice showed the value of LD_{50} was 150 mg/kg BW. TiO_2 NPs of 50 nm in size were injected intraperitoneally in mice with interval of one day up to two weeks and showed the acute behavior in the results like tremor, lethargy, and lack of appetite. The histopathological studies exhibited the lesions' effects due to penetration of certain number of TiO_2 NPs in the spleen. Small increase was also monitored in the aspartate aminotransferase (AST) and ALT levels as well as in the pulmonary vascular network, and thrombosis was detected. In another study by Ma et al., TiO_2 NPs of 5 nm in size showed the behavior of liver toxicity and injury of liver and inflammatory reactions also participating through NPs [195]. The assessment of enzyme-linked immunosorbent assay (ELISA) and real-time quantitative PCR (RT-PCR) through employment of TiO_2 NPs revealed that NPs caused the change in the protein articulation of various inflammatory tracks involving cross-reaction protein, interleukin (IL-4), IL-Iβ, IL-10, macrophage migration inhibitory factor (MMIF), and mRNA [196, 197], subsequently transferring TiO_2 NPs from abdominal cavity. NPs involved in the transformations of certain number of neurons to filamentous morphology remained shifted to inflammatory cells [198]. The intraperitoneally injection of TiO_2 NPs showed the systemic acute toxicity effects concerning biochemical and pathological sequel on major organs: the brain, heart, kidney, and liver.

Li et al. investigated the TiO_2 NPs effects on the erythrocytes, and results showed unpleasant symptoms like unusual hemagglutination, hemolysis, and sedimentation. These results were contrast to the TiO_2 FPs results of same treated cells. Another investigation was carried out through usage of TiO_2 NPs and FPs, outcomes of conducted experiment revealed that TiO_2 FPs exposure to erythrocytes showed the hemolysis 73 times more [199]. Although the plasma is the factor that can abrogate the hemolysis, accordingly *in vitro* state plasma can be helpful to stop hemolysis. In the experiment conducted on mouse macrophages (MH-S) cells, outcomes showed that anatase TiO_2 NPs of different sizes were less toxic [200]. Various studies *in vitro* exhibited the toxicity effects on circulatory cells through usage of TiO_2 NPs.

2.4.9 Sub-acute Toxicity of TiO_2

Rutile TiO_2 NPs of about 40 nm in size had coating of silicon dioxide (SiO_2) expose to lung tissues for two hours up to four weeks, and results of experiments showed the neutrophil attracted chemokine (CXCL 1), tumor necrosis factor (TNF)-α articulation, and pulmonary neutrophilia [201, 202]. Oberdorster et al. conducted the experiment to investigate the relationship between dose amount and TiO_2 particles (NPs and FPs) through intratracheal exposure to mice and rats [203]. The results showed the prominent effects of pulmonary

inflammatory factors that further involved in the increment of activity of LDH, acid α-glucosidase, and protein boost in BALF. The large surface area per mass of TiO_2 NPs was the suggested reason of the high toxicity. In another study Li et al. conducted an experiment on mice through intratracheal implant of TiO_2 NPs of size 3 nm with 12.2 mg/kg BW dose for four weeks (once a week) [204]. The results after four weeks of exposure showed adverse effects in the lungs and alter the alveolar-capillary wall. Furthermore, TiO_2 NPs were accessed to other pulmonary tissues like the kidney and liver through the blood circulation system and caused to injure the tissues up to significant level. The metabolomics assessment and standard methods were employed to investigate the oral toxicity effects against TiO_2 NPs in rats [205]. So by using main elements, 1H NMR and least squares assessments were held to examine the serum and urine. Furthermore, the chemical metabolic examination of urine revealed the increment of balance in citrate, histidine, citrulline, acetate, taurine, phenylacetylglycine (PAG), trimethylamine-*N*-oxide (TMAO), and α-ketoglutarate. Although in the balance of betaine, threonine, leucine, choline, 3-D-hydroxybutyrate, lactate, and pyruvate reduction were reported. The disturbances were showed in their investigations against amino acids, and energy balances may be the factors involved to create little adverse effects to the heart and liver through TiO_2 particles. Accordingly, to authors, to explore the NPs biochemical responses toward various instillations, the metabolomic assessment particularly based on nuclear magnetic resonance (NMR) can be more helpful and trustworthy.

2.4.10 Sub-chronic Toxicity of TiO_2 NPs

To compare pulmonary reactions against TiO_2 NPs, subchronic investigations were carried out on various species [206]. TiO_2 NPs with aerosol (0.5–10 mg/m^3) were employed on hamsters, female mice, and rats and results were observed against different intervals of time up to 13 weeks. After every interval, the selected lung activities, lymph nodes, and lung burdens were examined. Besides other activities lung burdens kept increasing with the control dose, and it showed maximum effects at the exposure closing in all under-examined species. At a point where the lung burdens balanced against TiO_2 NPs, rats showed high adverse inflammatory reactions than in mice. After this, improved fibroproliferative and epithelial alterations were reported. The disposal of TiO_2 NPs (10 mg/m^3) from the mice and rats' lungs were impaired, but in the case of hamsters, any dose concentration showed no significant effect during clearance.

In another investigation, Warheit et al. compared the intratracheal exposure to rats by employment of different TiO_2 NPs and FPs with diverse properties in term of size, crystalline morphology, and surface area [207]. Accordingly, the difference was large through two same size (100 and 25 nm) of particles in terms of surface area as 30-fold, but the reactions in lung inflammation had no significant diversity observed. So results suggested that surface area and size of particles are not the factors that make toxic effects on inflammatory responses. Wang et al. conducted an experiment to explore the effects of TiO_2 NPs of various sizes (25–155 nm) on female mice through intranasal way instillation on monoaminergic neurotransmitters with various interval up to 30 days [153]. To assay the effects of TiO_2 NPs in the area of murine brain, they engaged the

inductively coupled plasma mass spectrometry (ICP-MS). The reversed-phase high performance liquid chromatography (RP-HPLC) were used to make analysis about other neurotransmitters: 5-HT, dihydroxyphenylacetic acid (DOPAC), neurospora endonuclease (NE), homovanillic acid (HVA), domoic acid (DA), and 5-hydroxyindoleacetic acid (HIAA).

2.5 Alternative Perspective

There are reports demonstrating that TiO_2 NPs did not elicit significant biological responses and affect the cell-cycle progression [208], and they induce no significant cytotoxicity and inflammation [103, 197, 209, 210]. Under ambient conditions, it neither induces ROS generation nor oxidative stress in a lung-derived phagocytic cell line. Moreover, any toxic effects are neutralized by antioxidant defense mechanisms [103, 119, 210]. Its exposure does not affect cell morphology, cell proliferation, and survival [208, 211]. The study even reported no evidence of ROS-mediated oxidative stress in human intestinal cells (Caco-2); however, it suggested that the toxic potential is correlated with its surface area and the crystallinity [147]. No significant change in cell contractility and viability in human airway smooth muscle cells was observed after being exposed to TiO_2 (25 nm) [212]. It has also been reported as a biocompatible material for biomedical applications [15, 213–216].

The study reported no evidence of disruption in plasma membrane integrity, mitochondrial activity, and lysosomal function, thus suggesting negligible toxicity of the TiO_2 NPs [217]. Low concentration of TiO_2 NPs (<40 nm) neither show cell death nor disrupt epithelial integrity of intestinal cell lines [218], suggesting that NPs may be less toxic at low concentration [219]. No significant genotoxicity and oxidative stress are found after exposure of ultrafine and small-sized NPs (10 nm) [149, 152, 220].

ROS-induced oxidative stress is correlated with surface defects [221]. Therefore, surface passivation with silica or alumina may block ROS generation and ultimate oxidative stress. Moreover, protein corona also plays a crucial role in reducing toxicity [222]. Surface coating of TiO_2 NPs with biocompatible polymers, i.e. PEG, may minimize its toxicity [88, 145]. Though it is not considered a major problem [177], TiO_2 NPs of relatively small sizes are mainly eliminated via renal clearance [223, 224] and thus may induce minimum toxicity toward major organs. Therefore, the use of titanium in cosmetics, especially sunscreens, is also encouraged [73, 75].

Physicochemical properties, especially the size of TiO_2 NPs is found to be a critical factor in deciding the impact of toxicity [56, 85, 86, 220, 225–228], and minor changes in particle sizes may lead to significant alterations in inflammation and oxidative stress [85]. Micron-sized NPs might be less toxic than NPs [86, 220]. The studies point out that anatase TiO_2 NPs are more toxic than rutile TiO_2 NPs [18, 86], whereas TiO_2 possess minimum toxicity but may have the potential for long-term side effects, including epigenetic and mutagenic [229]. Indeed, there are conflicting data [18] about the toxicity of TiO_2 NPs that make it difficult to draw strong conclusions.

2.6 Conclusion

Nanotechnology and nanomedicine are the complementary disciplines having marvelous applications in many areas aimed at the improvement of human life; however, it is a double-edged sword. TiO_2 NPs are one of the most prevalent NMs. TiO_2 nano-products have a remarkable impact on society. However, there are numerous societal concerns about NPs exposure that may derail its promising applications. There are many challenges in recognizing and avoiding potential risks associated with TiO_2 NPs. Preventing exposure is the key that can be achieved with appropriate precautions and personal protection strategies.

TiO_2 NPs are capable to interact with biological systems as well as to cross various biological barriers. However, these interactions are heavily affected by the physiochemical properties of NPs and physiological systems. The physiological systems may have quite different strategies to counter toxicity and thus play a pivotal function in mitigating the adverse effects of NPs. Therefore, the biological activities and signaling pathways can be modulated by changing the physiochemical properties of NPs. The better understanding of underlying signaling pathways of cell death can be a straightforward approach to mitigate the unintended consequences.

The overwhelming majority of toxicological studies make it difficult to distinguish between the right and wrong. Notwithstanding, there is almost unanimous opinion among skeptics and proponents that the huge potential of TiO_2 NPs-based products requires immense attention to safety issues.

Acknowledgments

This work was supported by National Key R&D Program of China (2018YFC0910601, 2019YFA0405603), Natural Science Foundation of China (31971292, U1432114 to Aiguo Wu), Zhejiang Province Financial Supporting (2017C03042, LY18H180011), and the Science & Technology Bureau of Ningbo City (2015B11002, 2017C110022). Furthermore, the authors also acknowledge Shanghai Synchrotron Radiation Facility at Line BL15U (No. h15sr0021) for X-ray fluorescence imaging and National Synchrotron Radiation Laboratory in Hefei for soft X-ray imaging (No. 2016-HLS-PT-002193). Madiha Saeed thanks the Chinese Academy of Sciences (CAS) and The World Academy of Sciences (TWAS) for awarding her a CAS-TWAS President's PhD fellowship (2014A8017407006).

References

1 Xu, Z. et al. (2010). Interaction of nano-TiO_2 with lysozyme: insights into the enzyme toxicity of nanosized particles. *Environmental Science and Pollution Research* 17 (3): 798–806.

2 Monopoli, M.P. et al. (2012). Biomolecular coronas provide the biological identity of nanosized materials. *Nature Nanotechnology* 7 (12): 779.

3 Llop, J. et al. (2014). Uptake, biological fate, and toxicity of metal oxide nanoparticles. *Particle and Particle Systems Characterization* 31 (1): 24–35.
4 Oberdörster, G. (2010). Safety assessment for nanotechnology and nanomedicine: concepts of nanotoxicology. *Journal of Internal Medicine* 267 (1): 89–105.
5 Limo, M.J. et al. (2018). Interactions between metal oxides and biomolecules: from fundamental understanding to applications. *Chemical Reviews* 118 (22): 11118–11193.
6 Nel, A.E. et al. (2009). Understanding biophysicochemical interactions at the nano-bio interface. *Nature Materials* 8 (7): 543.
7 Septiadi, D. et al. (2018). Nanoparticle–cell interaction: a cell mechanics perspective. *Advanced Materials* 30 (19): 1704463.
8 Lundqvist, M. et al. (2008). Nanoparticle size and surface properties determine the protein corona with possible implications for biological impacts. *Proceedings of the National Academy of Sciences of the United States of America* 105 (38): 14265–14270.
9 Zhang, X., Li, W., and Yang, Z. (2015). Toxicology of nanosized titanium dioxide: an update. *Archives of Toxicology* 89 (12): 2207–2217.
10 Zhang, Y. et al. (2014). Perturbation of physiological systems by nanoparticles. *Chemical Society Reviews* 43 (10): 3762–3809.
11 Du, B., Yu, M., and Zheng, J. (2018). Transport and interactions of nanoparticles in the kidneys. *Nature Reviews Materials* 3: 358–374.
12 Buettner, K.M. and Valentine, A.M. (2011). Bioinorganic chemistry of titanium. *Chemical Reviews* 112 (3): 1863–1881.
13 Saeed, M., Ren, W., and Wu, A. (2018). Therapeutic applications of iron oxide based nanoparticles in cancer: basic concepts and recent advances. *Biomaterials Science* 6 (4): 708–725.
14 Rajh, T. et al. (2014). Titanium dioxide in the service of the biomedical revolution. *Chemical Reviews* 114 (19): 10177–10216.
15 Yin, Z.F. et al. (2013). Recent progress in biomedical applications of titanium dioxide. *Physical Chemistry Chemical Physics* 15 (14): 4844–4858.
16 Baan, R. et al. (2006). Carcinogenicity of carbon black, titanium dioxide, and talc. *The Lancet Oncology* 7 (4): 295–296.
17 Winkler, H.C. et al. (2018). Critical review of the safety assessment of titanium dioxide additives in food. *Journal of Nanobiotechnology* 16 (1): 51.
18 Shi, H. et al. (2013). Titanium dioxide nanoparticles: a review of current toxicological data. *Particle and Fibre Toxicology* 10 (1): 15.
19 Hendren, C.O. et al. (2011). Estimating production data for five engineered nanomaterials as a basis for exposure assessment. *Environmental Science & Technology* 45 (7): 2562–2569.
20 Cai, R. et al. (1992). Increment of photocatalytic killing of cancer cells using TiO_2 with the aid of superoxide dismutase. *Chemistry Letters* 21 (3): 427–430.
21 Fujishima, A. (1986). Behavior of tumor cells on photoexcited semiconductor surface. *Photomedicine and Photobiology* 8: 45–46.
22 Kubo, W. and Tatsuma, T. (2004). Detection of H_2O_2 released from TiO_2 photocatalyst to air. *Analytical Sciences* 20 (4): 591–593.

23 Nosaka, Y., Nakamura, M., and Hirakawa, T. (2002). Behavior of superoxide radicals formed on TiO_2 powder photocatalysts studied by a chemiluminescent probe method. *Physical Chemistry Chemical Physics* 4 (6): 1088–1092.

24 Murakami, Y. et al. (2006). Direct detection of OH radicals diffused to the gas phase from the UV-irradiated photocatalytic TiO_2 surfaces by means of laser-induced fluorescence spectroscopy. *The Journal of Physical Chemistry B* 110 (34): 16808–16811.

25 Chen, X. et al. (2011). Increasing solar absorption for photocatalysis with black hydrogenated titanium dioxide nanocrystals. *Science* 331 (6018): 746–750.

26 Hu, Y.H. (2012). A highly efficient photocatalyst—hydrogenated black TiO_2 for the photocatalytic splitting of water. *Angewandte Chemie International Edition* 51 (50): 12410–12412.

27 Ren, W. et al. (2015). A near infrared light triggered hydrogenated black TiO_2 for cancer photothermal therapy. *Advanced Healthcare Materials* 4 (10): 1526–1536.

28 Mou, J. et al. (2016). Black titania-based theranostic nanoplatform for single NIR laser induced dual-modal imaging-guided PTT/PDT. *Biomaterials* 84: 13–24.

29 Saeed, M. et al. (2019). Tunable fabrication of new theranostic Fe_3O_4-black TiO_2 nanocomposites: dual wavelength stimulated synergistic imaging-guided phototherapy in cancer. *Journal of Materials Chemistry B* 7 (2): 210–223.

30 Ren, W. et al. (2017). Black TiO_2 based core–shell nanocomposites as doxorubicin carriers for thermal imaging guided synergistic therapy of breast cancer. *Nanoscale* 9 (31): 11195–11204.

31 Guo, W. et al. (2017). TiO_{2-x} based nanoplatform for bimodal cancer imaging and NIR-triggered chem/photodynamic/photothermal combination therapy. *Chemistry of Materials* 29 (21): 9262–9274.

32 Miyoshi, N. et al. (2011). Application of titanium dioxide (TiO_2) nanoparticles in photodynamic therapy (PDT) of an experimental tumor. In: *AIP Conference Proceedings*. AIP.

33 Iqbal, M.Z. et al. (2018). A facile fabrication route for binary transition metal oxide-based Janus nanoparticles for cancer theranostic applications. *Nano Research* 11 (10): 5735–5750.

34 Zeng, L. et al. (2015). Doxorubicin-loaded $NaYF_4$: Yb/Tm–TiO_2 inorganic photosensitizers for NIR-triggered photodynamic therapy and enhanced chemotherapy in drug-resistant breast cancers. *Biomaterials* 57: 93–106.

35 Zeng, L. et al. (2013). Multifunctional Fe_3O_4–TiO_2 nanocomposites for magnetic resonance imaging and potential photodynamic therapy. *Nanoscale* 5 (5): 2107–2113.

36 Li, N., Xia, T., and Nel, A.E. (2008). The role of oxidative stress in ambient particulate matter-induced lung diseases and its implications in the toxicity of engineered nanoparticles. *Free Radical Biology and Medicine* 44 (9): 1689–1699.

37 Shukla, R.K. et al. (2011). ROS-mediated genotoxicity induced by titanium dioxide nanoparticles in human epidermal cells. *Toxicology In Vitro* 25 (1): 231–241.

38 Kramer, G.F. and Ames, B.N. (1987). Oxidative mechanisms of toxicity of low-intensity near-UV light in *Salmonella typhimurium*. *Journal of Bacteriology* 169 (5): 2259–2266.

39 Sinha, R.P. and Häder, D.-P. (2002). UV-induced DNA damage and repair: a review. *Photochemical and Photobiological Sciences* 1 (4): 225–236.

40 Song, Y., Li, X., and Du, X. (2009). Exposure to nanoparticles is related to pleural effusion, pulmonary fibrosis and granuloma. *European Respiratory Journal* 34 (3): 559–567.

41 Brain, J., Kreyling, W., and Gehr, P. (2010). To the editors: express concern about the recent paper by Song et al. *European Respiratory Journal* 35 (1): 226–227.

42 Bourquin, J. et al. (2018). Biodistribution, clearance, and long-term fate of clinically relevant nanomaterials. *Advanced Materials* 30 (19): 1704307.

43 Lara, Y. et al. (2011). Toxicological considerations of clinically applicable nanoparticles. *Nano Today* 6: 585–607.

44 Patton, J.S. and Byron, P.R. (2007). Inhaling medicines: delivering drugs to the body through the lungs. *Nature Reviews Drug Discovery* 6 (1): 67.

45 Rejman, J. et al. (2004). Size-dependent internalization of particles via the pathways of clathrin-and caveolae-mediated endocytosis. *Biochemical Journal* 377 (1): 159–169.

46 Kreyling, W.G. et al. (2012). Differences in the biokinetics of inhaled nano-versus micrometer-sized particles. *Accounts of Chemical Research* 46 (3): 714–722.

47 Oberdörster, G., Ferin, J., and Lehnert, B.E. (1994). Correlation between particle size, *in vivo* particle persistence, and lung injury. *Environmental Health Perspectives* 102 (Suppl. 5): 173–179.

48 Geiser, M. et al. (2005). Ultrafine particles cross cellular membranes by nonphagocytic mechanisms in lungs and in cultured cells. *Environmental Health Perspectives* 113 (11): 1555–1560.

49 Mühlfeld, C. et al. (2007). Re-evaluation of pulmonary titanium dioxide nanoparticle distribution using the "relative deposition index": evidence for clearance through microvasculature. *Particle and Fibre Toxicology* 4 (1): 7.

50 Geiser, M. and Kreyling, W.G. (2010). Deposition and biokinetics of inhaled nanoparticles. *Particle and Fibre Toxicology* 7 (1): 2.

51 Kreyling, W.G. et al. (2017). Quantitative biokinetics of titanium dioxide nanoparticles after intratracheal instillation in rats: Part 3. *Nanotoxicology* 11 (4): 454–464.

52 Knowles, M.R. and Boucher, R.C. (2002). Mucus clearance as a primary innate defense mechanism for mammalian airways. *The Journal of Clinical Investigation* 109 (5): 571–577.

53 Heyder, J. et al. (1986). Deposition of particles in the human respiratory tract in the size range 0.005–15 μm. *Journal of Aerosol Science* 17 (5): 811–825.

54 Weir, A. et al. (2012). Titanium dioxide nanoparticles in food and personal care products. *Environmental Science and Technology* 46 (4): 2242–2250.

55 McCracken, C., Dutta, P.K., and Waldman, W.J. (2016). Critical assessment of toxicological effects of ingested nanoparticles. *Environmental Science: Nano* 3 (2): 256–282.

56 Kreyling, W.G. et al. (2017). Quantitative biokinetics of titanium dioxide nanoparticles after oral application in rats: Part 2. *Nanotoxicology* 11 (4): 443–453.

57 Wang, J. et al. (2007). Acute toxicity and biodistribution of different sized titanium dioxide particles in mice after oral administration. *Toxicology Letters* 168 (2): 176–185.

58 Wang, Y. et al. (2013). Susceptibility of young and adult rats to the oral toxicity of titanium dioxide nanoparticles. *Small* 9 (9–10): 1742–1752.

59 Zhang, Y.-N. et al. (2016). Nanoparticle–liver interactions: cellular uptake and hepatobiliary elimination. *Journal of Controlled Release* 240: 332–348.

60 Setyawati, M. et al. (2013). Titanium dioxide nanomaterials cause endothelial cell leakiness by disrupting the homophilic interaction of VE–cadherin. *Nature Communications* 4: 1673.

61 Zhu, M. et al. (2012). Physicochemical properties determine nanomaterial cellular uptake, transport, and fate. *Accounts of Chemical Research* 46 (3): 622–631.

62 Schanen, B.C. et al. (2009). Exposure to titanium dioxide nanomaterials provokes inflammation of an *in vitro* human immune construct. *ACS Nano* 3 (9): 2523–2532.

63 Saldana, L. and Vilaboa, N. (2010). Effects of micrometric titanium particles on osteoblast attachment and cytoskeleton architecture. *Acta Biomaterialia* 6 (4): 1649–1660.

64 Septiadi, D. et al. (2018). Nanoparticle-cell interaction: a cell mechanics perspective. *Advanced Materials* 30 (19): e1704463.

65 Xu, J. et al. (2013). Acute toxicity of intravenously administered titanium dioxide nanoparticles in mice. *PLoS One* 8 (8): e70618.

66 Kreyling, W.G. et al. (2017). Quantitative biokinetics of titanium dioxide nanoparticles after intravenous injection in rats: Part 1. *Nanotoxicology* 11 (4): 434–442.

67 Mou, J. et al. (2017). A new green titania with enhanced NIR absorption for mitochondria-targeted cancer therapy. *Theranostics* 7 (6): 1531.

68 Saeed, M. et al. (2018). Controllable synthesis of Fe_3O_4 nanoflowers: enhanced imaging guided cancer therapy and comparison of photothermal efficiency with black-TiO_2. *Journal of Materials Chemistry B* 6 (22): 3800–3810.

69 Han, X. et al. (2018). Oxygen-deficient black titania for synergistic/enhanced sonodynamic and photoinduced cancer therapy at near infrared-II biowindow. *ACS Nano* 12 (5): 4545–4555.

70 Wang, M. et al. (2018). Rational design of multifunctional Fe@γ-Fe_2O_3@H-TiO_2 nanocomposites with enhanced magnetic and photoconversion effects for wide applications: from photocatalysis to

imaging-guided photothermal cancer therapy. *Advanced Materials* 30 (13): 1706747.

71 Kermanizadeh, A. et al. (2015). Nanomaterial translocation–the biokinetics, tissue accumulation, toxicity and fate of materials in secondary organs–a review. *Critical Reviews in Toxicology* 45 (10): 837–872.

72 Nohynek, G.J. et al. (2007). Grey goo on the skin? Nanotechnology, cosmetic and sunscreen safety. *Critical Reviews in Toxicology* 37 (3): 251–277.

73 Monteiro-Riviere, N.A. et al. (2011). Safety evaluation of sunscreen formulations containing titanium dioxide and zinc oxide nanoparticles in UVB sunburned skin: an *in vitro* and *in vivo* study. *Toxicological Sciences* 123 (1): 264–280.

74 Newman, M.D., Stotland, M., and Ellis, J.I. (2009). The safety of nanosized particles in titanium dioxide–and zinc oxide–based sunscreens. *Journal of the American Academy of Dermatology* 61 (4): 685–692.

75 Barry, B.W. (2001). Novel mechanisms and devices to enable successful transdermal drug delivery. *European Journal of Pharmaceutical Sciences* 14 (2): 101–114.

76 Lodén, M. et al. (2011). Sunscreen use: controversies, challenges and regulatory aspects. *British Journal of Dermatology* 165 (2): 255–262.

77 Clarke, P.G. (1990). Developmental cell death: morphological diversity and multiple mechanisms. *Anatomy and Embryology* 181 (3): 195–213.

78 Boya, P. and Kroemer, G. (2008). Lysosomal membrane permeabilization in cell death. *Oncogene* 27 (50): 6434.

79 Galluzzi, L. et al. (2012). Molecular definitions of cell death subroutines: recommendations of the Nomenclature Committee on Cell Death 2012. *Cell Death and Differentiation* 19 (1): 107.

80 Kroemer, G. et al. (2009). Classification of cell death: recommendations of the Nomenclature Committee on Cell Death 2009. *Cell Death and Differentiation* 16 (1): 3.

81 Sims, C.M. et al. (2017). Redox-active nanomaterials for nanomedicine applications. *Nanoscale* 9 (40): 15226–15251.

82 Zhao, F. et al. (2011). Cellular uptake, intracellular trafficking, and cytotoxicity of nanomaterials. *Small* 7 (10): 1322–1337.

83 Nel, A. et al. (2012). Nanomaterial toxicity testing in the 21st century: use of a predictive toxicological approach and high-throughput screening. *Accounts of Chemical Research* 46 (3): 607–621.

84 Soenen, S.J. et al. (2015). (Intra) cellular stability of inorganic nanoparticles: effects on cytotoxicity, particle functionality, and biomedical applications. *Chemical Reviews* 115 (5): 2109–2135.

85 De Stefano, D., Carnuccio, R., and Maiuri, M.C. (2012). Nanomaterials toxicity and cell death modalities. *Journal of Drug Delivery* 2012: 1–14.

86 Hussain, S. et al. (2009). Oxidative stress and proinflammatory effects of carbon black and titanium dioxide nanoparticles: role of particle surface area and internalized amount. *Toxicology* 260 (1–3): 142–149.

87 Wu, J., Sun, J., and Xue, Y. (2010). Involvement of JNK and P53 activation in G2/M cell cycle arrest and apoptosis induced by titanium dioxide nanoparticles in neuron cells. *Toxicology Letters* 199 (3): 269–276.

88 Park, E.-J. et al. (2008). Oxidative stress and apoptosis induced by titanium dioxide nanoparticles in cultured BEAS-2B cells. *Toxicology Letters* 180 (3): 222–229.

89 Boland, S., Hussain, S., and Baeza-Squiban, A. (2014). Carbon black and titanium dioxide nanoparticles induce distinct molecular mechanisms of toxicity. *Wiley Interdisciplinary Reviews* 6 (6): 641–652.

90 Hussain, S. et al. (2010). Carbon black and titanium dioxide nanoparticles elicit distinct apoptotic pathways in bronchial epithelial cells. *Particle and Fibre Toxicology* 7 (1): 10.

91 Tay, C.Y. et al. (2014). Nano-hydroxyapatite and nano-titanium dioxide exhibit different subcellular distribution and apoptotic profile in human oral epithelium. *ACS Applied Materials & Interfaces* 6 (9): 6248–6256.

92 Gurr, J.-R. et al. (2005). Ultrafine titanium dioxide particles in the absence of photoactivation can induce oxidative damage to human bronchial epithelial cells. *Toxicology* 213 (1–2): 66–73.

93 Shukla, R.K. et al. (2013). TiO_2 nanoparticles induce oxidative DNA damage and apoptosis in human liver cells. *Nanotoxicology* 7 (1): 48–60.

94 Hu, R. et al. (2011). Molecular mechanism of hippocampal apoptosis of mice following exposure to titanium dioxide nanoparticles. *Journal of Hazardous Materials* 191 (1–3): 32–40.

95 Shi, Y. et al. (2010). Titanium dioxide nanoparticles cause apoptosis in BEAS-2B cells through the caspase 8/t-Bid-independent mitochondrial pathway. *Toxicology Letters* 196 (1): 21–27.

96 Jin, C.-Y. et al. (2008). Cytotoxicity of titanium dioxide nanoparticles in mouse fibroblast cells. *Chemical Research in Toxicology* 21 (9): 1871–1877.

97 Chen, H.-W. et al. (2006). Titanium dioxide nanoparticles induce emphysema-like lung injury in mice. *The FASEB Journal* 20 (13): 2393–2395.

98 Zhu, Y., Eaton, J.W., and Li, C. (2012). Titanium dioxide (TiO_2) nanoparticles preferentially induce cell death in transformed cells in a Bak/Bax-independent fashion. *PLoS One* 7 (11): e50607.

99 Yoo, K.-C. et al. (2012). Titanium dioxide induces apoptotic cell death through reactive oxygen species-mediated Fas upregulation and Bax activation. *International Journal of Nanomedicine* 7: 1203.

100 Elmore, S. (2007). Apoptosis: a review of programmed cell death. *Toxicologic Pathology* 35 (4): 495–516.

101 Ravikumar, B. et al. (2010). Regulation of mammalian autophagy in physiology and pathophysiology. *Physiological Reviews* 90 (4): 1383–1435.

102 Kroemer, G. and Jäättelä, M. (2005). Lysosomes and autophagy in cell death control. *Nature Reviews Cancer* 5 (11): 886.

103 Zhao, Y. et al. (2013). Exposure to titanium dioxide nanoparticles induces autophagy in primary human keratinocytes. *Small* 9 (3): 387–392.

104 Zhang, X. et al. (2016). Nano-TiO_2 induces autophagy to protect against cell death through antioxidative mechanism in podocytes. *Cell Biology and Toxicology* 32 (6): 513–527.

105 Lopes, V.R. et al. (2016). Dose-dependent autophagic effect of titanium dioxide nanoparticles in human HaCaT cells at non-cytotoxic levels. *Journal of Nanobiotechnology* 14 (1): 22.

106 Kenzaoui, B.H. et al. (2012). Induction of oxidative stress, lysosome activation and autophagy by nanoparticles in human brain-derived endothelial cells. *Biochemical Journal* 441 (3): 813–821.

107 Pattingre, S. et al. (2005). Bcl-2 antiapoptotic proteins inhibit Beclin 1-dependent autophagy. *Cell* 122 (6): 927–939.

108 Kang, R. et al. (2011). The Beclin 1 network regulates autophagy and apoptosis. *Cell Death and Differentiation* 18 (4): 571.

109 Stern, S.T., Adiseshaiah, P.P., and Crist, R.M. (2012). Autophagy and lysosomal dysfunction as emerging mechanisms of nanomaterial toxicity. *Particle and Fibre Toxicology* 9: 20.

110 Braydich-Stolle, L.K. et al. (2009). Crystal structure mediates mode of cell death in TiO_2 nanotoxicity. *Journal of Nanoparticle Research* 11 (6): 1361–1374.

111 Gali, N.K. et al. (2016). Investigation on the mechanism of non-photocatalytically TiO_2-induced reactive oxygen species and its significance on cell cycle and morphology. *Journal of Applied Toxicology* 36 (10): 1355–1363.

112 Andón, F.T. and Fadeel, B. (2012). Programmed cell death: molecular mechanisms and implications for safety assessment of nanomaterials. *Accounts of Chemical Research* 46 (3): 733–742.

113 Arami, H., Mazloumi, M., Khalifehzadeh, R., and Sadrnezhaad, S.K. (2007). Sonochemical preparation of TiO_2 nanoparticles. *Materials Letters* 61 (23–24): 4559–4561.

114 Hirano, K., Nitta, H., and Sawada, K. (2005). Effect of sonication on the photo-catalytic mineralization of some chlorinated organic compounds. *Ultrasonics Sonochemistry* 12 (4): 271–276.

115 Parkin, I.P. and Palgrave, R.G. (2005). Self-cleaning coatings. *Journal of Materials Chemistry* 15 (17): 1689–1695.

116 Serpone, N., Salinaro, A., and Emeline, A. (2001). Deleterious effects of sunscreen titanium dioxide nanoparticles on DNA: efforts to limit DNA damage by particle surface modification. In: *Nanoparticles and Nanostructured Surfaces: Novel Reporters with Biological Applications*, vol. 4258, 86–98. International Society for Optics and Photonics.

117 Long, T.C. et al. (2006). Titanium dioxide (P25) produces reactive oxygen species in immortalized brain microglia (BV2): implications for nanoparticle neurotoxicity. *Environmental Science and Technology* 40 (14): 4346–4352.

118 Hidaka, H. et al. (1997). *In vitro* photochemical damage to DNA, RNA and their bases by an inorganic sunscreen agent on exposure to UVA and UVB radiation. *Journal of Photochemistry and Photobiology A* 111 (1–3): 205–213.

119 Hu, X. et al. (2009). *In vitro* evaluation of cytotoxicity of engineered metal oxide nanoparticles. *Science of the Total Environment* 407 (8): 3070–3072.

120 Hou, J. et al. (2019). Toxicity and mechanisms of action of titanium dioxide nanoparticles in living organisms. *Journal of Environmental Sciences* 75: 40–53.

121 Xia, T. et al. (2006). Comparison of the abilities of ambient and manufactured nanoparticles to induce cellular toxicity according to an oxidative stress paradigm. *Nano Letters* 6 (8): 1794–1807.

122 Aderem, A. and Underhill, D.M. (1999). Mechanisms of phagocytosis in macrophages. *Annual Review of Immunology* 17 (1): 593–623.

123 Rothen-Rutishauser, B.M. et al. (2006). Interaction of fine particles and nanoparticles with red blood cells visualized with advanced microscopic techniques. *Environmental Science and Technology* 40 (14): 4353–4359.

124 Kocbek, P. et al. (2010). Toxicological aspects of long-term treatment of keratinocytes with ZnO and TiO_2 nanoparticles. *Small* 6 (17): 1908–1917.

125 Xia, T. et al. (2008). Comparison of the mechanism of toxicity of zinc oxide and cerium oxide nanoparticles based on dissolution and oxidative stress properties. *ACS Nano* 2 (10): 2121–2134.

126 Long, T.C. et al. (2007). Nanosize titanium dioxide stimulates reactive oxygen species in brain microglia and damages neurons *in vitro*. *Environmental Health Perspectives* 115 (11): 1631–1637.

127 Dunford, R. et al. (1997). Chemical oxidation and DNA damage catalysed by inorganic sunscreen ingredients. *FEBS Letters* 418 (1–2): 87–90.

128 Uchino, T. et al. (2002). Quantitative determination of OH radical generation and its cytotoxicity induced by TiO_2–UVA treatment. *Toxicology In Vitro* 16 (5): 629–635.

129 Dodd, N.J. and Jha, A.N. (2009). Titanium dioxide induced cell damage: a proposed role of the carboxyl radical. *Mutation Research/Fundamental and Molecular Mechanisms of Mutagenesis* 660 (1–2): 79–82.

130 Wang, J. et al. (2008). Potential neurological lesion after nasal instillation of TiO_2 nanoparticles in the anatase and rutile crystal phases. *Toxicology Letters* 183 (1–3): 72–80.

131 Kang, J.L. et al. (2008). Comparison of the biological activity between ultrafine and fine titanium dioxide particles in RAW 264.7 cells associated with oxidative stress. *Journal of Toxicology & Environmental Health, Part A* 71 (8): 478–485.

132 Yazdi, A.S. et al. (2010). Nanoparticles activate the NLR pyrin domain containing 3 (Nlrp3) inflammasome and cause pulmonary inflammation through release of IL-1α and IL-1β. *Proceedings of the National Academy of Sciences of the United States of American* 107 (45): 19449–19454.

133 Lu, P.-J., Ho, I.-C., and Lee, T.-C. (1998). Induction of sister chromatid exchanges and micronuclei by titanium dioxide in Chinese hamster ovary-K1 cells. *Mutation Research/Genetic Toxicology and Environmental Mutagenesis* 414 (1–3): 15–20.

134 Toyooka, T., Amano, T., and Ibuki, Y. (2012). Titanium dioxide particles phosphorylate histone H2AX independent of ROS production. *Mutation Research/Genetic Toxicology and Environmental Mutagenesis* 742 (1–2): 84–91.

135 Rahman, Q. et al. (2002). Evidence that ultrafine titanium dioxide induces micronuclei and apoptosis in Syrian hamster embryo fibroblasts. *Environmental Health Perspectives* 110 (8): 797–800.

136 Xu, A. et al. (2009). Genotoxic responses to titanium dioxide nanoparticles and fullerene in gpt delta transgenic MEF cells. *Particle and Fibre Toxicology* 6 (1): 3.

137 Magdolenova, Z. et al. (2012). Impact of agglomeration and different dispersions of titanium dioxide nanoparticles on the human related *in vitro* cytotoxicity and genotoxicity. *Journal of Environmental Monitoring* 14 (2): 455–464.

138 Jugan, M.-L. et al. (2012). Titanium dioxide nanoparticles exhibit genotoxicity and impair DNA repair activity in A549 cells. *Nanotoxicology* 6 (5): 501–513.

139 Zucker, R. et al. (2010). Detection of TiO_2 nanoparticles in cells by flow cytometry. *Cytometry Part A* 77 (7): 677–685.

140 Saquib, Q. et al. (2012). Titanium dioxide nanoparticles induced cytotoxicity, oxidative stress and DNA damage in human amnion epithelial (WISH) cells. *Toxicology In Vitro* 26 (2): 351–361.

141 Scherbart, A.M. et al. (2011). Contrasting macrophage activation by fine and ultrafine titanium dioxide particles is associated with different uptake mechanisms. *Particle and Fibre Toxicology* 8 (1): 31.

142 Bhattacharya, K. et al. (2009). Titanium dioxide nanoparticles induce oxidative stress and DNA-adduct formation but not DNA-breakage in human lung cells. *Particle and Fibre Toxicology* 6 (1): 17.

143 Trouiller, B. et al. (2009). Titanium dioxide nanoparticles induce DNA damage and genetic instability *in vivo* in mice. *Cancer Research* 69 (22): 8784–8789.

144 Wang, J.J., Sanderson, B.J., and Wang, H. (2007). Cyto-and genotoxicity of ultrafine TiO_2 particles in cultured human lymphoblastoid cells. *Mutation Research/Genetic Toxicology and Environmental Mutagenesis* 628 (2): 99–106.

145 Kang, S.J. et al. (2008). Titanium dioxide nanoparticles trigger p53-mediated damage response in peripheral blood lymphocytes. *Environmental and Molecular Mutagenesis* 49 (5): 399–405.

146 Falck, G. et al. (2009). Genotoxic effects of nanosized and fine TiO_2. *Human & Experimental Toxicology* 28 (6–7): 339–352.

147 Mano, S.S. et al. (2012). Effect of polyethylene glycol modification of TiO_2 nanoparticles on cytotoxicity and gene expressions in human cell lines. *International Journal of Molecular Sciences* 13 (3): 3703–3717.

148 Petković, J. et al. (2011). DNA damage and alterations in expression of DNA damage responsive genes induced by TiO_2 nanoparticles in human hepatoma HepG2 cells. *Nanotoxicology* 5 (3): 341–353.

149 Gerloff, K. et al. (2012). Distinctive toxicity of TiO_2 rutile/anatase mixed phase nanoparticles on Caco-2 cells. *Chemical Research in Toxicology* 25 (3): 646–655.

150 Wan, R. et al. (2012). DNA damage caused by metal nanoparticles: involvement of oxidative stress and activation of ATM. *Chemical Research in Toxicology* 25 (7): 1402–1411.

151 Woodruff, R.S. et al. (2012). Genotoxicity evaluation of titanium dioxide nanoparticles using the Ames test and Comet assay. *Journal of Applied Toxicology* 32 (11): 934–943.

152 Linnainmaa, K., Kivipensas, P., and Vainio, H. (1997). Toxicity and cytogenetic studies of ultrafine titanium dioxide in cultured rat liver epithelial cells. *Toxicology In Vitro* 11 (4): 329–335.

153 Fisichella, M. et al. (2012). Intestinal toxicity evaluation of TiO_2 degraded surface-treated nanoparticles: a combined physico-chemical and toxicogenomics approach in caco-2 cells. *Particle and Fibre Toxicology* 9 (1): 18.

154 Warheit, D.B. et al. (2007). Development of a base set of toxicity tests using ultrafine TiO_2 particles as a component of nanoparticle risk management. *Toxicology Letters* 171 (3): 99–110.

155 Wang, J. et al. (2007). Influence of intranasal instilled titanium dioxide nanoparticles on monoaminergic neurotransmitters of female mice at different exposure time. *Zhonghua yu fang yi xue za zhi [Chinese journal of preventive medicine]* 41 (2): 91–95.

156 Ali, I. et al. (2018). Humidity-responsive gold aerogel for real-time monitoring of human breath. *Langmuir* 34 (16): 4908–4913.

157 Wang, J. et al. (2011). Disruption of zebrafish (Danio rerio) reproduction upon chronic exposure to TiO_2 nanoparticles. *Chemosphere* 83 (4): 461–467.

158 Hussain, S. et al. (2011). Lung exposure to nanoparticles modulates an asthmatic response in a mouse model. *European Respiratory Journal* 37 (2): 299–309.

159 Zhu, X. et al. (2008). Comparative toxicity of several metal oxide nanoparticle aqueous suspensions to Zebrafish (*Danio rerio*) early developmental stage. *Journal of Environmental Science and Health, Part A* 43 (3): 278–284.

160 Hougaard, K.S. et al. (2010). Effects of prenatal exposure to surface-coated nanosized titanium dioxide (UV-Titan). A study in mice. *Particle and Fibre Toxicology* 7 (1): 16.

161 Yamashita, K. et al. (2011). Silica and titanium dioxide nanoparticles cause pregnancy complications in mice. *Nature Nanotechnology* 6 (5): 321.

162 Komatsu, T. et al. (2008). The effects of nanoparticles on mouse testis Leydig cells *in vitro*. *Toxicology In Vitro* 22 (8): 1825–1831.

163 Setyawati, M.I. et al. (2013). Cytotoxic and genotoxic characterization of titanium dioxide, gadolinium oxide, and poly (lactic-co-glycolic acid) nanoparticles in human fibroblasts. *Journal of Biomedical Materials Research Part A* 101 (3): 633–640.

164 Borm, P.J., Schins, R.P., and Albrecht, C. (2004). Inhaled particles and lung cancer, Part B: paradigms and risk assessment. *International Journal of Cancer* 110 (1): 3–14.

165 Dankovic, D., Kuempel, E., and Wheeler, M. (2007). An approach to risk assessment for TiO_2. *Inhalation Toxicology* 19 (Supp 1): 205–212.

166 Kuempel, E. et al. (2006). Lung dosimetry and risk assessment of nanoparticles: evaluating and extending current models in rats and humans. *Inhalation Toxicology* 18 (10): 717–724.

167 Pott, F. (2005). Carcinogenicity study with nineteen granular dusts in rats. *European Journal of Oncology* 10: 249–281.

168 Bernard, B.K. et al. (1990). Toxicology and carcinogenesis studies of dietary titanium dioxide-coated mica in male and female Fischer 344 rats. *Journal of Toxicology & Environmental Health Part A: Current Issues* 29 (4): 417–429.

169 Xu, J. et al. (2011). Lack of promoting effect of titanium dioxide particles on ultraviolet B-initiated skin carcinogenesis in rats. *Food and Chemical Toxicology* 49 (6): 1298–1302.

170 Boffetta, P. et al. (2001). Exposure to titanium dioxide and risk of lung cancer in a population-based study from Montreal. *Scandinavian Journal of Work, Environment & Health* 27 (4): 227–232.

171 Fryzek, J.P. et al. (2003). A cohort mortality study among titanium dioxide manufacturing workers in the United States. *Journal of Occupational and Environmental Medicine* 45 (4): 400–409.

172 Morimoto, Y. et al. (2010). Hazard assessments of manufactured nanomaterials. *Journal of Occupational Health* 52 (6): 325–334.

173 Suttiponparnit, K. et al. (2011). Role of surface area, primary particle size, and crystal phase on titanium dioxide nanoparticle dispersion properties. *Nanoscale Research Letters* 6 (1): 27.

174 Lee, K., Trochimowicz, H., and Reinhardt, C. (1985). Pulmonary response of rats exposed to titanium dioxide (TiO_2) by inhalation for two years. *Toxicology and Applied Pharmacology* 79 (2): 179–192.

175 Wang, S. et al. (2011). Chronic exposure to nanosized, anatase titanium dioxide is not cyto-or genotoxic to Chinese hamster ovary cells. *Environmental and Molecular Mutagenesis* 52 (8): 614–622.

176 Vamanu, C.I. et al. (2008). Induction of cell death by TiO_2 nanoparticles: studies on a human monoblastoid cell line. *Toxicology In Vitro* 22 (7): 1689–1696.

177 Palomäki, J. et al. (2010). Engineered nanomaterials cause cytotoxicity and activation on mouse antigen presenting cells. *Toxicology* 267 (1–3): 125–131.

178 Moon, E.-Y. et al. (2011). An increase in mouse tumor growth by an *in vivo* immunomodulating effect of titanium dioxide nanoparticles. *Journal of Immunotoxicology* 8 (1): 56–67.

179 Nel, A. et al. (2006). Toxic potential of materials at the nanolevel. *Science* 311 (5761): 622–627.

180 Peters, A. et al. (2006). Translocation and potential neurological effects of fine and ultrafine particles a critical update. *Particle and Fibre Toxicology* 3 (1): 13.

181 Borm, P.J. et al. (2006). The potential risks of nanomaterials: a review carried out for ECETOC. *Particle and Fibre Toxicology* 3 (1): 11.

182 Liu, S. et al. (2010). Oxidative stress and apoptosis induced by nanosized titanium dioxide in PC12 cells. *Toxicology* 267 (1–3): 172–177.

183 Liu, X. et al. (2010). A protein interaction network for the analysis of the neuronal differentiation of neural stem cells in response to titanium dioxide nanoparticles. *Biomaterials* 31 (11): 3063–3070.

184 Scuri, M. et al. (2010). Effects of titanium dioxide nanoparticle exposure on neuroimmune responses in rat airways. *Journal of Toxicology & Environmental Health Part A* 73 (20): 1353–1369.

185 Ma-Hock, L. et al. (2009). Development of a short-term inhalation test in the rat using nano-titanium dioxide as a model substance. *Inhalation Toxicology* 21 (2): 102–118.

186 Grassian, V.H. et al. (2006). Inhalation exposure study of titanium dioxide nanoparticles with a primary particle size of 2 to 5 nm. *Environmental Health Perspectives* 115 (3): 397–402.

187 Nurkiewicz, T.R. et al. (2008). Nanoparticle inhalation augments particle-dependent systemic microvascular dysfunction. *Particle and Fibre Toxicology* 5 (1): 1.

188 Nurkiewicz, T.R., Porter, D.W., Hubbs, A.F. et al. (2011). Pulmonary particulate matter and systemic microvascular dysfunction. *Research Report (Health Effects Institute)* 164: 3–48.

189 LeBlanc, A. et al. (2009). Nanoparticle inhalation impairs endothelium-dependent vasodilation in subepicardial arterioles. *Journal of Toxicology & Environmental Health Part A* 72 (24): 1576–1584.

190 Sun, Q., Hong, X., and Wold, L.E. (2010). Cardiovascular effects of ambient particulate air pollution exposure. *Circulation* 121 (25): 2755–2765.

191 Liu, R. et al. (2009). Pulmonary toxicity induced by three forms of titanium dioxide nanoparticles via intra-tracheal instillation in rats. *Progress in Natural Science* 19 (5): 573–579.

192 Liu, R. et al. (2010). Small-sized titanium dioxide nanoparticles mediate immune toxicity in rat pulmonary alveolar macrophages in vivo. *Journal of Nanoscience and Nanotechnology* 10 (8): 5161–5169.

193 Liu, R. et al. (2010). The immune toxicity of titanium dioxide on primary pulmonary alveolar macrophages relies on their surface area and crystal structure. *Journal of Nanoscience and Nanotechnology* 10 (12): 8491–8499.

194 Shakeel, M. et al. (2016). Toxicity of nano-titanium dioxide (TiO_2-NP) through various routes of exposure: a review. *Biological Trace Element Research* 172 (1): 1–36.

195 Unnithan, J. et al. (2011). Aqueous synthesis and concentration-dependent dermal toxicity of TiO_2 nanoparticles in Wistar rats. *Biological Trace Element Research* 143 (3): 1682–1694.

196 Liu, H. et al. (2009). Biochemical toxicity of nano-anatase TiO_2 particles in mice. *Biological Trace Element Research* 129 (1–3): 170–180.

197 Ma, L. et al. (2009). The acute liver injury in mice caused by nano-anatase TiO_2. *Nanoscale Research Letters* 4 (11): 1275.

198 Saber, A.T. et al. (2012). Inflammatory and genotoxic effects of nanoparticles designed for inclusion in paints and lacquers. *Nanotoxicology* 6 (5): 453–471.

199 Sayes, C.M. et al. (2006). Correlating nanoscale titania structure with toxicity: a cytotoxicity and inflammatory response study with human dermal fibroblasts and human lung epithelial cells. *Toxicological Sciences* 92 (1): 174–185.

200 Ma, L. et al. (2010). Oxidative stress in the brain of mice caused by translocated nanoparticulate TiO_2 delivered to the abdominal cavity. *Biomaterials* 31 (1): 99–105.

201 Aisaka, Y. et al. (2008). Hemolysis caused by titanium dioxide particles. *Inhalation Toxicology* 20 (9): 891–893.

202 Zhang, J. et al. (2013). Cytotoxicity of different sized TiO_2 nanoparticles in mouse macrophages. *Toxicology and Industrial Health* 29 (6): 523–533.

203 Rossi, E.M. et al. (2009). Airway exposure to silica-coated TiO_2 nanoparticles induces pulmonary neutrophilia in mice. *Toxicological Sciences* 113 (2): 422–433.

204 Kan, H. et al. (2012). Pulmonary exposure of rats to ultrafine titanium dioxide enhances cardiac protein phosphorylation and substance P synthesis in nodose ganglia. *Nanotoxicology* 6 (7): 736–745.

205 Oberdörster, G. et al. (2000). Acute pulmonary effects of ultrafine particles in rats and mice. *Research Report (Health Effects Institute)* (96): 5–74; disc. 75–86.

206 Li, Y. et al. (2010). Systematic influence induced by 3 nm titanium dioxide following intratracheal instillation of mice. *Journal of Nanoscience and Nanotechnology* 10 (12): 8544–8549.

207 Bu, Q. et al. (2010). NMR-based metabonomic study of the sub-acute toxicity of titanium dioxide nanoparticles in rats after oral administration. *Nanotechnology* 21 (12): 125105.

208 Bermudez, E. et al. (2004). Pulmonary responses of mice, rats, and hamsters to subchronic inhalation of ultrafine titanium dioxide particles. *Toxicological Sciences* 77 (2): 347–357.

209 Warheit, D.B. et al. (2006). Pulmonary instillation studies with nanoscale TiO_2 rods and dots in rats: toxicity is not dependent upon particle size and surface area. *Toxicological Sciences* 91 (1): 227–236.

210 Setyawati, M.I., Tay, C.Y., and Leong, D.T. (2015). Mechanistic investigation of the biological effects of SiO_2, TiO_2, and ZnO nanoparticles on intestinal cells. *Small* 11 (28): 3458–3468.

211 Warheit, D., Kreiling, R., and Levy, L. (2016). Relevance of the rat lung tumor response to particle overload for human risk assessment—update and interpretation of new data since ILSI 2000. *Toxicology* 374: 42–59.

212 De Angelis, I. et al. (2013). Comparative study of ZnO and TiO_2 nanoparticles: physicochemical characterisation and toxicological effects on human colon carcinoma cells. *Nanotoxicology* 7 (8): 1361–1372.

213 Huang, S. et al. (2009). Disturbed mitotic progression and genome segregation are involved in cell transformation mediated by nano-TiO_2 long-term exposure. *Toxicology and Applied Pharmacology* 241 (2): 182–194.

214 Berntsen, P. et al. (2010). Biomechanical effects of environmental and engineered particles on human airway smooth muscle cells. *Journal of the Royal Society Interface* 7 (Suppl 3): S331–S340.

215 Carbone, R. et al. (2006). Biocompatibility of cluster-assembled nanostructured TiO_2 with primary and cancer cells. *Biomaterials* 27 (17): 3221–3229.

216 Karpagavalli, R. et al. (2007). Corrosion behavior and biocompatibility of nanostructured TiO_2 film on Ti6Al4V. *Journal of Biomedical Materials Research Part A* 83 (4): 1087–1095.

217 Popat, K.C. et al. (2007). Influence of engineered titania nanotubular surfaces on bone cells. *Biomaterials* 28 (21): 3188–3197.

218 Du, Y. et al. (2015). The enhanced chemotherapeutic effects of doxorubicin loaded PEG coated TiO_2 nanocarriers in an orthotopic breast tumor bearing mouse model. *Journal of Materials Chemistry B* 3 (8): 1518–1528.

219 Bermejo-Nogales, A. et al. (2017). Negligible cytotoxicity induced by different titanium dioxide nanoparticles in fish cell lines. *Ecotoxicology and Environmental Safety* 138: 309–319.

220 Koeneman, B.A. et al. (2010). Toxicity and cellular responses of intestinal cells exposed to titanium dioxide. *Cell Biology and Toxicology* 26 (3): 225–238.

221 Hussain, S. et al. (2005). *In vitro* toxicity of nanoparticles in BRL 3A rat liver cells. *Toxicology In Vitro* 19 (7): 975–983.

222 Fujita, K. et al. (2009). Effects of ultrafine TiO_2 particles on gene expression profile in human keratinocytes without illumination: involvement of extracellular matrix and cell adhesion. *Toxicology Letters* 191 (2–3): 109–117.

223 Jayaram, D.T. et al. (2017). Nanoparticle-induced oxidation of corona proteins initiates an oxidative stress response in cells. *Nanoscale* 9 (22): 7595–7601.

224 Runa, S. et al. (2016). TiO_2 nanoparticles alter the expression of peroxiredoxin antioxidant genes. *The Journal of Physical Chemistry C* 120 (37): 20736–20742.

225 Pérez-Campaña, C. et al. (2014). Production of 18F-labeled titanium dioxide nanoparticles by proton irradiation for biodistribution and biological fate studies in rats. *Particle and Particle Systems Characterization* 31 (1): 134–142.

226 Xie, G. et al. (2011). Tissue distribution and excretion of intravenously administered titanium dioxide nanoparticles. *Toxicology Letters* 205 (1): 55–61.

227 Sha, B. et al. (2015). The potential health challenges of TiO_2 nanomaterials. *Journal of Applied Toxicology* 35 (10): 1086–1101.

228 Sharifi, S. et al. (2012). Toxicity of nanomaterials. *Chemical Society Reviews* 41 (6): 2323–2343.

229 Li, M. et al. (2014). Mechanistic characterization of titanium dioxide nanoparticle-induced toxicity using electron spin resonance. *Journal of Food and Drug Analysis* 22 (1): 76–85.

230 Mu, Q. et al. (2014). Chemical basis of interactions between engineered nanoparticles and biological systems. *Chemical Reviews* 114 (15): 7740–7781.

3

Antibacterial Applications of TiO_2 Nanoparticles

Chen Xu[1,2], Jianjun Zheng[2,3], and Aiguo Wu[1]*

[1] Cixi Institute of Biomedical Engineering, CAS Key Laboratory of Magnetic Materials and Devices & Key Laboratory of Additive Manufacturing Materials of Zhejiang Province, Ningbo Institute of Materials Technology and Engineering, Chinese Academy of Sciences, 1219 Zhongguan West Road, Zhenhai District, Ningbo, 315201, P.R. China
[2] Hwa Mei Hospital, University of Chinese Academy of Sciences, Department of Experimental Medical Science, 41 Northwest Street, Haishu district, Ningbo, 315010, P.R. China
[3] Key Laboratory of Diagnosis and Treatment of Digestive System Tumors of Zhejiang Province, 175 Yongfeng North Road, Jiangbei District, Ningbo, 315016, P.R. China

CHAPTER MENU

Introduction, 105
Antibacterial Effect of TiO_2 Nanoparticle, 107
Ion-Doped TiO_2 Nanoparticles and Their Antibacterial Effect, 113
Antibacterial Agent-Doped TiO_2 Nanoparticles and Their Antibacterial Effect, 120
Antibacterial Applications of TiO_2-Based Nanoparticles, 124
Conclusion and Outlook, 126

3.1 Introduction

Extensive researches have been focused on TiO_2 nanoparticles for the inhibition and inactivation of various bacteria because of their photocatalytic performance. Since Matsunaga et al. [1] reported the bactericidal effect of TiO_2 based on the photocatalytic treatment in 1985, TiO_2-based nanoparticles have been investigated as a kind of photocatalysts extensively for disinfection of microorganism [2–4]. Electron–hole pairs will generate in the lattice of TiO_2 nanoparticles, when they are irradiated under light with energy equal to or greater than the band gap energy of TiO_2, inducing redox reactions on the surface of the nanoparticles. It is acknowledged that the disinfection process of TiO_2 nanoparticles on various bacteria involves the following steps [5–7]: firstly, when irradiated under light with energy equal to or greater than the band gap energy of TiO_2, electron–hole pairs will be produced and migrate subsequently to the surface of TiO_2; afterward, hydroxyl radicals with high reaction will be generated according to the

*Corresponding author: zhjjnb2@163.com

TiO_2 Nanoparticles: Applications in Nanobiotechnology and Nanomedicine,
First Edition. Edited by Aiguo Wu and Wenzhi Ren.
© 2020 Wiley-VCH Verlag GmbH & Co. KGaA. Published 2020 by Wiley-VCH Verlag GmbH & Co. KGaA.

reaction between the holes and their surrounding OH^- or H_2O, and superoxide ions will form through the reaction of the electrons with oxygen vacancies around; eventually, the bacterial cells adsorbed on the TiO_2 surface will be oxidized and damaged by the generated highly reactive oxygen species (ROS), leading to the bacteria death. Most of the early studies reported that ultraviolet (UV) light with a wavelength less than 400 nm was used as the excitation light source because the wide band gap of anatase–TiO_2 is about 3.2 eV [8–11]. However, the solar spectrum only contains about 5% UV light, and the UV light may be harmful to human [6, 11]. Thus, to reduce the adverse effects and make the best use of the visible light, developing novel TiO_2-based photocatalytic materials, which can bring high photocatalytic property under visible light, is necessary. Previous studies have used several methods to improve the photocatalytic activity of TiO_2 nanoparticles, including tailoring the surface area and particle size of TiO_2 nanoparticles and generating defects in TiO_2 lattice via anion and/or metal dopants [5, 12, 13]. Various mechanisms of antibacterial activity of nanoparticles are shown in Figure 3.1. TiO_2-based nanoparticles have small particle size and large surface area, and oxygen vacancies in TiO_2 lattice will increase with the dopants, thus generating ROS, which will endow the TiO_2 nanoparticles with excellent antibacterial activity [14]. The superoxide radicals (O^{2-}) and hydroxyl radicals ($OH^{\bullet}$) can penetrate into the bacterial cell membrane, then minerals, protein, and genetic material leak from the cell, causing death of the bacteria. This chapter summarizes the recent studies about antibacterial effect of TiO_2-based nanoparticles, including the antibacterial mechanism and the improvement of photocatalytic performance by doping anion or metal ions, and gives a brief introduction on its antibacterial applications.

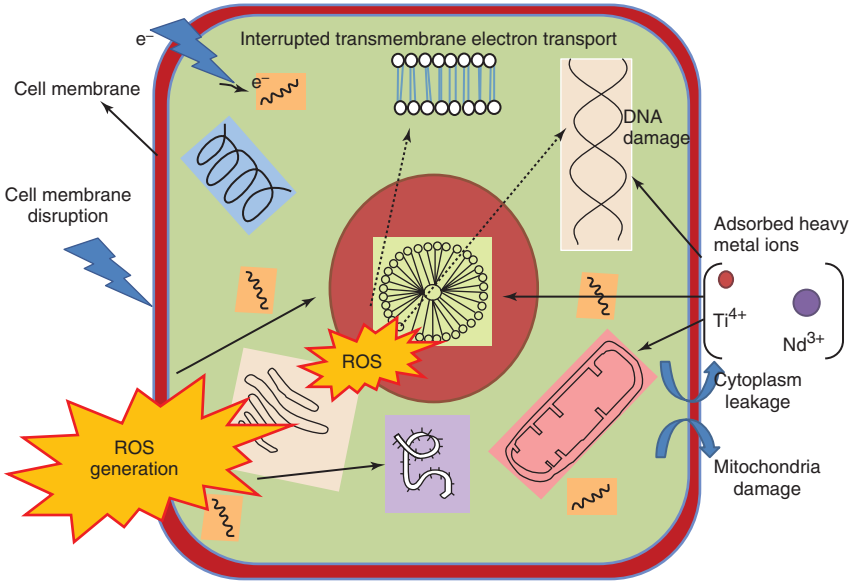

Figure 3.1 Typical diagram of mechanism of antibacterial activity of metal ion nanoparticles. Source: Reproduced with permission from Nithya et al. [14]. Copyright © 2018, Elsevier.

3.2 Antibacterial Effect of TiO_2 Nanoparticle

Many investigations have been directed to study TiO_2 nanoparticles to treat bacterial infections. First of all, TiO_2 nanoparticles have the potential to inactivate bacterial because the bacterial cells and TiO_2 nanoparticles have opposite charges, and the electrostatic attraction between bacterial cells and TiO_2 nanoparticles will result in disturbance of the cell membrane [15, 16]. When the nanoparticles surface and the bacteria carry the opposite charge, the electrostatic attraction would cause a close contact between the nanoparticles and bacteria. For example, the isoelectric point (IEP) of the TiO_2 nanoparticles of a commercially available product TKS201 is at pH 7.5. Their surface is negatively charged for pH >7.5 and positively charged for pH <7.5 [6, 17]. It is well known that the *Escherichia coli* K-12 cell surface has negative charge for pH >2.0. Thus, in the pH range of about 3.5–7.0, TiO_2 nanoparticles surfaces and *E. coli* carry opposite electric charge. When the cells were incubated with TiO_2 nanoparticles at pH range of 4.0–4.5, cell aggregates formed around the nanoparticles, resulting in the decrease of bacterial colony-forming units (CFUs) over 60 minutes [17, 18].

Extensive research about TiO_2-based nanoparticles for various bacteria disinfections has been conducted because of its unique photocatalytic performance. As shown previously, the TiO_2 nanoparticles activated by UV light irradiation are toxic to both Gram-negative and Gram-positive bacteria [5, 19]. Most studies have reported that when TiO_2 nanoparticles are irradiating under UV light, electron vacancies (h^+) and electrons will generate in their valence band and conduction band, respectively. The h^+ and electrons can produce ROS in aerobic aqueous environment, which show a strong oxidizing property toward bacteria by damaging their cell wall and membranes [5, 6]. Previous study indicated that the efficiency of TiO_2 nanoparticles on bacteria with UV light irradiation also depends on the interaction of nanoparticles with the bacterial [6]. When there was no formation of large aggregates, TiO_2 nanoparticles under UV light irradiation could not inactive bacteria. After treatment with UV light for different time, the bacteria within the TiO_2 aggregates tended to be inactive firstly, with the degree of cell compaction also increasing with the extension of treatment time, and some parts of the aggregates turned into an acellular mass eventually. After UV light irradiation, the aggregated bacteria closed to each other spontaneously and merged into larger aggregates gradually, which indicated that the mutual attraction of bacteria was enhanced by such UV light irradiation. To illustrate the antibacterial mechanism of TiO_2 nanoparticles, Zhukova analyzed the physiological status of *E. coli* K-12 cells incubated in TiO_2 suspension [6]. Either under UV-A irradiation or in the dark, the bacteria would be covered with TiO_2 nanoparticles because of electrostatic attraction, which played an important effect in the inactivation of bacteria when in an acidic medium. After incubated with TiO_2 nanoparticles for 60 minutes, bacteria aggregates formed without UV light irradiation, and the most bacteria lost the colony-forming ability. It was also confirmed by the acridine orange (AO) staining that after treatment with TiO_2 nanoparticles, most of the *E. coli* were dead, and the dead *E. coli* cells were

all located within the relatively large aggregates, when the active bacteria were detected at their periphery and in small aggregates. It was hypothesized that the direct contact of TiO_2 nanoparticles with *E. coli* caused the damage to the bacterial membrane, resulting in the death of the bacteria. On the contrary, when irradiated with UV light, 99.9% of the bacteria incubated with TiO_2 nanoparticles were killed after 30 minutes, while the bacteria with only UV light irradiation did not show significant CFUs changes during two hours. The results showed that the direct contact with TiO_2 nanoparticles alone is not sufficient to inactivate the bacteria, and the bacteria were inactivated only within bacteria aggregate, and the number of such bacteria was greater with the larger aggregate. It was assumed that the photoactivated TiO_2 nanoparticles generated powerful oxidants with the initiation of UV light irradiation, thus enhancing their antibacterial effect. The similar antibacterial mechanism of TiO_2 nanoparticles was also demonstrated in other studies [6, 20]. Previous studies have indicated that the TiO_2 nanoparticles have shown an antibacterial effect on *E. coli* with a dose-dependent manner, which might be attributed to the agglomeration of the nanoparticles [20]. Anjali et al. incubated *E. coli* on the Nutrient Agar plate with different concentrations of TiO_2 nanoparticles ranging from 5 to 100 mg/ml. After 14–16 hours, the number of bacteria colonies was found to be reduced with the increasing concentration of TiO_2 nanoparticles as compared with that in the control group. Specifically, there was no bacterial colonies after treatment with 50 and 100 mg/ml TiO_2 nanoparticles. However, bacteria were observed in the control group and also in the groups with TiO_2 nanoparticle concentration of 5, 10, and 25 mg/ml. The authors also hypothesized that TiO_2 nanoparticles were capable of attaching on the bacterial membrane by electrostatic interaction and disrupting the integrity of their membrane.

Liu et al. [21] put forward new insights about the mechanism of the toxicity of TiO_2 nanoparticles toward bacteria by investigating the expression of *prrF* RNA in *Pseudomonas brassicacearum* as an indicator of intracellular iron status. To study the effect of TiO_2 nanoparticles on the metabolism of *P. brassicacearum*, the authors prepared two shapes of anatase TiO_2 nanoparticles, and determined the bacterial activity by analyzing the interaction between TiO_2 and bacteria, as well as the influence of TiO_2 on the intracellular iron content, *prrF1* and *prrF2* sRNA expression of *P. brassicacearum*. Overall, it was demonstrated that the two type of TiO_2 nanoparticles did not affect the bacterial growth under dark conditions. By investigating the adaptive response of bacteria, the two types of TiO_2 nanoparticles could interact with the bacterial cell wall, increased the intracellular ROS levels in *P. brassicacearum*, and consequently decreased the intracellular Fe(II) homeostasis of the bacteria. In addition, with the increasing adsorption of TiO_2 nanoparticles on bacterial cells, the bacterial iron content significantly decreased, resulting in the increasing expression of *prrF1* and *prrF2* sRNA. Therefore, these findings showed the anatase TiO_2 nanoparticles clearly influenced the expression of *prrF* sRNAs in *P. brassicacearum*, and new insights about the toxic mechanism of TiO_2 nanoparticles toward bacteria were finally yielded.

Because of the photoactivated and antibacterial property of TiO_2 nanoparticles, nanostructured films with excellent antibacterial property can also be prepared by distributing TiO_2 nanoparticles uniformly in them [19]. Specifically,

colloidal solution of anatase TiO_2 nanoparticles was spin-coated on silicon monocrystal substrates to prepare thin films with UV light-induced antibacterial effects [19]. When exposing to UV light, the thin film containing TiO_2 nanoparticles would affect the viability of bacteria distinctly: the number of the bacterial colony formed on plates decreased about four times than that in the control group after five minutes irradiation, and no bacterial colony was found on plates after 20 minutes irradiation. They also studied the potential antibacterial effects of the thin film with TiO_2 nanoparticles in dark conditions: a slight decrease of viable bacteria was observed on the thin film in dark conditions, which was ascribed to the dehydration of the bacteria on the film surface. The results suggested that the photoactivation of TiO_2 nanoparticles indeed endowed the film with a high killing efficiency of bacteria with UV light irradiation. In addition, the thin film in this study was remarkably more effective in bacterial inactivation than the films designed in previous studies, which showed a long time to completely inactivated bacterial cells. According to the images of surviving luminescent bacteria, the prepared thin film effectively and rapidly inactivated *E. coli* cells. Overall, the morphology of bacterial cells changed as bacterial number decreased. In detail, the cellular outlines of the *E. coli* became more discursive with the length and the diameter increased, and the bacterial cell membrane was distorted. The results were corresponding to that in the quantitative analysis of bacterial activity, which showed that the number of the *E. coli* with damaged cell wall increased with the illumination of an increasing length of UV light. To be specific, after 10 minutes of exposure, it was seen that first distorted cell occurred, and then the number of viable bacteria decreased by two orders of magnitude. The bacteria cells cocultured with TiO_2 nanoparticle-based film enlarged, the cellular membrane distorted, and the cytoplasm tended to leak (Figure 3.2). After 20 minutes of exposure,

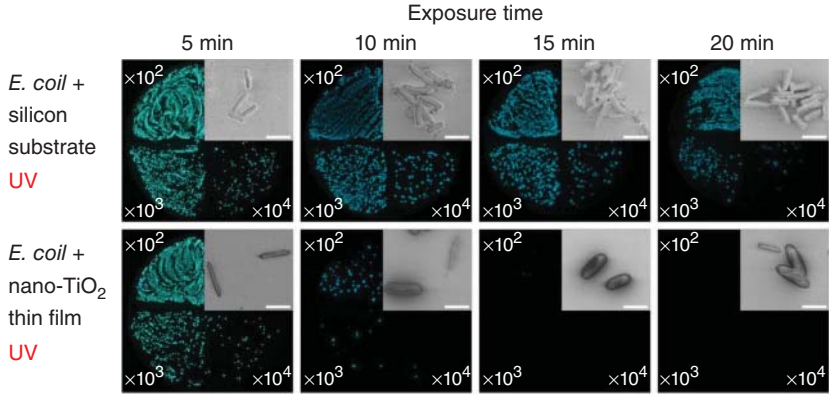

Figure 3.2 Images of surviving bacteria after exposure to UV light on Si-monocrystal substrates and on TiO_2 nanoparticle-based thin films. The photos were taken in the dark. Insets are SEM images of the bacteria. Scale bars is 2 μm. The significant morphological changes of bacteria can be observed in SEM images after 10 minutes UV irradiation on TiO_2 nanoparticle-based thin film. Source: Reproduced with permission from Joost et al. [19]. Copyright © 2015, Elsevier.

most of the *E. coli* cells distorted, and there were no viable cells according to the plate counts. It was also confirmed by scanning electron microscope (SEM) images that the damage of bacterial structures occurred when the bacteria were inactivated. However, SEM images showed that some cellular debris was still visible clearly, and the exposure time of 60 minutes was not long enough to achieve complete destroy of *E. coli* cells. Therefore, relative to the time needed to affect the viability of *E. coli*, it is necessary to take longer time to completely decompose bacterial cells on the surface of TiO_2-based film. In addition, X-ray photoelectron spectroscopy (XPS) analysis indicated that both unsaturated and saturated fatty acids are commonly present in the bacterial plasma membrane, and they would decompose after 10 minutes exposure of UV light on the surface of photoactivated TiO_2 nanoparticle-based thin film. Thus, the unsaturated and saturated fatty acids are two vital components of cell membrane, and the peroxidation and decomposition of the fatty acids might be one of the factors contributing to the morphological changes, leakage of the bacterial components, and ultimately death of bacteria.

It was demonstrated that a photokilling approach for pathogenic bacteria can be established by magnetic nanoparticles based on TiO_2 nanoparticles, such as iron oxide@titania (Fe_3O_4@TiO_2) core/shell magnetic nanoparticles [22]. The TiO_2 shell on the Fe_3O_4 core was used as a photocatalyst to kill pathogenic bacteria. The magnetic property of the nanoparticles allowed the targeted bacteria to flock together under an external magnetic field, and this magnetic separation method avoided the damage on non-target cells. It was confirmed that the Fe_3O_4@TiO_2 magnetic nanoparticles have a broad affinity with Gram-positive and Gram-negative bacteria, and they can also be used as a kind of photocatalyst to inactivate these bacteria. To demonstrate the feasibility of the Fe_3O_4@TiO_2 magnetic nanoparticles in the inactivation of the pathogenic bacteria, some nosocomial pathogenic bacteria, such as *Enterobacter cloacae*, *Haemophilus influenzae* type b, *Streptococcus pyogenes*, *Acinetobacter baumannii*, and antibiotic-resistant bacteria including methicillin-resistant *Staphylococcus aureus* (MRSA) and pan-drug-resistant *A. baumannii* (PDRAB), were used in the study [22]. It was demonstrated the Fe_3O_4@TiO_2 magnetic nanoparticles had the capability to inhibit the bacteria growth effectively by photochemical reactions within 15 minutes irradiation of UV light. In addition, it needed shorter time and less light power to inhibit the bacteria growth than those presented in previous studies, which might reduce the possibility to damage untargeted cells. Thus, it implied the feasibility of using the magnetic approach for antibacterial applications.

In wastewater treatment, TiO_2 nanoparticles also acted as catalysts for killing anaerobic bacterium. *Macrococcus caseolyticus* is isolated from the activated sludge in wastewater, and it was used as a representative bacteria to demonstrate the toxic effects of TiO_2 nanoparticles [23]. The cytotoxicity assessment of the nanoparticles was carried under dark conditions, UV light, and visible light, and the results revealed the reduction of bacterial viability was dependent on the dose of TiO_2 nanoparticles and light irradiation time. Without TiO_2 nanoparticles treatment, bacteria released exopolymeric substance (EPS) conventionally and then formed intact biofilm. With UV light treatment, there were maximum

clumping of cells in the biofilm, and the biofilm was more compact and secreted much more exopolymers as compared with the bacteria treated under dark conditions and visible light. Besides, the biofilm treated under dark condition was the least compact, and they tended to aggregate when treated with TiO_2 nanoparticles as compared with that in the control group. The results testified the photocatalytic response of biofilm and bacterial cell toward nanoparticles. In addition, the uptake of titanium ion by biofilm was analyzed by treating the biofilm under different conditions with different time interval. After treatment with TiO_2 nanoparticles under UV light, the biofilm was found to take in significantly higher dose of titanium as compared with that under dark conditions and visible light. It is well known that EPS is mainly composed of polysaccharides and proteins, and the uptake of nanoparticles can be affected by modifying the carbohydrates and proteins in the EPS. Mathur et al. observed the stress induced by the nanoparticles to the bacterial cell would bring about an increment of the nanoparticles in the EPS in a dose-dependent manner. After wastewater treatment, bacteria and EPS are the main constituent parts in activated sludge under the anaerobic condition, and the bacterial cells were protected by EPS from the bactericidal effect of UV light in the environment. To assess the biofilm, its density and thickness were chosen as major parameters. The results showed that the thickness and density of the biofilm were found to increase with the increasing concentration of TiO_2 nanoparticles and time interval, which can be corresponding to the results in bacterial viability studies. When the bacterial viability was not affected, the thickness of the biofilm was found to increase; when the toxicity toward bacteria was observed obviously, the thickness of the biofilm stopped increasing. For the density of the formed biofilm, it was directly related to the bacterial viability. Various physical interactions and chemical interactions, particularly electrostatic interactions, influenced the initial adsorption of nanoparticles onto the surface of the biofilm. The microscopic studies can give a better illumination of the changes in the biofilm formation process. In the present study, the changes of the biofilm treated under different conditions, such as dark, UV light, and visible light, were noticed. However, when treated under UV light, the thickness and density of the biofilm were higher than that under other luminous conditions, which might be because UV light irradiation enhanced the hydrophilicity of the TiO_2 nanoparticles. Moreover, SEM images showed that the biofilm in the control group was observed as segregated colonies. On the contrary, the biofilm tended to appear an inscrutable assemblage after treatment with the highest concentration of TiO_2 nanoparticles. To sum up, EPS persistently protected the biofilm from the toxicity of TiO_2 nanoparticles because of the following reasons: on the one hand, EPS provided a safer space for the formation of biofilm, and on the other hand, EPS captured the most toxic TiO_2 nanoparticles and inhibited the interaction between the nanoparticles with the most bacterial cells. Thus, the entrapment of nanoparticles by EPS could be utilized to enhance the bacterial potency to form biofilm after treatment with TiO_2 nanoparticles. Similarly, the investigation of *Listeria monocytogenes* further confirmed the results: the biofilm without any treatment appeared to be isolated cells and individual; on the contrary, after treatment with TiO_2 nanoparticles with the concentration of 1 mg/ml, the bacterial cells exhibited an increasing

release of exopolymers, and thereby formed more biofilm. This finding described that after counteracted with the antimicrobial effects of the TiO_2 nanoparticles, the released EPS had a protective action on biofilm.

It has been proven that TiO_2 nanoparticles can also be used to negatively affect aerobic denitrifiers, which can participate in the nitrogen cycle [24]. In order to investigate the cytotoxicity mechanism, the nanoparticle–bacteria interaction at the dark condition was investigated by exposing *Pseudomonas stutzeri* PCN-1 to different concentrations of TiO_2 nanoparticles, and the mechanism was elucidated in Figure 3.3 [25]. The results illustrated that the TiO_2 nanoparticles at different concentrations inhibited the aerobic denitrification; meanwhile they postponed the nitrate reduction and the accumulations of nitrous oxide and nitrite. To be specific, the removal rates of nitrate in the control group (without TiO_2 nanoparticles) were 12.5 mg-N/l h. After treatment with the TiO_2 nanoparticles with concentrations 1, 4, 16, 64, and 128 mg/l, the removal rates of nitrate were 3.64, 3.64, 5.10, 6.38, and 10.2 mg-N/L h, respectively. Notably, the increasing TiO_2 nanoparticles concentrations mitigated the inhibitory effect of TiO_2 nanoparticles, which indicated that the cytotoxicity of TiO_2 nanoparticles to the *P. stutzeri* PCN-1 was much higher at lower nanoparticles concentrations. However, in all the experimental groups within 28 hours, 100% of the nitrate was removed, which suggested that TiO_2 nanoparticles postponed the nitrate reduction. In addition, accompanied with the nitrate reduction, the authors observed a significant nitrite accumulation, and the maximal accumulation amount was similar at each exposure concentration. However, different concentrations of TiO_2 nanoparticles resulted in distinct patterns of the nitrite reduction, and TiO_2 nanoparticles concentrations lower than 16 mg/l could inhibit the nitrate reduction rates much more greatly. Accompanied by the

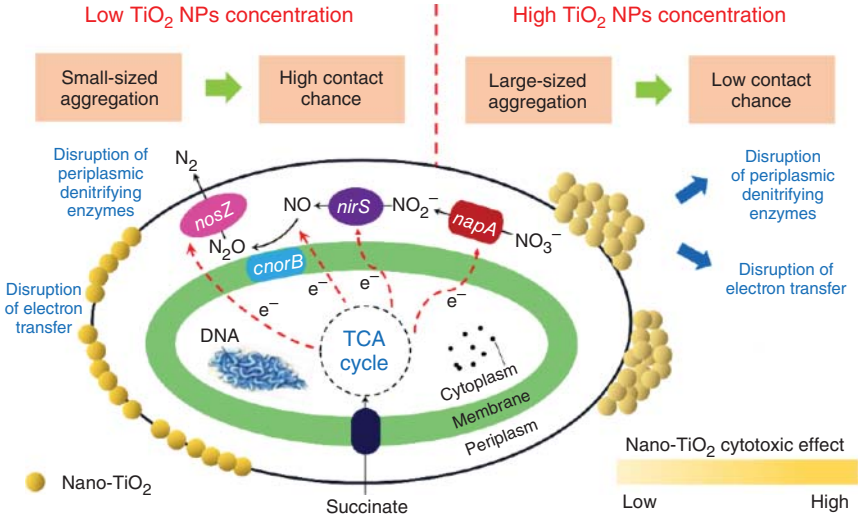

Figure 3.3 The mechanism of the cytotoxicity of TiO_2 nanoparticles to *Pseudomonas stutzeri* PCN-1. TCA, tricarboxylic acid. Source: Reproduced with permission from Liu et al. 2018 [25]. Copyright © 2018, Taylor & Francis.

nitrate reduction, the oxygen consumption occurred, which further confirmed the aerobic denitrification. Moreover, the oxygen utilization of *P. stutzeri* PCN-1 was also inhibited significantly by TiO_2 nanoparticles, and the uptake of oxygen for the bacteria would be inhibited at a lower concentration of TiO_2 nanoparticles. Furthermore, TiO_2 nanoparticles also inhibited the expression of aerobic denitrification genes. Specially, TiO_2 nanoparticles exhibited more significant inhibitory effect on *nirS* and *napA* genes than that on *cnorB* and *nosZ* genes, which might be responsible for the delay of the nitrate reduction and inhibition of the nitrite transfer. In addition, aggregates larger than 1000 nm would form when the concentration of TiO_2 nanoparticles was high, and the chance of interactions between bacterial cells and nanoparticles as well as the disturbance of denitrifying genes expressions reduced greatly, thus decreasing their toxicity. The findings previously mentioned contributed to the deep understanding of the mechanism of the cytotoxicity of TiO_2 nanoparticles and provided strategies for controlling the cytotoxicity of nanoparticles in the environment.

3.3 Ion-Doped TiO_2 Nanoparticles and Their Antibacterial Effect

However, traditional TiO_2 nanoparticles only have efficient antibacterial ability when irradiated with UV light, but it can also cause harm to human cells. The structure of the TiO_2 can be changed by doping or loading the other elements, which will enhance the adsorption in the visible light range. Until now, anion ions or/and metal ions, such as nitrogen [5, 11, 26, 27], carbon [5, 28], nickel [5, 29], neodymium [30, 31], have been doped into TiO_2 nanoparticles to alter their structure by the impact of defection. The band gap energy of TiO_2 nanoparticles can be reduced below 3.2 eV by doping elements, and its absorption band is possible to be extended into the visible light range from the UV range. Zane et al. prepared nitrogen (N)-doped TiO_2 nanoparticles using sol–gel method. The results of the UV–visible light spectroscopy showed a band of trap states, and it stated that the concentration of the nitrogen dopant led to an absorption that extended well to the visible range of wavelengths with increasing blue light absorption, and the extent of absorption in the visible light was dependent on the concentration of N–TiO_2 nanoparticles. They then examined the ability to produce free radicals in the synthesized N–TiO_2 nanoparticles that could be exploited to become an effective and potential antibacterial agent. It was shown that N–TiO_2 nanoparticles, which have been subjected to blue light, have been shown to induce ROS generation in a dose-dependent manner in comparison to phosphate buffered saline (PBS) controls. ROS manufacturing has undergone a significant change after the introduction of N–TiO_2 nanoparticles with the largest dose (200 μg/ml), and hydroxyl radicals and superoxide arose after the exposure of nanoparticles to visible light and oxygen. Moreover, the colony counts of *E. coli* were quantified following the treatment of ambient or blue light in the presence or absence of N–TiO_2 nanoparticles in order to investigate the prospective antibacterial property of N–TiO_2 nanoparticles with or without

light treatments. It showed that *E. coli* colonies decreased significantly due to the treatment with blue light alone, and when compared with exposure under ambient light conditions, *E. coli* colonies showed an obvious dose-dependent reduction under the treatment with N–TiO_2 nanoparticles under blue light irradiation. In order to confirm the antibacterial effect of N–TiO_2 nanoparticles, an additional set of the nanoparticles were also performed under light-emitting exposures. Live/dead staining showed bacterial viability changes in relation to the exposure to nanoparticles. To be specific, the number of the dead bacteria increased compared with live bacteria with an increasing concentration of nanoparticles, and the damaged bacteria underwent the treatment of nanoparticles and visible light tended to be swelling and undergoing morphology changes, which have proven their efficient antibacterial properties. The largest concentration of particles showed roughly 1-log decrease in the bacterial population. These observations were consistent with the morphological changes and the reduction of the number of live bacteria observed in the confocal microscopy [26]. TiO_2 nanoparticles doped with nickel ions have been synthesized using the sol–gel procedure, and few sites of Ti^{4+} in titania host lattice were replaced with Ni^{2+} [29]. UV–vis diffuse reflectance absorption measurement of Ni–TiO_2 nanoparticles showed an optical absorption in the visible light and confirmed the successful doping of nickel ions in the TiO_2 crystal lattice. The UV–vis absorption spectra for undoped TiO_2 and Ni–TiO_2 nanoparticles ranged from 300 to 700 nm demonstrated that a higher visible light absorption was observed for the Ni–TiO_2 nanoparticles, and this indicated the doping of Ni^{2+} reduced the band gap of TiO_2 lattice. The visible absorption of light was attributable to the fact that Ni^{2+}/Ni^{+} had an energy level underneath the conduction band and above the valance band of TiO_2. According to the energy level, these unique energies and oxygen vacancies produced by the metal doping process caused a bathochrome change in the band gap and the absorption of visible light through the transfer of charge between the doping elements and a conduction/valance band or d–d transition in the crystal field. After the nickel metal ions have been doped in TiO_2 lattice, the absorption of the samples in visible light region shifted because of the advent of a new energy level in TiO_2 semiconductor, which triggered the color changed from white to pale yellow in the doped samples. It was observed that the Ni–TiO_2 nanoparticles had higher photocatalytic bactericidal effect toward Gram-positive bacteria, such as *S. aureus*, *Bacillus subtilis* and to a lesser degree of Gram-negative bacteria, such as *E. coli* and *Salmonella abony*. With an increased concentration of nickel dopant in TiO_2, the photocatalytic inactivation of all the four bacterial strains increased in the presence of Ni–TiO_2 and light irradiation, and this might be because of newly generated energy levels in the band gap of TiO_2, causing the narrowing of the band gap and ultimately inducing more absorption of visible light. Besides, in the dark (with nanoparticles) and light condition (without any nanoparticles), the viable number of all species of bacteria was not affected, and this indicated that method to assess the antibacterial activity did not kill the bacteria during the whole experiment. Similar results have been obtained by Ananpattarachai et al. [32]. They prepared N-doped and Ni-doped TiO_2 nanoparticles and explored their bactericidal effect in the absence and presence of visible light. The *E. coli* and *S. aureus* were chosen

as an example of Gram-negative and Gram-positive bacteria, respectively [32]. The optical characterization of the undoped and doped TiO_2 nanoparticles showed that the undoped TiO_2 had a better absorbance in the UV light region ranging from 200 to 400 nm, and the TiO_2 nanoparticles doped with N and Ni element absorbed more visible light in the wavelength region from 400 to 800 nm. These findings showed that the range of light absorption of the TiO_2 was efficiently extended to the visible light range by doping Ni or N element. In the presence of Ni-doped, N-doped, and undoped TiO_2 nanoparticles, the greatest visibility of light absorption had been given with N-doped TiO_2, which led to a greater bactericidal effect for both *E. coli* and *S. aureus* than that of Ni-doped and undoped TiO_2. In detail, *S. aureus* in dark environment and under visible light alone were not inactivated within 180 minutes. However, a significant amount of *S. aureus* was inactivated after the treatment of the nanoparticles and visible light within 180 minutes. After a longer irradiation time of 300 minutes, only a small number of *S. aureus* colonies were observed in the experiment group treated with N-doped TiO_2 nanoparticles, while many bacterial colonies were found in the groups treated by Ni-doped and undoped TiO_2 nanoparticles. Furthermore, *E. coli* had a comparable tendency in the inactivation after the treatment of TiO_2-based nanoparticles. Under the dark conditions, the inactivation of *E. coli* was minimal, while the N–TiO_2 nanoparticles showed the most effective antibacterial activity under the irradiation of visible light, and only few *E. coli* colonies were observed after 180 minutes of irradiation. In this study, the concentrations ranged from 0 to 1000 mg/l for all three kinds of TiO_2 nanoparticles were chosen to clearly demonstrate the antibacterial activity. The results of photocatalytic inactivation of *S. aureus* and *E. coli* both showed that the N-doped TiO_2 was more lethal than the other types of TiO_2, and this could be due to the narrowing of the band gap, which lead to more absorption of visible light. Thus, the N-doped TiO_2 nanoparticles can achieve greater effectiveness in photocatalytic inactivation of bacteria. Moreover, the greater surface area of these smaller crystals was better to promote the photocatalytic response on the surface of the N-doped TiO_2, and then to produce greater levels of ROS and hydroxyl radicals than that of the Ni-doped TiO_2.

The modification of anion doping or/and transition metal ion was shown to be a successful approach to endow the TiO_2 nanoparticles with visible light activity. A powerful photocat system, palladium-modified nitrogen-doped titanium oxide (TiON/PdO), was created by Li et al. [33–35]. The concentration of palladium additive had a powerful impact on the structure, optical, and photocatalytic characteristics of TiON nanoparticles: the crystallization of the TiON was slightly interrupted by the increasing additive of palladium, and thus greatly improved its capacity of absorption of visible light as well as photocatalytic activity. Besides, the material had much greater photocatalytic activity than that of TiON within certain concentrations of palladium [33]. Based on the TiON/PdO nanoparticles, nano-sized TiON/PdO photocatalytic thin film and fiber samples were prepared and their photocatalytic properties were examined. For the TiON/PdO photocatalytic thin film, it was the first time to acquire the clear proof of photoelectron transfer between TiON matrix and PdO, and electron–hole pairs were

generated on the surface of PdO and in the TiON matrix by the nitrogen doping effect, then the photoelectrons were augmented on PdO when illuminated under visible light. The immediate result of the electron flow to PdO nanoparticles is, as disclosed by the in situ XPS assessment, that PdO is chemically reduced. Thus, the XPS analysis could be used to monitor the potential changes of the Pd additives valence with/without illumination of visible light. First, the TiON/PdO thin film was placed in the dark condition for five hours right before the XPS high-resolution scan over the 3d peak of Pd, and then, XPS scans were carried out concurrently with the illumination of visible light on the sample. There were obvious differences in the shape and position of the Pd 3d peak when the samples were in the dark and under illumination of visible light. In detail, the binding energy of Pd $3d_{5/2}$ was approximately 336.20 eV in darkness, suggesting that the existence form of Pd additives was PdO. However, the visible light broadened the peaks of Pd, and the binding energy of Pd $3d_{5/2}$ is changed to ~335.30 eV under the illumination of visible light. The broadened Pd $3d_{5/2}$ would be the greatest combination of Pd^0 $3d_{5/2}$ (speak at 335.2 eV) and Pd^{2+} $3d_{5/2}$ (speak at 336.2 eV), which obviously showed that the electron enhancement of the Pd additives in the thin TiON/PdO film had resulted in the reduction of PdO nanoparticles to metallic Pd^0 with the illumination of visible light. These Pd additive sites therefore trapped the photoelectrons, and the evidence that photoelectrons generated in the TiON matrix had flown to PdO nanoparticles had been clearly provided by the conversion of the valence state of Pd additives. With the switched-off visible light, the TiON matrix would stop generating the photoelectron, and there were no further photoelectrons flowing to the PdO nanoparticles, which resulted in the reversed direction of the charge transfer instead. It might be because that e^-/h^+ pairs could be generated in the TiON matrix with the illumination of visible light. The electrons generated from TiON would flow to PdO nanoparticles and then were captured locally by PdO nanoparticles, causing that the valence state of Pd shifted from +2 to 0. Subsequently, the e^-/h^+ pair recombination could decrease by the capture of charge carriers and thereafter the lifetime of the charge carriers was improved, which was beneficial to enhance its photoactivity. However, when visible light is switched off, the trapped electrons would be released and then might flow back to the TiON matrix. Particularly, if oxygen or water were present on the surface during the process, they would react with the released electrons to produce radicals. For the TiON/PdO fibers, the immobilization of TiON/PdO in the system eliminated the need for photocatalysts recycling in the powder form, and the contact efficiency of the TiON/PdO with bacteria was improved by the fiber network in water. To study the bactericidal effect of TiON/PdO fibers, the authors chose the *E. coli* AN 387 as a pathogenic model for post-exposure disinfection as well as photocatalytic disinfection. In the experiment of photocatalytic disinfection of *E. coli*, the cells were suspended in a buffer with TiON/PdO, and the system was irradiated under a visible light with the wavelength above 400 nm for different periods. After the treatment for one hour, the bacterial concentration in TiON/PdO group showed a much faster bacteria-killing kinetics compared with that of TiON group, and the higher killing rate reflected that the holes had a more durable antimicrobial ability due to the role of PdO nanoparticles in reducing

electron–hole pairs. To investigate the lasting time of the post-exposure disinfection ability of TiON/PdO fiber, the experiment was designed as follows: initially, the samples were irradiated with a lamp for about 10 hours; then the lamp was turned off so as to store the samples in a dark environment for 0–24 hours; at last, the disinfection experiments were conducted in the dark. The general tendency of the *E. coli* survival ratio demonstrated obviously that the TiON/PdO fibers did have the capability to kill the bacteria, and their bactericidal efficiency would gradually fall with the increase of the storing time in darkness. However, after stored in darkness for 24 hours following the illumination of visible light, the TiON/PdO fibers did lose their antibacterial property. On contrary, both of TiON/PdO and TiON were not poisonous to *E. coli* without light irradiation. It is thus concluded that the TiON/PdO fibers in darkness still had a post-exposure disinfection capability relying on the memory of the illumination of visible light. In the process, the initial illumination of visible light excited the charge flow from the TiON matrix to PdO nanoparticles, and after storing in the dark, the trapped electron would be released. In the study, the authors pointed out that when the visible light is switched off, the duration of post-illumination antibacterial property of the TiON/PdO fibers was mainly dependent on the release rate of electrons from PdO nanoparticles. Since the electron release rate is critical for the memory effect of the post-exposure disinfection, the oxygen or water in the surrounding would have a significant impact disinfection rate of the TiON/PdO fibers in darkness, which was because that the released electrons could react with the surrounding oxygen or water to generate radicals with high reactivity. In order to testify this hypothesis, the post-exposure disinfection effectiveness of TiON/PdO fibers on *E. coli* were contrasted in N_2 condition or in air, and the results clearly showed that the TiON/PdO fibers had much slower bactericidal rate in the N_2 environment. Thus, the oxygen concentration is the only difference in the two conditions. Thus, they have developed a distinctive catalytic disinfection system that can be tailored to a wide variety of bacteria with an ongoing operation in day and night.

The *Fusarium graminearum* macroconidium is generally consisted of 4–6 cells, and its size is about 25–70 μm in length and 3–5 μm in width. In addition, the *F. graminearum* macroconidium has a thicker cell wall and cell membrane than that of *E. coli* bacteria. Thus, it is necessary to develop a more powerful photocatalyst to inactivate the *F. graminearum* macroconidium effectively, since they have stronger resistance to the attack from ROS. Coincidentally, it was proven by Zhang et al. [11] that TiON/PdO nanoparticles even have an extremely efficient photocatalytic disinfection on *F. graminearum* macroconidia, which has bigger size and thicker cell wall and cell membrane, with the irradiation of visible light. When cultured with TiON/PdO nanoparticles, *F. graminearum* macroconidium tended to absorb abundance of the nanoparticles onto the surface, since the bacteria and TiON/PdO nanoparticles carried opposite surface charge. The electrostatic interaction was advantageous to enhance the bactericidal effect of the TiON/PdO nanoparticles on the bacteria. To demonstrate the photocatalytic disinfection capability of the nanoparticles, four different experimental groups were set as bacteria treated only with the illumination of visible light with the wavelength above 400 nm (control), bacteria with the

treatment of Degussa P25 TiO_2 nanoparticles and illumination of visible light, bacteria treated with TiON/PdO nanoparticles in darkness, and bacteria treated with TiON/PdO nanoparticles and illumination of visible light, respectively. After the above treatment, the survival ratio of the *F. graminearum* macroconidia was counted and compared with each other. No apparent loss of the bacteria was observed in the groups treated with only visible light illumination and with TiON/PdO nanoparticles in darkness. Interestingly, there was also no apparent loss of the wild-type *F. graminearum* macroconidia in the group treated by Degussa P25 TiO_2 and visible light, although Degussa P25 TiO_2 nanoparticles had been reported to have efficient photocatalytic disinfection capability on a number of bacteria under the irradiation of visible light. In contrast to the three groups, TiON/PdO nanoparticles showed a superior capability to inactivate the wild-type *F. graminearum* macroconidia with the irradiation of visible light, and the survival ratio of the bacteria declined rapidly in this group. In detail, the survival ratio decreased comparatively slowly to 79% and 48% after one hour irradiation and two hours irradiation, respectively, and then dropped sharply with the preceding irradiation. It has been reported that electron–hole pairs would be generated in the lattice TiON/PdO, and the lifetime of the charge carriers was improved by the additive of PdO. The holes with high reactivity produced more highly active $^{\bullet}OH$ radicals, and it was beneficial to enhance the photoactivity toward *F. graminearum* macroconidia. Moreover, the photocatalytic disinfection capability of the TiON/PdO nanoparticles could be enhanced by their attachment onto the surface of *F. graminearum* macroconidia.

Recently, TiO_2 doped with carbon has been found to inactivate a wide range of bacteria under the illumination of visible light [36]. All the tested pathogenic bacteria, including *Shigella flexneri*, *S. aureus*, and *A. baumannii*, were killed in a significantly higher proportion by the carbon-doped TiO_2 nanoparticles. Neodymium (Nd) can also be used to improve the photocatalytic disinfection capability of TiO_2. Different molar ratio of Nd can be doped into TiO_2 nanoparticles through sol–gel method [14]. By the addition of Nd element, the phase transition was identified, and crystal defects in TiO_2 lattice was demonstrated through photoluminescence spectroscopy. Different bacteria, such as *E. coli*, *S. aureus*, were used to evaluate the photocatalytic disinfection capability of Nd-doped TiO_2 nanoparticles. The water molecules (H_2O) were ionized into hydrogen ion (H^+) and hydroxyl radicals ($OH^{\bullet}$) by the electron–hole pairs in the TiO_2 nanoparticles. Meanwhile, the superoxide radical anions (O^{2-}) would be generated by the dissolved molecules of oxygen, and then produced HO_2^- radicals by its reaction with H^+. The HO_2^- radicals generated would interact with electrons in TiO_2 lattice to produce hydrogen peroxide anions ($H_2O_2^-$). Finally, hydrogen peroxide (H_2O_2) was generated by the reaction of the $H_2O_2^-$ and H^+, which would disturb the bacteria cell wall and then bring about their death [14, 37]. On this basis, the crystallite size also affects the antibacterial property of TiO_2-based nanoparticles. The crystallite size decreased with the addition of Nd dopant, and the diameter of the inhibition zone increased with the increasing content of Nd. Besides, the antibacterial effect toward *E. coli* (Gram-negative) is higher than that toward *S. aureus* (Gram-positive), which might be because of the differences in chemical composition and structure of Gram-negative and

Gram-positive bacteria. The Gram-positive bacterial cell wall includes dense peptidoglycan and teichoic acid, while the Gram-negative bacterial cell wall includes thin peptidoglycan and lipopolysaccharide [38], so Ti^{4+} easily attached to the Gram-negative bacteria, leading to cell death eventually. Moreover, the decreased particle size resulted in an easier penetration into the cell wall and cell death by rising content of Nd.

Another feasible approach, loading of metallic oxide nanoparticles into the photocatalyst, can be used to expand the absorption band of TiO_2 nanoparticles to visible light. Kim et al. [39] synthesized V_2O_5-loaded TiO_2 nanoparticles (V_2O_5–TiO_2) and compared the photocatalytic disinfection capability of V_2O_5–TiO_2 on *E. coli* with that of pure TiO_2 nanoparticles. When treated with fluorescent light, TiO_2 nanoparticles significantly reduced the activity of *E. coli*; however, the antibacterial activity was still much lower than that of V_2O_5–TiO_2 nanoparticles. It was supposed that the loading of V_2O_5 shifted the absorption band of TiO_2 into the visible light range. Liu et al. [40] designed selenium (Se) nanoparticles loaded into TiO_2 nanotubes (TNTs) to enhance the photocatalytic disinfection capability of TNTs. When compared with the unmodified TNTs, the TNT loaded with Se nanoparticles (TNT–Se) had an inhibitory effect on the activity of *E. coli* and *S. aureus*. As shown in the result, *E. coli* had intact membranes on both the untreated Ti substrate and TNTs. In contrast, the membranes of *E. coli* grown on TNT-Se samples became corrugated, and the disrupted *E. coli* membranes even adsorbed some Se nanoparticles. It is not yet clear whether this bacteria–Se contact is necessary to induce membrane damage, and further studies are needed to explain this interaction. Similarly, *S. aureus* grown on Ti substrate and TNTs were smooth and intact with typical spherical shapes. In contrast, the membranes of *S. aureus* on the TNT–Se–M substrate were grooved and even ruptured when contacting with Se. In addition, the ability of the samples to prevent bacterial growth was visualized and qualitatively assessed by confocal fluorescence microscopy and laser scanning (LSC) cytometry. After 24 hours in culture, there were more live bacteria on Ti substrate and TNT surfaces than the other samples, and the number of live bacteria decreased with the increasing content of Se in the TNT–Se samples. The LSC images, which showed the entire surface area of the samples, were consistent with the results obtained in the confocal, which also were in agreement with the quantitative data. Therefore, the results proved that TNT–Se samples reduced the activity of *E. coli* and *S. aureus*, and Se nanoparticles had a direct effect in destroying both Gram-negative and Gram-positive bacteria. Furthermore, to study the mechanism of the bactericidal effect of the TNT–Se, the expression of six genes of *E. coli* were monitored. The two genes, *ompA* and *ompF*, were down-regulated, indicating Se nanoparticles weakened *E. coli* membranes; *csgA* and *csgG* were gradually down-regulated with the rising content of Se nanoparticles, illustrating that the function of adhesion-mediating proteins decreased; the *ahpF* gene was up-regulated, indicating the production of damaging ROS was induced. Ultimately, it became clear that the TNT–Se samples attack bacteria by at least three ways: disruption of membrane functions, damage to the production of adhesion-mediating proteins, and production of damaging ROS.

3.4 Antibacterial Agent-Doped TiO_2 Nanoparticles and Their Antibacterial Effect

3.4.1 Ag-Doped TiO_2 Nanoparticles

One of the most fascinating antibacterial materials is Ag and related materials containing Ag [41, 42]. Generally, Ag^+ or Ag can approach and damage the cell wall and cell membrane of bacteria, and thus disrupt bacterial physiology. Besides, Ag can also activate visible light stimulation in TiO_2 as an antibacterial agent. It enhances the photoactivity of TiO_2 and its photocatalytic inactivation of bacteria by reducing the recombination rate of its photo-stimulated electrons/vacancies and/or offering a larger surface for the adsorption [43, 44]. It was also thought that the absorption of visible light by Ag's surface plasmon resonance caused electron transfer to TiO_2, leading to separation of charge and its activation under the illumination of visible light. Ag-doped TiO_2 nanoparticles therefore demonstrate excellent promise as photocatalytic materials that can react with visible light [45]. To acquire an enhanced photocatalytic disinfection under the illumination of visible light, a nitrogen-doped silver-modified titanium oxide ($TiON/Ag_2O$) nanoparticle was synthesized via a sol–gel process [46]. Silver is useful in this case to improve the crystallization, increase the surface area, increase volume of pores, and improve the absorption of visible light. The increased photocatalytic disinfection of *E. coli* by $TiON/Ag_2O$ was mainly due to the photocatalytic reaction of TiON and the following coupling between Ag_2O and TiON. Previous research revealed that good antibacterial properties of Ag nanoparticles on the TiON surfaces could be further improved by the illumination of visible light [47]. Its bad durability however significantly restricts the applications of this Ag–TiO_2 composites [48]. To improve the durability, Ag–TiO_2/Ag/α-TiO_2 nanocomposite film with an efficient storage of Ag nanoparticles has been prepared and used to explore the photo degradation of *E. coli* in the irradiation of visible light and solar light [8]. The bactericidal effect of the nanocomposite film on *E. coli* was much higher than that of the α-TiO_2 in darkness, and also greater than that of Ag/α-TiO_2 and α-TiO_2 as exposed to the solar light. In addition, because of the interdiffusion of silver and water, the durability of the nanocomposite film has been 11 times at least greater than that of Ag/α-TiO_2. These results demonstrated that the photocatalyst Ag–TiO_2/Ag/α-TiO_2 could be considered as an efficient and durable antibacterial material. Furthermore, TiO_2(N)/Ag/TiO_2(N) films [48] were developed with sandwiched structure, in which Ag is built into two layers of TiO_2N. The bactericidal durability in both dark and visible light environments of these thin films is significantly enhanced. *S. pyogenes*, *A. baumannii*, *E. coli*, and *S. aureus* could be efficiently eliminated.

Nanoparticles with core–shell structures have extraordinary physical, chemical, and biological characteristics. Novel core–shell structured TiO_2@Ag nanoparticles were manufactured by the ultrasound vibration of Ag–TiO_2 composite [49]. The Ag–TiO_2 nanoparticles, as well as the TiO_2@Ag core–shells, have powerful bactericidal activity on *E. coli* at a concentration of 20 μg/ml with the irradiation of laboratory light. Under the same conditions, the antimicrobial

activity of the core–shell structured TiO_2@Ag nanoparticles is somewhat higher than that of the Ag–TiO_2 nanoparticles, which might be due to the formation of larger agglomeration of TiO_2@Ag in the deionized water. Ultrasound vibration is known to allow agglomerated nanoparticles to be separated or scattered in water that will produce nanoparticles in minor sizes, and the nanoparticles with a smaller size were reported to be more effective than bigger ones in antibacterial activity. The Ag–TiO_2 compound and the core–shell structured TiO_2@Ag nanoparticles react differently with light, despite their optical absorbing spectrum were same. Thus, the unique core–shell structure is responsible for the slightly greater antibacterial activity than that of the Ag–TiO_2 compound. For the TiO_2@Ag nanoparticles, Ag served as the shell on the surface of TiO_2 and gave a larger interaction area between Ag and TiO_2. When the electrons were transported from the valance band to the conduction band of TiO_2 nanoparticles, the possibility of electrons combining or interacting with Ag nanoparticles is much higher than that of Ag–TiO_2 compound, which resulted in more opportunities of Ag in the TiO_2@Ag nanoparticles to interact with the microorganisms than that of Ag–TiO_2 compound. Therefore, TiO_2@Ag nanoparticles had an improved bactericidal effect because of the prevention of the formation of the Ag agglomerate by the deposition of TiO_2 as the shell [50]. This means that TiO_2@Ag nanoparticles in the core–shell structured form are better for the inactivation of various bacteria [51]. It should be noted that TiO_2 nanoparticles alone with hydroxyl groups (oxygen vacancies (O^-)) on the surface were not sufficient to inactivate the microorganisms [52], while these microorganisms would be effectively damaged by superoxide ions (O_2^-) and hydroxyl radical ($OH^•$) [53]. For the Ag–TiO_2 nanoparticles, two possible mechanisms are thought to be responsible to the death of microorganisms. The first one is the direct effect that the membrane of microorganisms interacted with the attached nanoparticles, leading to the damage and change of the cell membrane structure [54]. The second one is the indirect effect in which Ag ions released and ROS, such as OH^-, $OH^•$, and O_2^- formed under the irradiation of the ordinary light. These reactive species would react with the cell membrane, destroy the DNA and protein functions in the cell, and thus lead to cell to differentiation or death. To improve the bactericidal effect of the Ag–TiO_2 nanoparticles, the TiO_2 of anatase phase was chosen, since the photocatalytic activity of anatase TiO_2 was higher than that of amorphous TiO_2 [55]. It was demonstrated that the Ag–TiO_2 with anatase TiO_2 killed more bacteria in 90 minutes than that of Ag–TiO_2 with amorphous TiO_2 [56]. Yang et al. [57] also prepared and studied the antibacterial activity of the two typical structured nanoparticles: Ag–TiO_2 nanoparticles and core–shell structured Ag@TiO_2 nanoparticles. As shown in Figure 3.4, these two kinds of nanostructures have their distinctive functional characteristics in the inactivation of *E. coli*. To be specific, the Ag–TiO_2 nanoparticles were superior to the Ag@TiO_2 nanoparticles in inhibiting bacteria growth under standard incubation conditions, in which silver could play the leading role in the antibacterial process. However, the Ag@TiO_2 nanoparticles exhibited superior capacity to kill the bacteria than the Ag–TiO_2 nanoparticles when treated with UV light, which might be due to the production of more hydroxyl radicals during the irradiation process. Ag–TiO_2 and Ag@TiO_2

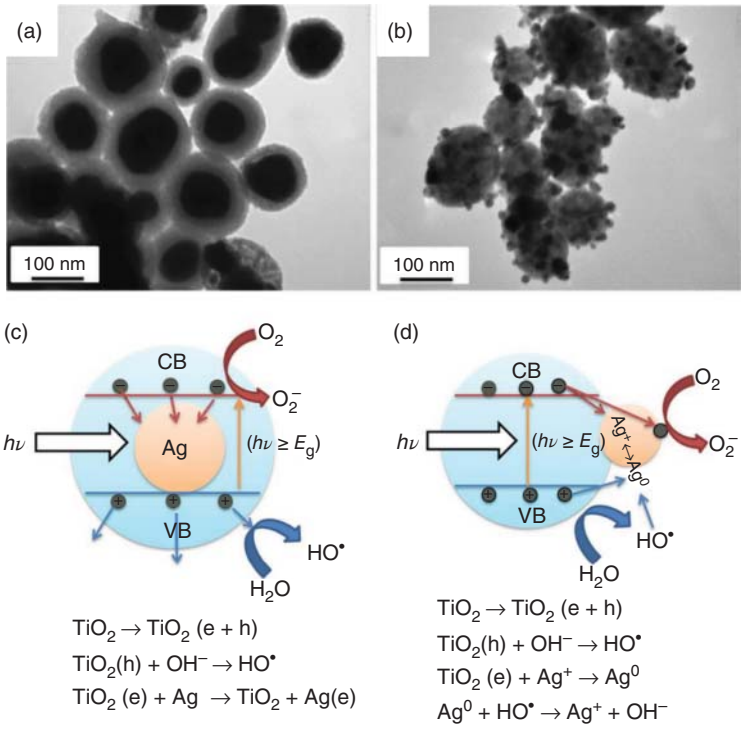

Figure 3.4 Transmission electron microscope (TEM) images of Ag@TiO_2 core–shell nanoparticles (a), Ag decorated TiO_2 (Ag–TiO_2) nanoparticles (b), and illustration of antibacterial mechanisms of Ag@TiO_2 (c), Ag–TiO_2 (d). Source: Reproduced with permission from Yang et al. 2014 [57]. Copyright © 2014, Springer Natures.

nanoparticles both demonstrated a bad ability to kill mature bacteria when there was no illumination of UV light. As shown in Figure 3.4c,d, the differences in the inactivation of the two nanoparticles might be attributed to the different antibacterial mechanisms. In particular, when the Ag@TiO_2 were stimulated by UV light, electrons at ground-state were excited into the conduction band. In a typical Schottky system, the electrons at the conductive band migrated to Ag and thus the Ag cores arrested more electrons from TiO_2 [58]. Thereafter hydroxyl radicals as well as superoxide anions would be produced. Furthermore, Ag cores might release Ag^+ ions due to the Ag_2O formation in this structure. Both of these variables would facilitate the inactivation of bacteria. In contrast, when irradiated with UV light, Ag–TiO_2 nanoparticles could lead to electrons being transferred to TiO_2 by the plasmon surface resonance of Ag, where the newly formed Ag^+ would accept the electrons generated by TiO_2 to form Ag^0 [59]. The hydroxyl radicals and superoxide anion are thought to play a more important role in the inactivation of bacteria than Ag^0 and Ag^+. These results were helpful in the design of antibacterial nanocomposites with desirable functionalities.

3.4.2 Zn-Doped TiO_2 Nanoparticles

Kumar et al. [60] explored the toxicity mechanism of ZnO and TiO_2 nanoparticles in *E. coli* and found that the two nanoparticles were internalized, uniformly distributed in *E. coli* without agglomeration, and caused significant DNA damage in *E. coli*. Because of their high chemical reactivity, it was of great interest that TiO_2 and ZnO nanoparticles could easily penetrate into the cells. *S. aureus* and *Staphylococcus epidermidis* are known as the prevalent bacteria in infected wound, TiO_2 and ZnO nanoparticles were to examine the antibacterial properties with visible light irradiation [61]. ZnO and TiO_2 nanoparticles have the capability of generating ROS when dispersed in water, and more amount of ROS would be produced if illuminated with blue light, which resulted in a significantly enhanced antibacterial activity of the nanoparticles. The high-quality of Zn-doped TiO_2 nanocrystals were developed by Kaviyarasu et al. [62], which delivered good inhibition on bacterial growth. It was confirmed the bactericidal effect of the material was closely relevant to the concentration of Zn and Ti for both Gram-negative and Gram-positive bacteria. However, with the treatment of Zn-doped TiO_2 nanoparticles and the irradiation of UV light, the bactericidal effect indicated that the inhibitory zones diameter of Gram-negative and Gram-positive bacteria both became larger with the rising content of TiO_2. Compared with Gram-negative bacteria, Gram-positive bacteria were more susceptible to the Zn-doped TiO_2 nanoparticles. It was related to the much thicker cell wall and polysaccharides in the Gram-negative bacteria, which stopped the nanoparticles penetrating into the bacterial cells, and the conclusion is consistent with that in other reports [14].

3.4.3 Cu-Doped TiO_2 Nanoparticles

In recent years, it has been proven that Cu-doped TiO_2 nanoparticles show great potential in enhanced bacterial inactivation when treated in darkness and the irradiation of weak UV and visible light [63, 64]. The antibacterial property of Cu-doped TiO_2 nanoparticles with diameter of 20 nm were assessed, and *Mycobacterium smegmatis* and *Shewanella oneidensis* MR-1 were selected as the model pathogenic strains because they are model bacterium of tuberculosis and environment-relevant bacterium. Both Cu-doped and non-doped TiO_2 nanoparticles with a diameter of 20 nm had the tendency to form larger aggregates, and such aggregates could not penetrate into the bacteria and thus failed to damage the cellular structures [64]. Cu-doped TiO_2 nanoparticles with a concentration lower than 100 mg/l significantly brought down the growth rate of *M. smegmatis*, but did not show an apparent bactericidal effect on *Sh. oneidensis* MR-1, while TiO_2 particles of the same concentration had no effects on either the growth of *M. smegmatis* and *Sh. oneidensis* MR-1. In addition, it was noted that Cu-doped TiO_2 nanoparticles had a higher bactericidal effect on *M. smegmatis* when compared with that of the equivalent amounts of Cu ions. Therefore, Cu^{2+} and TiO_2 nanoparticles might have a synergistic effect in the inhibition of *M. smegmatis*. TiO_2-based nanoparticles had the ability to adsorb Cu^{2+} since their surface was negatively charged, and thus the concentration of Cu^{2+} along the surface of TiO_2

nanoparticles tended to increase. Therefore, the presence of TiO_2 enhanced the antibacterial effect of Cu^{2+} to *M. smegmatis*. A large amount of EPS, especially extracellular protein, would be produced by *Sh. oneidensis* MR-1 when treated with Cu-doped TiO_2 nanoparticles, thus the toleration of the *Sh. oneidensis* MR-1 became higher with the increasing concentration of Cu doped. Moreover, the physical properties of the TiO_2 nanoparticles, such as size and crystal phase can be altered by the dopant of Cu into TiO_2 lattice, and the changes in the TiO_2 lattice can result in the shift of the light absorption to the visible light range. Sahu et al. [65] investigated the effects of such Cu-doped TiO_2 nanoparticles on the growth of *M. smegmatis* in darkness and under the irradiation of UV light and fluorescent light. In dark environment, Cu-doped TiO_2 showed insignificant antibacterial effect, and its bactericidal was enhanced with the increasing dopant of Cu. With the irradiation of fluorescent light, there was no obvious antibacterial effect for TiO_2, while Cu-doped TiO_2 nanoparticles showed an increasing inactivation with increasing dopant concentration. TiO_2 nanoparticles showed enhanced bacterial inactivation only under UV light irradiation. Meanwhile, the bacterial inactivation ability of Cu-doped TiO_2 nanoparticles was enhanced by irradiation of the UV light, and the bacterial cells resistance to UV light decreased over 99%. It was demonstrated in this study that when irradiated with light, three factors were responsible to the bactericidal effect of the Cu-doped TiO_2 nanoparticles, including (i) the interaction between the Cu^{2+} and bacterial cells, (ii) the increased products of reactive oxygen, and (iii) the enhanced photocatalytic reactions because of the decreased electron–hole pairs. When irradiated with light, the photoreactions of the Cu-doped TiO_2 nanoparticles were enhanced, which was attributed to the formation of more $OH^{\bullet}$ radicals resulted from the leaking Cu^{2+}. Therefore, it was suggested that the Cu-doped TiO_2 nanoparticles had a more effective potential in the inactivation of various bacteria than the conventional TiO_2 nanoparticles.

3.5 Antibacterial Applications of TiO_2-Based Nanoparticles

3.5.1 Medical Application

Surgical site infections and implant infections continue to be a common complication after surgery in clinic. Biomaterial surfaces must be modified to resist bacterial colonization *in vivo*, and coating an orthopedic implant with a TiO_2 film is demonstrated to decrease bacterial colonization [66, 67]. TiO_2-based nanoparticles have been used to inhibit bacteria formation because of their photocatalytic property [5, 66]. The big challenge in restorative dentistry is that secondary caries often be induced by the infection of bacteria because the biofilm tended to grow at the margin of a dental restoration. TiO_2-based nanoparticles were used to eliminate the biofilm on a novel dental adhesive through the photocatalytic reaction [68]. The results showed that with the treatment of TiO_2-based nanoparticles and the irradiation of UV light, the number of biofilm bacteria on the surface of the dental adhesives reduced by

one order of magnitude. Moreover, TiO_2 nanoparticles were also incorporated into poly(methylmethacrylate)/polyetheretherketone nanocomposite to prepare 3D printed stereo lithographic dental prosthesis with enhanced antibacterial characteristic [69]. The TiO_2 nanoparticles functionalized with carboxylic acid could be dispersed into the copolymer substrate uniformly, and they showed an antibacterial efficiency of 99% on both *E. coli* and *S. aureus* in darkness. This kind of antibacterial materials can be prepared facilely, and they have been efficiently used for the manufacturing of denture with the assistance of stereolithographic technique. Zane et al. [26] prepared TiO_2 nanoparticles without and with the dopant of nitrogen, and the particle size was in a range from 20 to 30 nm, and the authors extended their use in dental resins to reduce secondary caries caused by bacterial recolonization. When TiO_2 nanoparticles were coated on an orthopedic implant, Tsuang et al. [70] proposed to establish a relationship between the overall killing processes of TiO_2 nanoparticles. When incubated with TiO_2 nanoparticles, all the bacteria were nearly killed after 50 minutes UV irradiations. With the treatment of UV light, the TiO_2 nanoparticles can be used for medical apparatus and instruments to control the infection. *S. aureus* and *S. epidermidis* have been the most prevalent pathogenic bacteria in infections caused by implant since 1980 [71–73]. To inactivate the bacteria, TiO_2 can be used with the treatment of UV light by generating hydroxyl radicals and superoxide anion radicals in body fluid. For example, Toniatto et al. [73] constructed poly(lactic acid) (PLA) film loading with high dosage of TiO_2 nanoparticles by electrospinning method. With increasing the content of TiO_2, the PLA–TiO_2 film possessed higher bactericidal activity and showed no mammalian cell toxicity, thus the film loading with TiO_2 had the potential to be used extensively for biomedical applications.

3.5.2 Environmental Application

It was demonstrated that antibacterial activity can be enhanced by applying TiO_2-based nanoparticles doped with carbon nanotubes and metals including Cu, V, Ni, or the other elements with the irradiation of visible light [5]. Furthermore, specific aptamers can be used to endow the TiO_2 nanoparticles with enhanced specificity to the targeted bacteria, which can result in the effective transport of ROS to the targeted bacterial cells and also enhanced the inactivation of targeted bacteria in water [74]. It was observed that a high number of aptamers modified TiO_2 nanoparticles attached to the bacterial surface, leading to an effective and quick transportation of ROS to the bacteria. For example, aptamer related to *E. coli* modified TiO_2 nanoparticles only enhanced the bactericidal effect on *E. coli* in a mixed culture of *S. epidermidis* and *E. coli*. Thus, aptamer modified TiO_2 can be used to enhance inactivation target-specific bacteria in water. Also, TiO_2 nanoparticles and graphite were used as an additive to prepare a coating based on polyacrylic [75]. The modified coatings possessed excellent bactericidal effect on *Bacillus anthracis* and *S. aureus* in water environment, since they were hydrophilic, photocatalytic, and antibacterial. What's more – graphite also enhanced the inactivation activity toward bacteria by adsorbing bacteria in the surrounding of TiO_2 nanoparticles.

3.5.3 Food Safety Application

TiO_2 is a promising antibacterial coating for use in food safety application because of its photocatalytic performance. When coating on the surface of stainless steel, the TiO_2 nanoparticles coating possessed good antibacterial effect [76]. With increasing intensity of the UV light, the bacteria reduced for all the TiO_2 coatings. The results showed TiO_2 nanoparticles have a potential in developing coatings that possessed strong photocatalytic disinfection on the surface where food contacted. TiO_2 nanoparticles can also be deposited on steel or glass surfaces to construct different nanostructured thin films [77]. All the surfaces were cocultured with *L. monocytogenes* to develop biofilm, followed by the irradiation of UV light. The presence of the TiO_2 nanoparticles coated on steel or glass substrates both resulted in a fast and effective inactivation of biofilm. Thus, surface modification using nanostructured TiO_2 with photocatalytic performance is an inventive way to improve food safety.

3.6 Conclusion and Outlook

In this chapter, TiO_2-based nanoparticles have been introduced as a promising antibacterial agent because of its excellent photocatalytic performance under UV light as well as visible light. In order to endow TiO_2 nanoparticles with enhanced antibacterial property even under the illumination of visible light, many methods have been successfully carried out, including nitrogen, carbon, or other metal incorporated as substitutional or embedded state in TiO_2 lattice. On the basis of the TiO_2 nanoparticles doped with different elements, a variety of bacteria, such as *S. abony*, *S. aureus*, *B. subtilis*, *E. coli*, and *F. graminearum*, have been realized to be inactivated using UV or visible light illumination. It is thus proven that TiO_2-based nanoparticles are a type of promising antibacterial agents in medical, environmental, and other applications. However, the most antibacterial-related studies of TiO_2 nanoparticles based on their photocatalytic performance are only evaluated *in vitro*, and it is hard to acquire ideal antibacterial effect *in vivo* because of the lack of enough energy. Therefore, future investigations are needed to accomplish an enhanced antibacterial effect *in vivo*, as well as to keep a balance between inactivating targeted bacteria and affecting the mammalian cells in a minimal manner.

Acknowledgments

This work was supported by the National Key R&D Program of China (2018YFC0910601, 2019YFA0405603), the National Natural Science Foundation of China (31971292, U1432114), Zhejiang Province Financial Support (2017C03042, LGF18H180017, LY18H180011, LQ20H180002), and the Science & Technology Bureau of Ningbo City (2015B11002, 2017C110022, 2019A610202), Key Laboratory of Diagnosis and Treatment of Digestive System Tumors of Zhejiang Province (2019E10020). Furthermore, the authors also acknowledge Shanghai Synchrotron Radiation Facility at

+Line BL15U (No. h15sr0021) for X-ray fluorescence imaging and the National Synchrotron Radiation Laboratory in Hefei for soft X-ray imaging (No. 2016-HLS-PT-002193).

References

1 Matsunaga, T., Tomoda, R., Nakajima, T., and Wake, H. (1985). Photoelectrochemical sterilization of microbial cells by semiconductor powders. *FEMS Microbiology Letters* 29 (1–2): 211–214.

2 Sunada, K., Watanabe, T., and Hashimoto, K. (2003). Studies on photokilling of bacteria on TiO2 thin film. *Journal of Photochemistry and Photobiology A* 156 (1–3): 227–233.

3 Kim, B., Kim, D., Cho, D., and Cho, S. (2003). Bactericidal effect of TiO2 photocatalyst on selected food-borne pathogenic bacteria. *Chemosphere* 52 (1): 277–281.

4 Akhavan, O. and Ghaderi, E. (2009). Photocatalytic reduction of graphene oxide nanosheets on TiO2 thin film for photoinactivation of bacteria in solar light irradiation. *The Journal of Physical Chemistry C* 113 (47): 20214–20220.

5 Pelaez, M., Nolan, N.T., Pillai, S.C. et al. (2012). A review on the visible light active titanium dioxide photocatalysts for environmental applications. *Applied Catalysis, B: Environmental* 125: 331–349.

6 Zhukova, L.V. (2015). Evidence for compression of Escherichia coli K12 cells under the effect of TiO2 nanoparticles. *ACS Applied Materials & Interfaces* 7 (49): 27197–27205.

7 Hajipour, M.J., Fromm, K.M., Ashkarran, A.A. et al. (2012). Antibacterial properties of nanoparticles. *Trends in Biotechnology* 30 (10): 499–511.

8 Akhavan, O. (2009). Lasting antibacterial activities of Ag-TiO2/Ag/a-TiO2 nanocomposite thin film photocatalysts under solar light irradiation. *Journal of Colloid and Interface Science* 336 (1): 117–124.

9 Kim, S.-G., Dhandole, L.K., Seo, Y.-S. et al. (2018). Active composite photocatalyst synthesized from inactive Rh & Sb doped TiO2 nanorods: enhanced degradation of organic pollutants & antibacterial activity under visible light irradiation. *Applied Catalysis A* 564: 43–55.

10 Yeh, N., Lee, Y.C., Chang, C.Y., and Cheng, T.C. (2013). Anti-fish bacterial pathogen effect of visible light responsive Fe3O4@TiO2 nanoparticles immobilized on glass using TiO2 sol-gel. *Thin Solid Films* 549: 93–97.

11 Zhang, J., Liu, Y., Li, Q. et al. (2013). Antifungal activity and mechanism of palladium-modified nitrogen-doped titanium oxide photocatalyst on agricultural pathogenic fungi Fusarium graminearum. *ACS Applied Materials & Interfaces* 5 (21): 10953–10959.

12 Shieh, K.-J., Li, M., Lee, Y.-H. et al. (2006). Antibacterial performance of photocatalyst thin film fabricated by defection effect in visible light. *Nanomedicine: Nanotechnology, Biology and Medicine* 2 (2): 121–126.

13 Jang, H.D., Kim, S.-K., and Kim, S.-J. (2001). Effect of particle size and phase composition of titanium dioxide nanoparticles on the photocatalytic properties. *Journal of Nanoparticle Research* 3 (2–3): 141–147.

14 Nithya, N., Bhoopathi, G., Magesh, G., and Kumar, C.D.N. (2018). Neodymium doped TiO2 nanoparticles by sol-gel method for antibacterial and photocatalytic activity. *Materials Science in Semiconductor Processing* 83: 70–82.
15 Feris, K., Otto, C., Tinker, J. et al. (2009). Electrostatic interactions affect nanoparticle-mediated toxicity to gram-negative bacterium Pseudomonas aeruginosa PAO1. *Langmuir* 26 (6): 4429–4436.
16 Planchon, M., Ferrari, R., Guyot, F. et al. (2013). Interaction between Escherichia coli and TiO2 nanoparticles in natural and artificial waters. *Colloids and Surfaces B* 102: 158–164.
17 Zhukova, L.V., Kiwi, J., and Nikandrov, V.V. (2012). TiO2 nanoparticles suppress Escherichia coli cell division in the absence of UV irradiation in acidic conditions. *Colloids and Surfaces B* 97: 240–247.
18 Zhukova, L.V., Kiwi, J., and Nikandrov, V.V. (2010). Nanoparticles of TiO2 cause aggregation of Escherichia coli cells and suppress their division at pH 4.0–4.5 in the absence of UV irradiation. *Doklady Chemistry* 435: 279–282.
19 Joost, U., Juganson, K., Visnapuu, M. et al. (2015). Photocatalytic antibacterial activity of nano-TiO2 (anatase)-based thin films: effects on Escherichia coli cells and fatty acids. *Journal of Photochemistry and Photobiology. B* 142: 178–185.
20 Awasthi, A., Dube, A., Kumari, Y. et al. (2015). Toxicological evaluation of TiO2 nanoparticles in bacterial cell. *Macromolecular Symposia* 357 (1): 235–240.
21 Liu, W., Bertrand, M., Chaneac, C., and Achouak, W. (2016). TiO2 nanoparticles alter iron homeostasis in Pseudomonas brassicacearum as revealed by PrrF sRNA modulation. *Environmental Science: Nano* 3 (6): 1473–1482.
22 Chen, W.-J. and Chen, Y.-C. (2010). Fe3O4/TiO2 core/shell magnetic nanoparticle-based photokilling of pathogenic bacteria. *Nanomedicine* 5 (10): 1585–1593.
23 Mathur, A., Parashar, A., Chandrasekaran, N., and Mukherjee, A. (2017). Nano-TiO2 enhances biofilm formation in a bacterial isolate from activated sludge of a waste water treatment plant. *International Biodeterioration and Biodegradation* 116: 17–25.
24 Jomini, S., Clivot, H., Bauda, P., and Pagnout, C. (2015). Impact of manufactured TiO2 nanoparticles on planktonic and sessile bacterial communities. *Environmental Pollution* 202: 196–204.
25 Liu, S., Wang, M., Li, T., and Chen, Q. (2018). Response of an aerobic denitrifier to titanium dioxide nanoparticles exposure. *Environmental Technology*: 1–9.
26 Zane, A., Zuo, R., Villamena, F.A. et al. (2016). Biocompatibility and antibacterial activity of nitrogen-doped titanium dioxide nanoparticles for use in dental resin formulations. *International Journal of Nanomedicine* 11: 6459–6470.
27 Burda, C., Lou, Y.B., Chen, X.B. et al. (2003). Enhanced nitrogen doping in TiO2 nanoparticles. *Nano Letters* 3 (8): 1049–1051.

28 Park, J.H., Kim, S., and Bard, A.J. (2006). Novel carbon-doped TiO2 nanotube arrays with high aspect ratios for efficient solar water splitting. *Nano Letters* 6 (1): 24–28.

29 Yadav, H.M., Otari, S.V., Bohara, R.A. et al. (2014). Synthesis and visible light photocatalytic antibacterial activity of nickel-doped TiO2 nanoparticles against Gram-positive and Gram-negative bacteria. *Journal of Photochemistry and Photobiology A* 294: 130–136.

30 Li, W., Wang, Y., Lin, H. et al. (2003). Band gap tailoring of Nd3+-doped TiO2 nanoparticles. *Applied Physics Letters* 83 (20): 4143–4145.

31 Shah, S.I., Li, W., Huang, C.P. et al. (2002). Study of Nd3+, Pd2+, Pt4+, and Fe3+ dopant effect on photoreactivity of TiO2 nanoparticles. *Proceedings of the National Academy of Sciences of the United States of America* 99: 6482–6486.

32 Ananpattarachai, J., Boonto, Y., and Kajitvichyanukul, P. (2016). Visible light photocatalytic antibacterial activity of Ni-doped and N-doped TiO2 on Staphylococcus aureus and Escherichia coli bacteria. *Environmental Science and Pollution Research* 23 (5): 4111–4119.

33 Li, Q., Xie, R., Mintz, E.A., and Shang, J.K. (2007). Enhanced visible-light photocatalytic degradation of humic acid by palladium-modified nitrogen-doped titanium oxide. *Journal of the American Ceramic Society* 90 (12): 3863–3868.

34 Li, Q., Li, Y.W., Wu, P. et al. (2010). Palladium oxide nanoparticles on nitrogen-doped titanium oxide: accelerated photocatalytic disinfection and post-illumination catalytic "memory". *Advanced Materials* 20 (19): 3717–3723.

35 Wu, P., Xie, R., and Jian, K.S. (2010). Enhanced visible-light photocatalytic disinfection of bacterial spores by palladium-modified nitrogen-doped titanium oxide. *Journal of the American Ceramic Society* 91 (9): 2957–2962.

36 Cheng, C.-L., Sun, D.-S., Chu, W.-C. et al. (2009). The effects of the bacterial interaction with visible-light responsive titania photocatalyst on the bactericidal performance. *Journal of Biomedical Science* 16.

37 Bahadur, J., Agrawal, S., Panwar, V. et al. (2016). Antibacterial properties of silver doped TiO2 nanoparticles synthesized via sol-gel technique. *Macromolecular Research* 24 (6): 488–493.

38 Prashanth, G.K., Prashanth, P.A., Bora, U. et al. (2015). In vitro antibacterial and cytotoxicity studies of ZnO nanopowders prepared by combustion assisted facile green synthesis. *Karbala International Journal of Modern Science.* 1 (2): 67–77.

39 Kim, Y.S., Song, M.Y., Park, E.S. et al. (2012). Visible-light-induced bactericidal activity of vanadium-pentoxide (V2O5)-loaded TiO2 nanoparticles. *Applied Biochemistry and Biotechnology* 168 (5): 1143–1152.

40 Liu, W., Golshan, N.H., Deng, X. et al. (2016). Selenium nanoparticles incorporated into titania nanotubes inhibit bacterial growth and macrophage proliferation. *Nanoscale* 8 (34): 15783–15794.

41 de Faria, A.F., Martinez, D.S.T., Meira, S.M.M. et al. (2014). Anti-adhesion and antibacterial activity of silver nanoparticles supported on graphene oxide sheets. *Colloids and Surfaces B* 113: 115–124.

42 Lee, D., Cohen, R.E., and Rubner, M.F. (2005). Antibacterial properties of Ag nanoparticle loaded multilayers and formation of magnetically directed antibacterial microparticles. *Langmuir* 21 (21): 9651–9659.

43 Wang, H.-L. and Liu, X.-H. (2016). Preparation of silver nanoparticle loaded mesoporous TiO2 and its photocatalytic property. *Journal of Inorganic Materials* 31 (5): 555–560.

44 Uddin, M.J., Cesano, F., Scarano, D. et al. (2008). Cotton textile fibres coated by Au/TiO2 films: synthesis, characterization and self cleaning properties. *Journal of Photochemistry and Photobiology A* 199 (1): 64–72.

45 Jaksik, J., Phong, T., Galvez, V. et al. (2018). Advanced cotton fibers exhibit efficient photocatalytic self-cleaning and antimicrobial activity. *Journal of Photochemistry and Photobiology A* 365: 77–85.

46 Sun, C., Li, Q., Gao, S. et al. (2010). Enhanced photocatalytic disinfection of Escherichia coli bacteria by silver modification of nitrogen-doped titanium oxide nanoparticle photocatalyst under visible-light illumination. *Journal of the American Ceramic Society* 93 (11): 3880–3885.

47 Wong, M.S., Sun, D.S., and Chang, H.H. (2010). Bactericidal performance of visible-light responsive titania photocatalyst with silver nanostructures. *PLoS One* 5 (4).

48 Wong, M.-S., Chen, C.-W., Hsieh, C.-C. et al. (2015). Antibacterial property of Ag nanoparticle-impregnated N-doped titania films under visible light. *Scientific Reports* 5.

49 Hamad, A.H., Li, L., Liu, Z. et al. (2016). Sequential laser and ultrasonic wave generation of TiO2@Ag core-shell nanoparticles and their anti-bacterial properties. *Lasers in Medical Science* 31 (2): 263–273.

50 Dhanalekshmi, K. and Meena, K. (2014). Comparison of antibacterial activities of Ag@TiO2 and Ag@SiO2 core–shell nanoparticles. *Spectrochimica Acta Part A* 128: 887–890.

51 Chatterjee, K., Sarkar, S., Rao, K.J., and Paria, S. (2014). Core/shell nanoparticles in biomedical applications. *Advances in Colloid and Interface Science* 209: 8–39.

52 Quiñones-Jurado, Z.V., Waldo-Mendoza, M.Á., Aguilera-Bandin, H.M. et al. (2014). Silver nanoparticles supported on TiO2 and their antibacterial properties: effect of surface confinement and nonexistence of plasmon resonance. *Materials Sciences and Applications* 5 (12): 895.

53 Barudin, A., Hidayati, N., Sreekantan, S. et al. (eds.) (2013). Antibacterial activity of Ag-TiO2 nanoparticles with various silver contents. *Materials Science Forum* 756: 238–245.

54 Zhang, H. and Chen, G. (2009). Potent antibacterial activities of Ag/TiO2 nanocomposite powders synthesized by a one-pot sol–gel method. *Environmental Science & Technology* 43 (8): 2905–2910.

55 Ghanbary, F. and Jafarian, A. (2011). Preparation and photocatalytic properties of silver doped titanium dioxide nanoparticles and using artificial neural network for modeling of photocatalytic activity. *Australian Journal of Basic and Applied Sciences* 5: 2889–2898.

56 Amarjargal, A., Tijing, L.D., and Kim, C.S. (2011). One-pot synthesis of silver-titanium dioxide nanocomposites using ethylene glycol medium

and their antibacterial properties. *Digest Journal of Nanomaterials and Biostructures*.

57 Yang, X.H., Fu, H.T., Wang, X.C. et al. (2014). Yu AB. Synthesis of silver-titanium dioxide nanocomposites for antimicrobial applications. *Journal of Nanoparticle Research* 16 (8).

58 Chuang, H.Y. and Chen, D.H. (2009). Fabrication and photocatalytic activities in visible and UV light regions of Ag@TiO2 and NiAg@TiO2 nanoparticles. *Nanotechnology* 20 (10).

59 Cushing, S.K., Li, J., Meng, F. et al. (2012). Photocatalytic activity enhanced by plasmonic resonant energy transfer from metal to semiconductor. *Journal of the American Chemical Society* 134 (36): 15033–15041.

60 Kumar, A., Pandey, A.K., Singh, S.S. et al. (2011). Engineered ZnO and TiO2 nanoparticles induce oxidative stress and DNA damage leading to reduced viability of Escherichia coli. *Free Radical Biology & Medicine* 51 (10): 1872–1881.

61 Lipovsky, A., Gedanken, A., Nitzan, Y., and Lubart, R. (2011). Enhanced inactivation of bacteria by metal-oxide nanoparticles combined with visible light irradiation. *Lasers in Surgery and Medicine* 43 (3): 236–240.

62 Kaviyarasu, K., Geetha, N., Kanimozhi, K. et al. (2017). In vitro cytotoxicity effect and antibacterial performance of human lung epithelial cells A549 activity of Zinc oxide doped TiO2 nanocrystals: Investigation of bio-medical application by chemical method. *Materials Science & Engineering C-Materials for Biological Applications* 74: 325–333.

63 Yadav, H.M., Otari, S.V., Koli, V.B. et al. (2014). Preparation and characterization of copper-doped anatase TiO2 nanoparticles with visible light photocatalytic antibacterial activity. *Journal of Photochemistry and Photobiology A* 280: 32–38.

64 Wu, B., Huang, R., Sahu, M. et al. (2010). Bacterial responses to Cu-doped TiO2 nanoparticles. *The Science of the Total Environment* 408 (7): 1755–1758.

65 Sahu, M., Wu, B., Zhu, L. et al. (2011). Role of dopant concentration, crystal phase and particle size on microbial inactivation of Cu-doped TiO2 nanoparticles. *Nanotechnology* 22 (41): 415704.

66 Osumi, K., Matsuda, S., Fujimura, N. et al. (2017). Acceleration of wound healing by ultrasound activation of TiO2 in Escherichia coli-infected wounds in mice. *Journal of Biomedical Materials Research Part B* 105 (8): 2344–2351.

67 Liu, W., Su, P., Chen, S. et al. (2015). Antibacterial and osteogenic stem cell differentiation properties of photoinduced TiO2 nanoparticle-decorated TiO2 nanotubes. *Nanomedicine* 10 (5): 713–723.

68 Cai, Y., Stromme, M., Melhus, A. et al. (2014). Photocatalytic inactivation of biofilms on bioactive dental adhesives. *Journal of Biomedical Materials Research Part B* 102 (1): 62–67.

69 Chen, S., Yang, J., Li, K. et al. (2018). Carboxylic acid-functionalized TiO2 nanoparticle-loaded PMMA/PEEK copolymer matrix as a dental resin for 3D complete denture manufacturing by stereolithographic technique. *International Journal of Food Properties* 21 (1): 2557–2565.

70 Tsuang, Y.-H., Sun, J.-S., Huang, Y.-C., and Lu, C.-H. (2008). Chang WH-S, Wang C-C. Studies of photokilling of bacteria using titanium dioxide nanoparticles. *Artificial Organs* 32 (2): 167–174.

71 An, Y.H. and Friedman, R.J. (1996). Prevention of sepsis in total joint arthroplasty. *The Journal of Hospital Infection* 33 (2): 93–108.

72 Arciola, C.R., Campoccia, D., Ehrlich, G.D., and Montanaro, L. (2015). Biofilm-based implant infections in orthopaedics. In: *Biofilm-Based Healthcare-Associated Infections: Volume I. Cham* (ed. G. Donelli), 29–46. Germany: Springer International Publishing.

73 Toniatto, T.V., Rodrigues, B.V.M., Marsi, T.C.O. et al. (2017). Nanostructured poly (lactic acid) electrospun fiber with high loadings of TiO2 nanoparticles: insights into bactericidal activity and cell viability. *Materials Science and Engineering: C* 71: 381–385.

74 Song, M.Y., Jurng, J., Park, Y.-K., and Kim, B.C. (2016). An aptamer cocktail-functionalized photocatalyst with enhanced antibacterial efficiency towards target bacteria. *Journal of Hazardous Materials* 318: 247–254.

75 Nosrati, R., Olad, A., and Maryami, F. (2018). The use of graphite/TiO2 nanocomposite additive for preparation of polyacrylic based visible-light induced antibacterial and self-cleaning coating. *Research on Chemical Intermediates* 44 (10): 6219–6237.

76 Duncan, T.V. (2011). Applications of nanotechnology in food packaging and food safety: barrier materials, antimicrobials and sensors. *Journal of Colloid and Interface Science* 363 (1): 1–24.

77 Chorianopoulos, N.G., Tsoukleris, D.S., Panagou, E.Z. et al. (2011). Use of titanium dioxide (TiO2) photocatalysts as alternative means for Listeria monocytogenes biofilm disinfection in food processing. *Food Microbiology* 28 (1): 164–170.

4

Surface-Enhanced Raman Spectrum of TiO_2 Nanoparticle for Biosensing (TiO_2 Nanoparticle Served as SERS Sensing Substrate)

*Jie Lin and Aiguo Wu**

Cixi Institute of Biomedical Engineering, CAS Key Laboratory of Magnetic Materials and Devices, & Key Laboratory of Additive Manufacturing Materials of Zhejiang Province, Ningbo Institute of Materials Technology and Engineering, Chinese Academy of Sciences, No. 1219 Zhongguan West Road, Ningbo 315201, P.R. China

CHAPTER MENU

Introduction, 133
SERS Effect of Nanomaterial Substrate, 135
TiO_2 SERS Substrate Applied in Biosensing, 144
Conclusions and Future Perspectives, 150

4.1 Introduction

In 1977, Van Duyne and coworkers exhibited the effect of surface-enhanced Raman scattering (SERS) on the roughened silver electrode, which is an important breakthrough in Raman spectroscopy and a historic moment [1]. In 1974, Fleischmann et al. observed the robust Raman signal of the untreated pyridine molecules on silver electrodes by electrochemical methods [2]. Similar phenomena have been found. However, the authors attribute these high intensity Raman signal to the boosted adsorbed molecules and the surface area on the corrugated surface of the electrode. However, after careful and effective calculation, Van Duyne realized that the boosted Raman signal of the probe molecule was 10^5–10^6 times higher than bulk pyridine molecule. They concluded that the exceptionally strong Raman signal could not be explained only by increasing adsorbed molecules, but the real enhancement of Raman scattering efficiency mechanism. Jeanmail et al. and Albrecht et al. showed that the Raman enhancement is caused by local electromagnetic field around metal nanostructures [3]. This effect is called as SERS mechanism, which is also the origin of the SERS subject. The reported SERS phenomenon immediately attracted the interest of surface-enhanced Raman researchers, because ultrahigh molecular detection sensitivity is provided with SERS, which greatly expands the application of Raman spectroscopy. In addition, SERS technology is also used

*Corresponding author: aiguo@nimte.ac.cn

TiO_2 Nanoparticles: Applications in Nanobiotechnology and Nanomedicine,
First Edition. Edited by Aiguo Wu and Wenzhi Ren.
© 2020 Wiley-VCH Verlag GmbH & Co. KGaA. Published 2020 by Wiley-VCH Verlag GmbH & Co. KGaA.

at in situ detection fields, especially useful in the specially fields (electrochemical/aqueous), with ultra-high detection sensitivity and good nondestructive spectral resolution feature. It is noteworthy that the signals emitted by molecules adsorbed on the surface of noble metal nanoparticles (NPs) can be largely enhanced, while the molecular signals far from solutions remain unchanged. Therefore, it can effectively eliminate or reduce the interference of unabsorbed molecules in solution, which is a prominent advantage, and it also declares the irreplaceable position of Raman spectroscopy in sensing.

Traditional SERS substrate is largely relied on the surface plasma resonance effect, which is induced by the near-field interaction between light illumination and noble-metal materials (for example, Ag, Au, Cu) in the morphologies of different nanoparticles, nanofilms, nanostructures, and electrochemically roughened coinage metal interfaces. SERS substrate composed of noble metal nanomaterial can reach ultrahigh detection sensitivity even to single molecule level with the enhancement factor (EF) of 10^{12}–10^{15} based on the mechanism of electromagnetic enhancement [4–7]. Due to the hot spot effect for the noble metal substrate, the EF is high enough for detecting various target molecules. In the year of 1979, Creighton et al. group reported that yellow or purple sols were obtained with the synthesized method of monodisperse silver and gold colloids to enhance Raman scattering and sodium borohydride as reductant to prepare this sample [8]. The maximum extinction of silver sol is 400 nm and gold sol is 525 nm, which indicates that the size of silver sol solution is much smaller than the illumination laser. Pyridine molecule was added to the sol to enhance Raman signal. The enhancement depends on the extinction effect and the illuminated excitation wavelength, which indicates that surface plasmon oscillation is helpful to enhance Raman scattering. Moskovits' group results and Reighton's experimental result show these SERS substrates extend from rough coin nanoparticles, now known as NSs [9]. SERS technology extends the application of SERS from science report to materials and life science. Thanks to the rapid development of nanotechnology in 1990s, SERS effect has attracted increased interest and attention. In 1995, Natan and coworkers group prepared gold and silver NPs with monolayer polymer adsorbed substrates with mercaptan, amine, or cyanide functional groups [10]. These functional groups could interact strongly with noble material NPs. This is the first time noble metal nanoparticles with the matrix and a strong surface-enhanced Raman spectrum was obtained. Through these important and significant studies, a lot of new detection technology have been reported at the field of SERS with highly sensitive noble metal nanoparticles.

The observation of single-molecule SERS (SMSERS) effect was the biggest breakthroughs in SERS field, which was observed by Kneipp's and Nie's scientific groups [11, 12], respectively. Nie et al. group observed the reduction of Ag nanoparticles with nano-gap (nano-gap) by SMSERS on immobilized citrate using Rhodamine 6G (R6g) molecule [12]. They estimate the single nanoparticle with average R6G molecule at the concentration of 2×10^{-10} M. Compared with ordinary Raman, the additional SERS enhances by more than 10 orders of magnitude, which is equivalent to the one molecule fluorescence effect. At 1999, Xu group observed the Raman signal of a single hemoglobin protein molecule with silver nanoparticles separated or immobilized by SERS effect [13]. Connected with the scanning electron microscopy (SEM)/atomic force microscopy (AFM),

they observed that almost no Raman signal on a single silver nanoparticle; but, the active Raman signal were detected on dimers/trimers. In addition, in the high intensity dimer NPs, the axis which is paralleled with the illuminated wavelength, always produces high intensity SERS effect. It is noteworthy that the resonance coupling mechanism with light and nanoparticles, and junction between nanoparticles and nanoparticles (known as "hot spots") may produce stronger electromagnetic fields. The Raman signal of hot spot molecules is significantly improved. The single-molecule SERS effect overcome the limitations of molecular universality, making SERS one of the most promising trace analysis tools in biomedicine and a safe and environmental tool with single-molecule sensitivity. However, the non-selection enhancement, low spectra uniformity, and no good biocompatibility of the coinage materials seriously hinder their further applications, especially unable to satisfy the biological application [14, 15].

4.2 SERS Effect of Nanomaterial Substrate

4.2.1 Mechanism of Non-metal SERS Platforms

Recently, more and more scientific attention is focused on the SERS effect from noble metal to free metal materials exhibiting good SERS effect [16]. In particular, SERS-active substrates such as semiconductors and non-metal platforms (such as the graphene, carbon nanotubes) have been deeply studied. For non-metal material, graphene is the famous material in the science and nature and graphene is a real non-metallic system consisting of SP^2 carbon hexagonal networks with strong covalent bonds. Multilayer graphene can be stacked layer by layer in the form of Bernard or diamond by Van der Waals force coupling. High-quality single-layer graphene and multilayer graphene is prepared by the various methods, for example, micro-mechanical peeling, chemical deposition method, and epitaxy growth from SiC surface. Other manufactured routes for production, such as reduction of graphene oxide (Go) solution and organic synthesis, tend to introduce defects such as vacancies and dislocations in graphene and expose graphene to oxidation, hydrogenation, fluorination, and other chemical functionalization. Graphene nanomaterial's can also be decomposed into one-dimensional (1D) and zero-dimensional (0D) shapes such as graphene nanoribbons (GNR) and nanographene. All of these are ready for the application of graphene as a non-metallic material in the field of optoelectronics. Based on the advantages of noble metal, the advantage of semiconductor NPs lies in easy control of the interface properties. However, due to the economic cost, graphene served as SERS substrate is hindered, and other semiconductor materials have attracted our interest. It has been reported that the SERS effect can be generated from Ni, Pt, Rh, Pd, and Co NPs, but these transition metals always could not provide enough high enhancement [17]. The SERS substrates for non-metal substrate, semiconductor SERS substrates, have attracted increasing attention due to their high stability, reproducibility, and good biocompatibility. Currently, many groups have observed that semiconductor NPs have excellent SERS performance, such as silicon nanowire, $W_{18}O_{49}$

nanowires, ZnO NPs, InAs quantum dots, and Cu_2O NPs, and so on [18–22]. These materials served as SERS substrate would pave a good way for widely opening practical application with SERS sensing.

The mechanism for no-metal SERS platforms is attributed to photo-induced charge transfer (PICT) process with the semiconductor material and probe molecules. However, relatively weak EF ranging from 10 to 1000 seriously hinder the development of semiconductor-based SERS. Although SERS effect for the semiconductor is largely improved, the detection sensitivity for the no-metal SERS platforms can only arrive to 10^{-5} M, which is largely away from the noble metal SERS substrate (Au, Ag, Cu NPs). So a lot of methods are found for improving SERS detection property at semiconductor materials. Alessandri group made a large contribution to this field by using TiO_2-based spherical resonators [23]; the feature of the high-refractive index of the TiO_2 material and the multiple light scattering effect were responsible for the good SERS detection. Zhang group developed a new SERS substrate by introducing TiO_2 photonic microarray, attributed to the strong matter–light interaction and good multiple light scattering effect by the own feature of the microarray, and the SERS limit of detection for methylene blue (MB) probe molecules was 10^{-6} M [24]. Shi et al. group introduced the effect of strong morphology-induced light trapping by the Si nanowire arrays SERS substrate, and the R6G target molecules is detected at the concentration of 10^{-5} M [25]. Obviously, TiO_2 SERS substrate showed good potential materials for SERS technology, as it takes a key point provided by its own feature [26].

4.2.2 Advantages for TiO_2 SERS Substrate

TiO_2 has many advantages for SERS substrate compared with other semiconductor materials, as TiO_2 owns relatively high stability (spectrum stability), high index (enhancing light scattering), versatile interface functionalization (benefit for Raman signal), self-cleaning performance, and spectrum recyclability and also could arrive to the coupling with plasmonic nanoparticles (high enhancement); its good biocompatibility can help to make application in the biosensing [26]. These good optical properties are directly studied with the SERS-active platforms by superior prepared method and formed with good and multifunctional nanodevices, [27] but as non-metal materials, the EF feature of TiO_2 is always too smaller than that of Au and Ag SERS substrate, In order to improve the SERS property of TiO_2 substrate, a lot of methods were explored to enhance the SERS property [28]. Due to the changed particle size, different shape, and high and low doping technology, various of possibilities for the interface band structure of TiO_2NPs have been observed, and the band is easily modulated. For example, semiconductor materials with graphene, TiO_2 deposited on Si microarray, doping technology used in TiO_2 material, surface defect forming in TiO_2 material, making noble-material@TiO_2 complex SERS substrate, and building SiO_2@TiO_2 shell–core nanostructure with the feature of strongly light scattering effect have been observed to largely improve SERS performance and high detection sensitivity [29].

4.2.3 SERS Mechanism of TiO_2 SERS Substrate

TiO_2 served as SERS substrate exhibiting exciting performance, and many probe molecules were detected by TiO_2 substrate at relatively low concentrations. TiO_2 NPs are formed with the method of water hydrothermal, and the sizes for the TiO_2 nanoparticles are ranging at about 10 nm. TiO_2 nanoparticles adsorbed three probe thiophenol-related target molecules: [4-mercaptobenzoic acid (4-MBA) small molecules, 4-mercaptopyridine (4-MPY) small molecules, and 4-aminothiophenol (*p*-aminothiophenol, PATP) small molecules. The functional group (thiol) will bind to TiO_2 nanoparticles, and the molecules linked to the SERS substrate were strongly enhanced. Using the thiol group molecule, the Raman signal was largely enhanced compared with solution molecule. The Raman shift of the peak also exhibited significant difference compared with the powder references. In the SERS measurement, we always used 532 nm laser to excite the Raman signal. The energy of the excitation laser was 2.4 eV, and the energy is obviously no good to promote direct electron transfer from valence band (VB) structure to conduction band (CB) structure of TiO_2 nanoparticles. So the electron was transferred between target molecule and TiO_2 nanoparticles, and the enhancement for the three target molecules was followed by the results: 4-MBA > 4-MPY > PAYTP as shown in Figure 4.1 [29].

These results were in very good agreement with the attracting electron ability of the functional groups (the -SH group) and was not connected with Raman scattering cross section of the probe molecules as the cross section is almost the same. This result showed that the enhanced SERS signals of the target molecules adsorbed on TiO_2 nanoparticles were due to the contribution of the charge transfer (CT) process effect between the TiO_2 substrate and the probe molecule. The CT process effect between SERS platforms and the probe molecule could be mediated by many methods, and one is enhanced by Ti defect states. The surface defect states position is lied ~0.5 eV relatively lower than the position of the TiO_2 CB band edge. Due to the result of abundant surface defect states existing at the surface, the electron transition possibility between the TiO_2 nanoparticles and

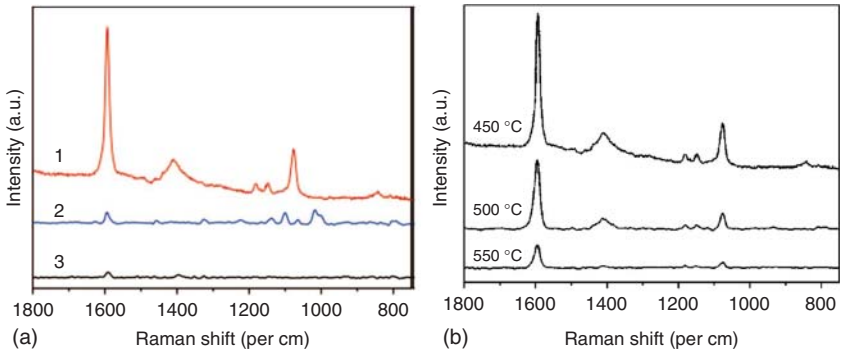

Figure 4.1 (a) SERS spectra of the 4-MBA (1), 4-MPY (2), and PATP (3) target molecules adsorbed on TiO_2 nanoparticles calcined at 450 °C. (b) SERS spectra of 4-MBA target molecules adsorbed on the TiO_2 nanoparticles calcined at different temperatures. Source: Reprinted with permission from Yang et al. 2008 [29]. Copyright 2008, American Chemical Society.

the target molecule would be largely promoted, which would strongly improve the target molecular polarizability tensor and largely boost the Raman scattering effect of this molecule based on the thermodynamically PICT transition rate in SERS-molecule surface complex. To some extent, the relatively numerous surface defects would result in relatively strong Raman intensity, especially for the b_2 Raman mode. In order to illustrate the surface defect playing an effectively effect in the enhancement of semiconductor SERS substrate, temperature-dependent TiO_2 nanoparticles SERS experiment is carried out. Based on this conjecture, a SERS experiment on the crystallinity feature was also took out to study the TiO_2 substrate-to-target molecule CT effect existed in the surface of TiO_2 substrate. Figure 4.2 illustrates 4-MBA adsorbed on TiO_2 nanoparticles SERS effect that are calcined by three temperatures. It is observed the SERS results based on the SERS signals of 4-MBA probe molecule on TiO_2 substrate were obviously decreased as the temperature increased from 450 to 550 °C. In the meantime, the crystallinity degree for the TiO_2 nanoparticles will become relatively higher, and the crystallite size for the SERS substrate becomes larger with the phenomenon of the increased calcination temperature, also simultaneously with the result of the specific surface area (SSA), and the amount of the interfacial defect content of TiO_2 nanoparticles will obviously decreased. We also studied that the decrease of adsorption effect for 4-MBA molecule on TiO_2 nanoparticles, the phenomenon

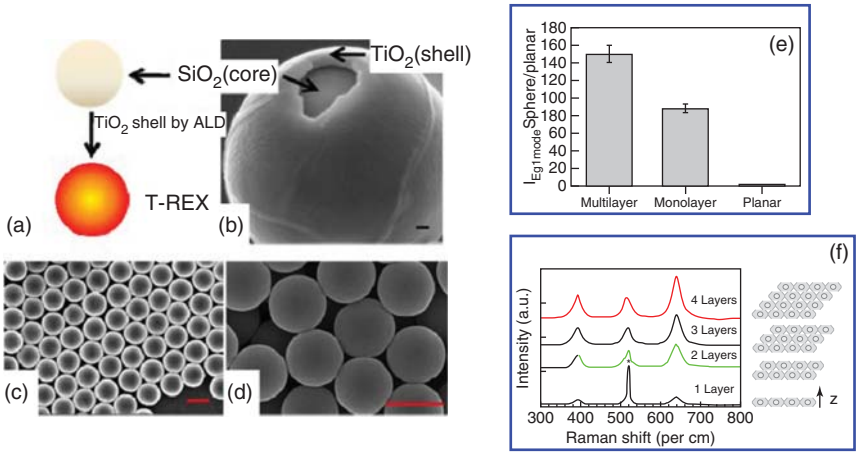

Figure 4.2 (a) Scheme of synthesis of TiO_2 spherical resonators (T-REX). The silica cores are covered with an amorphous titania thin shell through the ALD technology. Then annealing to 700 °C for six hours, promoting the formation of crystalline anatase; (b) SEM image of T-REX 100 sample. This image shows the SiO_2 core and evaluates the thickness of the TiO_2 layer. Scale bar: 100 nm; (c) low and (d) high magnification SEM images of T-REX 20 samples. Scale bars: 2 μm. (e) Assessment of the strength ratio of anatase $E_{g(1)}$ mode between T-REX 100 sample and corresponding plane reference. The data reported in the histogram are from Raman spectra obtained in 30 different regions of each sample and provide an indication of the Raman mode E_f; (f) Raman spectra are a function of the number of T-REX layers. The asterisk-denoted peak of Si substrate is used as a reference to evaluate the minimum number of T-REX layers required for light capture. Source: Reprinted with permission from Alessandri 2013 [23]. Copyright 2013, American Chemical Society.

caused by the decrease of the SSAs of TiO_2 with the calcination temperature rising, could be ruled out through the UV–vis measurements of 4-MBA probe molecule. The UV–vis result could make sure that the SSAs are not the important factor. These results indicated that we could not explain such decreased in intensity of SERS signals for the probe 4-MBA molecule adsorbed on TiO_2 SERS substrate (Figures 4.1a and 4.2) with the decreased SSA. Therefore, the remarkable phenomenon for the decrease in the intensity of the SERS signals for 4-MBA molecule adsorbed on TiO_2 nanoparticle with the heat temperature must due to the decrease of surface vacancy defect amount of TiO_2 substrate. The relatively higher the calcination temperature of TiO_2, the relatively higher the crystallinity, and relatively the lower surface defect amount, the relatively lower the capability of TiO_2 substrate-to probe molecule CT process and the relatively weaker SERS signals for the 4-MBA molecules adsorbed on the TiO_2 substrate. This result illustrates that the intrinsic TiO_2 substrate surface vacancy states (surface defect state) play a significant position in TiO_2 substrate-to-probe molecule CT process, both as freedom electron traps and effective center states for electron transfer from SERS substrate to probe molecules. The abundant surface defect states are beneficial for TiO_2 substrate-to-probe molecule CT process. This phenomenon also further confirmed the very important role of interfacial defects contributing to the TiO_2 SERS enhancement mechanism [30].

4.2.4 Novel Methods to Improve TiO_2 SERS Enhancement

The SERS EF for non-metal (semiconductors) SERS substrate is only about 10–1000, which is always originated from PICT process resonating with incident illumination. This effect is always hindered by the relatively low CT efficiency. But, observed on the coinage metals substrate, the relatively weak EF of semiconductors SERS substrates hinders the molecule sensing detection application and the biosensing applications fields. Fortunately in order to improve the SERS performance of TiO_2 nanoparticles, several useful novel strategies have been explored and reported [22]. Ivano Alessandri demonstrates TiO_2 spherical nanoparticle first, and an excellent enhancement of Raman enhancement has been acquired without the plasmonic nanostructures by the means of establishing TiO_2-based new spectrum resonators. The design is based on the high-refractive index feature of the shell layer of the TiO_2 NPs, and the morphology feature and the related sphere factors enhance the multiple light scattering for the Raman spectrum for both thin and ultrathin layers of anatase–TiO_2. This design could also direct monitor and effectively do the photocatalytic reactions at the in situ environment. And, due to the self-cleaning properties of TiO_2 spherical nanoparticle under ultraviolet (UV) illumination, these SERS substrates are obviously recyclable: Therefore, different target molecules and reactions can be done and directly acquired using the high SERS enhancement surface [23]. Figure 4.2a exhibits the feature of 100 nm-thick spherical TiO_2 deposited on the flat substrate, and micro-Raman spectra with T-REX 100 samples is obviously achieved with high enhancement intensity and good practically application. Raman spectra were obtained from single and multilayered regions and compared with planar films observed on the flat

platform during atomic layer deposition (ALD). The experimental design ensures the comparability between the obtained titanium dioxide layer under the same ALD cycle times and the fully annealed titanium dioxide layer under the same conditions. Compared with the plane reference, the Raman spectra of anatase NPs exhibit significant high intensity EF. With the same detected parameters, the Raman modes could be explained as $E_{g(1)}$, $E_{g(2)}$, $A_{1g} + B_{1g(2)}$, and $E_{g(3)}$ of T-REX in single and multilayered structures can be observed. Although the acquisition time is short, the signal is very strong and has a good signal-to-noise ratio. In other words, planar films are difficult to detect (see the magnification in Figure 4.2a). The information are limited to the main anatase peak ($E_{g(1)}$ mode), while $E_{g(2)}$ is undetectable. The other anatase Raman modes are close to the limit of detection, and the signal-to-noise ratio is very low.

Statistical useful analysis of normalizing the main peak of anatase ($E_{g(1)}$ model, about 143 per cm) of the T-REX 100 SERS nanoparticle to the strength ratio of the corresponding plane reference (Figure 4.2e) confirms the result. It shows that SERS intensity of the plane film is smaller than 2.5% of the strength displayed by T-REX monolayer and 1% of the strength realizable by T-REX monolayer. Raman scattering data are highly repeatable, indicating that the spectrum obtained from multiple layers is much stronger than that obtained from single layers, although ALD cycles (i.e. the amount of titanium dioxide deposited on the core) is the same. Compared with single layer and separated T-REX spheres, there is less difference in Raman scattering intensity. This result is explained by the transverse resolution of the laser beam size used in the current experimental device, which is less than 2 m, allowing a single T-REX sphere to be classified from a closed filling single layer. Detailed evaluation of the functional relationship between Raman scattering and T-REX layers shows that the layer number of T-REX is greater than 3, and the Si peaks originating from the underlying basement disappear (Figure 4.2f). The result shows that the excitation laser is completely bound to the T-REX colloidal crystal. Therefore, the total contribution to Raman scattering only comes from T-REX spheres, rather than dissipating through the interaction with the base. Based on these findings, it can be assumed that the significant enhancement of T-REX structure may be due to the synergistic effect of two main factors: titanium dioxide has a high refractive index feature (anatase is n−2.5) between two relatively low refractive index media (such as air, $n = 1$, and SiO_2, $n - 1.45$). The refractive index contrast result allows more efficient internal coupling of the light between the titanium dioxide shell and outside matter.

The feature of the evanescent interfacial electromagnetic field generated by the mentioned optical effects is expected to facilitate the detection of analytes adsorbed on the surface of the T-REX, and thus the related interface processes. As an experiment, we tested the detection of MB adsorbed on the surface of T-REX and its degradation under UV light. Specific spheroids were selected to monitor photodegradation by optical observed microscopy. Figure 4.3a shows the Raman spectrum of a T-REX 100 monolayer sample grown in a 10^{-5} M concentration MB solution. Although this concentration is lower than the detection limit of MB adsorbed on the TiO_2 flat film, the T-REX scaffold shows an MB spectrum with a strong mode and a good signal-to-noise ratio. This improved sensitivity may be due to the interfacial evanescent field produced at the TiO_2/MB surface.

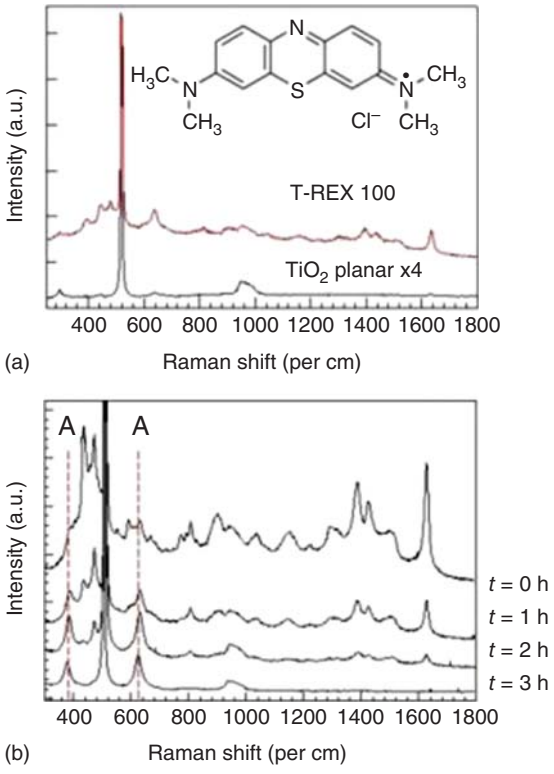

Figure 4.3 (a) Raman spectra of 10^{-5} mol MB solution adsorbed on T-REX 100 sphere. The spectra of the same solution adsorbed on the 100 nm thick anatase flat mask (multiplied by 4) were compared; (b) monitoring the MB-induced photo degradation of UV-induced adsorption on T-REX 100 spheres as a function of irradiation time. Initial concentration of MB solution ($t = 0$). Source: Reprinted with permission from Alessandri 2013 [23]. Copyright 2013, American Chemical Society.

Although detection sensitivity capability is far from the conventional metal-based Au and Ag SERS substrates, T-REX SERS platforms allow the Raman sensitivity to be extended to monitor many of the interest (degradation of organic pollutants, water decomposition, etc.). Most importantly, this process can be studied without interference from any metal reinforcers. In this case, we can observe that the MB signal gradually decreases with the time of irradiation and eventually disappears in the spectrum obtained three hours before irradiation (Figure 4.3b). A large number of MB are adsorbed on the interface of titanium dioxide in the dimer or molecular aggregate, as shown by strong CNC vibration. The bending mode is 450 per cm. One hour later, compared with 481 per cm thiazine rings in plane bending mode, the mode is obviously reduced. The characteristic of this mode is that the anatase mode becomes more obvious as MB target molecules are removed from the interface. Interestingly, as some MB target molecules are also adsorbed on the interface of titanium dioxide, the anatase signal obtained after two hours is slightly stronger than that obtained after three hours, that is, when MB is all removed (the Si peak is observed as compartment). This result is gone well with the observed phenomena reported by Lombardi and his colleagues on the enhancement of Raman modes of TiO_2 due to the coupling with the Raman molecules. This result and its relationship on wavelength laser and Raman probe molecule concentration are still unclear. In the long run, the refractive index platforms are applied and made into useful optical devices. This general method can

also be extended to infrared spectroscopy and fluorescence spectroscopy to fabricate multi-channel Raman sensors for detection features with different spectral intensity.

Sensitive SERS detection is implemented with a plasma-free titanium dioxide photonic artificial microarray, rapidly detected, and reused under simulated solar irradiation. In photonic microarrays, the interaction between matter and light is enhanced by repetition and multiple light scattering, thus obtaining sensitive detection performance. In addition, the sensitivity of SERS is different from the optical coupling resonance of microarrays with different photonic energy gaps [24]. The microarrays with the center of the band gap close to the laser wavelength show lower SERS signals because of the suppression of light propagation, while the microarrays with the edge of the band gap close to the laser wavelength show lower SERS signals. Due to the slow light effect, the sensitivity is higher. Here, the authors report a new and important photonic energy gap correlation sensitivity of titanium dioxide microarrays, which is reduced or improved by carefully matching the laser wavelength with the band gap position. By comparing porous and non-porous membranes, it is further proved that enhanced SERS detection sensitivity is related to enhanced with strong light–matter interaction by the photonic microarrays. In addition, the new SERS substrate is easily formed and reused from instantaneous sunlight.

Figure 4.4a shows the SERS spectra of MB target molecules adsorbed on the surface of TiO_2 (TiO_2-225) and titanium dioxide. Compared with the planar TiO_2 substrate, the inverse opal of TiO_2 has a very high sensitivity. The detection limit is even reduced to 6×10^{-6} M, which is equivalent to precious metals without help of hot spot effect. The peak intensity at 449 per cm decreases with the decrease of concentration of the molecular solution, indicating that monomers mainly exist at low concentration and aggregate at high concentration. The insertion SEM images show the titanium dioxide antiopal with a novel macroporous nanostructure and a higher SSA than the titanium dioxide plate. It can rule out that the enhanced SERS effect is attributed with the increased SSA effect. P25 material, a commercial product with a SSA almost same to that of titanium dioxide antiopal, is used as a reference matrix. Obviously, the SERS signal observed from the titanium dioxide antiopal is bigger than that from P25 (Figure 4.4a), which excludes the effect of SSA on the high SERS sensitivity of the titanium dioxide antiopal. However, the adsorption feature and enrichment of antiopal structure with higher SSA is still considerable compared with glass-borne slide, because even the no-SERS active substrates of SiO_2 antiopal exhibit higher signal intensity than glass-borne slide when detecting 10^{-3} M MB target molecule (Figure 4.4b). The improved signal of titanium dioxide antiopal may be due to the repeated scattering of lasers. Multiple scattering illumination wavelength improves the interaction between light and matter and provides stronger Raman scattering intensity.

In order to illustrate the boosted light–matter coupling resonance in photonic microarrays, titanium dioxide was injected into the inverse opal to fill the macropore. Obviously, the size of inverse opal decreases with the increase of casting times, and all the voids will disappear after three casting times (Figure 4.4c–f). The casting process is shown in Figure 4.4g. Due to gravity, the

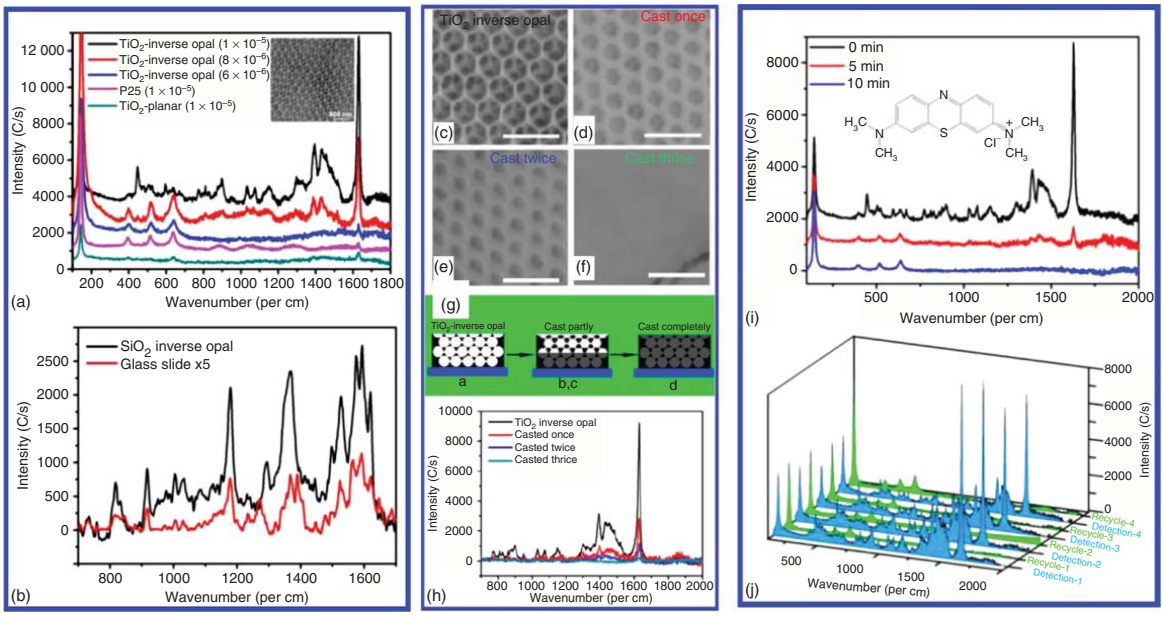

Figure 4.4 (a) Raman spectra of MB adsorbed on titanium dioxide antiopal, titanium dioxide plane, and P25 at different concentrations. The illustration shows the scanning electron microscopic image of titanium dioxide antiopal. (b) Raman spectra of 10^{-3} M MB adsorbed on SiO_2 antiopal substrates and glass slides (multiplied by 5). (c–f) Scanning electron microscopic images of 0, 1, 2, and 3 times cast titanium dioxide inverse opal (scale 500 nm); (g) casting process; (h) Raman spectra of 10^{-5} M MB adsorbed on 0, 1, 2, and 3 times cast substrates. (i) Raman spectra of 10^{-5} M MB adsorbed on the antiopal matrix of titanium dioxide under simulated sunlight for different time (0, 5, and 10 minutes). (j) Cyclic test of titanium dioxide antiopal matrix. The initial concentration of MB is 10^{-5} M, and the simulated solar irradiation time is 10 minutes. Source: Reprinted with permission from Qi et al. 2014 [24]. Copyright 2014, American Chemical Society.

solution of titanium dioxide precursor flows from the top of the substrate to the bottom, so in the first two casting processes, the lower macropore is completely immersed, while the higher macropore is only partially cast by the residual precursor (middle image in Figure 4.4h). The results show that after hydrolysis and calcination, the size of the upper macropore decreases and the bottom pore disappears completely. When an effective precursor solution is used, the macropore is completely filled (right figure in Figure 4.4g). The Raman spectra of MB on as-cast specimens show that the strength of MB decreases significantly with the increase of as-cast time (Figure 4.4h). The Raman intensity observed from the samples without multiple light scattering characteristics is as low as that from the TiO_2 plane. Therefore, the effective coupling of multiple light scattering effect to light substances plays a decisive role in sensitive SERS in situ detection application.

Due to the inherent self-cleaning ability of titanium dioxide, the antiopal matrix of titanium dioxide can decompose organic analytes under sunlight. Photodegradation of the 10^{-5} M MB target molecules on the antiopal matrix of TiO_2 detected under simulated sunlight (Figure 4.4i). After five minutes of irradiation, the peaks of MB were very few. After 10 minutes of irradiation, all the peaks of MB disappeared, indicating that MB was completely photodegraded. When MB with higher concentration is adsorbed, the matrix also shows good self-cleaning ability. This rapid and effective self-cleaning ability can also be attributed to the improvement of the daylighting ability of the antiopal of titanium dioxide. The stability of the SERS matrix is detected, and the recovery experiment was further carried out (Figure 4.4j). After three cycles, the matrix still showed good SERS activity. By this effective method, no-metal TiO_2 NPs SERS substrates were successfully prepared, and due to the boosted light–matter coupling resonance effect, the SERS EF is improved, so very high sensitive molecular detection could be achieved. The ultrahigh sensitivity is contributed by the energy gap position, and the highest sensitivity is from the photonic microarray energy gap resonance effect with the illuminated light. And, TiO_2 NPs exhibit excellent spectrum recyclability under the light irradiation, which is useful in the practical application.

4.3 TiO_2 SERS Substrate Applied in Biosensing

4.3.1 Cell Capture on TiO_2 Nanorod Arrays

Uniform TiO_2 nanorod arrays were fabricated by simple hydrothermal synthesis method, providing a "platform for multiscale interaction" used as cell capture. The overall concept is shown in Figure 4.5a. Titanium dioxide nanorods are densely stained on F-doped SnO_2 platforms with a diameter of ~160–300 nm, providing a 3D material surface for cell contact effect, and the nanorods are formed by 30–50 nanoparticles, which may further boost the terrain interaction between nanostructure N cell surface and titanium dioxide nanorod array. Albumin from bovine serum (BSA) is put into the nano-interface as a useful molecule to inhibit non-specific cell adhesion effect, which helps to decrease the

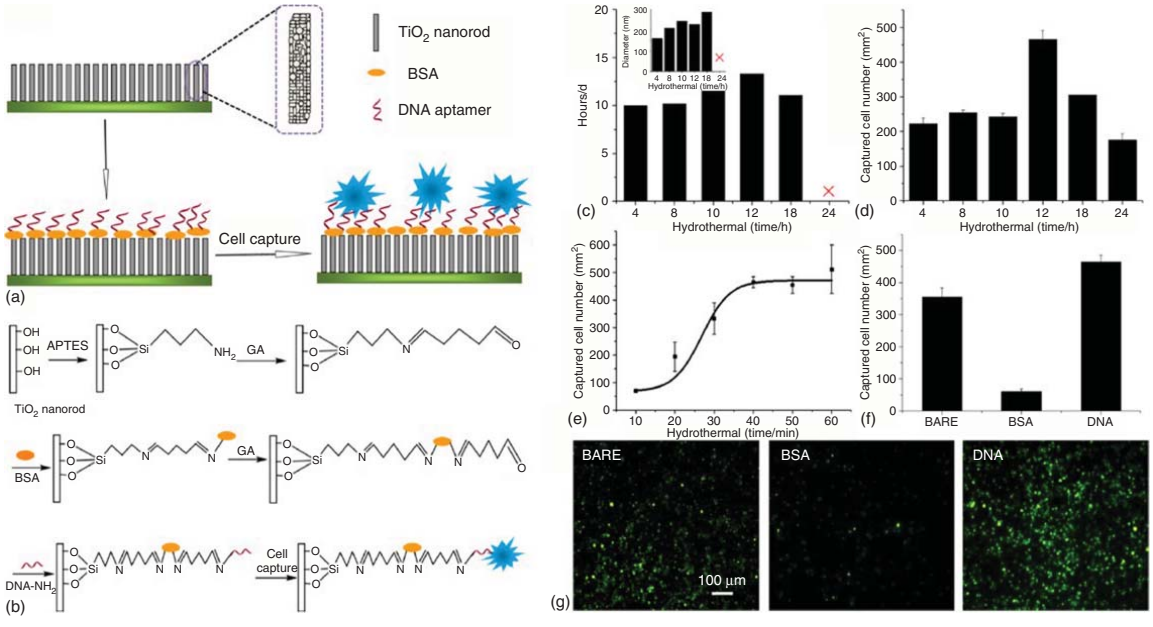

Figure 4.5 (a) Graphical description of cell capture on TiO_2 nanorod arrays. (b) Representation of biological interface fabrication on titanium dioxide nanorod arrays for specific capture of target cells. 3-aminopropyl triethoxysilane (APTES), glutaraldehyde (GA). (c) The aspect ratio of titanium dioxide nanorod arrays at different hydrothermal time. (d) The effect of ratio on cell capture rate. (e) The effect of culture time on capture performance. (f) The effects of BSA on non-specific cell adhesion and DNA aptamer-specific cell capture. (g) Compared with bare surface capture cells, BSA coated surface capture cells, and BSA aptamer modified TiO_2 nanorod surface capture cells, the scale bar in fluorescence image was 100 μm. Source: Reprinted with permission from Sun et al. 2016 [31]. Copyright 2016, American Chemical Society.

effect of capturing blood cells and improve the detection accuracy of circulating tumor cells (CTCs). The DNA adapter is then used to modify the multilevel interface to achieve specific capture of target cells, as shown in Figure 4.5b. The cell capture rate on the substrate of titanium dioxide nanorods array is as high as 93%. And, considerable sensitivity has been obtained from blood samples with a collection rate of more than 85% [31].

Cells were efficiently captured on the substrate of titanium dioxide nanorod array. The titanium dioxide nanorod array substrate was modified by BSA, and the cell capture DNA adapter was selected as the target of EpCAM cell. And 50 MCF-7 cells (breast cancer cell lines) were used as capture models of epithelial cell adhesion molecule (EpCAM) positive cancer cells. As shown in Figure 4.5c, the effects of titanium dioxide nanorod arrays on the capture rate of MCF-7 cells were studied. The results show that the capture rate of titanium dioxide nanorods increases with the increase of H/D ratio. After 12 hours of hydrothermal reaction, the maximum H/D value reached 465 MCF-7 cells/mm^2, which indicated that the height–diameter ratio of titanium dioxide nanorods was the vital factor affecting the capture efficiency of MCF-7 cells. When the nanorods stick together within 24 hours, the capture efficiency decreases sharply, which indicates that only 30–50 nanoscale nanostructures are ineffective in improving the capture efficiency. The results showed that the best capture conditions of BSA adapter modified titanium dioxide nanorod array matrix were the maximum H/D ratio and the average material diameter of 230 nm, and the hydrothermal reaction time was 12 hours.

In order to determine the optimal incubation time for cell capture, we tested the cell capture performance of the optimal titanium dioxide nanorod array matrix coated with BSA and DNA aptamers in 10–60 minutes incubation time. As shown in Figure 4.5d, with the more incubation time, the capture rate of MCF-7 cells increased significantly. From 40 minutes to after 40 minutes of cell culture, the density of captured cells could reach 465 MCF-7 cells per square millimeter, and the capture rate could reach 93%. In order to further understand the effect of modification surface effect about cell capture efficiency, we studied the capture performance of three substrates: bare substrates, immobilized BSA, and functionalized BSA adapters. As shown in panel Figure 4.5e–g the MCF-7 cells captured on bare matrix was $356 + 27$ cells/mm^2 ($71.2 + 5.4\%$), while the MCF-7 cells captured on BSA fixed matrix was significantly decreased to $60 + 9$ cells/mm^2, suggesting that BSA can effectively reduce non-specific cell adhesion. At the same time, the capture density of MCF-7 cells on BSA aptamer-fixed titanium nanorod array matrix reached $465 + 20$ cells/mm^2 ($93 + 4\%$), which was about eight times higher than that on BSA-modified matrix. This indicated that introducing DNA aptamer could effectively capture target cells. These results showed that multiscale TiO_2 nanorod arrays were prepared by the hydrothermal synthesis method. After BSA and DNA aptamer modification, target cells had good capture specificity and sensitivity. By comparing with different SERS platforms, we observed that even at low cell density, multilayer titanium dioxide nanorod substrates can effectively improve the capture performance of probe cancer cells. The capture rate of artificial blood with BSA aptamer titanium dioxide nanorods is as high as 85–95%,

which indicates the potential application of titanium dioxide nanorods in the efficient capture of the very few CTCs. This study provides a new platform for the capture of rare cancer cells. Multilayer high titanium dioxide nanorod arrays are expected to be used in clinical detection and early diagnosis.

4.3.2 Cell Capture Performance of TiO_2 Coatings

Since Fujishima Ming and his colleagues first discovered the phenomenon of photo-induced self-cleaning feature of TiO_2 NPs, which is deeply studied and widely studied in self-cleaning interface. Unlike the self-cleaning surfaces mentioned earlier, the self-cleaning properties of TiO_2 surface are derived from its inherent light response characteristics. In the process of photocatalysis, the useful superoxide radicals are introduced by effectively decomposing organic molecules on the interface of titanium dioxide materials into the carbon dioxide and water molecule by the illuminated light. Therefore, TiO_2 materials can be considered as the best candidate materials for the preparation of disposable devices such as highly sensitive nano-titanium dioxide. Besides, the water droplets are easily diffuse onto the surface of photo-induced super hydrophilic titanium dioxide to remove residual dust and impurities. Therefore, these photo response characteristics give promising self-cleaning properties to the surface of titanium dioxide. However, how to extend the self-cleaning properties of titanium dioxide materials to nano-biochips to isolate and detect cancer cells that can not only easily remove surface pollutants but also provide satisfactory cell capture performance has not been studied. In this work, the author developed a TiO_2 Nanosisal-like (TiNs) coating for the treatment of nano-biochip wastes through the self-cleaning characteristics of photo response of nano-biochips, which has been proven by nano-chips to be effective in detecting cancer cells [32]. Firstly, through the synergistic action of surface nanostructures and the specific molecules (i.e. the epithelial cell adhesion molecule antibodies, anti- EpCAM), targeted cancer cells in artificial whole blood samples can be effectively identified and captured. Then, the captured cancer cells are easily collected for downstream and effectively analyzed by the trypsin treatment, due to the unique 3D contact effect between the captured cells and nano-biochips, there is conducive to the entry of trypsin and the subsequent separation of captured cells. It is noteworthy that residual organic molecules (e.g. cell debris and EpCAM resistance) can be removed from the surface of nano-biochips by UV irradiation due to the unique light-driven self-cleaning properties of titanium dioxide coatings. Hence, this work paves a new way for eliminating the environmental pollution and health risks induced by the nano-biochip wastes.

SEM images exhibit that three nanostructured TiO_2 coatings can be fabricated accurately by changing the hydrothermal synthesis reaction time from 5 and 10 hours to 20 hours. The surface coverage (SCR) of TiN is about 24%, 45%, and 100%, representing low TiN (Figure 4.6a, TiN), medium TiN (Figure 4.6b, MTiNs), and high TiN (Figure 4.6c, HTiNs), respectively. X-ray diffraction (XRD) data exhibit that calcined TiN crystallizes better in rutile phase than before calcination (Figure 4.6d). In addition, transmission electron microscopy (TEM) analysis showed that the calcined TiN nanorods were rutile phase and grew

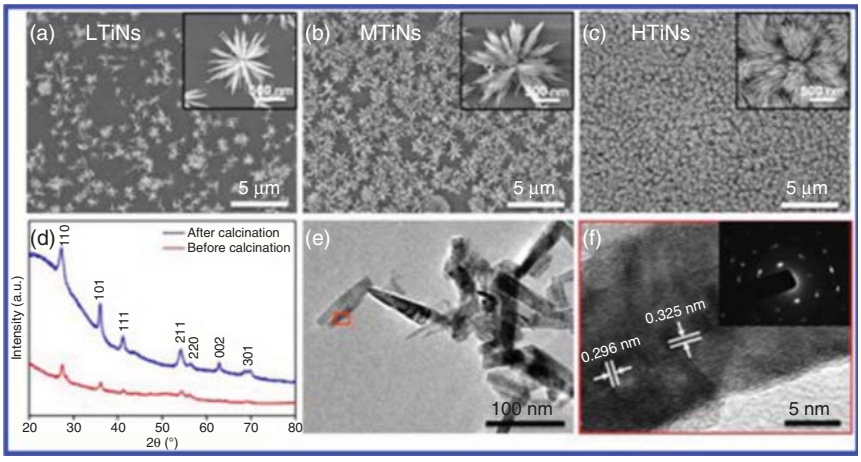

Figure 4.6 Morphology and characterization of TiN coatings. SEM and magnified SEM (illustration) images of three nanostructured coatings with TiN chips, including (a) low TiN (TiN), (b) medium TiN (MTiNs), and (c) high TiN (HTiNs). (d) XRD data of TiN coating before and after calcination. (e) Low-power TEM images of nanorods on TiN coatings and (f) corresponding high-power TEM images of single nanorods (red rectangle in figure (e)); illustrations in figure (f) show the corresponding selected area electron diffraction (SAED) patterns. XRD data and TEM images show that TiN coating crystallizes well in rutile TiO_2. Source: Reprinted with permission from Meng et al. 2015 [32]]. Copyright 2015, American Chemical Society.

along the (001) direction (Figure 4.6e, f). The distance of adjacent lattice fringes parallel to the nanorod wall is about 0.325 nm, which can be designated as the plane distance between the rutile stage (Figure 4.6f) plane (110). In addition, the distance of the edges perpendicular is about 0.296 nm, which corresponds to the plane distance of (001) planes in the rutile phase of titanium dioxide. Therefore, XRD data and TEM images show that the subsequent calcination process not only removes the organic pollutants adhering to the hydrothermal reaction but also gives TiN coating (bare TiN) better crystallization of rutile phase of TiO_2, which is conducive to the photocatalytic degradation of organic components. Therefore, nano-biochips with controllable TiN chips have been made, which provides a unique self-cleaning performance for the effective treatment of nano-biochip wastes.

The good specificity of TiN coating is determined by comparing the capture performance of naked cells, streptavidin coated, flat coated anti-EpCAM, and HTiNs-coated EpCAM-positive breast cancer cells (MCF7 cells). To illustrate the cell incubation time, EpCAM-positive MCF7 cells and two typical EpCAM-negative cancer cells are carefully compared, the cell capture effect (i.e. adherent HeLa cervical cancer cells and suspended Jurkat T lymphocytes) on anti- EpCAM-modified HTiNs coatings in static incubation for 5–90 minutes. In Figure 4.7a, the capture efficiency of targeted MCF7 cells initially increased with the prolongation of culture time, reaching its maximum at 60 minutes. In contrast, non-targeted Hela and Jurkat T cells always show negligible non-specific cell adhesion, regardless of the incubation time. To further reveal effect of SCR

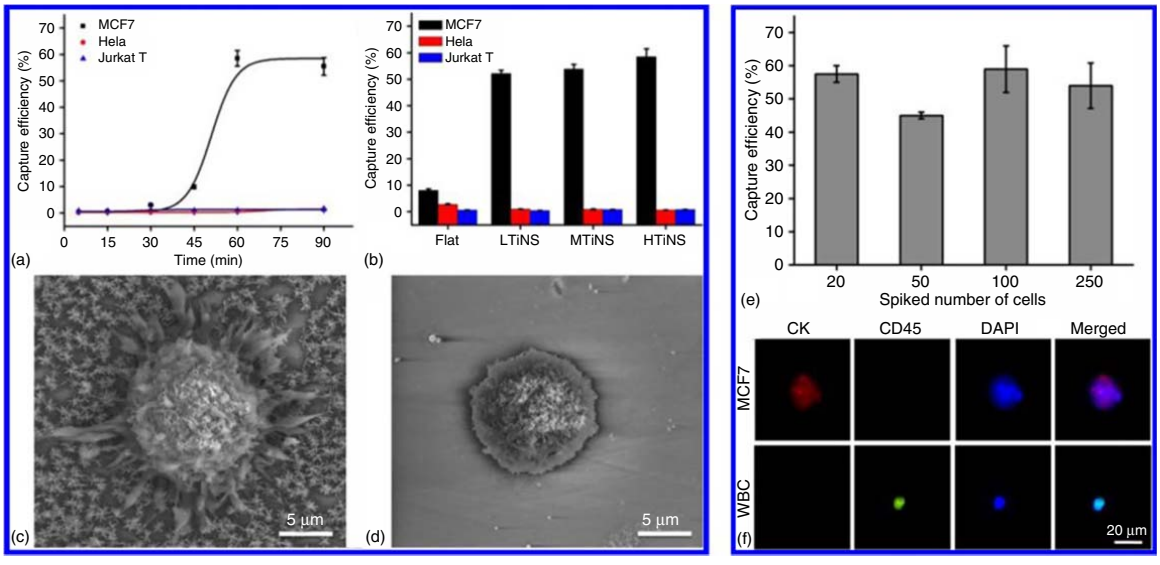

Figure 4.7 Cell capture performance of EpCAM-positive MCF7 cells and EpCAM-negative HeLa and Jurkat T cells on anti-EpCAM-modified TiO_2 coatings (a) in different culture periods of 5–90 minutes; (b) four anti-EpCAM-modified titanium dioxide coatings were used, including plate, TiN, MTiNs, and HTiNs. Typical environmental SEM (ESEM) images of MCF7 cells were taken on (c) HTiNs and (d) planes, respectively. The cells captured by HTiNs coating showed more filamentous pseudopodia than those on the plane, indicating that the terrain interaction between target MCF7 cells and HTiNs coating was enhanced. Error line: Standard error of average value ($n = 3$). Capture performance of anti-EpCAM-coated TiN coatings (i.e. HTiNs) for artificial whole blood samples spiked with rare cancer cells (i.e. MCF7). (e) The capture efficiency of prestained MCF7 cells is achieved on anti-EpCAM-coated HTiNs coatings for artificial whole blood samples with concentration of 20, 50, 100, and 250 cells/ml. (f) Three-color immunocytochemistry method for identifying spiked MCF7 cells from white blood cells (WBCs) including PE-labeled anti-CK (CK, a protein marker for epithelial cells), fluorescein isothiocyanate (FITC)-labeled anti-CD45 (CD45, a marker for WBCs) and diamidine phenyl indole (DAPI) for nuclear staining. Error bars: the standard error of mean ($n = 3$). Source: Reprinted with permission from Meng et al. 2015 [32]. Copyright 2015, American Chemical Society.

on EpCAM-resistant TiN, the cell capture properties of four EpCAM-resistant titanium dioxide coatings, including plate, TiN, MTiNs, and HTiNs (Figure 4.7b), were compared. Under the optimal incubation time (60 minutes), captured efficiency of the targeted MCF7 cells was 58.5%, which was significantly higher than that of other anti-EpCAM-modified titanium dioxide coatings (MTiNs 53.8%). At the same time, the captured MCF7 cells still had a high survival rate of about 97%, which was confirmed by live/dead staining. Unlike probed MCF7 cells, the non-specific adhesion of non-targeted Hela and Jurkat T cells to these EpCAM-resistant coatings can be completely ignored (Figure 4.7b). Compared with the anti-EpCAM modified plate, the cell capture rate of anti-EpCAM-modified TiN (such as HTiNs) coating is significantly higher, which can be explained by the obvious difference in morphology of captured cells. The environmental SEM pictures that exhibit the anti-EpCAM-modified HTiNs coating based on the cells captured (Figure 4.7c) not only have larger spreading area (Figure 4.7d) but also extend more silk feet than that of the anti-EpCAM-modified plane (Figure 4.7d), revealing the enhanced terrain interaction between the target cells and its HTiNs coating. Among them, the good specificity and ultrahigh sensitivity of Re and CTCs detection can be reached by optimum nano-chip and HTiNs coating at 60 minutes of incubation time due to enhanced terrain interaction between target cells and TiN coating and specific molecular recognition.

The potential clinical application based on the SERS is discussed in detail. The best cell capture methods for the spiked CTCs capturing capability was performed, and the result is provided (incubation time: 60 minutes). Artificial whole blood samples in the experiment was prepared by the method of spiking the mouse blood with DiD-prestained MCF7 cells at concentrations of approximately 20, 50, 100, and 250 cells/ml. Anti-EpCAM-modified HTiNs tips exhibit about 45–60% capture efficiency for the MCF7 cells shown in Figure 4.7e. The three-color immunocytochemistry study relied on the phycoerythrin (PE)-labeled anti-CK method have been introduced to observe the spiked MCF7 cells in the white blood cells (WBCs) as exhibited in Figure 4.7f. So, these works exhibit large applied potential of the TiNs material coatings in precision medicine for the cancer patients. This work has successfully developed a photosensitive TiN coating for the treatment of nano-biochip wastes. Using the effect of topological interaction and molecular recognition method, TiNs coating can effectively detect CTC in artificial whole blood samples with high activity. After the captured cells were separated and treated by trypsin, the residual organic components at nano-biochips could be completely treated by UV light based on the self-cleaning feature of titanium dioxide materials. This work will pave a new way for the development of the new generation disposable nano-biochips, so as to eliminate the old road of "pollution first, cleaning up later."

4.4 Conclusions and Future Perspectives

In summary, various types of metal and semiconductor NPs have been successfully developed and widely utilized in SERS field. Semiconductor NPs

with excellent biocompatibility are mainly developed based on the concept of "strategies for expanding SERS applications" to overcome the shortcoming of precious metal SERS materials. Therefore, the PICT mechanism was studied by semiconductor SERS method. In addition, semiconductor SERS substrates with super-strong EFs, such as defective TiO_2 nanoparticles and TiO_2 arrays with strong light coupling effect, have been developed. These methods can enhance the PICT effect and enhance SERS signal. The long-term limitation of precious metal materials in biological detection was overcome by increasing the EF of titanium dioxide. This is a good method to detect, characterize, and identify biological molecules on various no-metal materials and platforms, cancer cells, and so on. In addition, because of its ultrahigh sensitivity, good stability, and better simplicity, semiconductor SERS can be widely used in practical applications, such as biological analysis, pathological analysis, post-operative evaluation, early screening of cancer cells, and so on. Therefore, in various basic and practical research, there is great way to get new TiO_2 SERS energetic shell–core nanoparticles for further application on biosensor.

Acknowledgments

The authors would like to thank the continuous support by National Key R&D Program of China (2018YFC0910601, 2019YFA0405603), Natural Science Foundation of China (31971292, U1432114), Zhejiang Province Financial Supporting (2017C03042, LY18H180011), the Natural Science Foundation of Ningbo (2019A610024), China Postdoctoral Science Foundation (2019T120534 and 2018M640576) Zhejiang Province Key Research Project (2019C03058), STS project from the Chinese Academy of Sciences (KFJ-STS-ZDTP-061), Zhejiang Province Financial Supporting (Q20E020012) and the Science & Technology Bureau of Ningbo City (2015B11002, 2017C110022). Furthermore, the authors also acknowledge Shanghai Synchrotron Radiation Facility at Line BL15U (No. h15sr0021) for X-ray fluorescence imaging and National Synchrotron Radiation Laboratory in Hefei for soft X-ray imaging (No. 2016-HLS-PT-002193).

References

1 Jeanmaire, D.L. and Van Duyne, R.P. (1977). *Journal of Electroanalytical Chemistry and Interfacial Electrochemistry* 84 (1): 1–20.
2 Fleischmann, M., Hendra, P.J., and Mcquillan, A.J. (1974). *Chemical Physics Letters* 26 (2): 163–166.
3 Albrecht, M.G. and Creighton, J.A. (1977). *Journal of the American Chemical Society* 99 (15): 5215–5217.
4 Chen, W.J., Gui, X.C., Zheng, Y.J. et al. (2017). *Optical Materials* 5 (6): 1600715.
5 Huang, Z.L., Meng, G.W., Huang, Q. et al. (2010). *Advanced Materials* 22 (37): 4136–4139.

6 Li, J.F., Huang, Y.F., Ding, Y. et al. (2010). *Nature* 464 (7287): 27–27.
7 Li, J.F., Zhang, Y.J., Ding, S.Y. et al. (2017). *Chemical Reviews* 117: 5002–5069.
8 Creighton, J.A., Blatchford, C.G., and Albrecht, M.G. (1979). *Journal of the Chemical Society Faraday Transactions Molecular & Chemical Physics* 75 (75): 790–798.
9 Moskovits, M. (1985). *Reviews of Modern Physics* 57 (3): 783–826.
10 Mulvaney, S.P., Musick, M.D., Keating, C.D., and Natan, M.J. (2003). *Langmuir* 19 (11)): 4784–4790.
11 Kneipp, K., Wang, Y., Kneipp, H. et al. (1997). *Physical Review Letters* 78 (9): 1667.
12 Nie, S. and Emory, S.R. (1997). *Science* 275 (5303): 1102–1106.
13 Xu, H., Bjerneld, E.J., Käll, M., and Börjesson, L. (1999). *Physical Review Letters* 83 (21): 4357–4360.
14 Huh, S., Park, J., Kim, Y.S. et al. (2011). *ACS Nano* 5 (12): 9799–9806.
15 Lin, J., Shang, Y., Li, X.X. et al. (2017). *Advanced Materials* 29: 1604797.
16 Lin, J., Hao, W., Shang, Y. et al. (2018). *Small* 14: 1703274.
17 Shim, J., Oh, A., Kang, D.H. et al. (2016). *Advanced Materials* 28 (32): 6985–6992.
18 Heinemann, M., Eifert, B., and Heiliger, C. (2013). *Physical Review B* 87 (11): 46–50.
19 Jiang, L., You, T.T., Yin, P.G. et al. (2013). *Nanoscale* 5 (7): 2784–2789.
20 Ling, X., Fang, W.J., Lee, Y.H. et al. (2014). *Nano Letters* 14 (6): 3033–3040.
21 Quagliano, L.G. (2004). *Journal of the American Chemical Society* 126 (23): 7393–7398.
22 Zhao, K.Y., Lin, J., and Guo, L. (2015). *RSC Advances* 5 (66): 53524–53528.
23 Alessandri, I. (2013). *Journal of the American Chemical Society* 135 (15): 5541–5544.
24 Qi, D.Y., Lu, L., Wang, L.Z., and Zhang, J.L. (2014). *Journal of the American Chemical Society* 136 (28): 9886–9889.
25 Wang, X.T., Shi, W.S., She, G.W., and Mu, L.X.J. (2011). *American Chemical Society* 133 (41): 16518–16523.
26 Alessandri, I. and Lombardi, J.R. (2016). *Chemical Reviews* 116 (24): 14921–14981.
27 Ahmad, M., Agarwal, K., Kumari, N., and Mehta, B.R. (2017). *Applied Physics Letters* 111 (2): 1–11.
28 Hilty, F.W., Kuhlman, A.K., Pauly, F., and Zayak, A.T. (2015). *Journal of Physical Chemistry C* 119 (40): 23113–23118.
29 Yang, L.B., Jiang, X., Ruan, W.D. et al. (2008). *Journal of Physical Chemistry C* 112 (50): 20095–20098.
30 Tan, X.J., Melkersson, J., Wu, S.Q. et al. (2630). *Chemphyschem A European Journal of Chemical Physics & Physical Chemistry* 17 (17): 2016.
31 Sun, N., Li, X., Wang, Z. et al. (2016). *ACS Applied Materials & Interfaces* 8 (20): 12638.
32 Meng, J., Zhang, P., Zhang, F. et al. (2015). *ACS Nano* 9 (9): 9284–9291.

5

Cancer Theranostics of White TiO_2 Nanomaterials

*Yang Gao[1], Sijia Sun[1], Zhibin Yin[1], Yanhong Liu[1], Aiguo Wu[2], and Leyong Zeng[1]**

[1] Hebei University, College of Chemistry & Environmental Science, Key Laboratory of Medicinal Chemistry and Molecular Diagnosis of the Ministry of Education, Chemical Biology Key Laboratory of Hebei Province, Baoding 071002, P.R. China
[2] Cixi Institute of Biomedical Engineering, CAS Key Laboratory of Magnetic Materials and Devices, & Key Laboratory of Additive Manufacturing Materials of Zhejiang Province, Ningbo Institute of Materials Technology and Engineering, Chinese Academy of Sciences, No. 1219 Zhongguan West Road, Ningbo 315201, P.R. China

CHAPTER MENU

Introduction, 153
TiO_2 as Inorganic Photosensitizer for Photodynamic Therapy, 154
TiO_2 as Sonosensitizer for Sonodynamic Therapy, 162
TiO_2 as Multifunctional Nanoprobes for Visualized Theranostics, 167
Conclusions and Future Perspectives, 172

5.1 Introduction

White titanium dioxides (W-TiO_2), a kind of typical semiconductor materials with a band gap of 3.12 eV (for anatase structure), were well known as photocatalyst for degradation application [1, 2]. In the past decades, many efforts have been devoted to improving the photocatalytic performance of W-TiO_2 nanomaterials via functional tailoring and elemental doping [3–6]. Moreover, the excitation source can be red-shifted from ultraviolet (UV) to visible light, which improved the utilization efficiency of sunlight, and was closer to the practical application [7–10]. With the development of science and technology, W-TiO_2 nanomaterials have been applied in several applications, such as photocatalysts [11, 12], dye-sensitized solar cells [13–16], lithium batteries [17], photochromic devices [18], and so on. Especially, W-TiO_2 is widely used for photocatalytic degradation of organic compounds because of its high catalytic efficiency, stability, and relatively low cost. Under the irradiation of UV light, electron/hole pairs are generated by light and migrate to the surface of the crystal, eventually destroying contaminants [19–21].

*Corresponding author: zengly@hbu.cn, zengly@nimte.ac.cn

TiO_2 Nanoparticles: Applications in Nanobiotechnology and Nanomedicine,
First Edition. Edited by Aiguo Wu and Wenzhi Ren.
© 2020 Wiley-VCH Verlag GmbH & Co. KGaA. Published 2020 by Wiley-VCH Verlag GmbH & Co. KGaA.

In the past two decades, W-TiO_2 nanomaterials showed important potential in biomedical fields, especially in cancer theranostics, owing to good biocompatibility, high stability, and excellent light-/ultrasound-responsive properties. They were widely investigated as inorganic photosensitizers for photodynamic therapy (PDT), as inorganic sonosensitizers for sonodynamic therapy (SDT), as nanocarrier for drug delivery, and as multifunctional nanoprobes for visualized theranostics of cancers. In this chapter, the research progress of W-TiO_2 and their nanocomposites in cancer theranostics were systematically summarized and discussed, including UV-responsive PDT, near-infrared (NIR)-responsive PDT, dual-mode PDT, SDT, high intensity-focused ultrasound (HIFU) SDT, and visualized theranostics. Finally, the future perspectives of W-TiO_2 nanomaterials and their nanocomposites are also presented.

5.2 TiO_2 as Inorganic Photosensitizer for Photodynamic Therapy

5.2.1 Photodynamic Therapy Principle

PDT, which fights cancer, is non-invasive and tumor-specific, which typically uses an external physical light source to activate the photosensitizer and thus kill cancer cells [22, 23]. In PDT, photosensitizer is activated and then reactive oxygen species (ROS) are produced from molecular oxygen under the excitation of light with unique wavelength. These ROS destroy the biological structure directly or through a series of peroxidative chain reactions, and finally cancer cells are killed via apoptosis or necrosis [12, 24]. With the development of PDT, three main mechanisms were summarized on tumor killing [25]: (i) directly killing tumor cells by the ROS component, especially singlet oxygen, (ii) activating the body's anti-tumor immune response, and (iii) damaging the tumor-associated vasculature, resulting in ischemic death of the tumor. In PDT mode, three key factors are included: photosensitizer, light, and molecular oxygen, in which the light source is the foundation, the molecular oxygen is the guarantee, and the photosensitizer is the core.

Recently, two kinds of photosensitizers were widely investigated: organic and inorganic photosensitizers, in which organic photosensitizers were consisted of photosensitive molecules (chlorin e6 (Ce6), phthalocyanine (Pc), etc.) and inorganic photosensitizers included carbon-based and semiconductor nanomaterials (fullerenes, TiO_2, ZnO, etc.) [26–29]. Compared with traditional organic photosensitizers, TiO_2-based inorganic photosensitizers have high stability and low cytotoxicity, showing broad application in PDT of cancers [30, 31].

The PDT principle of W-TiO_2 is similar to other organic photosensitizers, in which W-TiO_2 is activated by UV light, and then the photogenerated electron/hole pairs can react with water and dissolved oxygen to form ROS (hydroxyl ($OH^{\bullet}$), hydrogen peroxide (H_2O_2), perhydroxyl ($HO_2^{\bullet}$), singlet oxygen ($^1O_2$), etc.) [32, 33]. A good photosensitizer must satisfy two factors: high separation efficiency of electron/hole pairs and strong optical absorption in special excitation zone. However, W-TiO_2 nanoparticles have weak absorption in visible and NIR zone, which limits their PDT application. To effectively

eliminate the recombination of electron/hole pairs, W-TiO_2 can be doped with impurities, including some metals, metal ions, and semiconductor oxides [34]. To effectively broaden the excitation wavelength, W-TiO_2 can be doped with inorganic non-metallic elements (N, C, etc.), or metallic elements (Fe, Pt, etc.) [34–37], or can be coupled with NIR-responsive upconversion luminescence (UCL) nanoparticles (UCNPs) [38], by which the excitation wavelength of W-TiO_2 can be changed from UV to visible, even to NIR zone.

5.2.2 Ultraviolet Light Responsive Photodynamic Therapy

Many researchers have investigated the application of W-TiO_2 nanoparticles in anti-bacteria [39] and anti-tumor [40–42], expanding the research content of W-TiO_2 nanoparticles in the treatment of cancers. The photo-induced biological activity of W-TiO_2 was investigated in terms of determining the conditions of photocatalytic treatment of cancer cells and exploring the molecular mechanisms involved in the process. Falaras and coworkers synthesized aqueous-dispersed W-TiO_2 using sol–gel method and investigated their photo-induced inhibition on MCF-7 and MDA-MB-468 breast cancer epithelial cells under the irradiation of UV light (wavelength of 350 nm), indicating the potential application of W-TiO_2 in PDT of cancers [43].

In 1991, Fujishima and coworkers reported the effect of W-TiO_2 particles on the viability of malignant HeLa cells under the irradiation of UV light. During 10 minutes UV irradiation, HeLa cells incubated with W-TiO_2 (100 μg/ml) were ultimately killed, but these particles (up to 360 μg/ml) showed little cytotoxicity without UV irradiation. Therefore, it was concluded that the irradiated W-TiO_2 particles killed the cells by $OH^{\bullet}$ and $HO_2^{\bullet}$ radicals produced by water, and the cells were oxidized by photogenerated holes of W-TiO_2, in which the cells were destroyed both in their cell membrane and cytoplasm [44]. Subsequently, Huang et al. studied the PDT performance of ultrafine W-TiO_2 on U937 cells, in which they concluded that the killing mechanism of W-TiO_2 was attributed to the DNA damage caused by the generated ROS [45].

Degussa P25 was considered to have excellent photocatalytic performance, which is also carried out originally for killing cells. In order to improve PDT performance, Cheon and coworkers synthesized rod-shaped single-crystalline W-TiO_2 nanoparticles with a diameter of 3.5 nm and a length of 10.4 nm for PDT of skin cancer cells under the irradiation of UV light. Compared with commercially available Degussa P25 nanoparticles, the PDT performance of single-crystalline W-TiO_2 was greatly improved, which can be attributed to the large surface-to-volume ratio and the single crystallinity [46].

In order to improve the dispersibility and the biocompatibility, the surface-modified W-TiO_2 was carried out [30, 47–51]. Ogino and coworkers reported polyacrylic acids (PAA) and antibody-modified W-TiO_2 for cell-specific PDT, in which the aggregation of W-TiO_2 was prevented, and the used nanoparticle concentration and the UV light dose were decreased due to the active targeting capability [52]. Wang and coworkers synthesized daunorubicin-loaded W-TiO_2 for chemotherapy and PDT against drug-resistant leukemia cells, in which UV irradiation had a significant effect on cancer cells with targeted resistance, indicating the excellent inhibition of drug

resistance under the combination of UV-responsive PDT and anti-cancer drugs [53]. In 2009, A. Rozhkova et al. reported 3,4-dihydroxyphenilacetic acid (DOPAC)-coated W-TiO_2 nanoparticles with a diameter of 5 nm for PDT in glioblastoma multiforme (GBM), by which the band gap can reduce from 3.2 to 1.6 eV, and the excitation light can correspondingly red-shift from 380 to 450 nm. As shown in Figure 5.1, antibody-linked DOPAC–TiO_2 nanoparticles showed excellent photocytotoxicity by damaging cell membrane, changing cell permeability, and finally killing cells due to the formation of ROS. Moreover, the biodistribution of nanoparticles was also directly observed by using synchrotron X-ray fluorescence microscopy [54].

To improve the separation efficiency of electron/hole pairs and broaden the zone of optical absorption, researchers developed different strategies by doping some metallic and non-metallic elements with W-TiO_2 [34–37, 55–57]. Liu et al. prepared Pt/W-TiO_2 nanocomposites to enhance the PDT performance of W-TiO_2 nanoparticles, in which precious metal nanoparticles are believed to play important role [37]. By doping Fe into W-TiO_2, the PDT performance can also be improved [35, 56, 57]. Huang et al. reported Fe-doped W-TiO_2 for PDT in leukemia HL60 cells based on the PDT reaction chamber of the LED light source, which showed that Fe doping can effectively improve the inactivation efficiency [57]. Mi and coworkers synthesized N-doped W-TiO_2 for PDT, in which the excitation light can red-shift to red light zone. Moreover, by conjugating organic photosensitizer of $AlPcS_4$, the ROS rate was greatly improved [36]. J. Balkus Jr. and coworkers synthesized S-nitrosocysteine-decorated PbS/TiO_2 nanotubes for enhanced PDT under the irradiation of visible light, in which cysteine-NO as photodonor, PbS as photosensitizer, and W-TiO_2 as photocatalyst [55].

5.2.3 980 nm Near-Infrared Light Responsive Photodynamic Therapy

It is known that W-TiO_2 can only be activated by UV light or rays with shorter wavelength due to the wide band gap. However, UV light has poor penetration depth and can damage to normal tissues, which limited the *in vivo* PDT application of W-TiO_2. Although several strategies have been developed to design visible light activated W-TiO_2 for PDT [36, 55], it is still not satisfying for *in vivo* PDT. NIR light with wavelength 700–1100 nm is the first optical window of body, which is safe and can penetrate tissues with large depth [58–61]. Therefore, many efforts have been devoted to developing NIR-responsive PDT of W-TiO_2 [62–64].

Rare-earth-doped UCL nanomaterials are good candidate as nanoprobes for fluorescent imaging and PDT, which can convert NIR to visible or UV via regulating rare-earth elements [65, 66]. Especially, Yb^{3+}/Tm^{3+} co-doped UCL nanoparticles can emit UV light under the excitation of a 980 nm laser [67–69]. Qin et al. reported Yb^{3+}/Tm^{3+} co-doped UCNPs–TiO_2 nanocomposites for NIR-responsive photocatalytic activity of organic contaminants under the irradiation of a 980 nm laser [70, 71]. Tang and coworkers synthesized $NaYF_4$: Yb,Tm@TiO_2 with core–shell structure, and then constructed photoelectrochemical aptasensing nanoplatform for sensitive detection of carcinoembryonic antigen, in which the UCL of NIR to UV can activate TiO_2 to generate photocurrent [72]. Therefore, by constructing W-TiO_2 and UCL nanocomposites, NIR-responsive PDT can be realized.

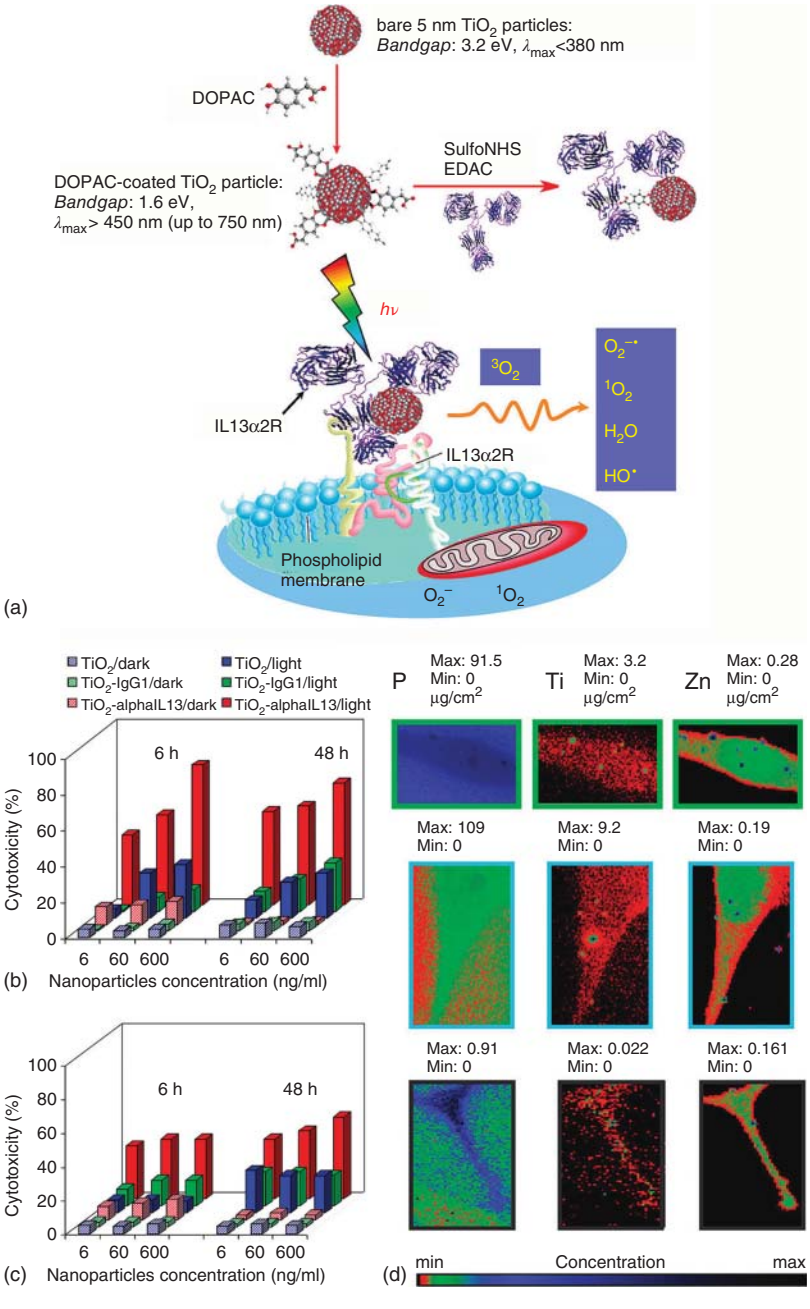

Figure 5.1 Antibody-linked DOPAC–TiO_2 nanoparticles for PDT in glioblastoma multiforme. (a) Diagrammatic sketch for the synthesis of antibody-linked DOPAC–TiO_2 nanoparticles and the proposal PDT mechanism; (b) photocytotoxicity of A172 GBM cells cultured with antibody-linked DOPAC–TiO_2 nanoparticles; (c) photocytotoxicity of U87 GBM cells cultured with antibody-linked DOPAC–TiO_2 nanoparticles; (d) X-ray fluorescence microscopy (XFM) images of antibody-linked DOPAC–TiO_2 nanoparticles in single A172 GBM cells.
Source: Reproduced with permission of Rozhkova et al. 2009 [54]. Copyright © 2009, American Chemical Society.

Idris et al. synthesized W-TiO_2 coated UCNPs for NIR-responsive PDT under the irradiation of a 980 nm laser, by upconverting high-permeability NIR light to UV light. Under the excitation of a NIR laser, a large amount of ROS can be produced, and the growth of cancer cells was effectively inhibited [38]. Xu et al. first reported N-doped TiO_2/$NaYF_4$: Yb/Tm nanocomposites for NIR-responsive PDT and also studied the drug release. Under the irradiation of a safe 980 nm laser, N-doped W-TiO_2 can be activated by visible light ($\lambda = 470$ nm) emitted by UCL nanoparticles ($NaYF_4$: Yb,Tm) to generate electron/hole pairs to destroy cancer cells [73]. By the combination of NIR-responsive drug delivery and PDT, the nanocomposites of UCL and W-TiO_2 further demonstrated the excellent treatment performance in cancers [63, 74, 75].

Zhang and coworkers synthesized UCNPs@SiO_2@TiO_2 nanocomposites with core–shell–shell structure for 980 nm NIR-responsive PDT, in which the uniform core–shell–shell structure achieved a repeatable loading and prevented any leakage of TiO_2 inorganic photosensitizer. As shown in Figure 5.2, the strong UCL peaks located at about 350 and 460 nm can be observed obviously under the excitation of a 980 nm laser [76]. Lin and coworkers synthesized Gd-based UCNPs, and then small W-TiO_2 nanoparticles were grown on the surface of UCNPs to construct 980 nm NIR-responsive nanoplatform, and they concluded the PDT efficiency can be attributed to the mitochondria-involved apoptosis [77]. Furthermore, Lin and coworkers also constructed a multifunctional core–shell structure (TiO_2@$Y_2Ti_2O_7$@YOF:Yb, Tm) for simultaneous 980 nm responsive PDT, photothermal therapy (PTT), UCL imaging, and CT imaging [62].

In our previous work, UCNPs–TiO_2 nanocomposites with core–shell and Janus structure were, respectively, synthesized for 980 nm NIR-responsive PDT [78, 79]. As shown in Figure 5.3, Yb/Tm co-doped Gd-based UCNPs were firstly synthesized, which can upconvert UV to activate W-$TiO_2$for PDT. Under the irradiation of a 980 nm laser, the MCF-7 tumors were nearly disappeared after 14-day treatment. Moreover, the PDT mechanism can be attributed to the UV light and ROS, which was demonstrated by irradiating NIR laser on cells incubated with UCNPs [79].

5.2.4 808 nm Near-Infrared Light Responsive Photodynamic Therapy

980 nm NIR-responsive PDT overcomes the weak penetration disadvantage and tissue damage of W-TiO_2. However, it is still a threat to safe PDT due to the overheating effect of 980 nm laser, in which the water absorption is very strong [80, 81]. It is well known that 808 nm is located at the center of the first optical window, which is deeper penetrable than 980 nm laser. Importantly, the water absorption is very weak under the irradiation of 808 nm laser, which can powerfully avoid the heating effect [82, 83].

It was previously reported that Nd^{3+}-doped UCNPs possess excellent UCL performance under the excitation of 808 nm laser [84, 85]. Researchers have made many efforts to improve their UCL performance of Nd^{3+}-doped UCNPs [86, 87]. In our previous work, Nd^{3+}-doped UCNPs with core–shell–shell structure were also synthesized for 808 nm responsive fluorescent imaging and PDT [88]. Therefore, it is urgent of developing 808 nm NIR-responsive PDT of W-TiO_2.

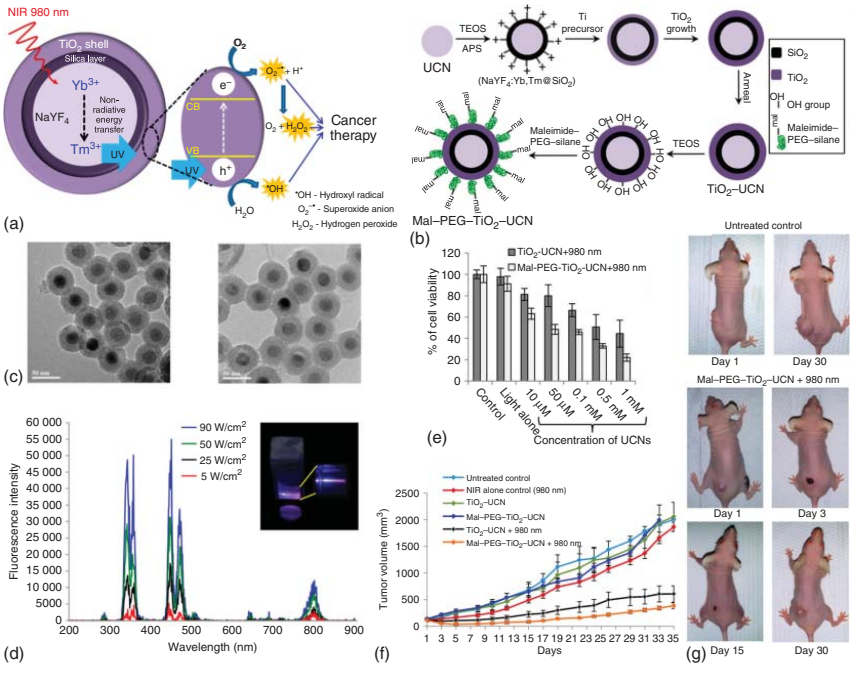

Figure 5.2 980 nm NIR-responsive nanoplatform for deep-penetration PDT based on UCNPs@SiO_2@TiO_2 nanocomposites. (a) Diagrammatic sketch for the proposal PDT mechanism by energy transfer from Tm^{3+} to TiO_2; (b) diagrammatic sketch for the synthesis of UCNPs@SiO_2@TiO_2 nanocomposites; (c) Transmission electron microscopy (TEM) images of UCNPs@SiO_2@TiO_2 nanocomposites before (left) and after (right) surface modification of maleimide-PEG-silane; (d) UCL spectra of UCNPs@SiO_2@TiO_2 nanocomposites with different power density under the excitation of a 980 nm laser; (e) *in vitro* PDT performance; (f) *in vivo* PDT performance; (g) photographs of mice with tumors in control group and in PDT group. Source: Reproduced with permission from Lucky et al. 2015 [76]. Copyright © 2015 American Chemical Society.

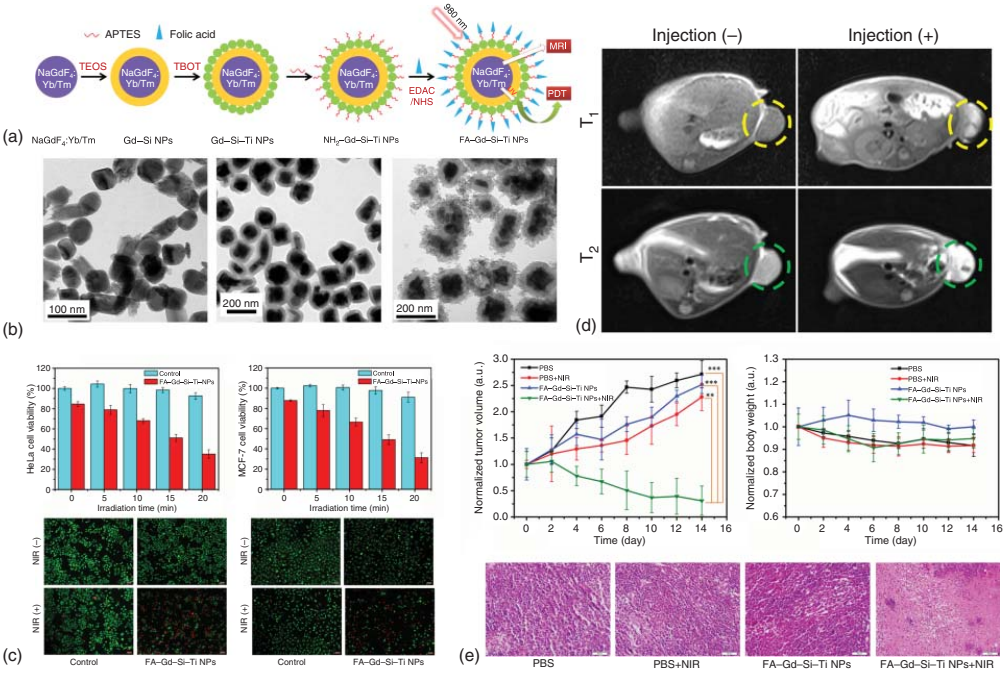

Figure 5.3 980 nm NIR-responsive nanoplatform for deep-penetration PDT based on Gd-based UCL-TiO_2 nanocomposites. (a) Diagrammatic sketch for the synthesis of Gd-based UCL-TiO_2 nanocomposites; (b) TEM images of Gd-based UCNPs (left), Gd-Si nanocomposites (middle), and Gd-Si-Ti nanocomposites (right); (c) *in vitro* PDT performance under the irradiation of a 980 nm laser; (d) T_1-weighted *in vivo* MRI performance; (e) *in vivo* PDT performance under the irradiation of a 980 nm laser. Source: Reproduced with permission from Zhang et al. 2015 [79]. Copyright © 2015, Elsevier.

Lin and coworkers innovatively designed the nanocomposites of Nd^{3+}-doped UCNPs and W-TiO_2 for 808 nm NIR-responsive PDT, in which anatase W-TiO_2 nanoparticles were successfully grown on the surface of Nd^{3+}-doped UCNPs due to the low surface area of UCNPs. Due to the difficulty of growing more W-TiO_2 nanoparticles on the surface of UCNPs, they constructed UCNPs–TiO_2 nanocomposites with a distinct core–shell structure (UCNPs@mSiO_2@TiO_2), in which the nucleus three-layer structure of UCNPs eliminated the detrimental cross-relaxation between Tm^{3+} and Nd^{3+} and maintained the UCL emission intensity of the core due to the presence of an internal quenching layer, also by which the loading rate of W-TiO_2 was obviously increased and the PDT performance was also effectively improved under the excitation of an 808 nm laser [89].

5.2.5 Organic/Inorganic Dual-Mode Photodynamic Therapy

By coupling organic photosensitizer and W-TiO_2 inorganic photosensitizer, the better PDT can be achieved under the combination of organic and inorganic dual-mode PDT, in which the production rate of ROS is greatly improved. W-TiO_2 nanoparticles modified with organic photosensitizers have been synthesized and have been demonstrated to be potential photosensitizers in dual-mode PDT applications [90]. Generally, in dual-mode PDT, organic photosensitizer was activated by visible light, but W-TiO_2 was activated by UV or NIR light. Therefore, in the dual-mode PDT, both single excitation source and dual-excitation sources were used based on the properties of photosensitizers.

In early reports, UV-responsive W-TiO_2 was commonly conjugated with organic photosensitizers for dual-mode PDT. Mi and coworkers synthesized N-doped W-TiO_2 conjugated with Pc (N-TiO_2-Pc) and investigated the ROS production irradiated by a tungsten halogen lamp, which exhibited a much higher photokilling performance than single Pc and W-TiO_2. Moreover, N-doping can significantly enhance the formation of $^1O_2$ and $^{\bullet}O_2^-$ [10]. Frochot and coworkers reported Ce6-conjugated W-TiO_2 for dual-mode PDT under the irradiation of a 652 nm laser, in which Ce6 was covalently attached to the modified W-TiO_2, demonstrating the prepared Ce6–TiO_2 nanosystem had good PDT efficiency, and multiple ROS ($^1O_2$ and $HO^{\bullet}$) were responsible for the dual-mode PDT [91].

In order to realize NIR-responsive dual-mode PDT, UCNP–TiO_2 nanocomposites were used as carrier to modify organic photosensitizers. Hou et al. synthesized Nd^{3+}-doped multi-shell UCNPs, and then W-TiO_2 nanoparticles were grown on the surface of UCNPs; further hypocrellin A (HA) were modified to build NIR-responsive dual-mode PDT nanoplatforms (UCNP@TiO_2@HA), which converted 808 nm NIR light into UV and blue light to excite W-TiO_2 and HA, resulting in ROS causing destruction of the mitochondrial membrane [92].

As a carrier of organic photosensitizers, the nanocomposites of inorganic W-TiO_2 and organic photosensitizers had more outstanding effects than the single organic photosensitizers, and the inorganic/organic dual-mode PDT should show better tumor-killing effect and provide a basis for the synergistic therapy in cancers.

5.3 TiO_2 as Sonosensitizer for Sonodynamic Therapy

Ultrasound (US) is a mechanical sound wave whose frequency is higher than the periodic vibration of human hearing (20 kHz). US was widely used for diagnostic imaging due to its non-radiative and low tissue attenuation coefficient. Moreover, US can also be used for treatment, which can achieve deeper penetration in biological tissues, compared with light excitation. Based on previous reports, W-TiO_2 can produce ROS under the action of US. Therefore, instead of light, W-TiO_2 can be applied for SDT under the excitation of US.

5.3.1 Sonodynamic Therapy Principle

Generally, US can cause two main effects: thermal effect and non-thermal effect. First, the thermal effect means the energy is converted into heat due to the friction effect due to the ultrasonic wave during the production process. Second, the non-thermal effects of US, a complex mechanism, includes stabilization and inertial cavitation, microfluidics, and radiation forces, in which inertial cavitation can induce the generation of ROS [93–96].

Recently, people have considerable attention in ROS formation under the excitation of US, in which different mechanisms have been proposed for explaining the generation of ROS [97, 98]. Bogdan et al. summarized the SDT mechanism, in which W-TiO_2 nanoparticles can provide additional nuclei, which increased the formation of air bubbles caused by US. The bubble collapse causes a local high-temperature rise, and OH radicals can be generated by water pyrolysis. In addition, thermal excitation and photoexcitation of sonoluminescence of W-TiO_2 caused by bubble implosion can be also responsive for the generation of OH radicals [53, 98, 99].

5.3.2 Sonodynamic Therapy

By changing intensity and frequency, US is currently used to achieve the purpose of diagnosis and treatment in medicine [93]. Compared with other excitation modes, US showed deeper penetration in tissues, which is safe and reasonable instrument [96, 100]. US can enhance the echogenicity and obtain 2D and 3D images under the action of microbubble contrast agents. In addition, US can also be used to treat a variety of pathologies, including the treatment of soft tissue injury, treatment of stones and cosmetic surgery [101–103]. US therapy has been accepted in medicine for many years. Since the 1950s, US with low power (1 MHz) has been widely used in physical therapy, such as tendinitis and bursitis. In the 1980s, high-pressure amplitude shock waves began to be used to mechanically resolve kidney stones and replaced surgical therapy as the most common treatment. US therapy continues to expand its use in medicine and approved applications in many fields, including SDT in cancers and other diseases [101].

US has a high depth of tissue penetration and is a benefit for SDT in internal organs, which makes it a promising source of external physical triggers for multifunctional biomedical applications. Similarly to photosensitizers in PDT, sonosensitizers is the core of SDT. However, most sonosensitizers molecules

were hydrophobic to accumulate in aqueous media and reduced the production rate of ROS. In order to develop high-efficiency sonosensitizers, nano-sized sonosensitizers have been attracted, owing to some advantages of large surface area and easy-functionalization [104]. W-TiO_2 can be promoted to generate ROS by exposing them under US, and subsequent cavitation collapse. Therefore, W-TiO_2 can be good candidate as sonosensitizers applied in SDT [105, 106].

To assess the ability of W-TiO_2 to destroy cells under UV or US, S. Yamaguchi et al. prepared water-dispersed W-TiO_2 nanoparticles and tested their cytotoxicity under the irradiation of UV (5.0 mW/cm^2) or US (1.0 MHz, 1.0 W/cm^2), in which the photodynamic cytotoxicity of W-TiO_2 was almost completely inhibited by the radical scavenger, but the inhibition of sonodynamic cytotoxicity was not significant, indicating that W-TiO_2 may be treated with SDT for malignant glioma [107]. To improve the biocompatibility of W-TiO_2, A. Harada et al. successfully prepared a core–shell structured micelle embedded W-TiO_2 by modifying polyallylamine bearing polyethylene glycol (PEG) grafts on the surface of the micelles, which showed the micelles have negligible cytotoxicity, and the W-TiO_2 was still sonicated to maintain its ability to produce ROS for SDT [108]. By using dual-frequency US, the SDT performance can be greatly improved. K. Ninomiya et al. demonstrated enhanced OH radicals generation of W-TiO_2 under the irradiation of dual-frequency US (0.5 MHz, 0.8 W/cm^2 and 1 MHz, 0.4 W/cm^2), by which the viability of HepG2 cells was inhibited by 46% [97].

In order to improve SDT performance, the targeted W-TiO_2 nanoprobes were designed. C. Ogino et al. synthesized pre-S1/S2 protein of Hepatitis B virus immobilized W-TiO_2 nanoparticles to target specifically liver cells, in which the liver cells were damaged under US at an ultrasonic radiation intensity of 0.4 W/cm^2 [106]. Subsequently, they examined the 24 hours uptake behavior of HepG2 cells using pre-S1/S2 modified W-TiO_2, in which the viability of HepG2 cells cultured with W-TiO_2 was obviously inhibited after irradiated by 1 MHz ultrasonic waves (0.1 W/cm^2, 30 seconds). Moreover, the tumor growth was also obviously inhibited under the ultrasonic irradiation (1 MHz, 1.0 W/cm^2, 60 seconds) [109]. K. Ninomiya et al. prepared avidin-modified W-TiO_2 for targeted SDT specially toward breast cancer cells (MCF-7). 80% of MCF-7 cells showed good uptake for avidin-modified W-TiO_2 nanoparticles, and ROS produced by W-TiO_2 can kill cells after applying 1-MHz ultrasound (0.1 W/cm^2, 30 seconds) [110].

For *in vivo* evaluation, Y. Harada et al. demonstrated the effect of the combination of US and W-TiO_2 on the viability of melanoma cells (C32). The C32 cells in the control group and the experimental group were irradiated by US, respectively (1 MHz, 0.5 and 1.0 W/cm^2 for 10 seconds), by which the cell survival was found to be significantly reduced only by the experimental group after US irradiation, and the combination of W-TiO_2 and US radiation (1 MHz, 1.0 W/cm^2, 2 minutes) inhibited tumor growth, demonstrating the high supersensitive SDT efficiency of W-TiO_2 in *in vivo* treatment [111].

Although SDT has become a potential replacement for traditional PDT, the low quantum yield of W-TiO_2 nanoparticles remains a major problem. Park and coworkers synthesized hydrophilized Au–W-TiO_2 (HAu–W-TiO_2) nanocomposites as sonosensitizers for improved SDT. As shown in Figure 5.4,

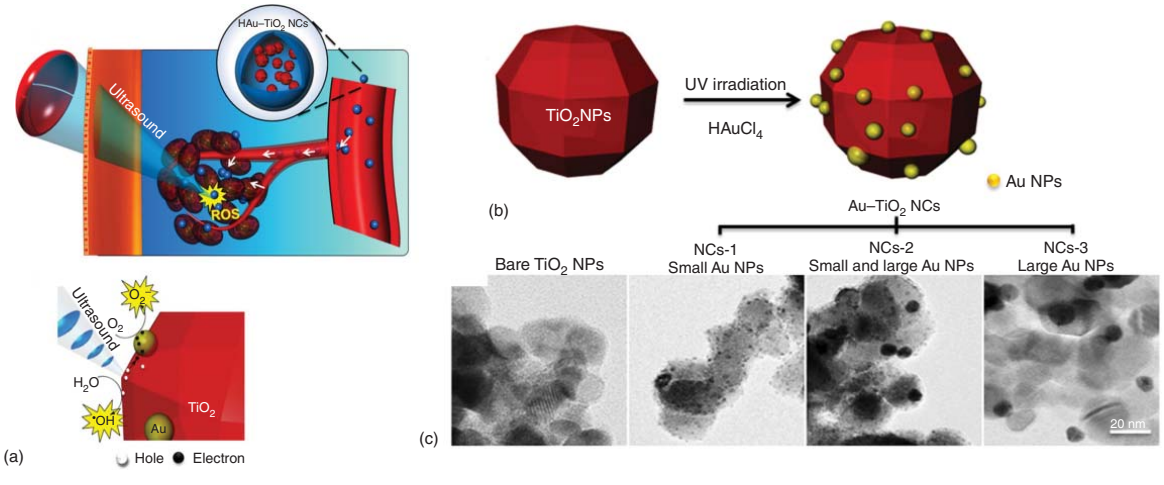

Figure 5.4 Improved SDT nanoplatform based on HAu–W-TiO_2 nanocomposites. (a) Diagrammatic sketch for the proposal SDT mechanism of HAu–TiO_2 nanocomposites; (b) diagrammatic sketch for the synthesis of HAu–TiO_2 nanocomposites; (c) TEM images of TiO_2 nanoparticles (left 1) and Au–TiO_2 nanocomposites with different magnification (left 2–4); (d) element distribution in the samples of H–TiO_2 and HAu–TiO_2 obtained using energy sispersive X-ray spectroscopy (EDS) mapping; (e) *in vitro* ROS generation the samples of H–TiO_2 and HAu–TiO_2 under the irradiation of US; (f) *in vivo* SDT performance of tumor-nearing mice in different groups; (g) survival rate of tumor-nearing mice in different groups with and without SDT. Source: Reproduced with permission from Deepagan et al. 2016 [112]. Copyright © 2016, American Chemical Society.

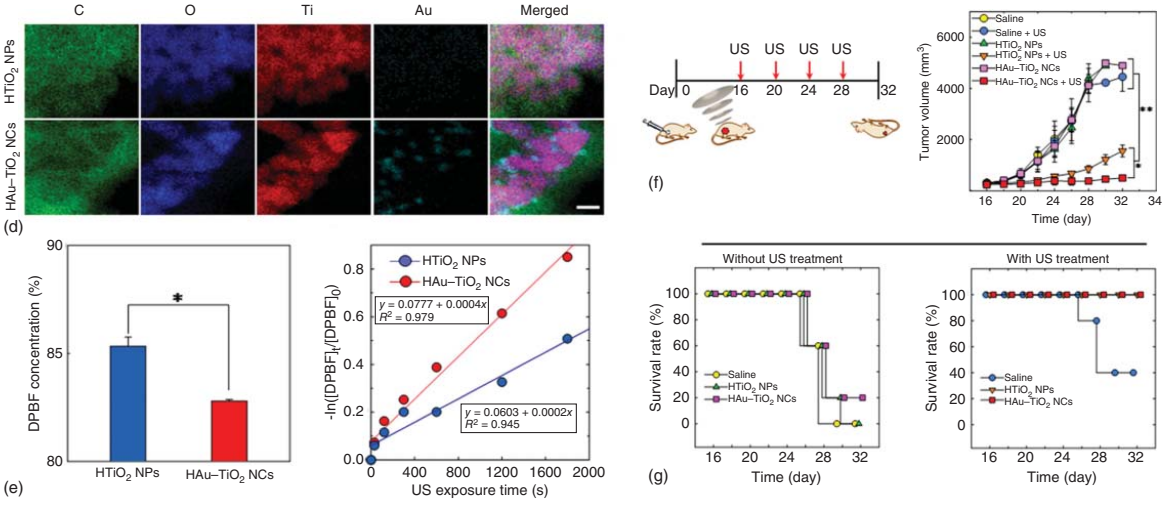

Figure 5.4 (*Continued*)

a large amount of ROS was produced, and the complex of gold and W-TiO_2 significantly increased the level of ROS production, resulting in enhanced therapeutic efficacy, when HAu–W-TiO_2 nanocomposites were exposed to US [112]. You et al. designed hydrophilized W-TiO_2 nanoparticles as sonosensitizers for *in vivo* SDT, in which they demonstrated that hydrophilized W-TiO_2 nanoparticles have long circulation in the body and can inhibit the growth of deep liver tumors by at least 15-fold, compared with that in control group [113]. Chen and coworkers designed mesoporous anatase W-TiO_2 nanoparticles with single-crystal structure for improved SDT, in which they demonstrated that high crystallinity of W-TiO_2 can avoid the recombination of electron/hole pairs under the action of US [114]. Dai et al. loaded W-TiO_2 nanoparticles onto the surface of graphene for enhanced SDT, by which the separation efficiency of electron/hole pairs was accelerated and the SDT performance was significantly improved, owing to the high conductivity of graphene [115].

Multifunctional SDT nanoplatforms based on W-TiO_2 were also developed. J.J. Shi et al. developed a novel type of mesoporous W-TiO_2 nanoparticles for simultaneous docetaxel (DTX) loading and SDT, in which β-cyclodextrin is coupled onto W-TiO_2 via a ROS-sensitive linker to prevent drug leakage, and the release of DTX was accelerated under ultrasound [116]. Yuan and Song developed a multifunctional system of W-TiO_2:Gd@DOX/FA nanomaterials for SDT and pH-responsive release of doxorubicin (DOX), in which Gd-doping increased ROS levels and improved the acoustic dynamics of W-TiO_2 [117]. Shen et al. designed DOX-loaded multifunctional dual-core@shell nanocomposites for synergistic SDT and chemotherapy, in which W-TiO_2 acted as sonosensitizers for tumor SDT in deep tissues, and the US obviously enhanced the apoptosis of cells, suggesting the importance of acoustic chemotherapy in cancer treatment [118].

5.3.3 High Intensity-Focused Ultrasound Therapy

HIFU, a non-invasive method of applying high-intensity ultrasound in the focal region, may cause the temperature to rise above 80 °C through absorbing ultrasound energy, leading to coagulative necrosis and irreversible apoptosis in the focal region, and achieve the minimum possibility of thermal damage to normal tissues outside the irradiation area [93, 95, 119]. It can also utilize different exposure times, pulse counts, and duty cycle modulation to limit temperature rise in the focus area [120]. HIFU has been studied to treat various types of tumors. In addition, HIFU is also a benefit for the targeted uptake, because US irradiation can temporarily increase cell permeability [121].

Although HIFU has many uses, it needs to increase the sound power or exposure time to increase the temperature in the depth of the tissue, and at the same time, it can cause side effects such as skin burns and nerve damage [122]. Therefore, different microbubbles were developed for therapeutic and diagnostic imaging under HIFU. These microbubbles enhance the mechanical effects associated with HIFU from therapeutic goals at low ultrasound intensity and low exposure time [123]. Y. Harada et al. reported that W-TiO_2 can be combined with HIFU for improved SDT without damaging the surrounding normal structure for cancer [111].

The use of SDT and HIFU is one of the challenges in SDT. The activation of the sonosensitizers depend on the cavitation process, and the presence of the sonosensitizers provides a nucleation site for the cavitation and reduces the cavitation threshold. It is necessary to develop some nanoparticles that help to reduce the power and time of SDT and HIFU irradiation for cancer treatment in the future.

5.4 TiO_2 as Multifunctional Nanoprobes for Visualized Theranostics

With the development of nanomedicine, multifunctional nanoprobes are becoming popular, which can integrate different modes of diagnosis and therapy in a single nanoprobe. One of the disadvantages of W-TiO_2 is the lack of imaging performance, and it is important for coupling imaging functions or other therapy functions into W-TiO_2, other than PDT and SDT functions [124–126]. Therefore, by synthesizing W-TiO_2 nanocomposites, multifunctional nanoprobes can be constructed for visualized theranostics in cancers, for example, imaging-guided PDT (or SDT) nanoprobes, synergistic therapy nanoprobes, and so on.

5.4.1 Magnetic Resonance Imaging and Phototherapy

MRI and PDT have potential applications in the early diagnosis and therapy, as well as in the prognosis assessment of cancers. Different elements such as iron, cobalt, and nickel can be used as T_2-weighted MRI agents, and Gd element can be used as T_1-weighted MRI agents. If these elements were doped into the crystal structure of W-TiO_2, or were coupled with W-TiO_2 to form nanocomposites, multifunctional nanoprobes of MRI and PDT can be designed for visualized theranostics in cancers, as a medical imaging agent. At present, Gd-complexes have been used as commercial T_1-weighted MRI contrast agents in hospitals [127], and Gd-based UCNPs were also good candidate as T1-weighted MRI contrast agents [128]. Due to good compatibility and high magnetism, iron oxide nanomaterials showed potential application in T_2-weighted MRI contrast agents [129, 130].

Yu et al. synthesize Fe_3O_4@TiO_2@mTiO_2 nanocomposites with core–shell–shell structure for MRI and PDT, and further for siRNA and DOX delivery due to the coating of mesoporous W-TiO_2, in which the pore TiO_2 shell allows controlled release of siRNA by a pH reversible hydrazone linkage [131]. In our previous work, Janus-structured Fe_3O_4–TiO_2 nanocomposites were synthesized for T_2-weighted MRI and UV-responsive PDT. Compared with core–shell structure, the designed Janus structure can maintain the magnetic performance and avoid the recombination of electron/hole pairs. As shown in Figure 5.5, Fe_3O_4–TiO_2 nanocomposites had a size of about 30–40 nm and an r_2 value of about 54.691/mM s, and the cell viability cultured with Fe_3O_4–TiO_2 nanocomposites can be reduced from about 85% to 39%, showing strong PDT performance [132]. Iglič and coworkers prepared Gd-doped mesoporous TiO_2 nanobeads for simultaneous MRI and PDT under the irradiation of UV light. The results indicated that Gd-doped TiO_2 exhibited red emission at 637 nm,

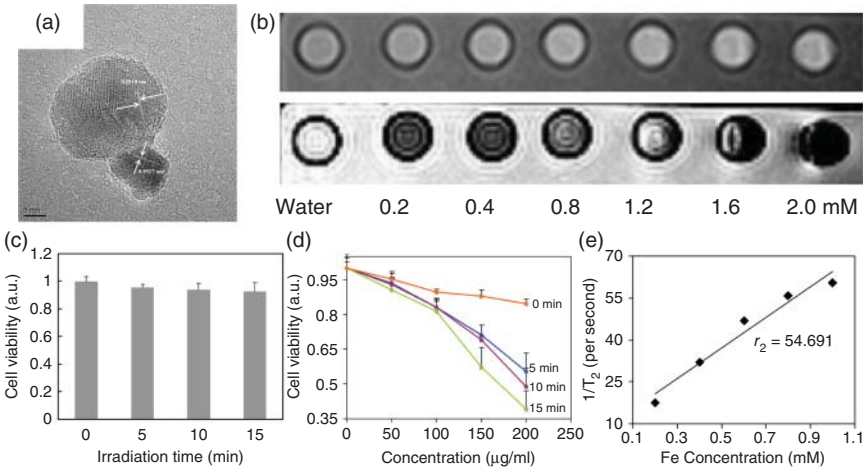

Figure 5.5 Multifunctional Fe_3O_4–TiO_2 nanocomposites for T_2-weighted MRI and UV-responsive PDT. (a) TEM images of Fe_3O_4–TiO_2 nanocomposites with Janus structure; (b) T_1- and T_2-weighted MR images of Fe_3O_4–TiO_2 nanocomposites with different concentrations; (c) viability of free MCF-7 cells irradiated by UV light for 0, 5, 10, and 15 minutes; (d) *in vitro* PDT performance of Fe_3O_4–TiO_2 nanocomposites toward MCF-7 cells under the irradiation of UV light; (e) T_2-weighted MR relaxation curve of Fe_3O_4–TiO_2 nanocomposites. Source: Reproduced with permission from Zeng et al. 2013 [132]. Copyright © 2013, Royal Chemical Society.

which favored optical imaging and significantly improved MRI performance, and showed enhanced ROS generation capability, compared with undoped TiO_2 nanobeads and commercial P25 [4].

NIR-responsive W-TiO_2 nanoparticles have been widely investigated for PDT [76, 77, 89], and it is very useful to develop multifunctional MRI and PDT reagents based on NIR-responsive W-TiO_2 nanocomposites [79]. In our previous work, Gd-based UCL–TiO_2 nanocomposites were synthesized for T_1-weighted MRI and NIR-responsive PDT under the irradiation of a 980 nm laser, in which the r_1 value is as high as 4.53/mM s, as shown in Figure 5.3 [79].

5.4.2 Fluorescent Imaging and Phototherapy

Because of the lack of accuracy in PDT, fluorescence imaging provided the right choice for the early diagnosis of cancers, which can be a perfect replacement for invasive surgery in modern medicine [133]. Therefore, the integration of diagnosis and treatment of W-TiO_2 nanocomposites has broad prospects for development [99]. Many nanomaterials can be used to synthesize W-TiO_2-based nanocomposites for simultaneous fluorescent imaging and phototherapy.

Synthesizing UCL–TiO_2 nanocomposites for simultaneous UCL imaging and PDT is very interesting. Moreover, the NIR-responsive PDT of W-TiO_2 can be realized. Zhang and coworkers Yb/Tm co-doped $NaYF_4$ nanoparticles, and then coated W-TiO_2 to form core–shell structure for UCL imaging and NIR-responsive PDT, in which UCNPs acted as a photosensor and TiO_2 shell acted as a photocatalyst under the excitation of a 980 nm laser [38]. However, various structures currently developed have certain limitations. If the loaded

photosensitizers were instable, the detachment and leakage were possible, thus reducing the therapeutic effects of photosensitizers and limiting their application in PDT. Zhang and coworkers subsequently prepared silica-coated UCNPs by uniformly coating TiO_2, which completely prevented the leakage of the photosensitizers, ensured effective stability for good PDT performance and enhanced the fluorescence intensity of the tumor sites [76].

Rheumatoid arthritis (RA) is a disease that affected progressive joint inflammation in humans, and the number of patients with illness accounts for 1% of the total population. Zhao et al. synthesized a new nanocomposite using W-TiO_2 and teterasulfonatophenyl porphyrin (TSPP) for fluorescent imaging and PDT, which indicated that TSPP–TiO_2 nanocomposites can significantly reduce the concentration of TNF-α and increase the body weight of mice, demonstrating excellent theranostics in RA [134].

Two-photon absorption nanomaterials are also an ideal clinical diagnostic material for deep tissues. Metalloporphyrin, zinc-5,10,15,20-tetra(4-pyridyl)-21H,23H-porphine (ZnTPyP), is one of the photonic nanomaterials, and ZnTPyP self-assembled nanocrystals (ZSN) are good photoluminescent materials with single-photon and two-photon absorption characteristics, which can emit red fluorescence while generating electron/hole pairs [135, 136]. Liu et al. successfully prepared a hexagonal nanocomposite system by uniformly coating W-TiO_2 on the outer layer of ZSN for deep tissue fluorescence imaging and PDT, in which ZSN can produce red fluorescence electron/hole pairs, and TiO_2 can accept photoelectron transferred from ZSN and acted as a photosensitizer for PDT to kill tumor cells. Under the combined action of ZSN and TiO_2, the high-efficiency PDT was achieved, which caused a significant increase in cell death rate [137].

5.4.3 Multi-mode Imaging and Phototherapy

Besides MRI and fluorescent imaging, multi-mode imaging will show promising application in accurate diagnosis. Moreover, by coupling W-TiO_2 and multi-mode imaging elements, multifunctional nanoprobes with simultaneous multi-mode imaging and phototherapy can be successfully constructed for accurate theranostics.

Lukeš and coworkers prepared multimodal therapeutic nanoprobe of TiO_2@RhdGd for simultaneous dual-mode imaging of MR and fluorescence and PDT, in which the tumor was accurately located by MRI and fluorescent imaging, and the PDT was applied directly to the tumor site under the irradiation of UV light, avoiding non-specific damage to surrounding tissue [138]. Wu et al. designed mesoporous TiO_2-coated magnetic nanoparticles (Fe_3O_4@mTiO_2) for siRNA delivery and PDT by modifying flavin mononucleotide (FMN) and polyethyleneimine (PEI), in which FMN was fluorescent probe, Fe_3O_4 was MRI probe, and PEI-linked mesoporous TiO_2 was used as siRNA delivery carrier for gene therapy, which all showed important potential as photosensitizers for PDT [139].

Recently, UCNPs–TiO_2 nanocomposites have been popular for NIR-responsive PDT, also for magnetic/fluorescent imaging [76]. Lin et al. designed

UCNPs@mSiO_2@TiO_2 with multi-shell structure for simultaneous multi-mode imaging of UCL, CT and MR, and PDT under the irradiation of a single 808 nm laser (Figure 5.6) [89]. Zhou et al. successfully constructed indocyanine green (ICG)-coated and rare-earth doped W-TiO_2 for multi-mode imaging and dual-mode phototherapy, in which ICG acted as fluorescent imaging and PTT, rare-earth ions acted as UCL imaging and W-TiO_2 acted as PDT under the irradiation of an 808 nm laser [140]. Lv et al. synthesized TiO_2@$Y_2Ti_2O_7$@YOF nanocomposites with uniform core–shell structure for multi-modal imaging of UCL/CT, and dual-modal phototherapy of PDT/PTT under the irradiation of a single 980 nm laser, in which the combination of electron/hole pairs can produce thermal effects due to non-radiative transition [62].

5.4.4 Drug Delivery and Synergistic Therapy

Besides the application in PDT and SDT, W-TiO_2 nanoparticles can also serve as nanocarrier for drug delivery due to their large surface area and good biocompatibility. Generally, W-TiO_2 can be used as nanocarrier for drug delivery [24]. Moreover, by constructing W-TiO_2-based nanocomposites, visualized delivery nanosystem can also be developed.

DOX is one of the most common chemotherapy drugs used in clinical treatment for solid tumors. Qin et al. synthesized DOX-loaded W-TiO_2 nanoparticles for improved chemotherapy using covalent coupling method, by which DOX can enter the nucleus, but TiO_2–DOX was mainly located in the cytoplasm [141]. Wu et al. synthesized mesoporous W-TiO_2 nanoparticles functionalized with a phosphate-containing fluorescent molecule (flavin mononucleotide) and loaded with DOX for fluorescent imaging and chemotherapy, which is the first report of highly biocompatible mesoporous W-TiO_2 nanoparticles for fluorescence imaging and drug carriers [142].

Flak et al. prepared hybrid ZnPc@TiO_2 nanocomposites for fluorescence imaging, DOX delivery and PDT under the irradiation of UV light, in which DOX was electrostatically adsorbed onto the hybrid nanocomposites, and was effectively delivered to the cytoplasm and ensured uniform distribution [143]. In our previous report, DOX-loaded UCL–TiO_2 nanocomposites were synthesized for enhanced chemotherapy and NIR-responsive PDT to overcome multidrug resistance in breast cancer. As shown in Figure 5.7, under the combination of enhanced chemotherapy and NIR-responsive PDT, the multidrug resistance of breast cancer was successfully overcome, in which the inhibition rate of MCF-7/ADR tumors was up to 96.74% [78].

In addition to DOX, paclitaxel (PTX) is also one of the most commonly used chemotherapy drugs. Kumar and coworkers synthesized PTX-loaded, PEG, and FA-modified W-TiO_2 nanoparticles for targeted drug delivery [144]. Wang et al. innovatively prepared PTX-loaded porous W-TiO_2 nanoparticles for PDT and chemotherapy, in which PTX was loaded into the pores of porous W-TiO_2, and can be released under the irradiation of UV light [145].

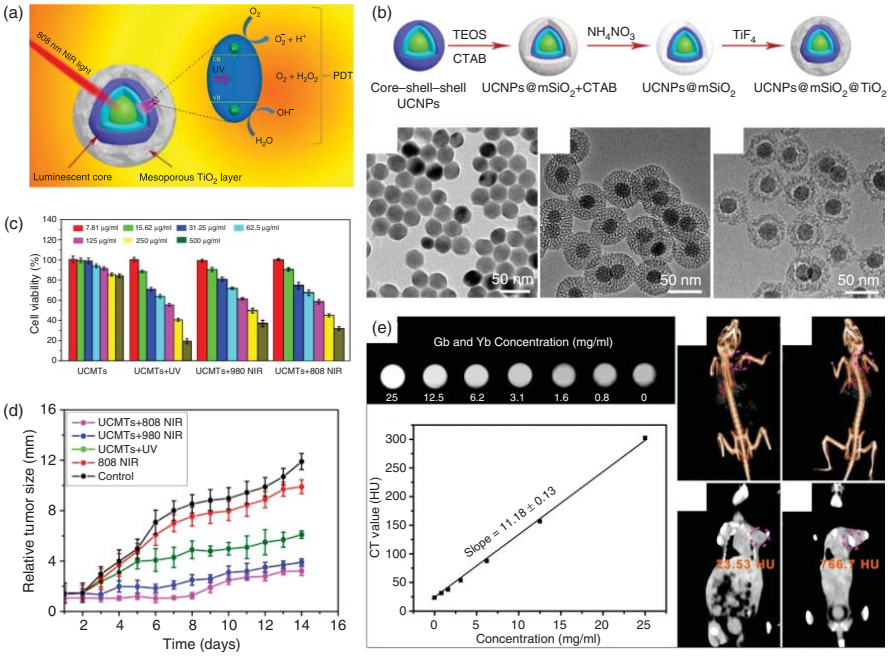

Figure 5.6 Tri-modal imaging of UCL/MRI/CT and NIR-responsive PDT multifunctional nanoplatform based on UCNPs@mSiO$_2$@TiO$_2$ under the irradiation of an 808 nm laser. (a) Diagrammatic sketch for the proposal PDT mechanism of UCNPs@mSiO$_2$@TiO$_2$ nanocomposites; (b) diagrammatic sketch for the synthesis of UCNPs@mSiO$_2$@TiO$_2$ nanocomposites, and TEM images of UCNPs (left), UCNPs@mSiO$_2$ (middle), and UCNPs@mSiO$_2$@TiO$_2$ (right); (c) *in vitro* PDT performance; (d) *in vivo* PDT performance; (e) *in vivo* MRI/CT imaging. Source: Reproduced with permission from Yang et al. 2015 [89]. Copyright © 2015, American Chemical Society.

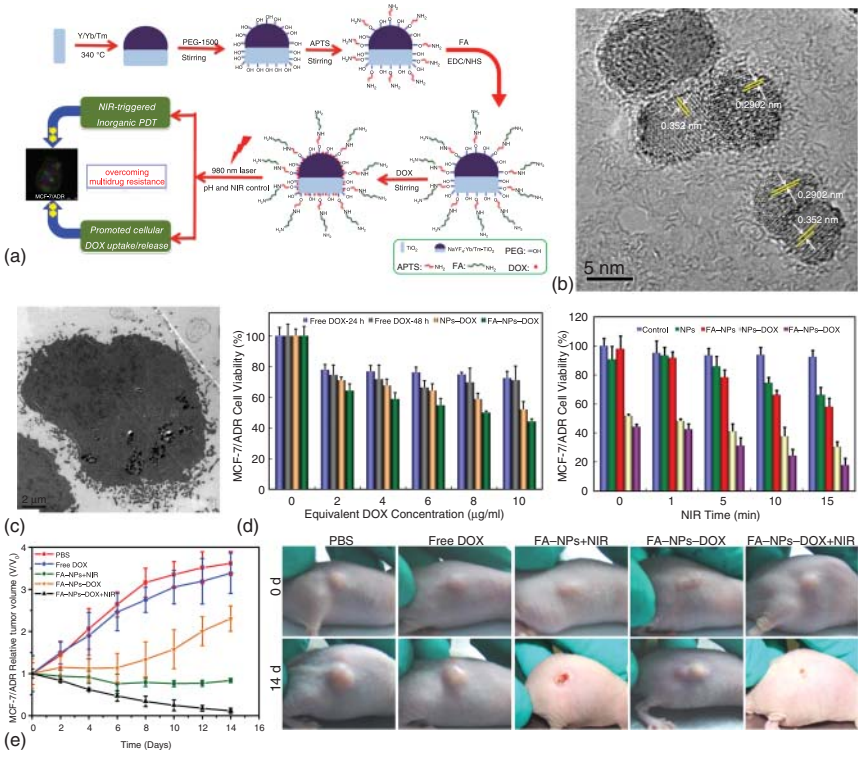

Figure 5.7 DOX-coated UCL–TiO_2 nanocomposites for simultaneous improved chemotherapy and 980 nm NIR-responsive PDT, overcoming the multidrug resistance in breast cancer. (a) Diagrammatic sketch for the synthesis of DOX-coated UCL–TiO_2 nanocomposites; (b) high-resolution TEM images of UCL–TiO_2 nanocomposites with Janus structure; (c) cellular uptake of UCL–TiO_2 nanocomposites by drug-resistant breast cancer cells of MCF-7/ADR, characterized by TEM; (d) *in vitro* chemotherapy and synergistic chemotherapy/PDT performance of UCL–TiO_2 nanocomposites toward MCF-7/ADR cells; (e) *in vivo* chemotherapy and synergistic chemotherapy/PDT performance toward tumor-bearing mice in different groups. Source: Reproduced with permission from Zeng et al. 2015 [78]. Copyright © 2015, Elsevier.

5.5 Conclusions and Future Perspectives

W-TiO_2 nanoparticles and their nanocomposites have been widely investigated and showed important potential in tumor treatment and visualized theranostics. Especially, as inorganic photosensitizers for PDT, W-TiO_2 nanoparticles showed many advantages of photostability, biocompatibility, and long circulation, compared with organic photosensitizers. By doping and coupling, the excitation wavelength of PDT can also be modulated, which can increase the penetration depth and reduce the tissue damage. As an alternative treatment mode, SDT based on W-TiO_2 nanoparticles is becoming promising due to its non-radiation damage and non-photo damage. Furthermore, due to easy functionalization, W-TiO_2 nanoparticles can be modified with drugs and be coupled with other

nanostructure, thus multifunctional nanostructures can be constructed for drug delivery, multi-mode imaging, and visualized theranostics.

However, in order to accelerate the clinical application of W-TiO_2 and their nanocomposites, many significant challenges need to be overcome, including:

(1) How to precisely control the size, composition, shape, and water dispersibility of W-TiO_2 nanoparticles to modulate the performance of PDT and SDT?
(2) How to combine W-TiO_2 nanoparticles with other materials to achieve enhanced *in vivo* diagnosis and treatment?
(3) How to control the safety dose of W-TiO_2 nanoparticles and their nanocomposites to achieve the optimized *in vivo* visualized theranostics?

Acknowledgments

This work was financially supported by the National Natural Science Foundation of China (51772074, U1732127 to Leyong Zeng, and 31971292, U1432114 to Aiguo Wu), National Key R&D Program of China (2018YFC0910601, 2019YFA0405603), Key Basic Research Foundation of Science & Technology Department of Hebei Province (17961302D), Youth Top-notch Talents of Education Department of Hebei Province (BJ2017002), Advanced Talents Incubation Program of the Hebei University (521000981076) (L.Y. Zeng), and Zhejiang Province Financial Supporting (2017C03042, LY18H180011), as well as the Science & Technology Bureau of Ningbo City (2015B11002, 2017C110022).

References

1 Chen, X. and Mao, S.S. (2007). Titanium dioxide nanomaterials: synthesis, properties, modification, and applications. *Chemical Reviews* 107: 2891–2959.
2 Hashimoto, K., Irie, H., and Fujishima, A. (2005). TiO_2 photocatalysis: a historical overview and future prospects. *Japanese Journal of Applied Physics* 44: 8269–8285.
3 Deshmukh, S.P., Mullanil, S.B., Koli, V.B. et al. (2018). Ag nanoparticles connected to the surface of TiO_2 electrostatically for antibacterial photoinactivation studies. *Photochemistry and Photobiology* 94: 1249–1262.
4 Imani, R., Dillert, R., Bahnemann, D.W. et al. (2017). Multifunctional gadolinium-doped mesoporous TiO_2 nanobeads: photoluminescence, enhanced spin relaxation, and reactive oxygen species photogeneration, beneficial for cancer diagnosis and treatment. *Small* 13: 1700349.
5 Cheng, Y., Chang, Y., Feng, Y.L. et al. (2017). Simulated sunlight-mediated photodynamic therapy for melanoma skin cancer by titanium-dioxide nanoparticle-gold-nanocluster-graphene heterogeneous nanocomposites. *Small* 13: 1603935.
6 Ahamed, M., Khan, M.A.M., Akhtar, M.J. et al. (2017). Ag-doping regulates the cytotoxicity of TiO_2 nanoparticles *via* oxidative stress in human cancer cells. *Scientific Reports* 7: 17662.

7 Zeni, P.F., Santos, D.P.D., Canevarolo, R.R. et al. (2018). Photocatalytic and cytotoxic effects of nitrogen-doped TiO_2 nanoparticles on melanoma cells. *Journal of Nanoscience and Nanotechnology* 18: 3722–3728.

8 Zhou, J., Luo, P., Sun, C. et al. (2017). A "win–win" nanoplatform TiO_2:Yb,Ho,F for NIR light-induced synergistic therapy and imaging. *Nanoscale* 9: 4244–4254.

9 Yu, N., Hu, Y., Wang, X.Y. et al. (2017). Dynamically tuning near-infrared-induced photothermal performances of TiO_2 nanocrystals by Nb-doping for imaging guided photothermal therapy of tumors. *Nanoscale* 9: 9148–9159.

10 Pan, X.B., Liang, X.Y., Yao, L.F. et al. (2017). Study of the photodynamic activity of N-doped TiO_2 nanoparticles conjugated with aluminum phthalocyanine. *Nanomaterials* 7: 338.

11 Kamat, P.V. (2002). Photophysical, photochemical and photocatalytic aspects of metal nanoparticles. *The Journal of Physical Chemistry B* 106: 7729–7744.

12 Subramanian, V., Wolf, E., and Kamat, P.V. (2001). Semiconductor-metal composite nanostructures. To what extent do metal nanoparticles improve the photocatalytic activity of TiO_2 films. *The Journal of Physical Chemistry B* 105: 11439–11446.

13 Hagfeldt, A. and Gratzel, M. (1995). Light-induced redox reactions in nanocrystalline systems. *Chemical Reviews* 95: 49–68.

14 Yan, S.G., Prieskorn, J.S., Kim, Y., and Hupp, J.T. (2000). In search of the inverted region: chromophore-based driving force dependence of interfacial electron transfer reactivity at the nanocrystalline titanium dioxide semiconductor/solution interface. *The Journal of Physical Chemistry B* 104: 10871–10877.

15 Lemon, B.I. and Hupp, J.T. (1999). EQCM investigations of dye-functionalized nanocrystalline titanium dioxide electrode/solution interfaces: does luminescence report directly on interfacial electron transfer kinetics. *The Journal of Physical Chemistry B* 103: 3797–3799.

16 Kamat, P.V. (1993). Photochemistry on nonreactive and reactive (semiconductor) surfaces. *Chemical Reviews* 93: 267–300.

17 Wagemaker, M., Krol, R., Kentgens, A.P.M. et al. (2001). Two phase morphology limits lithium diffusion in TiO_2 (anatase): a ^{7}Li MAS NMR study. *Journal of the American Chemical Society* 123: 11454–11461.

18 Iuchi, K., Ohko, Y., Tatsuma, T., and Fujishima, A. (2004). Cathode-separated TiO_2 photocatalysts applicable to a photochromic device responsive to backside illumination. *Chemistry of Materials* 16: 1165–1167.

19 Hotsenpiller, P.A.M., Bolt, J.D., and Farneth, W.E. (1998). Orientation dependence of photochemical reactions on TiO_2 surfaces. *The Journal of Physical Chemistry B* 102: 3216–3226.

20 Lowekamp, J.B. and Rohrer, G.S. (1998). Anisotropic photochemical reactivity of bulk TiO_2 crystals. *The Journal of Physical Chemistry B* 102: 7323–7327.

21 Wilson, J.N. and Idriss, H. (2002). Structure sensitivity and photocatalytic reactions of semiconductors. Effect of the last layer atomic arrangement. *Journal of the American Chemical Society* 124: 11284–11285.

22 Chatterjee, D.K., Fong, L.S., and Zhang, Y. (2008). Nanoparticles in photodynamic therapy: an emerging paradigm. *Advanced Drug Delivery Reviews* 60: 1627–1637.

23 Shen, Y.Z., Shuhendler, A.J., Ye, D. et al. (2016). Two-photon excitation nanoparticles for photodynamic therapy. *Chemical Society Reviews* 45: 6725–6741.

24 Xu, J., Sun, Y., Huang, J.J. et al. (2007). Photokilling cancer cells using highly cell-specific antibody-TiO_2 bioconjugates and electroporation. *Bioelectrochemistry* 71: 217–222.

25 Dolmans, D.E.J.G.J., Fukumura, D., and Jain, R.K. (2003). Photodynamic therapy for cancer. *Nature Reviews Cancer* 3: 380–387.

26 Zhao, J., Wu, W., and Guo, S. (2013). Triplet photosensitizers: from molecular design to applications. *Chemical Society Reviews* 42: 5323–5351.

27 Voon, S.H., Kiew, L.V., Lee, H.B. et al. (2014). *In vivo* studies of nanostructure-based photosensitizers for photodynamic cancer therapy. *Small* 10: 4993–5013.

28 Zhang, H., Chen, B., Jiang, H. et al. (2011). A strategy for ZnO nanorod mediated multi-mode cancer treatment. *Biomaterials* 32: 1906–1914.

29 Shi, J., Wang, L., Gao, J. et al. (2014). A fullerene-based multi-functional nanoplatform for cancer theranostic applications. *Biomaterials* 35: 5771–5784.

30 Zhang, H., Shi, R.H., Xie, A.J. et al. (2013). Novel TiO_2/PEGDA hybrid hydrogel prepared *in situ* on tumor cells for effective photodynamic therapy. *ACS Applied Materials & Interfaces* 5: 12317–12322.

31 Chen, Y.H., Tong, R.H., An, N. et al. (2017). DOX-UCNPs@mSiO_2-TiO_2 nanocomposites for near-infrared photocontrolled chemo/photodynamic therapy. *New Journal of Chemistry* 41: 7292–7301.

32 Wang, J., Guo, Y.W., Gao, J.Q. et al. (2011). Detection and comparison of reactive oxygen species (ROS) generated by chlorophyllin metal (Fe, Mg and Cu) complexes under ultrasonic and visible-light irradiation. *Ultrasonics Sonochemistry* 18: 1028–1034.

33 Dodd, N.J.F. and Jha, A.N. (2009). Titanium dioxide induced cell damage: a proposed role of the carboxyl radical. *Mutation Research/Fundamental and Molecular Mechanisms of Mutagenesis* 660: 79–82.

34 Li, F.B., Li, X.Z., and Hou, M.F. (2004). Photocatalytic degradation of 2-mercaptobenzothiazole in aqueous La^{3+}–TiO_2 suspension for odor control. *Applied Catalysis B* 48: 185–194.

35 Ivanković, S., Gotić, M., Jurin, M., and Musić, S. (2003). Photokilling squamous carcinoma cells SCCVII with ultrafine particles of selected metal oxides. *Journal of Sol-Gel Science and Technology* 27: 225–233.

36 Pan, X.B., Xie, J., Li, Z. et al. (2015). Enhancement of the photokilling effect of aluminum phthalocyanine in photodynamic therapy by conjugating with nitrogen-doped TiO_2 nanoparticles. *Colloids and Surfaces B* 130: 292–298.

37 Liu, L., Miao, P., Xu, Y.Y. et al. (2010). Study of Pt/TiO_2 nanocomposite for cancer-cell treatment. *Journal of Photochemistry and Photobiology B* 98: 207–210.

38 Idris, N.M., Lucky, S.S., Li, Z.Q. et al. (2014). Photoactivation of core–shell titania coated upconversion nanoparticles and their effect on cell death. *Journal of Materials Chemistry B* 2: 7017–7026.

39 Muñoz-Bonilla, A., Cerrada, M.L., Fernández-García, M. et al. (2013). Biodegradable polycaprolactone-titania nanocomposites: preparation, characterization and antimicrobial properties. *International Journal of Molecular Sciences* 14: 9249–9266.

40 Cai, R., Hashimoto, K., Kubota, Y., and Fujishima, A. (1992). Increment of photocatalytic killing of cancer cells using TiO_2 with the aid of superoxide dismutase. *Chemistry Letters* 21: 427–430.

41 Sakai, H., Baba, R., Hashimoto, K. et al. (1995). Selective killing of a single cancerous T24 cell with TiO_2 semiconducting microelectrode under irradiation. *Chemistry Letters* 24: 185–186.

42 Stefanou, E., Evangelou, A., and Falaras, P. (2010). Effects of UV-irradiated titania nanoparticles on cell proliferation, cancer metastasis and promotion. *Catalysis Today* 151: 58–63.

43 Lagopati, N., Kitsiou, P.V., Kontos, A.I. et al. (2010). Photo-induced treatment of breast epithelial cancer cells using nanostructured titanium dioxide solution. *Journal of Photochemistry and Photobiology A* 214: 215–223.

44 Cai, R., Hashimoto, K., Itoh, K. et al. (1991). Photokilling of malignant cells with ultra TiO_2 powder. *Bulletin of the Chemical Society of Japan* 64: 1268–1273.

45 Huang, N.P., Xu, M.H., Yuan, C.W., and Yu, R.R. (1997). The study of the photokilling effect and mechanism of ultrafine TiO_2 particles on U937 cells. *Journal of Photochemistry and Photobiology A* 108: 229–233.

46 Seo, J., Chung, H., Kim, M. et al. (2007). Development of water-soluble single crystalline TiO_2 nanoparticles for photocatalytic cancer-cell treatment. *Small* 3: 850–853.

47 Feng, X.H., Zhang, S.K., and Lou, X. (2013). Controlling silica coating thickness on TiO_2 nanoparticles for effective photodynamic therapy. *Colloids and Surfaces B: Biointerfaces* 107: 220–226.

48 Yamaguchi, S., Kobayashi, H., Narita, T. et al. (2010). Novel photodynamic therapy using water-dispersed TiO_2-polyethylene glycol compound: evaluation of antitumor effect on glioma cells and spheroids *in vitro*. *Photochemistry and Photobiology* 86: 964–971.

49 Polyakov, N.E., Leshina, T.V., Meteleva, E.S. et al. (2010). Enhancement of the photocatalytic activity of TiO_2 nanoparticles by water-soluble complexes of carotenoids. *The Journal of Physical Chemistry B* 114: 14200–14204.

50 Yin, Y., Zhu, W.W., Guo, L.P. et al. (2013). RGDC functionalized titanium dioxide nanoparticles induce less damage to plasmid DNA but higher cytotoxicity to HeLa cells. *The Journal of Physical Chemistry B* 117: 125–131.

51 Thevenot, P., Cho, J., Wavhal, D. et al. (2008). Surface chemistry influences cancer killing effect of TiO_2 nanoparticles. *Nanomedicine: Nanotechnology, Biology and Medicine* 4: 226–236.

52 Matsui, K., Karasaki, M., Segawa, M. et al. (2010). Biofunctional TiO_2 nanoparticle-mediated photokilling of cancer cells using UV irradiation. *Medicinal Chemistry Communications* 1: 209–211.

53 Song, M., Zhang, R.Y., Dai, Y.Y. et al. (2006). The *in vitro* inhibition of multidrug resistance by combined nanoparticulate titanium dioxide and UV irradition. *Biomaterials* 27: 4230–4238.

54 Rozhkova, E.A., Ulasov, I., Lai, B. et al. (2009). A high-performance nanobio photocatalyst for targeted brain cancer therapy. *Nano Letters* 9: 3337–3342.

55 Ratanatawanate, C., Chyao, A., and Balkus, K.J. (2011). S-nitrosocysteine-decorated PbS QDs/TiO_2 nanotubes for enhanced production of singlet oxygen. *Journal of the American Chemical Society* 133: 3492–3497.

56 Lu, K.Q., He, Q.Y., Chen, L. et al. (2015). The comparative PDT experiment of the inactivation of HL60 on modified TiO_2 nanoparticles. *Journal of Nanomaterials*: 540247.

57 Huang, K.Q., Chen, L., Liao, M.X., and Xiong, J.W. (2012). The photocatalytic inactivation effect of Fe-doped TiO_2 nanocomposites on leukemic HL60 cells-based photodynamic therapy. *International Journal of Photoenergy* 2012: 367072.

58 Szacilowski, K., Macyk, W., Drzewiecka-Matuszek, A. et al. (2005). Bioinorganic photochemistry: frontiers and mechanisms. *Chemical Reviews* 105: 2647–2694.

59 Hemmer, E., Benayas, A., Légaré, F., and Vetrone, F. (2016). Exploiting the biological windows: current perspective on fluorescent bioprobes emitting above 1000 nm. *Nanoscale Horizons* 1: 168–184.

60 Vogel, A. and Venugopalan, V. (2003). Mechanisms of pulsed laser ablation of biological tissues. *Chemical Reviews* 103: 577–644.

61 Ju, Q., Chen, X., Ai, F. et al. (2015). An upconversion nanoprobe operating in the first biological window. *Journal of Materials Chemistry C* 3: 3548–3555.

62 Lv, R.C., Zhong, C.N., Li, R.M. et al. (2015). Multifunctional anticancer platform for multimodal imaging and visible light driven photodynamic/photothermal therapy. *Chemistry of Materials* 27: 1751–1763.

63 Yin, M.L., Ju, E.G., Chen, Z.W. et al. (2014). Upconverting nanoparticles with a mesoporous TiO_2 shell for near-infrared-triggered drug delivery and synergistic targeted cancer therapy. *Chemistry A European Journal* 20: 14012–14017.

64 Lee, C., Hong, C., Kim, H. et al. (2010). TiO_2 nanotubes as a therapeutic agent for cancer thermotherapy. *Photochemistry and Photobiology* 86: 981–989.

65 Prodi, L., Rampazzo, E., Rastrelli, F. et al. (2015). Imaging agents based on lanthanide doped nanoparticles. *Chemical Society Reviews* 44: 4922–4952.

66 Zheng, W., Huang, P., Tu, D. et al. (2015). Lanthanide-doped upconversion nano-bioprobes: electronic structures, optical properties, and biodetection. *Chemical Society Reviews* 44: 1379–1415.

67 Wang, G.F., Qin, W.P., Wang, L.L. et al. (2008). Intense ultraviolet upconversion luminescence from hexagonal $NaYF_4$:Yb^{3+}/Tm^{3+} microcrystals. *Optics Express* 16: 11907–11914.

68 Qin, W., Cao, C., Wang, L. et al. (2008). Ultraviolet upconversion fluorescence from ^6D_J of Gd^{3+} induced by 980 nm excitation. *Optics Letters* 33: 2167–2169.

69 Mahalingam, V., Naccache, R., Vetrone, F., and Capobianco, J.A. (2009). Sensitized Ce^{3+} and Gd^{3+} ultraviolet emissions by Tm^{3+} in colloidal $LiYF_4$ nanocrystals. *Chemistry A European Journal* 15: 9660–9663.

70 Qin, W.P., Zhang, D.S., Zhao, D. et al. (2010). Near-infrared photocatalysis based on YF_3:Yb^{3+},Tm^{3+}/TiO_2 core/shell nanoparticles. *Chemical Communications* 46: 2304–2306.

71 Tang, Y.N., Di, W.H., Zhai, X.S. et al. (2013). NIR-responsive photocatalytic activity and mechanism of $NaYF_4$:Yb,Tm@TiO_2 core–shell nanoparticles. *ACS Catalysis* 3: 405–412.

72 Qiu, Z.L., Shu, J., and Tang, D.P. (2018). Near-infrared-to-ultraviolet light-mediated photoelectrochemical aptasensing platform for cancer biomarker based on core–shell $NaYF_4$:Yb,Tm@TiO_2 upconversion microrods. *Analytical Chemistry* 90: 1021–1028.

73 Xu, Q.C., Zhang, Y., Tan, M.J. et al. (2012). Anti-cAngptl4 Ab-conjugated N-TiO_2/NaYF4:Yb,Tm nanocomposite for near infrared-triggered drug release and enhanced targeted cancer cell ablation. *Advanced Healthcare Materials* 1: 470–474.

74 Tong, R.H., Lin, H.M., Chen, Y.H. et al. (2017). Near-infrared mediated chemo/photodynamic synergistic therapy with DOX-UCNPs@mSiO_2/TiO_2-TC nanocomposite. *Materials Science and Engineering C* 78: 998–1005.

75 Yu, Z.Z., Sun, Q.Q., Pan, W. et al. (2015). A near-infrared triggered nanophotosensitizer inducing domino effect on mitochondrial reactive oxygen species burst for cancer therapy. *ACS Nano* 9: 11064–11074.

76 Lucky, S.S., Idris, N.M., Li, Z.Q. et al. (2015). Titania coated upconversion nanoparticles for near-infrared light triggered photodynamic therapy. *ACS Nano* 9: 191–205.

77 Hou, Z.Y., Zhang, Y.X., Deng, K.R. et al. (2015). UV-emitting upconversion-based TiO_2 photosensitizing nanoplatform: near-infrared light mediated *in vivo* photodynamic therapy *via* mitochondria-involved apoptosis pathway. *ACS Nano* 9: 2584–2599.

78 Zeng, L.Y., Pan, Y.W., Tian, Y. et al. (2015). Doxorubicin-loaded $NaYF_4$:Yb/Tm-TiO_2 inorganic photosensitizers for NIR-triggered photodynamic therapy and enhanced chemotherapy in drug-resistant breast cancers. *Biomaterials* 57: 93–106.

79 Zhang, L.E., Zeng, L.Y., Pan, Y.W. et al. (2015). Inorganic photosensitizer coupled Gd-based upconversion luminescent nanocomposites for *in vivo* magnetic resonance imaging and near-infrared-responsive photodynamic therapy in cancers. *Biomaterials* 44: 82–90.

80 Weissleder, R. (2001). A clearer vision for imaging. *Nature Biotechnology* 19: 316–317.

81 Zhan, Q., Qian, J., Liang, H. et al. (2011). Using 915 nm laser excited Tm^{3+}/Er^{3+}/Ho^{3+}-doped $NaYbF_4$ upconversion nanoparticles for *in vitro*

and deeper *in vivo* bioimaging without overheating irradiation. *ACS Nano* 5: 3744–3757.

82 Xie, X. and Liu, X. (2012). Upconversion goes broadband. *Nature Materials* 11: 842–843.

83 Jayakumar, M.K.G., Idris, N.M., Huang, K., and Zhang, Y. (2014). A paradigm shift in the excitation wavelength of upconversion nanoparticles. *Nanoscale* 6: 8441–8443.

84 Wang, Y.F., Liu, G.Y., Sun, L.D. et al. (2013). Nd^{3+}-sensitized upconversion nanophosphors: efficient *in vivo* bioimaging probes with minimized heating effect. *ACS Nano* 7: 7200–7206.

85 Xie, X., Gao, N., Deng, R. et al. (2013). Mechanistic investigation of photon upconversion in Nd^{3+}-sensitized core–shell nanoparticles. *Journal of the American Chemical Society* 135: 12608–12611.

86 Wen, H.L., Zhu, H., Chen, X. et al. (2013). Upconverting near-infrared light through energy management in core–shell–shell nanoparticles. *Angewandte Chemie International Edition* 52: 13419–13423.

87 Li, X.M., Guo, Z.Z., Zhao, T.C. et al. (2016). Filtration shell mediated power density independent orthogonal excitations–emissions upconversion luminescence. *Angewandte Chemie International Edition* 128: 2510–2515.

88 Zeng, L., Pan, Y., Zou, R. et al. (2016). 808 nm-excited upconversion nanoprobes with low heating effect for targeted dual-modality imaging and high-efficacy photodynamic therapy in HER2-overexpressed breast cancer. *Biomaterials* 103: 116–127.

89 Yang, G.X., Yang, D., Yang, P.P. et al. (2015). A single 808 nm near-infrared light-mediated multiple imaging and photodynamic therapy based on titania coupled upconversion nanoparticles. *Chemistry of Materials* 27: 7957–7968.

90 Lopez, T., Ortiz, E., Alvarez, M. et al. (2010). Study of the stabilization of zinc phthalocyanine in sol–gel TiO_2 for photodynamic therapy applications. *Nanomedicine: Nanotechnology, Biology and Medicine* 6: 777–785.

91 Youssef, Z., Jouan-Hureaux, V., Colombeau, L. et al. (2018). Titania and silica nanoparticles coupled to Chlorin e6 for anti-cancer photodynamic therapy. *Photodiagnosis and Photodynamic Therapy* 22: 115–126.

92 Hou, Z.Y., Deng, K.R., Li, C.X. et al. (2016). 808 nm light-triggered and hyaluronic acid-targeted dual-photosensitizers nanoplatform by fully utilizing Nd^{3+}-sensitized upconversion emission with enhanced anti-tumor efficacy. *Biomaterials* 11: 32–46.

93 Shibaguchi, H., Tsuru, H., Kuroki, M., and Kuroki, M. (2011). Sonodynamic cancer therapy: a non-invasive and repeatable approach using low-intensity ultrasound with a sonosensitizer. *Anticancer Research* 31: 2425–2429.

94 Santos, H.M., Lodeiro, C., and Capelo-Martínez, J.-L. (2009). The power of ultrasound. In: *Ultrasound in Chemistry* (ed. J.-L. Capelo-Martínez), 1–16. Wiley-VCH.

95 Dubinsky, T.J., Cuevas, C., Dighe, M.K. et al. (2008). High-intensity focused ultrasound: current potential and oncologic applications. *American Journal of Roentgenology* 190: 191–199.

96 Rosenthal, I., Sostaric, J.Z., and Riesz, P. (2004). Sonodynamic therapy–a review of the synergistic effects of drugs and ultrasound. *Ultrasonics Sonochemistry* 11: 349–363.

97 Ninomiya, K., Noda, K., Ogino, C. et al. (2014). Enhanced OH radical generation by dual-frequency ultrasound with TiO_2 nanoparticles: its application to targeted sonodynamic therapy. *Ultrasonics Sonochemistry* 21: 289–294.

98 Bogdan, J., Pławińska-Czarnak, J., and Zarzyńska, J. (2017). Nanoparticles of titanium and zinc oxides as novel agents in tumor treatment: a review. *Nanoscale Research Letters* 12: 225–240.

99 Rehman, F.U., Zhao, C., Jiang, H., and Wang, X. (2016). Biomedical applications of nano-titania in theranostics and photodynamic therapy. *Biomaterials Science* 4: 40–54.

100 Urban, C., Urban, A.S., Charron, H., and Joshi, A. (2013). Externally modulated theranostic nanoparticles. *Translational Cancer Research* 2: 292–308.

101 Miller, D.L., Smith, N.B., Bailey, M.R. et al. (2012). Overview of therapeutic ultrasound applications and safety considerations. *Journal of Ultrasound in Medicine* 31: 623–634.

102 Lingeman, J.E., McAteer, J.A., Gnessin, E., and Evan, A.P. (2009). Shock wave lithotripsy: advances in technology and technique. *Nature Reviews Urology* 6: 660–670.

103 Kennedy, J., Verne, S., Griffith, R. et al. (2015). Non-invasive subcutaneous fat reduction: a review. *Journal of the European Academy of Dermatology and Venereology* 29: 1679–1688.

104 Tuziuti, T., Yasui, K., Sivakumar, M., and Iida, Y. (2005). Correlation between acoustic cavitation noise and yield enhancement of sonochemica reaction by particle addition. *The Journal of Physical Chemistry. A* 109: 4869–4872.

105 Shimizu, N., Ninomiya, K., Ogino, C., and Rahman, M.M. (2010). Potential uses of titanium dioxide in conjunction with ultrasound for improved disinfection. *Biochemical Engineering Journal* 48: 416–423.

106 Ogino, C., Shibata, N., Sasai, R. et al. (2010). Construction of protein-modified TiO_2 nanoparticles for use with ultrasound irradiation in a novel cell injuring method. *Bioorganic and Medicinal Chemistry Letters* 20: 5320–5325.

107 Yamaguchi, S., Kobayashi, H., Narita, T. et al. (2011). Sonodynamic therapy using water-dispersed TiO_2-polyethylene glycol compound on glioma cells: comparison of cytotoxic mechanism with photodynamic therapy. *Ultrasonics Sonochemistry* 18: 1197–1204.

108 Harada, A., Ono, M., Yuba, E., and Kono, K. (2013). Titanium dioxide nanoparticle-entrapped polyion complex micelles generate singlet oxygen in the cells by ultrasound irradiation for sonodynamic therapy. *Biomaterials Science* 1: 65–73.

109 Ninomiya, K., Ogino, C., Oshima, S. et al. (2011). Targeted sonodynamic therapy using protein-modified TiO_2 nanoparticles. *Ultrasonics Sonochemistry* 19: 607–614.

110 Ninomiya, K., Fukuda, A., Ogino, C., and Shimizu, N. (2014). Targeted sonocatalytic cancer cell injury using avidin-conjugated titanium dioxide nanoparticles. *Ultrasonics Sonochemistry* 21: 1624–1628.

111 Harada, Y., Ogawa, K., Irie, Y. et al. (2011). Ultrasound activation of TiO_2 in melanoma tumors. *Journal of Controlled Release* 149: 190–195.

112 Deepagan, V.G., You, D.G., Um, W. et al. (2016). Long-circulating Au-TiO_2 nanocomposite as a sonosensitizer for ROS-mediated eradication of cancer. *Nano Letters* 16: 6257–6264.

113 You, D.G., Deepagan, V.G., Um, W. et al. (2016). ROS-generating TiO_2 nanoparticlesfor non-invasive sonodynamic therapy of cancer. *Scientific Reports* 6: 23200: 1–12.

114 Wang, X., Wang, W.P., Yu, L.D. et al. (2017). Site-specific sonocatalytic tumor suppression by chemically engineered single-crystalline mesoporous titanium dioxide sonosensitizers. *Journal of Materials Chemistry B* 5: 4579–4586.

115 Dai, C., Zhang, S.J., Liu, Z. et al. (2017). Two-dimensional graphene augments nanosonosensitized sonocatalytic tumor eradication. *ACS Nano* 11: 9467–9480.

116 Shi, J.J., Chen, Z.Y., Wang, B.H. et al. (2015). Reactive oxygen species-manipulated drug release from a smart envelope-type mesoporous titanium nanovehicle for tumor sonodynamic-chemotherapy. *ACS Applied Materials & Interfaces* 7: 28554–28565.

117 Yuan, P. and Song, D.K. (2018). MRI tracing non-invasive TiO_2-based nanoparticles motivated by ultrasound for multi-mechanism therapy of prostatic cancer. *Nanotechnology* 29: 1–18.

118 Shen, S., Guo, X.M., Wu, L. et al. (2014). Dual-core@shell-structured Fe_3O_4-$NaYF_4$@TiO_2nanocomposites as a magnetic targeting drug carrier for bioimaging and combined chemosonodynamic therapy. *Journal of Materials Chemistry B* 2: 5775–5784.

119 Hoogenboom, M., Eikelenboom, D., Brok, M.H.D. et al. (2015). Mechanical high-intensity focused ultrasound destruction of soft tissue: working mechanisms and physiologic effects. *Ultrasound in Medicine & Biology* 41: 1500–1517.

120 Leinenga, G. and Götz, J. (2015). Scanning ultrasound removes amyloid-β and restores memory in an Alzheimer's disease mouse model. *Science Translational Medicine* 7: 278ra33.

121 Hana, H., Lee, H., Kim, K., and Kim, H. (2017). Effect of high intensity focused ultrasound (HIFU) in conjunction with ananomedicines-microbubble complex for enhanced drug delivery. *Journal of Controlled Release* 266: 75–86.

122 Yildirim, A., Chattaraj, R., Blum, N.T. et al. (2017). Phospholipid capped mesoporous nanoparticles for targeted high intensity focused ultrasound ablation. *Advanced Healthcare Materials* 6: 1700514.

123 You, Y.F., Wang, Z.G., Ran, H.T. et al. (2016). Nanoparticle-enhanced synergistic HIFU ablation and transarterial chemoembolization for efficient cancer therapy. *Nanoscale* 8: 4324–4339.

124 Rajh, T., Dimitrijevic, N.M., Bissonnette, M. et al. (2014). Titanium dioxide in the service of the biomedical revolution. *Chemical Reviews* 114: 10177–10216.

125 Wu, L., Su, Y.H., Yin, Z.F., and Yang, H.G. (2013). Recent progress in biomedical applications of titanium dioxide. *Physical Chemistry Chemical Physics* 15: 4844–4858.

126 Wu, S., Weng, Z., Liu, X. et al. (2014). Functionalized TiO_2 based nanomaterials for biomedical applications. *Advanced Functional Materials* 24: 5464–5481.

127 Na, H.B., Song, I.C., and Hyeon, T. (2009). Inorganic nanoparticles for MRI contrast agents. *Advanced Materials* 21: 2133–2148.

128 Wang, F., Tan, W.B., Zhang, Y. et al. (2006). Luminescent nanomaterials for biological labelling. *Nanotechnology* 17: R1–R13.

129 Hu, F.Q., Wei, L., Zhou, Z. et al. (2006). Preparations of biocompatible magnetite nanocrystals for *in vivo* magnetic resonance detection of cancer. *Advanced Materials* 18: 2553–2556.

130 Liu, D.F., Wu, W., Ling, J.J. et al. (2011). Effective PEGylation of iron oxide nanoparticles for high performance *in vivo* cancer imaging. *Advanced Functional Materials* 21: 1498–1504.

131 Yu, Q., Sun, J., Zhu, X. et al. (2017). Mesoporous titanium dioxide nanocarrier with magnetic-targeting and high loading efficiency for dual-modal imaging and photodynamic therapy. *Journal of Materials Chemistry B* 5: 6081–6096.

132 Zeng, L., Ren, W., Xiang, L. et al. (2013). Multifunctional Fe_3O_4-TiO_2 nanocomposites for magnetic resonance imaging and potential photodynamic therapy. *Nanoscale* 5: 2107–2113.

133 Lai, C.W., Wang, Y.H., Lai, C.H. et al. (2008). Iridium-complex-functionalized Fe_3O_4/SiO_2 core/shell nanoparticles: a facile three-in-one system in magnetic resonance imaging, luminescence imaging, and photodynamic therapy. *Small* 4: 218–224.

134 Zhao, C.Q., Rehman, F.U., Yang, Y.L. et al. (2015). Bio-imaging and photodynamic therapy with tetra sulphonatophenyl porphyrin (TSPP)-TiO_2 nanowhiskers: new approaches in rheumatoid arthritis theranostics. *Scientific Reports* 5: 11518–11528.

135 Zhong, Y., Wang, J.F., Zhang, R.F. et al. (2014). Morphology-controlled self-assembly and synthesis of photocatalytic nanocrystals. *Nano Letters* 14: 7175–7179.

136 Kim, H.M., An, M.J., Hong, J.H. et al. (2008). Two-photon fluorescent probes for acidic vesicles in live cells and tissue. *Angewandte Chemie International Edition* 47: 2231–2234.

137 Liu, Y.Y., Meng, X.F., Wang, H. et al. (2018). Photoelectron transfer at ZnT-PyP self-assembly/TiO_2 interfaces for enhanced two-photon photodynamic therapy. *ACS Applied Materials & Interfaces* 10: 1492–1498.

138 Řehoř, I., Vilímová, V., Jendelová, P. et al. (2011). Phosphonate–titanium dioxide assemblies: platform for multimodal diagnostic–therapeutic nanoprobes. *Journal of Medicinal Chemistry* 54: 5185–5194.

139 Wu, J., Liu, Y., Li, W. et al. (2014). Magnetically guided survivin-siRNA delivery and simultaneous dual-modal imaging visualization based on Fe_3O_4@TiO_2 nanospheres for breast cancer. *Journal of Materials Chemistry B* 2: 7756–7764.

140 Zhou, J., Meng, L., Sun, C. et al. (2018). A "protective umbrella" nanoplatform for loading ICG and multi-modal imaging-guided phototherapy. *Nanomedicine: Nanotechnology, Biology and Medicine* 14: 289–301.

141 Qin, Y., Sun, L., Li, X.X. et al. (2011). Highly water-dispersible TiO_2 nanoparticles for doxorubicin delivery: effect of loading mode on therapeutic efficacy. *Journal of Materials Chemistry* 21: 18003–18010.

142 Wu, K.C.-W., Yamauchi, Y., Hong, C.-Y. et al. (2011). Biocompatible, surface functionalized mesoporous titania nanoparticles for intracellular imaging and anticancer drug delivery. *Chemical Communications* 47: 5232–5234.

143 Flak, D., Yate, L., Nowaczyk, G., and Jurga, S. (2017). Hybrid ZnPc@TiO_2 nanostructures for targeted photodynamic therapy, bioimaging and doxorubicin delivery. *Materials Science and Engineering C* 78: 1072–1085.

144 Venkatasubbu, G.D., Ramasamy, S., Ramakrishnan, V., and Kumar, J. (2013). Folate targeted PEGylated titanium dioxide nanoparticlesas a nanocarrier for targeted paclitaxel drug delivery. *Advanced Powder Technology* 24: 947–954.

145 Wang, T.Y., Jiang, H.T., Wan, L. et al. (2015). Potential application of functional porous TiO_2 nanoparticles in light-controlled drug release and targeted drug delivery. *Acta Biomaterialia* 13: 354–363.

6

Cancer Theranostics of Black TiO_2 Nanoparticles

Ting Dai[1, 2], *Wenzhi Ren*[1*], *and Aiguo Wu*[1]

[1] *Cixi Institute of Biomedical Engineering, CAS Key Laboratory of Magnetic Materials and Devices, & Key Laboratory of Additive Manufacturing Materials of Zhejiang Province, Ningbo Institute of Materials Technology and Engineering, Chinese Academy of Sciences, No. 1219 Zhongguan West Road, Ningbo 315201, P.R. China*
[2] *The Affiliated Hospital of School of Medicine of Ningbo University, Department of Cardiology, 247 Renmin road, Jiangbei District, Ningbo Zhejiang Province, 315020, P.R. China*

CHAPTER MENU

Introduction, 185
Preparations and Properties of Black TiO_2 Nanomaterials, 187
Black TiO_2 for Phototherapy, 189
Black TiO_2 for Imaging-Guided Phototherapy, 195
Black TiO_2 for Synergistic Chemo-phototherapy, 199
Black TiO_{2-x} for Synergistic of Sonodynamic–Photothermal Therapy, 202
Overview and Further Perspective, 205

6.1 Introduction

6.1.1 Limitations of White TiO_2 Nanoparticles in Cancer Treatment

Traditional white TiO_2 nanomaterials have been widely applied in cancer treatment, which mainly attribute to their good biocompatibility, very low toxicity, stable structure, and excellent photocatalytic properties [1–5]. So far, the most important purpose of white TiO_2 nanoparticles is used as photosensitizers for photodynamic therapy (PDT) of malignant tumors over the last three decades [6–10]. White TiO_2 nanoparticles are wide band gap semiconductor materials, for example, the band gap energy of TiO_2 with anatase crystalline is 3.23 eV, which is equivalent to the energy of ultraviolet (UV) light at wavelength of 385 nm. Therefore, white TiO_2 nanoparticles require UV light to generate reactive oxygen species (ROS) for cancer PDT [11, 12]. It is well known that UV light is harmful to normal cells and its' biological tissue penetration is very shallow, which makes white TiO_2 nanomaterials meet serious obstacles for their clinical applications of

*Corresponding author: renwzh@nimte.ac.cn

TiO_2 Nanoparticles: Applications in Nanobiotechnology and Nanomedicine,
First Edition. Edited by Aiguo Wu and Wenzhi Ren.
© 2020 Wiley-VCH Verlag GmbH & Co. KGaA. Published 2020 by Wiley-VCH Verlag GmbH & Co. KGaA.

cancer PDT. To overcome this problem, many studies were carried out to move the excitation light from UV light to visible light region by modifying ligand or doping materials [13–15]. Though visible light is safe, its tissue penetration is still not deep. Compared with UV or visible light, NIR light is safe and its tissue penetration is deeper. Therefore, the development of NIR-stimulated TiO_2 for cancer treatment is the research trend in this field.

Recently, researchers have prepared a series of nanocomposites of white TiO_2 coated or coupled with upconversion materials. The prepared nanocomposites utilize the anti-Stokes luminescence properties of upconversion materials in which the upconversion materials can be excited by NIR light to emit ultraviolet light, and then white TiO_2 components are stimulated by ultraviolet light to generate ROS for cancer PDT. However, because of the limitation of upconversion luminescence efficiency and the general hypoxia in tumor tissue, the therapeutic effect of this kind of nanocomposites still needs to be improved. Compared with PDT, photothermal therapy (PTT) directly converts the absorbed light energy into heat, which can avoid the limitation of reduced therapeutic effect of PDT caused by hypoxia in tumor tissues. Therefore, development of a NIR light-stimulated TiO_2 nanomaterials for PTT of cancer will break the bottleneck of TiO_2-based tumor treatment and greatly promote its application in nano- and biomedical field.

6.1.2 Advantages of Black TiO_2 Nanoparticles in Cancer Treatment

It is very fortunate that a novel hydrogenated black TiO_2 nanomaterial was reported by S. Mao's group in 2011. The reported black TiO_2 nanomaterials, with internal crystallization-surface amorphous core–shell structure, are the reduction products of traditional white TiO_2 under high temperature. Because of Ti^{4+} is reduced to Ti^{3+}, a great number of oxygen vacancies is doped to form amorphous layer on surface of materials. The changed surface structure narrows the band gap energy from 3.2 to 1.54 eV, which represents the excitation have moved from 380 nm of UV light to 806 nm of NIR light. Meanwhile, the absorption is expanded to 1200 nm of NIR light (1.0 eV), which makes black TiO_2 exhibit property of full spectrum absorption. The changed optical properties make black TiO_2 can convert absorbed NIR light into heat or be stimulated by NIR light to generate photogenerated electrons and holes. Attributing to its excellent narrow band gap performance, black TiO_2 nanomaterials have attracted worldwide research interest in the fields of photodegradation of organic pollutants, photolysis of aquatic hydrogen, and dye-sensitized solar cells and supercapacitors. In addition, the excellent optical performance also makes black TiO_2 be promising to break the problem of UV light-stimulated white TiO_2-based cancer treatment. In this chapter, we briefly summarize the preparations and properties of black TiO_2. Then we overview recent advances of black TiO_2-based nanoparticles in cancer phototherapy (including PTT and PDT), sonodynamic therapy, and combined therapy and therapeutic visualization. Finally, we summarize the existed problems and the possible research directions of black TiO_2-based nanomaterials in the field of cancer theranostics in future.

6.2 Preparations and Properties of Black TiO_2 Nanomaterials

As a novel and high performance of photocatalytic material, black TiO_2 nanomaterials have attracted tremendous attentions in the field of energy and environment. There are many kinds of preparation methods of black TiO_2, including hydrogenation reduction, hydrogen plasma, chemical reduction, and so on. By regulating the reaction conditions of preparation methods, black TiO_2 nanomaterials with various optical properties (reduction degree) can be synthesized.

6.2.1 Hydrogenation Reduction Method

Hydrogenation reduction refers to the reduction of Ti^{4+} to Ti^{3+} on surface of TiO_2 or other reduced state of titanium through a high temperature reaction at a certain time in hydrogen atmosphere. Hydrogenation reduction results in corresponding changes in oxygen vacancy defect, amorphous, and lattice on the surface of white TiO_2 nanomaterial, thus obtaining hydrogenate black TiO_2 nanoparticles. It is seemed that hydrogenation reduction is a simple and direct method. However, the final properties of black TiO_2 products are often different, which are influenced by the amount of material and chemical properties, hydrogen pressure and concentration, reaction time, and temperature. According to the purity of hydrogen, reaction pressure and whether mixed protective gases in the reaction system, the hydrogenation reduction methods can be divided into many kinds, such as high-pressure pure hydrogen method, environmental or low-pressure pure hydrogen method, and environmental hydrogen-nitrogen and environmental hydrogen–argon methods [16–18].

Xiaobo Chen et al. prepared black TiO_2 nanomaterials through heating white TiO_2 at 200 °C for five days in pure H_2 atmosphere at the pressure of 20.0 bar. The introduction of Ti^{3+} in TiO_2 nanomaterials results in a large number of oxygen defects appearing on the surface crystal, which form an amorphous layer on the exterior of TiO_2 nanomaterials. These surface structural changes reduce the band gap energy of black TiO_2 to 1.54 eV, which makes black TiO_2 be stimulated by visible and NIR light to generate photogenerated electrons and holes. Therefore, black TiO_2 nanomaterials exhibit high performance on hydrogen generation from solar decomposed water and degradation of organic pollutants [19]. Li and coworkers heated the white TiO_2 nanowires in circumstance of ultra-high purity hydrogen at 200–550 °C for three hours under ambient pressure to prepare hydrogenated rutile nanowires. As shown in Figure 6.1, the colors of hydrogenated nanowires mainly depend on the reaction temperature, which the nanowires show yellow-green below 350 °C and exhibit black at or above 450 °C [20].

6.2.2 Hydrogen Plasma Method

By using P25 white TiO_2 as raw material (a kind of anatase and rutile mixed phase TiO_2 with an average particle size of 25 nm), Huang and coworkers using

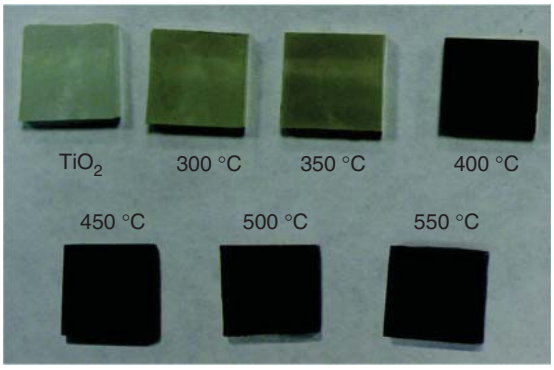

Figure 6.1 TiO_2 nanowires with rutile crystal form hydrogenated at various temperatures from 300 to 550 °C for three hours, which can obtain yellow to black color of nanomaterials. Source: Image is adapted with permission from Wang et al. 2011 [20]. Copyright 2011, American Chemical Society.

a thermal plasma furnace to synthesize hydrogenated black TiO_2 nanomaterials through hydrogen plasma reaction at 500 °C for four to eight hours. The synthesized black TiO_2 nanomaterials have obvious absorption in visible and NIR regions. The visible and NIR absorption of black TiO_2 nanoparticles increases rapidly, when the wavelength is more than 400 nm [21].

6.2.3 Chemical Reduction Method

In a chemical reduction method, black TiO_2 nanoparticles are prepared by heating of high temperature and protection of inert gas, which uses metal or reducing compounds as reducing agents. In preparation of black TiO_2 by chemical reduction method, aluminum and zinc are the commonly used metals, and sodium borohydride and imidazole are usually used as reducing compounds [22–25]. Huang and coworkers used aluminum as reductant to prepare black TiO_2 nanomaterials. In this study, white TiO_2 power and aluminum are placed in a two-zone tubular furnace. After vacuuming less than 0.5 Pa, aluminum power are heated to 800 °C, and white TiO_2 power are treated at 300–600 °C for 6–20 hours. In this reaction, the melt of aluminum causes continuous low oxygen partial pressure and results in the release of oxygen atoms from white TiO_2, which leads to form reduced black TiO_2 nanoparticles [22].

6.2.4 Properties of Black TiO_2 Nanomaterials

Good biocompatibility and unique optical properties are the basis of biomedicine application of black TiO_2 nanoparticles. Under light irradiation, black TiO_2 nanoparticles not only exhibit high photothermal conversion efficiency but also exhibit photo-induced redox activity, which provides a basis for the biomedical application of TiO_2. When TiO_2 is excited by the light that is stronger than its band gap energy, the valence band electron of TiO_2 will transit to the conduction band and leave an electron vacancy with positive charge in the valence band. These photogenerated electrons and holes can be recombined to generate thermal energy or can be delivered to the surface of nanoparticles to response to redox electrons in solution, exhibiting photocatalytic activity. Therefore, the surface of TiO_2 nanoparticles has both of anode and cathode chamber.

The molecules attached to the surface of TiO_2 nanomaterials can be oxidized and reduced simultaneously. The charge separation efficiency and the selectivity of photogenerated electron pairs dictate the efficiency of redox reaction [26]. More importantly, attributing to the appearance of Ti^{3+} on the surface, a large quantity of oxygen vacancy defects are doped in the amorphous layer of TiO_2 surface. The changes of structure results in the absorption of black TiO_2 reduced to 1.0 eV (equivalent to the energy of 1200 nm photons) and the bandgap energy reduced to 1.54 eV (equivalent to the energy of 806.8 nm photons) [16, 17, 27]. Therefore, black TiO_2 nanoparticles can be excited by visible and NIR light to generate photogenerated electrons and holes or convert absorbed light energy into heat energy. Compared with UV light, NIR light has more deep tissue penetration ability and is safe and harmless. Therefore, black TiO_2 has more efficient and extensive application prospect in the field of biomedical in comparison with traditional white TiO_2 nanomaterials.

Under aerobic conditions, reactive oxygen radicals with different redox properties and reactivity can be produced by irradiation white TiO_2 and/or black TiO_2 nanoparticles with excitation light in aqueous solution. Photogenerated holes can response with free radicals and water, which attached to the surface of TiO_2 to form hydroxyl radicals (OH, the strongest active oxygen radical, Eox = 2.7 V), while photogenerated electrons are eliminated by oxygen molecules to produce superoxide anion free radicals. These reactions are very effective in the solution of TiO_2 which establishes a foundation for TiO_2 nanomaterials' application in the field of nanomedicine [26]. These produced free radicals possess different redox characteristics, diffusion coefficients, and diffusion distances. For instance, $OH^{\bullet}$ radical contains the strongest oxidation potential and even higher diffusion coefficient. Nevertheless, because the reactivity is very high, the diffusion distance of $OH^{\bullet}$ and singlet oxygen ($_1O^2$) is very short in water, in which diffusion distance of $OH^{\bullet}$ is shorter than 20 nm, and $_1O^2$ is from 20 to 220 nm. While superoxide anion radicals ($O^{2-\bullet}$) and H_2O_2 attributing to the moderate oxidation potential, their diffusion distances can reach hundreds of microns [28]. Because of their various of reactivity and redox properties, the previously mentioned free radicals can react with biological macromolecules and proteins on the surface of cells in different distances, affect cell function, and ultimately lead to cell death, which is the property basis of the application of black TiO_2 nanoparticles in cancer diagnosis and treatment.

6.3 Black TiO_2 for Phototherapy

Phototherapy, which possesses the advantages of specific spatial/temporal selectivity and minimal invasiveness, has been generally recognized as one of the most promising cancer treatment methods. Phototherapy includes two types – one is PDT and another one is PTT. The mechanism of PDT is based on the aggregation of photosensitizers in a tumor. Light of a specified wavelength is applied to irradiate tumor site. After absorbing light energy, the photosensitizers are stimulated from ground state to excitation state and produces a large quantity of reactive oxygen radicals (mainly singlet oxygen) in the process of de-excitation.

The produced reactive oxygen radicals then destroy biological macromolecules and induce apoptosis of cancer cells. PDT has the advantages of high selectivity, non-invasiveness, and controllability [29–31]. As an effective treatment method for cancer therapy, the mechanism of PTT is mainly on account of the aggregation of photothermal agents in the tumor lesion that absorbs NIR laser and translates it into heat energy to kill the tumor cells [32–34]. Compared with traditional therapeutic methods of tumor, such as radiotherapy, chemotherapy, and surgery, phototherapy has the advantages of tumor targeting, noninvasive, and consequently highly effective; besides, it does not have the side effects that traditional treatments involved. More importantly, PTT converts absorbed light energy into heat directly, avoiding the limitation that PTT-dependent reactive oxygen radicals to achieve treatment, while tumor tissue is mostly in a hypoxic state. Therefore, PTT is a more effective treatment compared with PDT. The type of phototherapy agent is an essential factor for phototherapy and has aroused numerous concerns of many researchers. Because of the superior NIR absorption of black TiO_2 nanomaterials, it is much promising to establish a novel NIR-induced photothermal agent in both diagnosing and treating of cancer.

6.3.1 Black TiO_2 for Photothermal Therapy

The first black TiO_2-based phototherapy was reported by our group [35]. In this work, polyethylene glycol (PEG) was attached to the NIR light-induced hydrogenated black TiO_2 nanomaterials to enhance the stability in physiological environment. Then, we measured the photothermal property of PEG-coated H–TiO_2 (H–TiO_2–PEG) nanoparticles and calculated photothermal conversion efficiency. Furthermore, the toxicity and PTT performance of H–TiO_2–PEG nanoparticles were systematically studied in normal mice and breast cancer-bearing mice. Our findings proved that the photothermal conversion efficiency of H–TiO_2–PEG nanoparticles was 40.8% and the toxicity *in vitro* and *in vivo* was very low. It is clearly indicated in Figure 6.2 that PEG coating improves the dispersion of black TiO_2, after that H–TiO_2–PEG nanoparticles were irradiated by 808 nm NIR light at 2 W/cm^2 of power density for 600 seconds. The temperature of H–TiO_2–PEG nanoparticles increased to 66 °C rapidly, while pure water only reached to 28.5 °C at the same conditions, which suggests black TiO_2 is a high efficiency photothermal agent. Followed, H–TiO_2–PEG nanoparticles were injected into tumor and irradiated by 808 nm NIR laser for 300 seconds. Photothermal images show that temperature increases to 52.6 °C in H–TiO_2–PEG injected tumor, while physiological saline injected tumor only 36.5 °C at same irradiation conditions, which is tissue acceptability and tolerance. It has been considered that when the temperature exceeds 50 °C, the cancer cells will be killed in a few minutes. Therefore, the previously mentioned experimental results indicate that black TiO_2 can quickly achieve the thermal ablation of mice tumors. Therefore, on the 14th day of NIR irradiation of the H–TiO_2–PEG nanoparticles injected tumor, the tumor disappeared and leaved only smooth scars on the original tumor site. Our results demonstrated that the hydrogenated black TiO_2 nanoparticles are high performance cancer PTT agent.

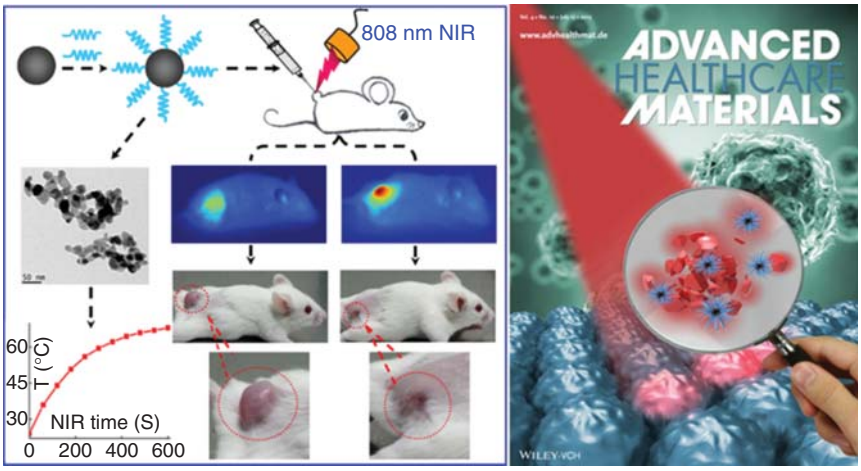

Figure 6.2 Near-infrared (NIR) light-triggered PEG-coated black TiO_2 for photothermal imaging-guided breast cancer photothermal therapy and its back-cover. Source: Image is adapted with permission from Ren et al. 2015 [35]. Copyright 2015, John Wiley & Sons.

Meanwhile, the photothermal mechanism was also discussed in this paper. Compared with traditional white TiO_2, the white H–TiO_2 nanoparticles turns to black; therefore the absorption of H–TiO_2 nanoparticles increased in visible and NIR region. The enhanced spectrum absorption of H–TiO_2 is probably related to a great amount of deep Ti^{3+} defects on the surface of nanoparticle after hydrogenation treatment. The electron paramagnetic resonance (EPR) spectrum shows that there is no signal in white TiO_2, indicating few numbers of defects in white TiO_2; while H–TiO_2 shows very strong signal, suggesting a large amount of Ti^{3+} in H–TiO_2. It has been considered that new electronic state will be formed below the materials' conduction band during Ti^{3+} reduced by hydrogenation. In this situation, attributing to the valence band of TiO_2 changes to new electronic states or translate new electronic states to the conduction band of TiO_2, the absorption of H–TiO_2 is significantly enhanced in visible and NIR regions.

To reveal the photothermal process, light-induced EPR was carried out. The results show that compared with white TiO_2 nanoparticles, H–TiO_2 exhibits more efficiency in photogenerated electrons separated from holes. Furthermore, the O^- signal intensity of H–TiO_2 nanoparticles decreases significantly, and the inverted broad resonance appears at 1.957 of average g value. The results indicate the decrease of Ti^{3+} in H–TiO_2 during irradiation may be because the photogenerated holes and locally Ti^{3+} combine together.

It has been considered that the releasing of phonons in nonradiative recombination is the major way for photogenerated charge-annihilation in semiconductor with high concentration deep level defect. In this process, energy exchanged with the form of lattice vibration; therefore the thermal energy in the material increased, which means the thermal energy is produced through lattice vibration in the materials [27]. During this procedure, energy converted in the form

of lattice vibration increases thermal energy of the material. Therefore, the photothermal performance of black TiO_2 nanoparticles may be due to the significant enhancement of non-radiative recombination caused by Ti^{3+} deep-level defects. These findings indicate that the prepared black TiO_2 nanoparticles are as promising as PTT agents for cancer treatment study in the field of nanomedicine. As a back-cover paper, this work was published on Advanced Healthcare Materials in 2015 and has attracted much attentions in the field of cancer theranostics.

As a photothermal agent, photothermal efficiency and biocompatibility are two key factors for cancer PTT. The safety of TiO_2 nanomaterials have been demonstrated by variously applied TiO_2 as food additives [27, 36, 37]. However, how to explain the photothermal process of the black TiO_2 and how to improve the materials' photothermal performance are still challenges of the field. Followed, in 2016, a titanium oxide-based photothermal agent was reported by Liu and coworkers; this nanoplatform possesses high photothermal efficiency and good biocompatibility for cancer PTT [38]. The reported Ti_8O_{15} nanomaterials with Magnéli-phase were synthesized by the arc-melting method, which can absorb more than 98% of NIR light and an excellent PTT efficiency in the tumor-bearing mice. In addition, the Ti_8O_{15} nanomaterials also exhibit a good biocompatibility.

Although titanium oxide-based photothermal agents has been fascinated in the field of cancer theranostics, regulation of their photothermal performance is still limited. High photothermal conversion is a major performance for photothermal agent. Much effort has been explored to improve the photothermal conversion of black TiO_2. In 2017, Miao Yu and coworkers used $NaBH_4$ as reducing agent to supply H_2 under high temperature, prepared core–shell structured black TiO_2 nanomaterials for cancer PTT by this relative mild method [39]. The reported black TiO_2 nanomaterials shows an interior crystalline core and exterior amorphous layer with about 1 nm of thickness. The characterization results show different from the traditional white TiO_2 nanomaterials that exhibits 95% reflectance in visible and NIR region; the core–shell black TiO_2 nanomaterials possess enhanced absorption from 420 to 1000 nm, which covers NIR region. More importantly, the prepared black TiO_2 nanomaterials show 55.2% of high photothermal conversion. The excellent photothermal performance makes the core–shell black TiO_2 exhibits high efficiency of tumor ablation. This study also explored photothermal mechanism of black TiO_2 nanomaterials. The enhanced optical property is mainly induced by hydrogenation caused by oxygen vacancies that results defect levels on surface of the nanoparticles. However, it is very interesting that excessive oxygen vacancies induced large quantities of surface defects will decrease instead of increase the thermal conductivity, which weaken photothermal conversion efficiency of prepared black TiO_2 nanomaterials. Therefore, the photothermal performance of black TiO_2 will be mainly decided by how to regulate the degree of hydrogenated reduction as well as find the appropriate ratio of crystallization and amorphous on surface of black TiO_2. In short, the findings about the photothermal mechanism of black TiO_2 will provide a guideline for synthesis high photothermal performance of black TiO_2 as well as hydrogenated semiconductor materials, which will improve black TiO_2's application study in the field of nanomedicine.

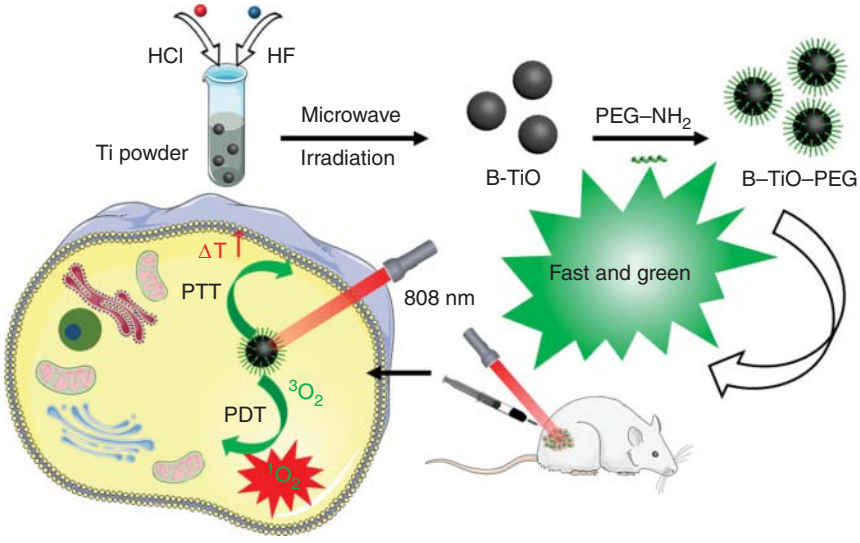

Figure 6.3 Preparation of black TiO nanomaterials by microwave-assisted method and their application in photothermal–photodynamic synergistic therapy of tumor-bearing mice. HF, hydrogen fluorid. Source: Image is adapted with permission from Shu et al. 2018 [40]. Copyright 2011, American Chemical Society.

More and more studies have shown that black TiO_2 nanomaterials have become new stars in the field of light-triggered cancer treatment due to the excellent photothermal properties and good biosafety of black TiO_2. However, the preparation of black TiO_2 nanomaterials generally requires high temperature, inert gas protection, and hydrogen reduction, which are complex and are consuming a lot of time. Therefore, it will be a realistic need to develop a new and simple method to prepare black TiO_2 for phototherapy of cancer. Very recently, Xuejun Zhang and coworkers reported a one-step synthesis for preparation of black TiO_2 nanoparticles through microwave-assisted hydrothermal method. As shown in Figure 6.3, the black TiO_2 can be fast facile prepared with only Ti powder, hydrofluoric acid, and hydrochloric acid, but without the reducing agent as well as high-temperature [40]. The reported black TiO_2 nanomaterials is about 52 nm, which possess as high as 50% of photothermal conversion efficiency and excellent ROS generation performance under irradiation of 808 nm light. Consequently, the prepared black TiO_2 nanomaterials exhibit significant synergistic effect of photothermal and PDT induced by a single 808 nm of NIR laser. In brief, the microwave-assisted method reported in this study provides a simple and fast synthesis of black titanium nanomaterials and therefore promotes the application of black titanium-based materials in nanomedicine.

Compared with ultraviolet and visible light, the traditional NIR light (NIR-I, 700–900 nm) do increase the tissue penetration depth, but the penetration depth is still not satisfying. Therefore, researchers turn sight to the NIR-II light (1000–1700 nm), which possess better tissue penetration depth and large excitation wavelength range. However, related reports about NIR-II photothermal

nanoparticles are very limited, thus Zeng et al. developed hyaluronic acid modified Ti_2O_3 nanoparticles as NIR-II PTT platform to enhance light absorption and photothermal conversion ability. Because of these advantages, the Ti_2O_3 nanoparticles showed strong ability to kill cancer cells and excellent therapeutic effects under NIR-II laser irradiation [41].

6.3.2 Black TiO_2 for Photodynamic Therapy

TiO_2 nanoparticles have the advantages of low toxicity, stable structure, and photoresponse capability and have promising prospects in PDT for cancer treatment; however, they possess good capability of PDT only under ultraviolet excitation. It is well known that ultraviolet irradiation is a significant factor of genetic mutations, which damages healthy cells, and has very shallow penetration depth. Therefore, cancer PDT with TiO_2 encountered bottleneck due to ultraviolet excitation. Although researchers can dope or modify nanoparticles surface to change the excitation wavelength of TiO_2 from ultraviolet to visible light, the penetration ability is still weak [13]. Compared with ultraviolet and the light in the visible region, NIR light is a safe electromagnetic wave with strong tissue penetration force. Besides, deeply penetrating NIR laser can be converted into ultraviolet light to stimulate ROS by synthesizing upconversion-based TiO_2 photosensitizing nanoplatform [31]. But due to the limit of low upconversion efficiency, the therapeutic effects of these nanocomposites still need to be further improved. Using NIR laser to directly excite TiO_2 for generating ROS for PDT can avoid ineffective treatment caused by low upconversion luminescence efficiency. Accordingly, developing a NIR laser-triggered TiO_2-based nanoplatform for cancer PDT will considerably promote future applications of TiO_2 in biomedicine.

Recently, Yang et al. reported excellent photodynamic activity by using Au clusters anchored black anatase TiO_{2-x} nanotubes. The Au nanoclusters were used as PDT agent, and the nanotube structure provides a direct channel for electron transition, and the density of Ti^{3+} in the surface of TiO_2 enhanced due to the gaseous reduction process of anatase TiO_2, which can suppress the electron and hole pairs recombinant effectively and expend the light region as well as tissue penetration depth. In addition, the charge separation efficiency increased after modification of Au clusters. All the previously mentioned features contribute to the markedly improved therapeutic efficacy [42].

6.3.3 Black TiO_2 for Synergistic Photothermal and Photodynamic Therapy

As mentioned earlier, traditional white TiO_2, with 3.2 eV of band gap, can be excited by UV light to produce ROS for cancer PDT. When it comes to black TiO_2, most studies applied these nanomaterials as photothermal agent for cancer PTT. Recently, Mancheng Gong and coworkers reported novel black TiO_2 nanoparticles that can be use as both PDT and PTT [43]. Using a facile calcination way to prepare the reported nanoparticles, the narrow band gap of nanoparticles were ~2.32 eV, which can be stimulated by 808 nm of NIR. Their results suggested the

black TiO_2 nanoparticles, as efficient photosensitizers for PDT and PTT, exhibited low toxicity as well as high antitumor activity *in vitro*. In summary, these works provide experimental models for application of black TiO_2 nanoparticles in cancer therapy. Their results confirmed that NIR-triggered-PTT/PDT can overcome the limitations of UV light-stimulated PDT and broaden the applications of TiO_2 in biomedicine.

Besides single NIR laser-induced combination treatment of PTT and PDT, black TiO_2 can be also combined with other functional materials to achieve multifunctional therapy and promote wound healing. Like Xiaochen Wang et.al who reported in their research that they incorporated nanosized black TiO_2 into the chitosan-based thermosensitive hydrogel, which can fill irregular parts, defend against microorganisms, and deliver therapeutic nanoplatforms to the damaged areas as well as promote wound healing. In addition, these composite nanoplatform possesses PTT and PDT effects simultaneously under single wavelength NIR laser excitation, which can eliminate residual cancer cells in a short time and promote skin tissue regeneration in the prognosis. All of the advantages contribute to the exceptional therapeutic performance of these nanoplatform on skin tumors both *in vitro* and *in vivo* [44].

6.4 Black TiO_2 for Imaging-Guided Phototherapy

Imaging-guided tumor therapy can monitor the therapeutic effect, improve the therapeutical accuracy, regulate the treatment plan in time, and reduce the damage to health tissues. In addition, nanoparticle-based imaging can monitor and dynamically evaluate the operation, accumulation, and metabolism of nanoparticles *in vivo*; therefore, it is a developing trend in the field of cancer theranostics [45–49]. At present, there are eight kinds of main medical imaging technologies, which are photothermal imaging (PTI), photoacoustic imaging (PAI), magnetic resonance imaging (MRI), fluorescence imaging (FI), ultrasound imaging (USI), computed tomography (CT), emission computed tomography (ECT), and Raman imaging (RI), respectively [50–54]. Each imaging modality has its advantages and limits. For instance, PTI has good temperature sensitivity and can be used for real-time monitoring, but its spatial resolution is poor. For FI, its benefits are high sensitivity and multi-color imaging, however, the disadvantages include low spatial resolution and poor tissue permeability which make FI only suitable for surface imaging [55]. MRI is a method of performing images of the human body by the interaction of an external magnetic field and an object, such as a hydrogen proton. The advantages of MRI are high spatial resolution, none-limited tissue penetration ability, and safety of no-radioactivity, but its sensitivity needs to improve, and the required time of imaging is very long. PAI is a newly emerging biomedical imaging technique, which is non-invasive and non-ionizing radiation. When the biological tissues are irradiated by the laser radiation, it absorb the light and convert it to heat. In the meantime, biological tissues can generate supersonic wave by thermal vibration, and these acoustic signals are stimulated by light and thus produce photoacoustic signal. The photoacoustic signal generated by biological tissues possesses absorption characteristics of the tissues and can convert

optical absorption to visual images specifically by detecting and reconstructing the photoacoustic signal. PAI possesses many advantages, including deep penetration of USI and high sensitivity of optical imaging, and it can also realize deeper *in vivo* optical imaging with more than 50 mm penetration depth and the resolution up to micron even submicron. Compared with PTI and MRI, PAI exhibits very higher resolution and also possesses more depth tissue penetration than that of FI, but imaging speed of PAI is still not enough for clinical application [56, 57]. In order to improve resolution and sensitivity of cancer imaging, as well as to overcome limits of each single imaging modality, nanoparticle-based dual modal or multimodal imaging has become the development direction [58–60].

Among the several imaging modalities, when it comes to black TiO_2-based imaging-guided phototherapy, the most reported dual modal or multimodal imaging combines PTI with PAI or MRI, which is determined by the essential attributes of black TiO_2 nanoparticles. As a photothermal agent, black TiO_2 can convert its absorbed NIR into heat, then record and reconstruct image by infrared thermal imager. Because of photothermal effect, black TiO_2 aggregated in tumors can cause thermal vibration of tumors tissue. The vibration ultrasound generated by black TiO_2 can be reconstructed into tumors image after receiving by PAI system. Therefore, black TiO_2 itself can act as both PAI and PTI contrast agent.

It has been considered that PTI/PAI dual-model imaging not only combine the advantages of good temperature sensitivity, very high resolution, real-time monitoring, and depth tissue penetration but also avoid the limitations of each single imaging mode [61]. In 2016, Hangrong Chen and Jianlin Shi's group reported a single NIR-triggered black TiO_2 nanoplatform for PTI/PAI dual-modal imaging-guided phototherapy [62]. Under guidance of PTI/PAI dual-modal imaging, combination of PDT and PTT can avoid the decrease of PDT effect caused by hypoxia of tumor tissue, and produce synergistic therapeutic effect. Their results show PTI of the tumor-bearing mice after different treatments. As we expected, under the excitation of 808 nm NIR laser, there is a significant PTI enhancement after the mice administration with black TiO_2, which demonstrates that photothermal nanomaterial is a high performance of PTI contrast agent. Meanwhile, the results show three-dimensional USI/PAI of the tumor injected with or without black TiO_2 at different time intervals. It can be observed that PAI exhibits much higher resolution and distribution of black TiO_2 in tumor. Furthermore, PAI shows the strongest signal at the first five second post-injection of the nanoparticles, when it is compared with other time points after administration of the black TiO_2. According to the author's explanation, it attributes to the rapid clearance of black TiO_2 in blood circulation.

As a commonly used clinical imaging method, MRI has the advantages of high resolution of soft tissue, infinite penetration depth, precise target location, no radioactive contamination, and can display the blood supply characteristics of solid tumor [63–66]. Therefore, MRI has become a commonly used imaging method for cancer diagnosis. Furthermore, the diagnostic effect on the lesion location can be further improved by using the contrast agent of MRI. Currently, there are two types of MRI contrast agent. One is superparamagnetic contrast agents for T_1 weighted imaging, such as Gd^{3+} chelate; another is paramagnetic

contrast agent that is suitable for enhancement of T_2 weighted imaging, such as Fe_3O_4 nanoparticles [67–69]. Considering the advantages of MRI, black TiO_2 nanoparticles have been combined with MRI contrast agents for MRI-guided phototherapy.

Among all kinds of cancers, pancreatic cancer has high malignancy, rapid metastasis, and poor prognosis, which make the five-year survival of pancreatic cancer patients less than 8% [70, 71]. It has been demonstrated that pancreatic cancer stem cells (PCSCs), with high expression of transmembrane glycoprotein CD133, show resistance to chemotherapy and tumorigenesis, which is therefore the major cause of pancreatic cancer's metastasis and recurrence [72]. Recently, our group constructed black TiO_2-based nanoprobes for phototherapy of pancreatic cancer stem-like cells under the guidance of T_1-weighted MRI [73]. Figure 6.4a is the synthesis process of $bTiO_2$–Gd–CD133mAb nanoprobes. The $bTiO_2$ nanoparticles were loaded with DOTA–Gd and conjugated with CD133 monoclonal antibodies (CD133mAbs) to form the $bTiO_2$–Gd–CD133mAb nanoprobes with PCSC targeted T_1-weigthed MRI ability. As Figure 6.4b,c illustrated, dispersibility of the nanoprobes is enhanced after modified with NH_2–PEG–COOH and conjugated with CD133mAbs. Energy dispersive spectrometer (EDS) spectrum of $bTiO_2$–Gd–CD133mAb shows Ti and Gd elements contained in the nanoprobes, which suggests successful loading of DOTA–Gd on $bTiO_2$ nanoparticles. In Figure 6.4a, when the cells incubated with $bTiO_2$–Gd–CD133mAb or $bTiO_2$–Gd, the colors show dark gray, which

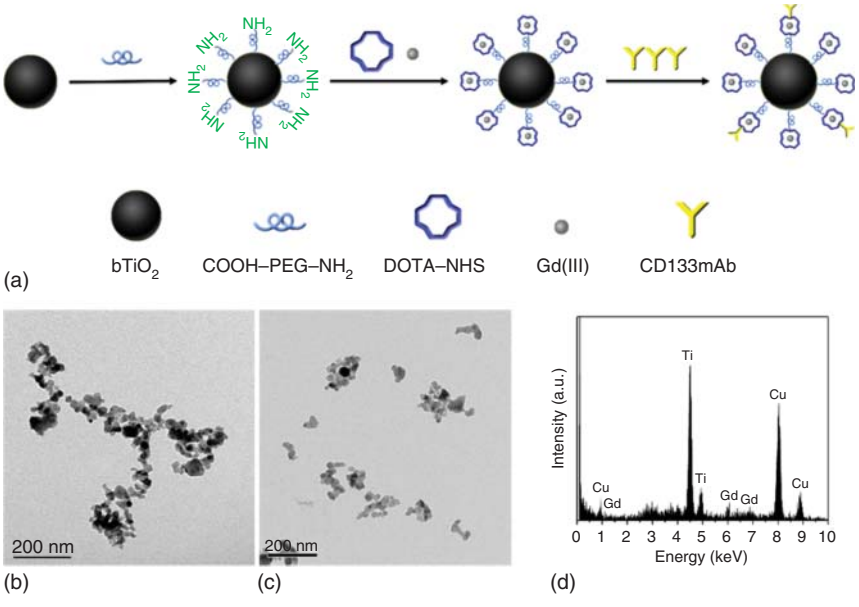

Figure 6.4 (a) Scheme of the synthesis process of Gd loaded, CD133mAb-conjugated black TiO_2 ($bTiO_2$–Gd–CD133mAb) nanoprobes. (b) TEM images of $bTiO_2$. (c, d) TEM and EDS images of $bTiO_2$–Gd–CD133mAb nanoprobes. Source: Image is reproduced with permission from Wang et al. [73]. The Royal Society of Chemistry.

suggests the black TiO_2 nanoprobes were uptake by the stem-like cells. Furthermore, $bTiO_2$–Gd–CD133mAb incubated cells show darker than that of $bTiO_2$–Gd group, which indicates CD133mAb conjugation gives the nanoprobes targeting ability on pancreatic cancer stem-like cells. T_1-weighted MR images in Figure 6.4b shows that the Magnevist, a commercial contrast agent, cannot stain the stem-like cells. However, $bTiO_2$–Gd–CD133mAb incubated stem-like cells manifest much brighter T1-weighted MR images than $bTiO_2$–Gd group, its main attribute to conjugation of CD133mAb. This phenomenon is further proved by quantitative MR signal intensity. The values are 148 ± 4.1, 163 ± 3.7 and 195 ± 4.4 in control, $bTiO_2$–Gd, and $bTiO_2$–Gd–CD133mAb group, respectively. These results support that prepared $bTiO_2$–Gd–CD133mAb are promising nanoprobes for targeted T1-weighted MRI guided PTT on pancreatic cancer stem-like cells.

Although Gd-based MRI contrast agents are widely used in clinic, rare earth Gd is a heavy metal element, which has potential safety risks. Thanks to an essential element of human body, iron-based MRI contrast agents, such as Fe_3O_4 nanoparticles, which has become a hot field of cancer theranostics at present [74–78]. Recently, our group prepared tunable fabricated Fe_3O_4–black TiO_2 nanocomposites for MRI-guided dual wavelength triggered synergistic phototherapy of cancer [79, 80]. As shown in Figure 6.5a, the b-TiO_2 nanoparticles were anchored on the surface of Fe_3O_4 nanoparticles through a smart strategy to form Fe_3O_4–black TiO_2 nanoplatforms (Fe–Ti NCs). Under the irradiation of 671 and 808 nm of laser, the Fe–Ti NCs can generate both ROS and heat. It is very interesting that under the irradiation of 671 nm laser at lower power density, a brighter green fluorescence can be seen in Figure 6.5b, which suggests the Fe–Ti NCs generate more ROS under a shorter wavelength stimulation. Figure 6.5c gives an enhanced dark imaging signal (T_2 MRI) of the tumor after intratumor injection of Fe–Ti NCs. Under the guidance of T_2-weigthed tumor MRI, compared with Phosphate Buffer Saline (PBS), PBS + irradiation, and Fe–Ti NCs groups, both Fe–Ti NCs + 808 nm and Fe–Ti NCs + 671 nm group exhibit significant tumor ablation effect. Our results verify the as-prepared Fe–Ti nanocomposites are high performance nanoprobes for imaging-guided cancer phototherapy.

As mentioned in multimodal imaging, consideration of the high complementarity of MRI, PAI and PTI in resolving, sensitivity, three-dimensional imaging, temperature sensitive, and imaging depth, multimodal imaging of MRI/PAI/PTI can obtain more comprehensive information, such as high resolution, high sensitivity, and accurate imaging information for lesion localization. By using one-step hydrogen reduction, Professor Lin Jun's group reported multifunctional Fe@γ-Fe_2O_3@H–TiO_2 nanoplatforms, which obtained a multilayer structure [81]. According to the calculation using Vienna ab initio simulation package based on the density functional theory, H–TiO_2 and γ-Fe_2O_3 show more circuit loops for electron transitions, which improves photothermal transition efficiency of Fe@γ-Fe_2O_3@H–TiO_2 NCs. Their results indicated that H–TiO_2 shell played dual functions as photothermal agent and catalytic agent at the same time with the structure of Fe@γ-Fe_2O_3@H–TiO_2 NCs, and Fe@γ-Fe_2O_3 core can be used not only as magnetic-separation agent but also as magnetic-targeted agent. In addition to the solar light-responsive

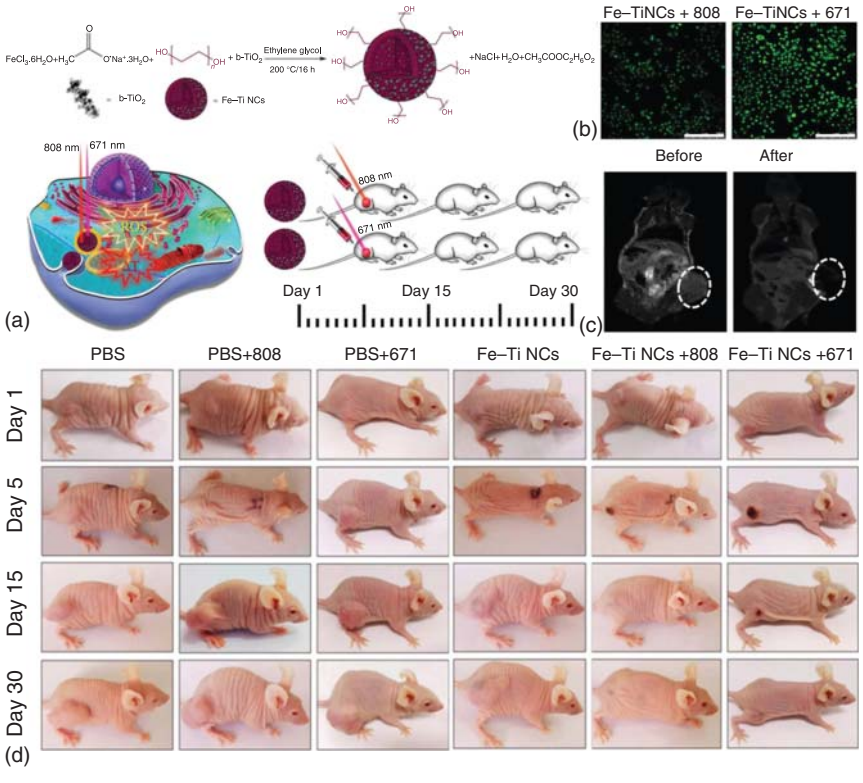

Figure 6.5 (a) Illustration of synthesis of dual wavelength of 671 and 808 nm triggered synergistic PDT and PTT in breast tumor-bearing mice. (b) Cellular ROS detection by 2′,7′-dichlorofluorescin (DCF) in MCF-7 cells under 1.3 W/cm^2 of 808 nm and 1.0 W/cm^2 of 671 nm laser irradiations in presence of Fe–Ti NCs. Scale bar: 250 mm. (c) T_2-weigthed MRI of the human breast cells seeded tumor-bearing mice before and after injected Fe–Ti NCs (0.5 mg/ml). (d) Tumor ablation images of mice after different treatments from 1st to 30th day. Source: Image is reproduced with permission from Saeed et al. 2019 [80]. Royal Society of Chemistry.

photocatalyst, which aims to degrade organic dyes and can be separated and recovered by a magnet, the as-prepared nanocomposites can also be applied for NIR-triggered magnetic-targeted PTT under the guidance of multimodal imaging of MRI/PAI/PTI.

6.5 Black TiO_2 for Synergistic Chemo-phototherapy

Due to the lack of targeting, chemotherapeutic drugs are easy to damage normal tissues while killing cancer cells. In the late years, phototherapeutic agent-based drug carriers have been developed very well, in combination of each treatment's advantages. The nanocarriers take drugs safely and accurately to the lesion site, then controlled release the drugs by some stimulations, reduce the loss of chemotherapeutic drugs, enhance therapeutic efficiency, and protect normal

tissues. Furthermore, because of thermal ablation, cancer cells become more sensitive to chemotherapeutic drugs, not only overcomes the limited penetration depth of NIR light resulted incomplete ablation of tumors, but also shows the synergistic combination of PTT and chemotherapy. Therefore, controlled-release chemotherapeutic drugs using phototherapy-nanomaterials as carriers has become the development trend in the field of cancer theranostics [82–85].

TiO_2 based-nanoplatforms have been investigated systematically both *in vitro* and *in vivo* with respect to the drug delivery [86–89]. Our previous research has proved that doxorubicin (DOX) integrated TiO_2 nanoplatforms can get over multiple drug resistance of breast cancer cells. In addition, *in vivo* researches have indicated that TiO_2 nanoplatforms possess the ability to decrease the systemic toxicity of the drug and increase anticancer efficacy of DOX [90, 91]. Two key properties in drug carriers are the high content drug loading and the controlled drug release. Nevertheless, in most reported TiO_2 nanoplatforms, the drugs were usually carried on the surface of TiO_2. Therefore, drug loading capacity was insufficient because the surface area of TiO_2 nanoparticles are limited. Just like mesoporous silica ($mSiO_2$) drug carriers, an ideal drug carrier usually obtain excellent dispersibility as well as large loading capacity in aqueous solution [92–94]. It is essential to synthesize $mSiO_2$-coated TiO_2 core–shell nanocarriers, because it can improve TiO_2's drug loading capacity and aqueous dispersibility. In the meantime, the synergistic therapy ability of TiO_2 nanoparticles are preserved after coating with a mesoporous structure. In 2017, our group prepared a novel kind of 808 nm NIR laser-induced $mSiO_2$-coated black TiO_2 core–shell nanoplatform to enhance drug loading capacity of TiO_2 nanocarriers and to strengthen the treatment performance of synergistic chemo-phototherapy [95]. Our previous research has proved that folic acid (FA) has the specific targeting ability to target breast cancer cells, because the membrane of the cancer cells expresses FA receptor strongly [96]. As we can see in Figure 6.6a, FA is loaded onto core–shell nanoplatforms of $mSiO_2$-coated black TiO_2 to increase the uptake ability of nanocarriers *in vivo*, after that, DOX is integrated to the nanoplatforms for 808 nm NIR laser-induced PTT coordinated chemotherapy of breast cancer. Figure 6.6b gives the transmission electron microscope (TEM) results of as-prepared core–shell $mSiO_2$-black TiO_2 nanocomposites. The results demonstrated that DOX-loaded FA integrated $mSiO_2$-coated black TiO_2 core–shell nanoplatforms are not only pH-responsive but also NIR-accelerated drug-release carriers. The drug release curves of these nanocomposites in buffer solution at pH 5.0 and 7.4 with or without NIR laser excitation are demonstrated in Figure 6.6c. The accumulative release of DOX up to 74.1% at pH 5.0 and 60.6% at pH 7.4 in 48 hours indicates that the nanocomposites are pH responsive. When pH value of the buffer solution is 5.0, DOX accumulative release increase to 91.3% after irradiated by NIR laser, which is the result of the photothermal effect based on our previous study [97]. Figure 6.6d shows the different state of tumor after treatments on the 1st day and 14th day. It is clearly indicated that the size of tumor in the NC–FA–DOX + NIR group is remarkably suppressed compared with the NC–FA + NIR or NC–FA–DOX groups, suggesting that the combination treatment is more effective and promising than single PTT or chemotherapy. In summary, this research investigated a black TiO_2-based

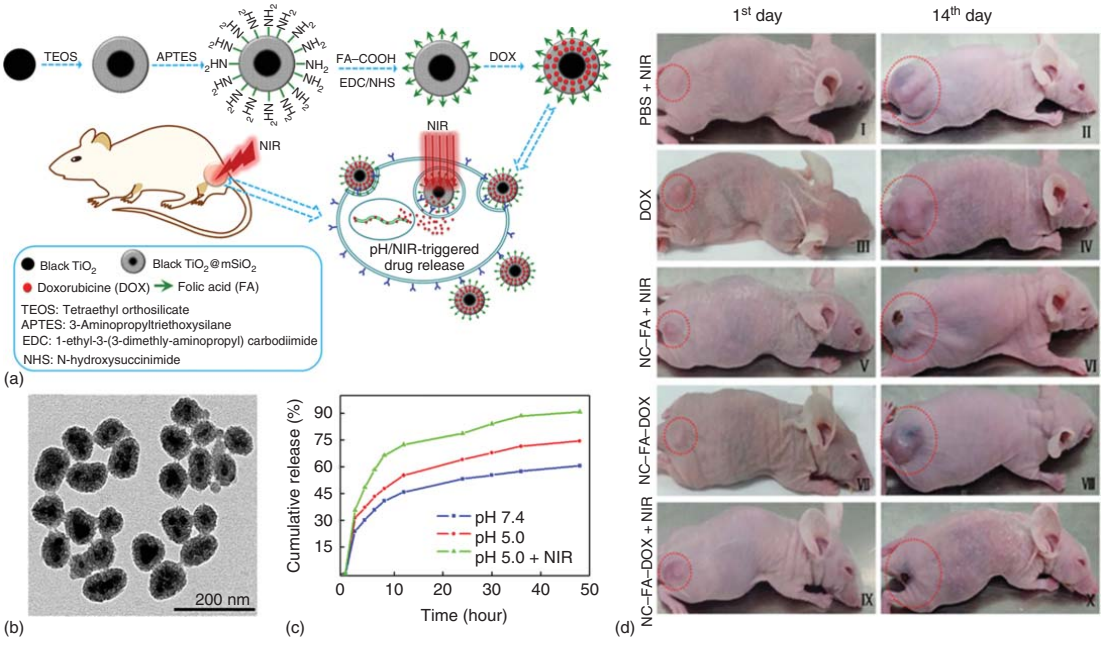

Figure 6.6 (a) Scheme of synthesis of the folic acid conjugated, doxorubicine loaded, mesoporous SiO_2-coated black TiO_2 (NC–FA–DOX) nanomaterials and their application in 808 nm NIR-stimulated photothermal therapy synergistic chemotherapy for breast cancer model. (b) High resolution TEM images of black TiO_2@SiO_2 nanomaterials. (c) The drug release-curve of NC–FA–DOX nanomaterials exhibiting pH responsive and NIR accelerated property. The group of pH 5.0 + NIR was irradiated by 2 W/cm^2 of 808 nm NIR laser for 15 minutes before detection of DOX at each time point. (d) Digital photos of human breast cancer MCF-7 cells seeded tumor-bearing mice undergoing various of therapies and their tumor changes at the 1st and 14th after treatments. Source: Image is reproduced with permission from Ren et al. 2017 [95]. Royal Society of Chemistry.

emerging core–shell nanocomposite for associative PTT–chemotherapy of breast cancer, and extended TiO_2 nanoparticles' application in the field of nanomedicine simultaneously.

Benefits from imaging-guided tumor therapy, professor Shaoqin Liu's group reported FI/PAI bimodal cancer imaging as well as NIR-induced chemotherapy–PDT–PTT, three model synergistic therapy based on black TiO_{2-x} nanoparticle [98]. Their results suggest that, in the NIR region, the sphere matrix of TiO_{2-x} nanoparticle obtains very strong optical absorption, and after NIR laser excitation, it can generate both hyperthermia and ROS and therefore exhibits triple functions of PDT, PTT, and photoacoustic tomography (PAT) imaging accordingly. In addition, the TiO_{2-x} sphere matrix contains ordered mesoporous channels in it, which make it possible for the nanocomposite to obtain drug loading capacity after encapsulated by the polydopamine layer. The polydopamine layer is sensitive to pH value and possesses a shell with photothermally sensitive ability for DOX controlled releasing. In the end, attaching a fluorescent molecule, named Cy5.5, to the outer layer of polydopamine can realize the fluorescence tumor imaging. Both *in vitro* and *in vivo* anti-cancer studies showed the advantages of triple synergistic treatments, which can significantly restrain the growth of cancer and even completely eliminate the solid tumor. The mechanism of anti-cancer effect was proved as combined effects of DNA damage caused by DOX, as well as mitochondrial dysfunction/change of membrane induced by PDT/PTT. Moreover, B-mode ultrasonography observed that the eradication of solid tumors is caused by the liquefaction necrosis of the tumor tissue.

6.6 Black TiO_{2-x} for Synergistic of Sonodynamic–Photothermal Therapy

Nowadays, the main methods based on ultrasonic wave for cancer therapy in clinic are ultrasound cavitation (UC) and high intensity-focused ultrasound (HIFU). UC is a process that microbubbles exist in the liquid, namely, cavitation nuclei, vibrate, get bigger, and continue to accumulate ultrasonic energy owing to the effect of ultrasonic; when the accumulated energy researches some threshold, these microbubbles collapse and explode rapidly. The energy released by the explosion can generate instantaneous high temperature and high pressure, as a result, having the killing effect on the nearby cancer cells [99–101]. However, the time needed for the energy released by the explosion is very short, the killing effect of UC needs to be improved. HIFU is a non-invasive ablation technique for cancer. It can focus high energy ultrasonic on lesion and can lead to tissue necrosis in ablation area by the instantaneous high temperature and high pressure produced by ultrasonic. Compared with the traditional treatment, HIFU have several advantages, such as safe, no need of operation, no bleeding, eliminate superficial tumors entirely, stimulate the body's immune system, and so on, therefore performing good therapeutic effect on the treatment of solid tumors [102–104]. The ultrasonic energy attenuate rapidly because it absorbed by tissue in the process of transmission *in vivo*. As a result, the ablation

effect of HIFU is not satisfied enough for the deep-sited tumor. Enhancing the output power do compensate for the tissue absorption in clinic; however, it will lead to tissue damage on the ultrasonic transmission pathway. In conclusion, the treatment techniques based on the ultrasonic, whether UC or HIFU, all need an efficient sensitizer to improve the therapy effects. Consequently, the sonodynamic therapy, which is based on the principle of PDT, provides an ideal sensitizer for both UC and HIFU [105–108].

Sound dynamic therapy (SDT) is a novel method of cancer therapy based on the theory and technology of PDT [109]. The basic principle of SDT is to stimulate the sonosensitizers accumulated in the tumor tissue by the specific frequency and power of ultrasound, which can produce ROS and kill the tumor cells. SDT has the advantages of non-invasive and selective of PDT, and deeper penetration depth (5–10 cm) and focus ability [110–112]. At present, most of used organic sonosensitizers have some phototoxic side effects, and their structures are unstable in presence of ultrasound produced ROS. In 2011, Terasaka's group from Hokkaido University reported ultrasound-stimulated white TiO_2 as inorganic sonosensitizers for cancer SDT [113]. Compared with organic sonosensitizers, inorganic sonosensitizers of white TiO_2 has the advantages of non-phototoxicity, stable structure, and the increased ability of permeability and retention in tumor. Therefore, the treatments of cancers with white TiO_2-based SDT has attracted much attentions of researchers [114–119].

However, considering the excellent natures of black TiO_2 introduced earlier, it is very fascinating to explore the black TiO_2-based SDT. In addition, NIR light with 808 nm has been widely used in black TiO_2-based photothermal and photodynamic therapies. Although 808 nm of NIR has increased the penetration depth of light for phototherapy, the treatment effects of it in tumor are still not quite satisfactory and ideal. Recent studies about photo-based therapy has been concentrated on wavelength from 1000 to 1350 nm (NIR-II biowindow), because the wavelength region of NIR-II biowindow is very long, which can increase the penetration depth and make the maximum permissible exposure become larger [120–123]. Therefore, NIR-II triggered black TiO_2-based phototherapy is more promising in future for treatment of deep tumor. Recently, based on the black TiO_2 nanoparticle, professor Jun Lin's group first reported a simultaneous SDT and PTT treatment in the NIR-II biowindow [124]. Figure 6.7a shows scheme of the fabricated core/shell-structured black TiO_2 nanoplatform by using a facile aluminum-reduction progress. To promote the dispersity in aqueous solution and enhance the biomedical applications, NH_2–PEG was attached to the surface of black TiO_2 nanoparticles. Figure 6.7b is the diagrammatic sketch of synergistic interactions of PTT and SDT by PEG coated black TiO_2 to treat cancer. Figure 6.7c is high-resolution TEM of black TiO_2 nanoplatform, which clearly showed that the nanoplatform possesses a classic core/shell structure, which the surface of the nanoplatform obtains a distinct oxygen-deficient amorphous shell and inside is a single-crystalline core. Inset of Figure 6.7c is the selected area electron diffraction (SAED) pattern that shows the single-crystalline structure of black TiO_2 nanoplatform. As shown in Figure 6.7d, compared with PTT or SDT alone, the tumor was totally eliminated by the combined photothermal ablation and US irradiation; what's more, it had no recurrence in the subsequent

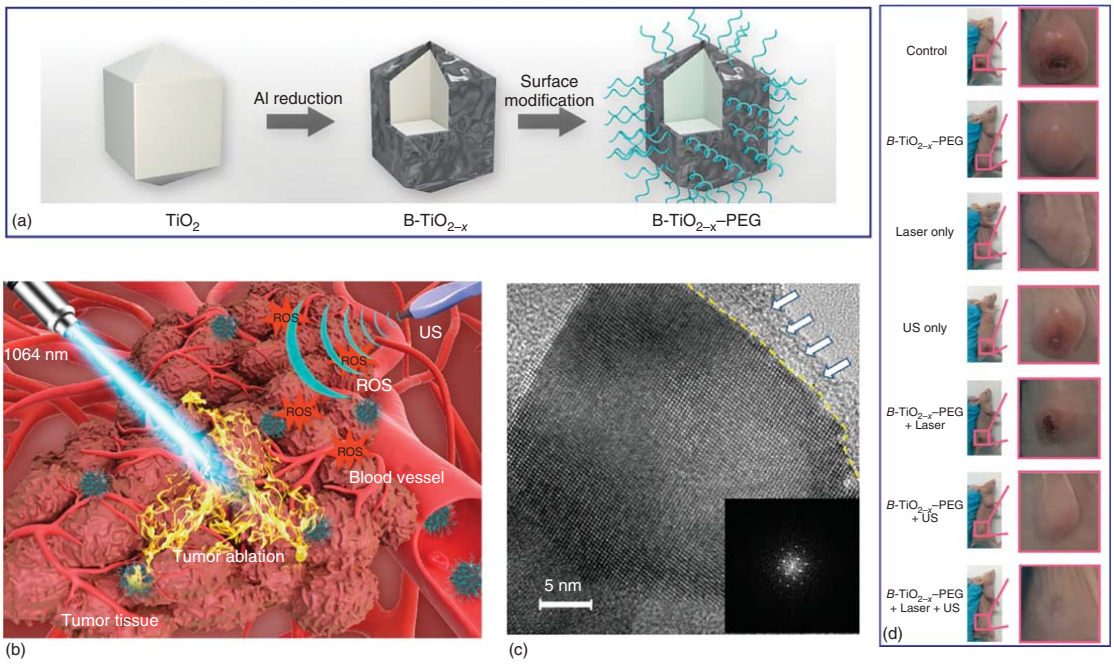

Figure 6.7 (a) Illustration of the preparation of black TiO_2 nanomaterials by using aluminum reduction method. (b) Scheme of combined PTT and SDT as synergistic treatments of tumor by PEG-coated black TiO_2 nanomaterials. (c) High resolution TEM and SAED images of black TiO_2 nanomaterials. (d) Pictures of tumor-bearing mice model after various of therapies at the 15th day and the changes of tumor sites. Source: Image is adapted with permission from Harada et al. 2011 [114]. Copyright 2018, American Chemical Society.

monitoring duration, proving that the synergistic efficacy of simultaneous PTT as well as SDT treatment is very high.

6.7 Overview and Further Perspective

In this chapter, we introduce the application of black TiO_2 in cancer theranostics. Compared with the traditional white TiO_2-based PDT, which requires ultraviolet irradiation to stimulate ROS production for tumor killing, the advantage of black TiO_2 is that its band gap energy can be reduced to about 1.5 eV, and therefore it can be stimulated by NIR to produce ROS for cancer PDT. In addition, due to the full spectrum absorption and combination of non-radiation, black TiO_2 can convert absorbed light energy into heat and result PTT for ablation of tumors. Furthermore, based on the principle of photothermal conversion, black TiO_2 can be used as contrast agents for both PTI and PAI. Therefore, under single-wavelength NIR irradiation, such as 808 nm NIR, black TiO_2 has four functions, which can be used in PDT and PTT of tumors guided by PTI or PAI. In addition, black TiO_2 can be constructed with other imaging materials, such as MRI contrast agent, FI contrast agent, or with chemotherapeutic drugs to develop multimodal imaging and synergistic therapeutic nanoprobes for cancer theranostics.

As a multifunctional nanoprobe, black TiO_2 can be excited by NIR light or ultrasound and therefore has a wide and bright clinical application prospect. However, in order to achieve the clinical application of black TiO_2, there are still many problems to be clarified or overcome:

(1) In the progress of preparing the material, first reducing Ti^{4+} from the crystalline structure of white TiO_2 nanoparticle to Ti^{3+}, and during the reduction reaction, it produces a large number of oxygen vacancies and surface defects, which contribute to the synthesis of black TiO_2. As an inorganic semiconductor nanoparticle, its metabolic process *in vivo* is one of the most concerned problems. There are now substantial studies suggesting that the nanoparticles can excrete from the body by glomerular filtration when the size is below 5 nm. Accordingly, researchers can solve the metabolic problems by controlling the size of black TiO_2 less than 5 nm. However, preliminary research results indicated that the stability of nanoparticles may become worse because of the quantum effects when the size of black TiO_2 less than 5 nm. After storage for a period of time, the color of black TiO_2 turns gray gradually, and becomes white in the end, which indicate the black TiO_2 are oxidized. Therefore, the next step of the research is to figure out how to maintain the stability of black TiO_2 in 5 nm. Furthermore, the emergence of metal–organic frameworks (MOFs) offers a new research path to degrade inorganic nanomaterials *in vivo*. Synthesizing black Ti-based MOF nanoplatform can combine the feature of MOF with black TiO_2 and solve the degradation and metabolism problems of black TiO_2 *in vivo* at the same time. Thus it can be seen that the preparation of black Ti-based MOF nanoparticles might be the potential work in the direction of future studies to further explore.

(2) In terms of optical properties, black TiO_2 not only has excellent absorption ability of NIR light but also can be triggered by NIR laser to generate ROS, which are used for the PDT therapy in tumor. Based on the existing literature and combined with our thesis, we consider the deep level defects in Ti^{3+} led to the increased non-radiative recombination and electron annihilation, thereby causing the absorbed light energy to generate heat energy by lattice vibration, as a result, black TiO_2 possesses photothermal effect. According to the reports, the amorphous layer of TiO_2 surface form a mass of oxygen vacancies defects because of the reduction reaction of Ti^{4+}, which cause the band gap of black TiO_2 reduced to 1.54 eV (806.8 nm), making it possible for black TiO_2 to produce electrons and holes under NIR laser, and thus achieving PDT treatment. Nevertheless, black TiO_2 produce heat energy or ROS under NIR laser are based on photo-induced holes and electrons, if the photo-induced holes and electrons are recombined again, it will produce heat energy, while if the photo-induced electrons are transported to the surface of nanoparticles, then react with the redox couple in solution, it will generate the ROS. According to the description earlier, it is not hard to find that one photogenerated electron–hole cannot generate heat energy and ROS at the same time, but we observed that black TiO_2 do produce a few ROS as well as heat energy simultaneously under NIR excite (data not shown). Therefore, the mechanism of optical performance of black TiO_2 needs to be further explained, and the proportion of Ti^{3+} and Ti^{4+} in the amorphous layer may be an important factor to determine the photothermal effect and photocatalytic effect.

(3) In the aspect of surface modification, black TiO_2 as a kind of inorganic nanoparticles, modifying or coating with hydrophilic polymer on the surface of nanoparticles is an important prerequisite for the diagnosis and therapy of cancer. Different from other nanoparticles prepared in solvent, black TiO_2 are synthesized by the reduction of white TiO_2 and are in the state of dried powder. These nanoparticles are easy to agglomerate when dispersed into liquid, and it is difficult to obtain monodisperse black TiO_2 nanoparticles in water even after the modification of hydrophilic polymer, and the agglomeration of nanomaterials has negative impacts in morphology, size, and photothermal performance, which severely affected the application *in vivo*. As a result, using hydrophilic polymer to modify and optimize black TiO_2 nanoparticles to acquire excellent monodisperse compound nanomaterials is an essential issue in the next step.

(4) As a novel nanoparticle for cancer diagnosis, metabolic and biological toxicity of black TiO_2 *in vivo* need more complete and systemic research in future, including the metabolic pathways, acute and chronic toxicity, neurotoxicity, genotoxicity, immunotoxicity and the immune mechanism, etc.

(5) To broaden the application fields of black TiO_2, more explorative researches can be performed in terms of multifunction diagnostic and therapeutic for cancer. It can realize visualization treatment and coordination therapy for cancer by compositing with other functional materials. For instance, black TiO_2 can compound with MRI imaging materials, like Fe_3O_4 and Gd, to achieve MRI visualization therapy. Besides, black TiO_2 can be

combined with Gd upconversion materials to realize visualization treatment under dual-functional fluorescence-MRI composite imaging. In addition, black TiO_2 can also associate with gold nanoparticles to achieve the CT imaging-guided visualization treatment.

Acknowledgments

This work was supported by National Key R&D Program of China (2018YFC 0910601, 2019YFA0405603), Natural Science Foundation of China (31971292, U1432114), and Zhejiang Province Financial Supporting (2017C03042, LY18H180011, LGF19C100001), Key Laboratory of Diagnosis and Treatment of Digestive System Tumors of Zhejiang Province (2019E10020), the Science & Technology Bureau of Ningbo City (2015B11002, 2017C110022). Furthermore, the authors also acknowledge Shanghai Synchrotron Radiation Facility at Line BL15U (No. h15sr0021) for X-ray fluorescence imaging and National Synchrotron Radiation Laboratory in Hefei for soft X-ray imaging (No. 2016-HLS-PT-002193).

References

1 Paunesku, T., Rajh, T., Wiederrecht, G. et al. (2003). Biology of TiO_2–oligonucleotide nanocomposites. *Nature Materials* 2: 343–346.
2 Yamaguchi, S., Kobayashi, H., Narita, T. et al. (2010). Novel photodynamic therapy using water-dispersed TiO_2-polyethylene glycol compound: evaluation of antitumor effect on glioma cells and spheroids *in vitro*. *Photochemistry and Photobiology* 86: 964–971.
3 Paunesku, T., Ke, T., Dharmakumar, R. et al. (2008). Gadolinium-conjugated TiO_2-DNA oligonucleotide nanoconjugates show prolonged intracellular retention period and T_1-weighted contrast enhancement in magnetic resonance images. *Nanomedicine* 4: 201–207.
4 Sun, N., Li, X., Wang, Z. et al. (2016). A multiscale TiO_2 nanorod array for ultrasensitive capture of circulating tumor cells. *ACS Applied Materials & Interfaces* 8: 12638–12643.
5 Xu, P., Wang, R., Ouyang, J., and Chen, B. (2015). A new strategy for TiO_2 whiskers mediated multi-mode cancer treatment. *Nanoscale Research Letters* 10: 94.
6 Zeng, L., Ren, W., Xiang, L. et al. (2013). Multifunctional Fe_3O_4-TiO_2 nanocomposites for magnetic resonance imaging and potential photodynamic therapy. *Nanoscale* 5: 2107–2113.
7 Zhao, C., Rehman, F.U., Yang, Y. et al. (2015). Bio-imaging and photodynamic therapy with tetra sulphonatophenyl porphyrin (TSPP)-TiO_2 nanowhiskers: new approaches in rheumatoidb arthritis theranostics. *Scientific Reports* 5: 11518.
8 Wang, T., Jiang, H., Wan, L. et al. (2015). Potential application of functional porous TiO_2 nanoparticles in light-controlled drug release and targeted drug delivery. *Acta Biomaterialia* 13: 354–363.

9 Feng, X., Zhang, S., Wu, H., and Lou, X. (2015). A novel folic acid-conjugated TiO_2–SiO_2 photosensitizer for cancer targeting in photodynamic therapy. *Colloids and Surfaces B* 125: 197–205.

10 Song, M., Zhang, R., Dai, Y. et al. (2006). The *in vitro* inhibition of multidrug resistance by combined nanoparticulate titanium dioxide and UV irradiation. *Biomaterials* 27: 4230–4238.

11 Seo, J.-W., Chung, H., Kim, M.-Y. et al. (2007). Development of water-soluble single-crystalline TiO_2 nanoparticles for photocatalytic cancer. *Small* 3: 850–853.

12 Rozhkova, E.A., Ulasov, I., Lai, B. et al. (2009). A high-performance nanobio photocatalyst for targeted brain cancer therapy. *Nano Letters* 9 (9): 3337–3342.

13 Lopez, T., Ortiz, E., Alvarez, M. et al. (2010). Study of the stabilization of zinc phthalocyanine in sol–gel TiO_2 for photodynamic therapy applications. *Nanomedicine* 6: 777–785.

14 Lee, J., Lee, Y.H., Choi, J.S. et al. (2015). Hydrothermal synthesis of defective TiO_2 nanoparticles for long-wavelength visible light-photocatalytic killing of cancer cells. *RSC Advances* 5: 99789–99796.

15 An, H.-R., Park, S.Y., Kim, H. et al. (2016). Advanced nanoporous TiO_2 photocatalysts by hydrogen plasma for efficient solar-light photocatalytic application. *Scientific Reports* 6: 29683.

16 Ullattil, S.G., Narendranath, S.B., Pillai, S.C., and Periyat, P. (2018). Black TiO_2 nanomaterials: a review of recent advances. *Chemical Engineering Journal* 343: 708–736.

17 Chen, X., Liu, L., and Huang, F. (2015). Black titanium dioxide (TiO_2) nanomaterials. *Chemical Society Reviews* 44 (7): 1861–1885.

18 Burda, C., Chen, X., Narayanan, R., and El-Sayed, M.A. (2005). Chemistry and properties of nanocrystals of different shapes. *Chemical Reviews* 105 (4): 1025–1102.

19 Chen, X., Liu, L., Yu, P.Y., and Mao, S.S. (2011). Increasing solar absorption for photocatalysis with black hydrogenated titanium dioxide nanocrystals. *Science* 331: 746–750.

20 Wang, G., Wang, H., Ling, Y. et al. (2011). Hydrogen-treated TiO_2 nanowire arrays for photoelectrochemical water splitting. *Nano Letters* 11 (7): 3026–3033.

21 Wang, Z., Yang, C., Lin, T. et al. (2013). H-doped black titania with very high solar absorption and excellent photocatalysis enhanced by localized surface plasmon resonance. *Advanced Functional Materials* 23 (43): 5444–5450.

22 Wang, Z., Yang, C., Lin, T. et al. (2013). Visible-light photocatalytic, solar thermal and photoelectrochemical properties of aluminium-reduced black titania. *Energy & Environmental Science* 6 (10): 3007.

23 Lin, T., Yang, C., Wang, Z. et al. (2014). Effective nonmetal incorporation in black titania with enhanced solar energy utilization. *Energy & Environmental Science* 7 (3): 967.

24 Tan, H., Zhao, Z., Niu, M. et al. (2014). A facile and versatile method for preparation of colored TiO_2 with enhanced solar-driven photocatalytic activity. *Nanoscale* 6 (17): 10216–10223.

25 Zou, X., Liu, J., Su, J. et al. (2013). Facile synthesis of thermal- and photostable titania with paramagnetic oxygen vacancies for visible-light photocatalysis. *Chemistry A European Journal* 19 (8): 2866–2873.

26 Schweitzer, C. and Schmidt, R. (2003). Physical mechanisms of generation and deactivation of singlet oxygen. *Chemical Reviews* 103 (5): 1685–1757.

27 Hu, Y.H. (2012). A highly efficient photocatalyst—hydrogenated black TiO_2 for the photocatalytic splitting of water. *Angewandte Chemie International Edition* 51 (50): 12410–12412.

28 Redmond, R.W. and Kochevar, I.E. (2006). Spatially resolved cellular responses to singlet oxygen. *Photochemistry and Photobiology* 82 (5): 1178–1186.

29 Zeng, L., Xiang, L., Ren, W. et al. (2013). Multifunctional photosensitizer-conjugated core–shell Fe_3O_4@$NaYF_4$:Yb/Er nanocomplexes and their applications in T_2-weighted magnetic resonance/upconversion luminescence imaging and photodynamic therapy of cancer cells. *RSC Advances* 3: 13915–13925.

30 Zeng, L., Pan, Y., Tian, Y. et al. (2015). Doxorubicin-loaded $NaYF_4$:Yb/Tm–TiO_2 inorganic photosensitizers for NIR-triggered photodynamic therapy and enhanced chemotherapy in drug-resistant breast cancers. *Biomaterials* 57: 93–106.

31 Hou, Z., Zhang, Y., Deng, K. et al. (2015). UV-emitting upconversion-based TiO_2 photosensitizing nanoplatform: near-infrared light mediated *in vivo* photodynamic therapy *via* mitochondria-involved apoptosis pathway. *ACS Nano* 9: 2584–2599.

32 Huang, Y., He, S., Cao, W. et al. (2012). Biomedical nanomaterials for imaging-guided cancer therapy. *Nanoscale* 4: 6135–6149.

33 Zhang, Z., Wang, L., Wang, J. et al. (2012). Mesoporous silica-coated gold nanorods as a light-mediated multifunctional theranostic platform for cancer treatment. *Advanced Materials* 24: 1418–1423.

34 Jiang, R., Cheng, S., Shao, L. et al. (2013). Mass-based photothermal comparison among gold nanocrystals, PbS nanocrystals, organic dyes, and carbon black. *The Journal of Physical Chemistry C* 117: 8909–8915.

35 Ren, W., Yan, Y., Zeng, L. et al. (2015). A near infrared light triggered hydrogenated black TiO_2 for cancer photothermal therapy. *Advanced Healthcare Materials* 4: 1526–1536.

36 Shi, H., Magaye, R., Castranova, V., and Zhao, J. (2013). Titanium dioxide nanoparticles: a review of current toxicological data. *Particle and Fibre Toxicology* 10: 15.

37 Wu, S., Weng, Z., Liu, X. et al. (2014). Functionalized TiO_2 based nanomaterials for biomedical applications. *Advanced Functional Materials* 24: 5464–5481.

38 Ou, G., Li, Z., Li, D. et al. (2016). Photothermal therapy by using titanium oxide nanoparticles. *Nano Research* 9: 1236–1243.

39 Sun, L., Li, Z., Li, Z. et al. (2017). Design and mechanism of core-shell TiO_2 nanoparticles as a high-performance photothermal agent. *Nanoscale* 9: 16183.

40 Shu, G., Wang, H., Zhao, H.-X., and Zhang, X. (2018). Microwave-assisted synthesis of black titanium monoxide for synergistic tumor phototherapy. *ACS Applied Materials & Interfaces* https://doi.org/10.1021/acsami.8b17418.

41 Zeng, J., Wu, M., Lan, S. et al. (2018). Facile preparation of biocompatible Ti_2O_3 nanoparticles for second near-infrared window photothermal therapy. *Journal of Materials Chemistry B* 6 (47): 7889–7897.

42 Yang, D., Gulzar, A., Yang, G. et al. (2017). Au nanoclusters sensitized black TiO_{2-x} nanotubes for enhanced photodynamic therapy driven by near-infrared light. *Small* 13 (48): 1703007.

43 Ni, W., Li, M., Cui, J. et al. (2017). 808 nm light triggered black TiO_2 nanoparticles for killing of bladder cancer cells. *Materials Science and Engineering C* 81: 252–260.

44 Wang, X., Ma, B., Xue, J. et al. (2019). Defective black nano-titania thermogels for cutaneous tumor-induced therapy and healing. *Nano Letters* 19 (3): 2138–2147.

45 Medintz, I.L., Uyeda, H.T., Goldman, E.R., and Mattoussi, H. (2005). Quantum dot bioconjugates for imaging, labelling and sensing. *Nature Materials* 4: 435–446.

46 Gong, Q., Zou, R., Xing, J. et al. (2018). A ultrasensitive near-infrared fluorescent probe reveals pyroglutamate aminopeptidase 1 can be a new inflammatory cytokine. *Advanced Science* 5: 1700664.

47 Wang, J., Gu, X., Ma, H. et al. (2018). A facile strategy for realizing room temperature phosphorescence and single molecule white light emission. *Nature Communications* 9: 2963.

48 Shen, Z., Song, J., Zhou, Z. et al. (2018). Dotted core–shell nanoparticles for T1-weighted MRI of tumors. *Advanced Materials* 30: 1803163.

49 Li, J., Tian, Y., Shan, D. et al. (2017). Neuropeptide Y Y 1 receptor-mediated biodegradable photoluminescent nanobubbles as ultrasound contrast agents for targeted breast cancer imaging. *Biomaterials* 116: 106–117.

50 Shen, Z., Chen, T., Ma, X. et al. (2017). Multifunctional theranostic nanoparticles based on exceedingly small magnetic iron oxide nanoparticles for T_1-weighted magnetic resonance imaging and chemotherapy. *ACS Nano* 11: 10992–11004.

51 Fan, Q., Cheng, K., Hu, X. et al. (2014). Transferring biomarker into molecular probe: melanin nanoparticle as a naturally active platform for multimodality imaging. *Journal of the American Chemical Society* 136 (43): 15185–15194.

52 Liu, C., Luo, L., Zeng, L. et al. (2018). Porous gold nanoshells on functional NH_2-MOFs: facile synthesis and designable platforms for cancer multiple therapy. *Small* 14: 1801851.

53 Kwon, S.-P., Jeon, S., Lee, S.-H. et al. (2018). Thrombin-activatable fluorescent peptide incorporated gold nanoparticles for dual optical/computed tomography thrombus imaging. *Biomaterials* 150: 125–136.

54 Liu, Z., Li, X., Tabakman, S.M. et al. (2008). Multiplexed multicolor Raman imaging of live cells with isotopically modified single walled carbon nanotubes. *Journal of the American Chemical Society* 130 (41): 13540–13541.

55 Kowada, T., Maed, H., and Kikuchi, K. (2015). BODIPY-based probes for the fluorescence imaging of biomolecules in living cells. *Chemical Society Reviews* 46 (35): 4953–4972.

56 Fu, Q., Zhu, R., Song, J. et al. (2019). Photoacoustic imaging: contrast agents and their biomedical applications. *Advanced Materials* 31: 1805875.

57 Kang, J., Kim, D., Wang, J. et al. (2018). Enhanced performance of a molecular photoacoustic imaging agent by encapsulation in mesoporous silicon nanoparticles. *Advanced Materials* 30 (27): 1800512.

58 Wu, X., Li, C., Liao, S. et al. (2014). Silica-encapsulated Gd^{3+}-aggregated gold nanoclusters for in vitro and in vivo multimodal cancer imaging. *Chemistry* 20 (29): 8876–8882.

59 Deng, H., Dai, F., Ma, G., and Zhang, X. (2015). Theranostic gold nanomicelles made from biocompatible comb-like polymers for thermochemotherapy and multifunctional imaging with rapid clearance. *Advanced Materials* 27: 3645–3653.

60 Qin, H., Zhou, T., Yang, S. et al. (2013). Gadolinium (III)–gold nanorods for MRI and photoacoustic imaging dual-modality detection of macrophages in atherosclerotic inflammation. *Nanomedicine* 8 (10): 1611–1624.

61 Mou, J., Liu, C., Li, P. et al. (2015). A facile synthesis of versatile $Cu_{2-x}S$ nanoprobe for enhanced MRI and infrared thermal/photoacoustic multimodal imaging. *Biomaterials* 57: 12–21.

62 Mou, J., Lin, T., Huang, F. et al. (2016). Black titania-based theranostic nanoplatform for single NIR laser induced dual-modal imaging-guided PTT/PDT. *Biomaterials* 84: 13–24.

63 Rao, L., Cai, B., Bu, L.-L. et al. (2017). Microfluidic electroporation-facilitated synthesis of erythrocyte membrane-coated magnetic nanoparticles for enhanced imaging-guided cancer therapy. *ACS Nano* 11 (4): 3496–3505.

64 Liang, X., Li, Y., Li, X. et al. (2015). PEGylated polypyrrole nanoparticles conjugating gadolinium chelates for dual-modal MRI/photoacoustic imaging guided photothermal therapy of cancer. *Advanced Functional Materials* 25: 1451–1462.

65 Jiang, Z., Tian, Y., Shan, D. et al. (2018). pH protective Y1 receptor ligand functionalized antiphagocytosis BPLP-WPU micelles for enhanced tumor imaging and therapy with prolonged survival time. *Biomaterials* 170: 70–81.

66 Shen, Z., Wu, A., and Chen, X. (2017). Iron oxide nanoparticles-based contrast agents for magnetic resonance imaging. *Molecular Pharmaceutics* 14: 1352–1364.

67 Yu, Z., Xia, Y., Xing, J. et al. (2018). Y1 receptor ligand functionalized ultrasmall upconversion nanoparticles for tumor-targeted trimodality imaging and photodynamic therapy with low toxicity. *Nanoscale* 10 (36): 17038–17052.

68 Guo, Z., Gao, M., Song, M. et al. (2016). Superfluorinated PEI derivative coupled with ^{99m}Tc for ASGPR targeted ^{19}F MRI/SPECT/PA tri-modality imaging. *Advanced Materials* 28: 5898–5906.

69 Rao, L., Bu, L.-L., Meng, Q.-F. et al. (2017). Antitumor platelet-mimicking magnetic nanoparticles. *Advanced Functional Materials* 27: 1604774.

70 Siegel, R.L., Miller, K.D., and Jemal, A. (2018). Cancer statistics, 2018. *CA: A Cancer Journal for Clinicians* 68: 7–30.

71 Shackleton, M., Quintana, E., Fearon, E.R., and Morrison, S.J. (2009). Heterogeneity in cancer: cancer stem cells versus clonal evolution. *Cell* 138: 822–829.

72 Maeda, S., Shinchi, H., Kurahara, H. et al. (2008). CD133 expression is correlated with lymph node metastasis and vascular endothelial growth factor-C expression in pancreatic cancer. *British Journal of Cancer* 98: 1389–1397.

73 Wang, S., Ren, W., Wang, J. et al. (2018). Black TiO_2 based nanoprobes for T1-weighted MRI guided photothermal therapy in CD133 high expressed pancreatic cancer stem-like cells. *Biomaterials Science* 6: 2209–2218.

74 Zhang, H., Li, L., Liu, X.L. et al. (2017). Ultrasmall ferrite nanoparticles synthesized *via* dynamic simultaneous thermal decomposition for high-performance and multifunctional T_1 magnetic resonance imaging contrast agent. *ACS Nano* 11 (4): 3614–3631.

75 Tromsdorf, U.I., Bruns, O.T., Salmen, S.C. et al. (2009). A highly effective, nontoxic T_1 MR contrast agent based on ultrasmall PEGylated iron oxide nanoparticles. *Nano Letters* 9: 4434–4440.

76 Kim, B.H., Lee, N., Kim, H. et al. (2011). Large-scale synthesis of uniform and extremely small-sized iron oxide nanoparticles for high-resolution T_1 magnetic resonance imaging contrast agents. *Journal of the American Chemical Society* 133: 12624–12631.

77 Wei, H., Bruns, O.T., Kaul, M.G. et al. (2014). Exceedingly small iron oxide nanoparticles as positive MRI contrast agents. *Proceedings of the National Academy of Sciences of the United States of America* 114: 2325–2330.

78 Pellico, J., Ruiz-Cabello, J., Saiz-Alía, M. et al. (2016). Fast synthesis and bioconjugation of ^{68}Ga core-doped extremely small iron oxide nanoparticles for PET/MR imaging. *Contrast Media & Molecular Imaging* 11: 203–210.

79 Saeed, M., Iqbal, M.Z., Ren, W. et al. (2018). Controllable synthesis of Fe_3O_4 nanoflowers: enhanced imaging guided cancer therapy and comparison of photothermal efficiency with black-TiO_2. *Journal of Materials Chemistry B* 6: 3800–3810.

80 Saeed, M., Iqbal, M.Z., Ren, W. et al. (2019). Tunable fabrication of new theranostic Fe_3O_4-black TiO_2 nanocomposites: dual wavelength stimulated synergistic imaging-guided phototherapy in cancer. *Journal of Materials Chemistry B* 7: 210–223.

81 Wang, M., Deng, K., Lü, W. et al. (2018). Rational design of multifunctional Fe@γ-Fe_2O_3@H-TiO_2 nanocomposites with enhanced magnetic and photoconversion effects for wide applications: from photocatalysis to imaging-guided photothermal cancer therapy. *Advanced Materials* 30: 1706747.

82 Li, Y., Deng, Y., Tian, X. et al. (2015). Multipronged design of light-triggered nanoparticles to overcome cisplatin resistance for efficient ablation of resistant tumor. *ACS Nano* 9: 9626–9637.

83 Zheng, M., Yue, C., Ma, Y. et al. (2013). Single-step assembly of DOX/ICG loaded lipid-polymer nanoparticles for highly effective chemo-photothermal combination therapy. *ACS Nano* 7: 2056–2067.

84 Yan, H.-W., Lu, Y.-J., Lin, K.-J. et al. (2013). EGRF conjugated PEGylated nanographene oxide for targeted chemotherapy and photothermal therapy. *Biomaterials* 34: 7204–7214.

85 Jana, A., Saha, B., Banerjee, D.R. et al. (2013). Photocontrolled nuclear-targeted drug delivery by single component photoresponsive fluorescent organic nanoparticles of acridin-9-methanol. *Bioconjugate Chemistry* 24: 1828–1839.

86 Xu, J., Zhou, X., Gao, Z. et al. (2016). Visible-light-triggered drug release from TiO_2 nanotube arrays: a controllable antibacterial platform. *Angewandte Chemie International Edition* 55: 593–597.

87 Xie, C., Li, P., Liu, Y. et al. (2016). Preparation of TiO_2 nanotubes/mesoporous calcium silicate composites with controllable drug release. *Materials Science and Engineering C: Materials for Biological Applications* 67: 433–439.

88 Torres, C.C., Campos, C.H., Diáz, C. et al. (2016). PAMAM-grafted TiO_2 nanotubes as novel versatile materials for drug delivery applications. *Materials Science and Engineering C: Materials for Biological Applications* 65: 164–171.

89 Rajh, T., Dimitrijevic, N.M., Bissonnette, M. et al. (2014). Titanium dioxide in the service of the biomedical revolution. *Chemical Reviews* 114: 10177–10216.

90 Ren, W., Zeng, L., Shen, Z. et al. (2013). Enhanced doxorubicin transport to multidrug resistant breast cancer cells *via* TiO_2 nanocarriers. *RSC Advances* 3: 20855–20861.

91 Du, Y., Ren, W., Li, Y. et al. (2015). The enhanced chemoth erapeutic effects of doxorubicin loaded PEG coated TiO_2 nanocarriers in an orthotopic breast tumor bearing mouse model. *Journal of Materials Chemistry B* 3: 1518–1528.

92 Pan, L., He, Q., Liu, J. et al. (2012). Nuclear-targeted drug delivery of TAT peptide-conjugated monodisperse mesoporous silica nanoparticles. *Journal of the American Chemical Society* 134: 5722–5725.

93 Peng, F., Cao, Z., Ji, X. et al. (2015). Silicon nanostructures for cancer diagnosis and therapy. *Nanomedicine (London, England)* 10 (13): 2109–2123.

94 Croissant, J.G., Fatieiev, Y., and Khashab, N.M. (2017). Degradability and clearance of silicon, organosilica, silsesquioxane, silica mixed oxide, and mesoporous silica nanoparticles. *Advanced Materials* 29: 1604634.

95 Ren, W., Iqbal, M.Z., Zeng, L. et al. (2017). Black TiO_2 based core–shell nanocomposites as doxorubicin carriers for thermal imaging guided synergistic therapy of breast cancer. *Nanoscale* 9: 11195–11204.

96 Wu, X., Xia, Y., Huang, Y. et al. (2016). Improved SERS-active nanoparticles with various shapes for CTC detection without enrichment process with supersensitivity and high specificity. *ACS Applied Materials & Interfaces* 8 (31): 19928–19938.

97 Pan, Y., Zhang, L.'e., Zeng, L. et al. (2016). Gd-based upconversion nanocarriers with yolk–shell structure for dual-modal imaging and enhanced chemotherapy to overcome multidrug resistance in breast cancer. *Nanoscale* 8: 878–888.

98 Guo, W., Wang, F., Ding, D. et al. (2017). TiO_{2-x} based nanoplatform for bimodal cancer imaging and NIR-triggered chem/photodynamic/photothermal combination therapy. *Chemistry of Materials* 29: 9262–9274.

99 Miller, D.L., Pislaru, S.V., and Greenleaf, J.F. (2002). Sonoporation: mechanical DNA delivery by ultrasonic cavitation. *Somatic Cell and Molecular Genetics* 27: 115–134.

100 Schlicher, R.K., Radhakrishna, H., Tolentino, T.P. et al. (2006). Mechanism of intracellular delivery by acoustic cavitation. *Ultrasound in Medicine & Biology* 32 (6): 915–924.

101 Frenkel, V. (2008). Ultrasound mediated delivery of drugs and genes to solid tumors. *Advanced Drug Delivery Reviews* 60 (10): 1193–1208.

102 Kennedy, J.E. (2005). High-intensity focused ultrasound in the treatment of solid tumours. *Nature Reviews Cancer* 5: 321–327.

103 Illing, R.O., Kennedy, J.E., F, W. et al. (2005). The safety and feasibility of extracorporeal high-intensity focused ultrasound (HIFU) for the treatment of liver and kidney tumours in a Western population. *British Journal of Cancer* 93: 890–895.

104 Wang, X., Chen, H., Zhang, K. et al. (2014). An intelligent nanotheranostic agent for targeting, redox-responsive ultrasound imaging, and imaging guided high-intensity focused ultrasound synergistic therapy. *Small* 10: 1403–1411.

105 Gao, Z., Kennedy, A.M., Christensen, D.A., and Rapoport, N.Y. (2008). Drug-loaded nano/microbubbles for combining ultrasonography and targeted chemotherapy. *Ultrasonics* 48 (4): 260–270.

106 Zhu, H., Zhou, K., Zhang, L. et al. (2009). High intensity focused ultrasound (HIFU) therapy for local treatment of hepatocellular carcinoma: role of partial rib resection. *European Journal of Radiology* 72: 160–166.

107 Chen, Y., Chen, H., Sun, Y. et al. (2011). Multifunctional mesoporous composite nanocapsules for highly efficient MRI-guided high-intensity focused ultrasound cancer surgery. *Angewandte Chemie International Edition* 50: 12505–12509.

108 Zhang, X., Zheng, Y., Wang, Z. et al. (2014). Methotrexate-loaded PLGA nanobubbles for ultrasound imaging and synergistic targeted therapy of residual tumor during HIFU ablation. *Biomaterials* 35: 5148–5161.

109 Xu, J., Xia, X., Leung, A.W. et al. (2011). Sonodynamic action of pyropheophorbide-a methyl ester induces mitochondrial damage in liver cancer cells. *Ultrasonics* 51: 480–484.

110 Wang, X., Wang, Y., Wang, P. et al. (2011). Sonodynamically induced anti-tumor effect with protoporphyrin IX on hepatoma-22 solid tumor. *Ultrasonics* 51: 539–546.

111 Chen, H.-J., Huang, X.-R., Zhou, X.-B. et al. (2015). Potential sonodynamic anticancer activities of artemether and liposome-encapsulated artemether. *Chemical Communications* 51: 4681–4684.

112 Nomikou, N., Fowley, C., Byrne, N.M. et al. (2012). Microbubble–sonosensitiser conjugates as therapeutics in sonodynamic therapy. *Chemical Communications* 48: 8332–8334.

113 Yamaguchi, S., Kobayashi, H., Narita, T. et al. (2011). Sonodynamic therapy using water-dispersed TiO_2-polyethylene glycol compound on glioma cells: comparison of cytotoxic mechanism with photodynamic therapy. *Ultrasonics Sonochemistry* 18: 1197–1204.

114 Harada, Y., Ogawa, K., Irie, Y. et al. (2011). Ultrasound activation of TiO_2 in melanoma tumors. *Journal of Controlled Release* 149: 190–195.

115 Ninomiya, K., Noda, K., Ogino, C. et al. (2014). Enhanced OH radical generation by dual-frequency ultrasound with TiO_2 nanoparticles: its application to targeted sonodynamic therapy. *Ultrasonics Sonochemistry* 21: 289–294.

116 Harada, A., Ono, M., Yuba, E., and Kono, K. (2013). Titanium dioxide nanoparticle-entrapped polyion complex micelles generate singlet oxygen in the cells by ultrasound irradiation for sonodynamic therapy. *Biomaterials Science* 1: 65–73.

117 Guo, Y., Cheng, C., Wang, J. et al. (2011). Detection of reactive oxygen species (ROS) generated by TiO_2(R), TiO_2(R/A) and TiO_2(A) under ultrasonic and solar light irradiation and application in degradation of organic dyes. *Journal of Hazardous Materials* 192: 786–793.

118 Ninomiya, K., Ogino, C., Oshima, S. et al. (2012). Targeted sonodynamic therapy using protein-modified TiO_2 nanoparticles. *Ultrasonics Sonochemistry* 19: 607–614.

119 Davids, L.M. and Kleemann, B. (2011). Combating melanoma: the use of photodynamic therapy as a novel, adjuvant therapeutic tool. *Cancer Treatment Reviews* 37: 465–475.

120 Hong, G., Lee, J.C., Robinson, J.T. et al. (2012). Multifunctional *in vivo* vascular imaging using near-infrared II fluorescence. *Nature Medicine* 18: 1841––1846.

121 Dai, C., Chen, Y., Jing, X. et al. (2017). Two-dimensional tantalum carbide (MXenes) composite nanosheets for multiple imaging-guided photothermal tumor ablation. *ACS Nano* 11: 12696–12712.

122 Kim, S., Lim, Y.T., Soltesz, E.G. et al. (2004). Near-infrared fluorescent type II quantum dots for sentinel lymph node mapping. *Nature Biotechnology* 22: 93–97.

123 Hong, G., Tabakman, S.M., Welsher, K. et al. (2011). Near-infrared-fluorescence-enhanced molecular imaging of live cells on gold substrates. *Angewandte Chemie International Edition* 50: 4644–4648.

124 Han, X., Huang, J., Jing, X. et al. (2018). Oxygen-deficient black titania for synergistic/enhanced sonodynamic and photoinduced cancer therapy at near infrared-II biowindow. *ACS Nano* 12 (5): 4545–4555.

7

Neurodegenerative Disease Diagnostics and Therapy of TiO_2-Based Nanoparticles

Xiang Gao[1], Jieling Qin[2], Zhenqi Jiang[3], Juan Li[3], and Aiguo Wu[3]*

[1] Ningbo First Hospital, Department of Neurosurgery specialist, Liuting Street 59, Ningbo 315201, P.R. China
[2] Sungkyunkwan University, School of Chemical Engineering, 2066, Seobu-ro, Jangan-gu, Suwon-si, Gyeonggi-do, 16419, Korea
[3] Cixi Institute of Biomedical Engineering, CAS Key Laboratory of Magnetic Materials and Devices, & Key Laboratory of Additive Manufacturing Materials of Zhejiang Province, Ningbo Institute of Materials Technology and Engineering, Chinese Academy of Sciences, No. 1219 Zhongguan West Road, Ningbo 315201, P.R. China

CHAPTER MENU

Introduction, 217
The Symptoms of Neurodegenerative Disease, 219
Traditional Diagnosis and Treatment for NDs, 220
Nanoparticles in the Diagnosis and Treatment of NDs, 221
The Diagnosis of NDs Using TiO_2, 222
The Therapy of NDs Using TiO_2, 225
The Dilemma Situation of TiO_2 in the NDs, 226
Conclusion, 228

7.1 Introduction

Neurodegenerative diseases (NDs) are kinds of diseases that are caused by the loss of neurons and/or myelin deterioration over time and affect millions of people worldwide [1–4]. There are four main causes of these adverse reactions:

1) *Oxidative stress* [3, 5, 6]: Oxidative stress is due to excessive free radical production and/or insufficient free radical elimination, *in vivo* oxidation and antioxidant imbalance, and body cells and is caused by tissue damage. Free radicals are atoms or groups having unpaired electrons, including hydroxyl radicals (OH^-), superoxide anions (O^-), nitric oxide (NO), and the like. Nowadays, the NDs, such as amyotrophic lateral sclerosis (ALS), Alzheimer's disease (AD), Huntington's disease (HD), Parkinson's disease (PD), etc. have found the deterioration of nerve tissue causing oxidative damage.
2) *Mitochondrial dysfunction* [7–10]: Most of them are the mitochondrial DNA (mtDNA) deficiencies and abnormal oxidative phosphorylation in

*Corresponding author: Lij@nimte.ac.cn

TiO_2 Nanoparticles: Applications in Nanobiotechnology and Nanomedicine,
First Edition. Edited by Aiguo Wu and Wenzhi Ren.
© 2020 Wiley-VCH Verlag GmbH & Co. KGaA. Published 2020 by Wiley-VCH Verlag GmbH & Co. KGaA.

NDs patients' brains. Polymerase chain reaction (PCR) and Western blotting revealed mtDNA breaks, base deletions, and missense mutations in brain tissue of patients with sporadic NDs. Electron microscopic observation confirmed that the structure of mitochondria was deteriorated with the increase of the concentrations of mitochondria especially for the appearance of the lamellar crystalline inclusion bodies sometimes. Furthermore, neuronal mitochondrial dysfunction in patients with neurotrophic disorders leads to insufficient energy supply to neurons to release excess amount of reactive oxygen species (ROS) and damage caused by the oxidative stress, calcium regulation disorder, and neuronal apoptosis finally.

3) *Excitatory toxins* [11–14]: Excessive intercellular glutamate concentration can cause neurotoxicity, leading to degeneration and eventual death of neuron. This excitatory toxic effect of glutamate is closely related to the occurrence and development of various neural stem cells and is one of the important mechanisms leading to the death of neural stem cells.
4) *Immune inflammation* [15–17]: There is much evidence that inflammation is of importance during the pathogenesis of NDs. The natural immune defense function, namely, the innate immune system (IIS), is formed with the development and evolution of species and can quickly respond to numerous harmful substances to protect the body compared with other immune response. Moreover, the activation of the IIS itself is a double-edged sword, together with which the long-term and uncontrollable contact of harmful substances can cause the brain damage. NDs can be divided into acute NDs and chronic NDs. The former mainly contains cerebral ischemia (CI), brain injury (BI), and epilepsy, while the latter includes AD, PD, HD, ALS, and different types of spinocerebellar ataxia (SCA), Pico disease, etc. The pathological changes associated with NDs are irreversible, which means, as some symptoms that are assigned to NDs happen in a patient, his/her disease has already come in the middle and late stages. And the general treatment can just relieve the deterioration and slow the development of NDs instead of completely cure the damage of neural network. Hence, for the NDs, the diagnosis and treatment should be as early as possible to prevent further development of the disease.

Nanotechnology involves manipulating particles with the diameter around 100 nm [18–20]. Compared with micro or larger scale, the particles with the size in nanoscale have the unique morphology, biological, and physicochemical characteristics with the significant effect on cell localization. The advent of nanotechnology provides a platform for closer integration with diagnosis and treatment. Strict research has been conducted on NP-based therapies to discover the starting point of therapeutic development, which is widely used in imaging and therapy, as well as in the development of targeted drugs for cancer, diabetes, immune disorders, genetic disorders, and the NDs [21, 22].

With the rapid development of nanotechnology, nano-titanium dioxide (TiO_2), with a large specific surface area and excellent photocatalytic performance, has also been widely concerned and applied in the field of biomedicine for its good biocompatibility and excellent photocatalytic performance [23–25]. Some reports have reported that TiO_2 was used as the substrate to detect the biomarkers of NDs [26, 27].

In this chapter, we try to discuss the major problem of NDs and introduce several diagnostic and therapeutic methods in NDs using TiO_2.

7.2 The Symptoms of Neurodegenerative Disease

NDs are age-dependent disorders that represent a major threat to human health and become increasing prevalent in recent years because of the aging population [28]. NDs such as ALS, HD, PD, and AD are similar in their symptoms showing one or more forms including memory loss, cognitive impairment, emotion difficulty, or movement disorder [29]. The symptoms of NDs are generally mild, but over time, the symptoms become more severe and begin to interfere with daily life. In the case of AD, the earliest symptom of most patients is memory loss, especially since they cannot remember recent happening and learn new info. For the hippocampus plays the central role in the daily memory, the previously mentioned symptoms occur because the hippocampus is damaged in the beginning of AD. However, with the exacerbation of AD, issues such as memory loss, communication, reasoning, and orientation have become more serious. In this case, the patient needs more daily support from the nurse. In addition, many people with intermediate AD tend to have behaviors that appear to be unusual or inconsistent, including anxiety, repeating the same problem or disrupting sleep patterns, and so on, which can be a great of challenge for their career. Finally, people in the late stages may find it difficult to eat or walk without help and become increasingly weak. Their daily activities need help. Therefore, it is very urgent to find an effective method to diagnose and treat AD and other NDs [30].

Before the diagnosis and treatment of the NDs, the biomarkers of each NDs need to be clarified clearly first. Ross and Poirier reported that all the NDs have common cellular as well as molecular mechanisms including protein aggregation and elementary body (sometimes called inclusion body) formation [30].

Specifically, AD includes the two major types of protein aggregates. One is neuritic plaque, such as the aggregated amyloid beta peptide (Aβ)-sourced proteolysis of the amyloid precursor protein (APP), while another one is tau proteins, called neurofibrillary tangles on the microtubes.

The possible cause of PD is the destruction of monoaminergic neuronal (in other brain stem) as well as dopaminergic neurons (in substantia nigra) [31]. The increased gene dosage α-synuclein can induce the PD, according to the gain-of-function mechanism. While considering the loss-of-function mechanism, the mutations in the PINK1, DJ-1, or the genes encoding Parkin may also cause the PD [32]. In addition, the Lewy body including α-synuclein protein, is the important biomarker for the PD.

HD, which is caused by single gene mutations, has become a typical model for studying the pathogenesis of NDs. In the disease caused by Huntington's protein, the amount of polyglutamine extended is greater than or equal to 36, and less than or equal to 35 does not have a significant threshold effect.

ALS is another ND caused by gradual degeneration of lower/upper motor neurons of the lateral horn of the spinal cord and cerebral cortex, respectively, leading to progressive motor weakness [33]. The cause of rare early-onset familial

ALS may be a mutation in the superoxide dismutase (*SOD1*) gene. In addition, recent studies have found that there are some ubiquitin aggregates in the brain of patients, but *SOD1* is usually not detected in sporadic cases or form a fibrous structure *in vitro*.

Hence, generally, the deposition of the abnormal proteins in neurons, cells, or extracellular, e.g. Aβ, α-synuclein, polyglutamine/ubiquitin, and ubiquitin, causes the degeneration of neurons for the pathologies of AD [34], PD [35], HD [36, 37], and ALS [38], respectively.

7.3 Traditional Diagnosis and Treatment for NDs

7.3.1 Current Methods for the Diagnosis of NDs

There are two important reasons for early and accurate NDs differential diagnosis. On one hand, the early diagnosis together with current treatment can relieve hospital stay [39]; once disease-modifying drugs are acquired, the importance of early diagnosis will increase significantly [40]. On the other hand, the development of new treatments requires early and accurate diagnosis, especially the identification of the right target population, which may explain the failure of several previous drug trials [41].

Up to now, a variety of strategies have been introduced to diagnose the NDs such as Neurodegenerative Disease Sleep Questionnaire (NDSQ) [42], functional imaging [43–45] including MRI and CT, enzyme-linked immunosorbent assay (ELISA) [46, 47], nuclear magnetic resonance (NMR) spectroscopy [48], electrochemical immunoassay [49, 50], photo-electrochemistry [51], surface-enhanced Raman spectroscopy [52, 53], colorimetric assay [54, 55], and localized surface plasmon resonance (SPR) [56].

7.3.2 Current Medicine for the Treatment of NDs

Considering the NDs' mechanism, the concept of neuroprotection has been proposed in recent years. Specifically, there are three general ways to protect nerve cells from degenerative changes, i.e. (i) inhibitors of neurodegenerative changes (Abet, NO, free radicals, excitotoxicity, and inflammatory cytokines, for instance) [57, 58], (ii) Blocking the signal transduction process of neurodegenerative changes (such as apoptosis) [58, 59], and (iii) endogenous neuroprotective mechanisms (e.g. neurotrophic factors) [60–62].

According to the pathways earlier, the current medicine can be subsequently divided into five categories, that is:

1) *Neuroprotective agents*: The conventional neuroprotective agents, namely, calcium antagonist [63, 64], antioxidants [65, 66], *N*-methyl-D-aspartate (NMDA) receptor antagonist [67, 68], and anti-inflammatory drugs [69, 70] that can have therapeutic effects on PD, cardiovascular and cerebrovascular diseases, AD, and stroke, respectively.
2) *Antiapoptotic drugs*: Antiapoptotic drugs [71, 72], such as ginsenoside Rg1, jun-N-terminal kinase (JNK) inhibitors, and CFP-1347, can protect the activity of choline acetyltransferase and can be used to treat AD and PD.

3) *Neurotrophic factor*: Neurotrophic factor (NTF) [73–75] is a type of protein or polypeptide molecule secreted by a target cell of a neuron. After specifically binding to a corresponding receptor, it is taken up by the axon terminal and transported retrogradely to the neuronal cell body by axoplasmic processes to promote and maintain neurons.
4) *Neural stem cell transplantation*: Neural stem cell transplantation [76, 77], such as unipotent stem cells and pluripotent stem cells, is the idea of using neural stem cells to replace the NDs that begins with localized lesions such as PD and HD has achieved satisfactory results in the experiment.
5) *RNA interference*: RNA interference [78, 79] can explore the pathogenesis of NDs, revealing the pathogenesis of these diseases, reducing the production of pathogenic proteins, and delaying the occurrence of diseases.

7.4 Nanoparticles in the Diagnosis and Treatment of NDs

7.4.1 The Diagnosis of ND Using NPs

As we mentioned before, the ELISA, through the enzymatic amplification of the signals, is widespread in clinical and biochemical analysis [80, 81]. However, this method has inherent shortcomings that are labor-intensive and relatively high cost enzyme-linked antibodies for analyte recognition. Alternatively, the application of NPs in the diagnosis of NDs have attracted widespread attention. For the diagnosis of AD, Georganopoulou et al. utilized bio-barcoded gold nanoparticles (AuNPs) to detect the approximation concentration of amyloid-beta-derived diffusible ligands (ADDL) [82], and Neely et al. combined antibody-coated AuNP and two-photon scattering to detect tau protein [83]. Roney et al. prepared the polymer (*N*-butyl-2-cyanoacrylate), which encapsulates 125I-CQ and which can cross the blood–brain barrier (BBB) and increase the relative length of AD transgenic mice [84]. To establish an *in vitro* diagnostic technique for partial discharge, Yu and Lyubchenko developed a new determination based on α-synuclein single-molecule nanomanipulation, which was characterized by atomic force microscope (AFM) for folding errors and self-assembly [85]. Baron et al. used plasma uptake and AuNP to establish an *in vitro* quantitative assay for neurotransmitters involved in PD pathology [86].

In addition, nuclear power sources, especially those composed of iron oxide, are used as specific tissue-targeted superparamagnetic particles during MRI for diagnostic purposes including AD, PD, HD, ALS, etc. [87]. Petry et al. [88] injected the iron oxide nuclear power source into the bloodstream and then captured by the reticuloendothelial system (RES). Once in these cells, such as macrophages, MRI can be used to track the iron oxide nuclear power source, considering that the integrity of the BBB is compromised in certain disease states [89], injected the iron oxide nuclear power source into the bloodstream, and then captured by the RES. Machtoub et al. used ultra small paramagnetic iron oxide nanoparticles (USPIO-NP) to inject T-Cell-labeled *ex vivo* magnetic resonance imaging, and the probe injected with anti-CD4 antibody was able to detect the pathological region of the ALS rat model [90, 91].

7.4.2 The Treatment of ND Using NPs as Drug Delivery

Although the previously mentioned drugs are effective in the treatment of NDs, the BBB is an obstacle to its treatment and diagnosis in view of its presence as a central nervous system (CNS) disease [92]. Traditional drugs, such as protein macromolecules, limit their clinical application due to their low bioavailability and pharmacokinetic properties. Therefore, the study of nanoparticles (NPs) with neurotrophic effects has become a new hotspot in the research field of NDs [93].

Nanobiotechnology is a field that specializes in the application of nanoscale objects (i.e. less than 100 nm) to pharmaceutical and biomedical systems. In view of the changes in the properties of materials of this size, nanobiotechnology is attracting increasing interest as a way to overcome the problems raised by BBB in the treatment of CNS diseases [94]. In particular, systems involving NPs provide an alternative means of targeting drug delivery to the CNS as well as new therapeutic applications [95]. In addition, the ability of nuclear power sources to cross the BBB provides additional opportunities for early diagnosis of CNS disease prior to BBB inflammation and provides an opportunity to monitor and detect further disease progression [87].

NPs can be used as a carrier system to aid in drug therapy for the CNS. The drug is typically combined with the NP using either by merging during NP production or by surface adsorption onto pre-formed NP [96]. Drugs that bind to NP are more susceptible to degradation by the RES and phagocytosis [97]. In addition, drugs that bind to nuclear power sources have a more sustained release pattern, resulting in slow drug release [98]. There are many ways in which solute can pass through the BBB, where diffusion is a very simple passive transport process that depends on the concentration gradient that may exist across the membrane (i.e. across cells) or between cells (i.e. by cell transport). In addition, the accumulation of ROS to decompose Aβ under the action of laser is a new way to solve AD, and the diffusion process depends on the size and lipophilicity of the solute [99]. Gobbi et al. have developed nanoliposomes (NL) that have phosphoric acid or cardiolipin functions and are useful for washing effects [100]. Canovi et al. synthesized modified anti-Aβ monoclonal antibody NL to have high *in vitro* or *in vitro* affinity for Aβ on autopsy and brain specimens [101]. Liu et al. prepared NP from polystyrene and the iron chelator (2-methyl-*N*-(2-aminoethyl)-3-hydroxy-4-pyridinone) was coupled on this NP and demonstrated its protection against neurons *in vitro* [102]. On the other hand, NP can also be used as a transfection vector in PD gene therapy, as an alternative virus to limit the risk of excessive immune response and mutations. Trapani et al. prepared chitosan NP to adsorb dopamine acid (DA) outside, which is less cytotoxic and can reach the brain. And the amount of DA with the chitosan NPs in the striatum is higher than that of DA alone [103].

7.5 The Diagnosis of NDs Using TiO_2

Among the NPs, the TiO_2-based methods are of great interest owning to its non-toxicity, environmental safety, and biocompatibility. Tan and his group prepared

a porous nylon substrate with the modification of TiO_2 NPs as the membrane for phosphopeptides enrichment from p-tau digests [104]. A membrane having a submicron pore size allows for the adsorption of phosphopeptides without mass transfer restriction, and the high surface area of the nylon matrix and the TiO_2 NPs provides a material having high phosphorus peptide binding ability. Finally, membrane enrichment coupled with tandem mass spectrometry revealed seven phosphorylation sites for phosphorylated tau (p-tau) protein *in vivo*, which are associated with AD.

In addition, because of the particular powerful photocatalytic activity [51], the usage of TiO_2 in the photoelectrochemical method receives significant attention for the diagnosis of NDs. Wang et al. reported a TiO_2 nanorods on the fluorine-doped tin oxide (FTO) glass followed by the attachment of 3-mercaptopropionic acid (MPA) to immobilize $A\beta_{1-28}$ for the peptide detection with the excitation by wavelength of 470 nm as an acceptable photocurrent, which could have less damage to biorelated species comparing to UV illumination. The application of TiO_2 in the photoelectrochemical sensor can provide place for the separation of charge carriers and promote the transfer of electron or holes to solution. Finally, 15% increases of photocurrent could be achieved by this illumination that is proven for larger signal for AD detection [105].

Moreover, Curulli synthesized a nanoporous TiO_2-modified Si electrode to determine the catecholamines for the diagnosis of PD. TiO_2 nanomaterials have strong electrocatalytic activity for catecholamines, combined with the high ion selectivity induced by the "chemical surface" characteristics of titanium dioxide nanostructured oxides, and differential voltammetry is used to give a good analytical resolution of the anode peaks rate (DPV method). This titanium dioxide-based sensor is actually a widely used technique for detecting biomolecules in clinical research [106]. Furthermore, another stochastic microsensors based on gold (Au)–TiO_2–graphene and silver (Ag)–TiO_2–graphene composites were also fabricated with the modification of basic porphyrin, and two azulenes: 2,6-bis((E)-2-(furan-2-yl)vinyl)-4-(4,6,8-trimethylazulen-1-yl)pyridine (A1) and 2,6-bis((E)-2-(thiophen-3-yl)vinyl)-4-(4,6,8-trimet hylazulen-1-yl)pyridine (A2) [107]. The prepared stochastic microsensors was effective to DA because of the channel conductivity. Specifically, the addition of DA would block the channel and make the current drop to zero for the recognition DA in the whole blood and urine samples. In addition, another the photoelectrochemical immunosensor was designed using Au-doped TiO_2 nanotube-modified titanium (Ti) foil to detect α-synuclein for the early diagnosis of PD [51]. The TiO_2 nanotubes facilitated the improvement of the photoelectrochemical performance as well as the immobilization of primary antibodies. After the immobilization of primary antibody (Ab_1), the α-synuclein was detected by photoelectrochemical method, and then the [Ab_2–Au–GOx] bioconjugate is attached, which was characterized in that the secondary antibody (Ab_2) and glucose oxidase (GOx) tags are linked to Au NPs. The higher amount of α-synuclein could increase the immobilization of [Ab_2–Au–GOx] bioconjugates and catalytic conversion of glucose to gluconic acid and H_2O_2. Finally, the high yielded H_2O_2 activated high amount of TiO_2 and increased the photocurrent (Figure 7.1).

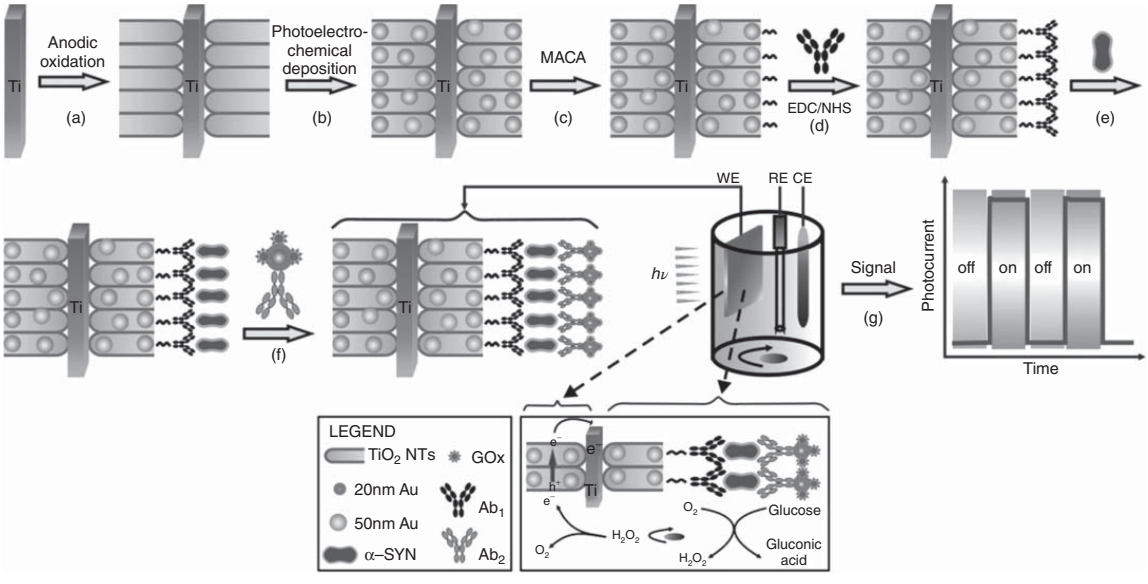

Figure 7.1 Schematic illustration for the synthesis of the TiO_2–Au–Ab_1–α-synuclein-[Ab_2–Au–GOx] immunosensor as well as the mechanism for the photoelectrochemical detection of α-synuclein [51]. Source: Reproduced with permission from An et al. 2010 [51]. Copyright © 2010, Wiley.

7.6 The Therapy of NDs Using TiO_2

Due to mechanism of NDs, the methods that can modulate, inhibit, and clear the special proteins' aggregation may be the effective means for the therapy of NDs.

7.6.1 The Therapy of NDs Using TiO_2 as Drug Delivery Platform

BBB is an important structure between the CNS and the cerebral circulatory system. It consists of endothelial cells, basal layer, astrocyte foot, and pericytes. The main functions of BBB are to protect the selected solute as a carrier for transporting nutrients to the brain and to remove brain metabolites. Recent studies have shown that changes in BBB and its transporters affect the entry of drugs for the treatment of NDs [108, 109].

Although the effects of TiO_2 on BBB function are unknown so far, several experiments found that the TiO_2 can pass through BBB and cause BBB dysfunction [110], and the usage of TiO_2 as a drug delivery platform for the treatment of NDs receives increasing interests. For example, TiO_2 nanowires can penetrate cell membranes with the load of drugs and stem cells without damaging the cell membrane and releasing extracellular or intracellular contents, thereby effectively treating NDs.

Sharma et al. found that histamine antibody was able to reduce BBB breakdown 30–40% higher than the Aβ peptide (AβP) alone group after four-week infusion [111]. After the addition of TiO_2 nanowire, the degree of the BBB breakdown was increased from 30–40% to 60–75% effectively. With the addition of TiO_2 nanowire delivery of cerebrolysin (CBL), the neuroprotection happened via attenuating the deposition of AβP and decreasing the tau phosphorylation. The coadministration of TiO_2 nanowire histamine antibodies with nanowire CBL in AβP model resulted in over 85–90% reduction in BBB breakdown to further enhance the neuroprotection in AD. On the other hand, since neprilysin (NPL) is an endogenous enzyme that promotes the degradation of AβP, the entry of mesenchymal stem cells (MSCs) into the cerebral cistern can reduce the accumulation of AβP by increasing the concentration of NPL. The combination of TiO_2 nanowire MSC and nanowire CBL can significantly increase the concentration of NPL in the brain, which can significantly reduce the AβP level in AD patients [112].

It is worth noting that the use of TiO_2 to transport CBL not only inhibits the aggregation of AβP to AD but also promotes the improvement of morphological function by activating the survival pathway after dopamine depletion, which is an effective method for the treatment of PD [113]. Specifically, CBL in the PD model reduces oxidative stress, restores dopamine levels, and improves behavioral outcomes. TiO_2 nanowires are a promising strategy as a delivery system that penetrates the CNS more quickly and extends into a wide range of areas to increase drug delivery in the CNS [114]. On the other hand, non-pharmacological methods, such as feeding in a rich environment (enriched environment (EE), physical exercise combined with social, visual, and cognitive stimuli), have demonstrated a neuroprotective/neurorestorative effects on different pathological situations.

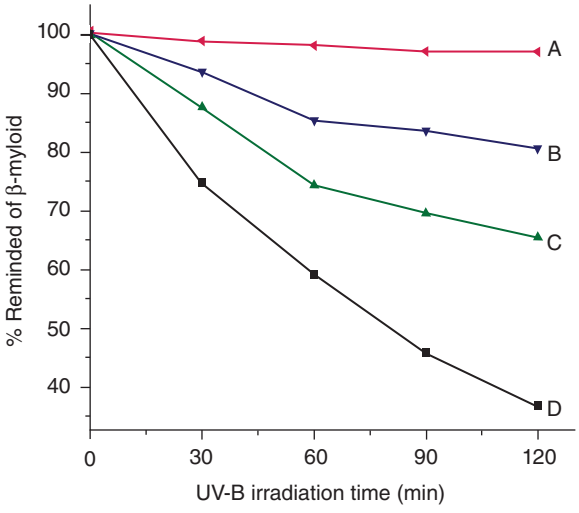

Figure 7.2 Aβ concentration (50 µl, 20 µm) decreased; Aβ deposited on the surface of stainless steel (A) and Ag–Ag–TiO_2 (B); ultraviolet irradiation of Aβ on stainless steel without photocatalyst (C); ultraviolet light of Aβ on Ag–TiO_2 (D) [115]. Source: Reproduced with permission from Ahmed et al. 2013 [115]. Copyright © 2013, Elsevier.

7.6.2 The Therapy of NDs Using TiO_2 as Light-Responsive Material

Owing to its strong oxidizing power, TiO_2 is utilized as a photocatalyst to generate ROS to inhibit these special proteins through photodynamic reactions for the treatment of NDs. In AD, for instance, the possible mechanism of the phototherapy is the ROS, received from TiO_2 after light irradiation, extracts an electron from the tyrosine of Aβ generating a reactive form and then undergoes cross-linking with the neighbors to prevent further aggregation [34].

It has been found that loading TiO_2 surface with silver NPs (Ag–TiO_2) can highly enhance photocatalysis by improving the electron–hole transfer, increasing the charge-carrier separation sites, as well as providing more activated surface area. Hence, Ag–TiO_2 caused a further conformational change of Aβ after exposure to ultraviolet B irradiation, which slightly suppressed the formation of amyloid fibers for treating AD (Figure 7.2) [115].

In addition, the TiO_2 can also be applied to modulate HD by hindering the polyglutamine aggregates [37]. With the UV irradiation, the H_2O_2 that are generated on the TiO_2 acts as the oxidation agent to catalyze the Methionine^7 (Met^7) oxidation, resulting in the incomplete aggregation of the peptide/protein. Hence, the utility of TiO_2 for the Met^7 oxidation could be considered as one of the efficient methods to delay the progress of HD.

7.7 The Dilemma Situation of TiO_2 in the NDs

Even though the TiO_2 has diverse applications for the diagnosis and treatment of NDs, several studies also report that the presence of TiO_2 can promote the aggregation of the proteins, thus may be considered as a probable risk for NDs. Particularly, according to the kinetics of formation of Aβ fibrillation, the Aβ is formed by closely related concentration of nucleation-dependent mechanism. While the presence of TiO_2 NPs may increase local concentration of Aβ monomers around

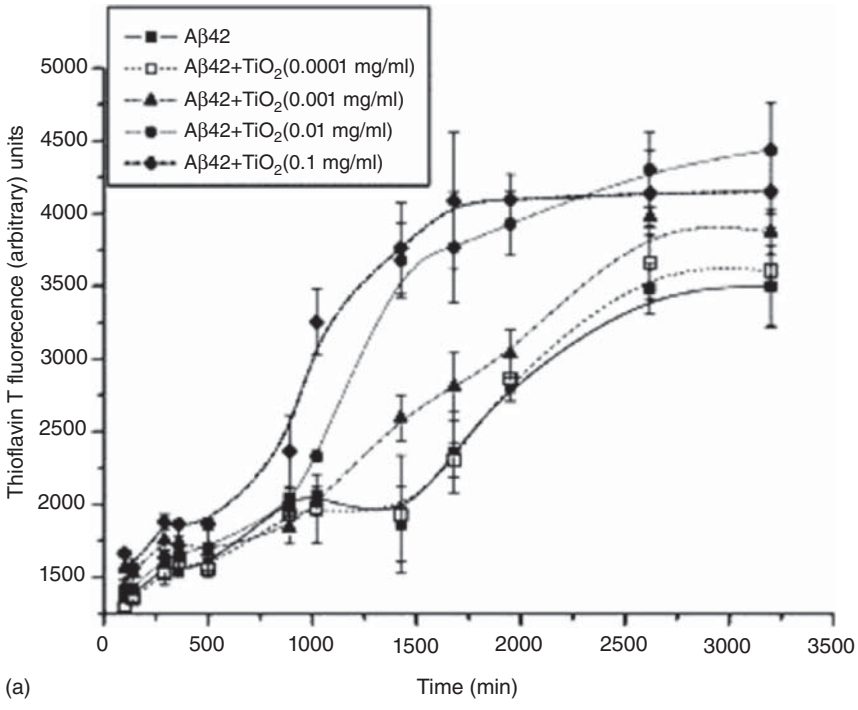

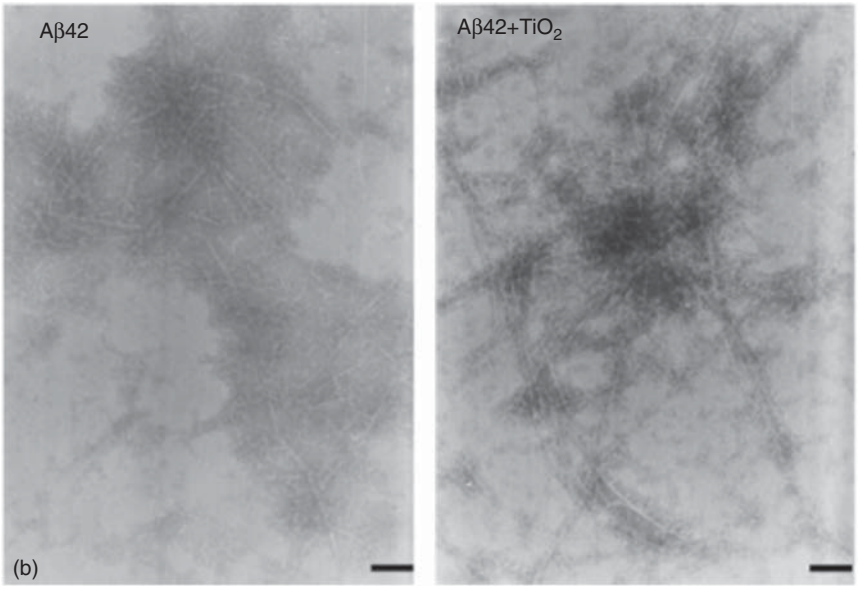

Figure 7.3 Fibrillation of Aβ with TiO_2 NPs. (a) Aβ fibrillation for kinetic curves with different concentrations of TiO_2 NPs. (b) TEM of Aβ fibrillation with TiO_2 nanoparticles. 20 μM Aβ was incubated with 0 (left) and 0.01 mg/ml (right) TiO_2 NPs incubated in neutral PBS at 37 °C after 24 hours (scale bar = 100 nm). Source: Reproduced with permission from Wu et al. 2008 [116]. Copyright © 2017, Elsevier.

the particle surface to facilitate the aggregation of Aβ. Moreover, the NPs can further make it easier for fibril formation for the reduced energetic barriers to aggravate the AD (Figure 7.3) [116].

Similarly, the TiO_2 can accelerate the aggregation of α-synuclein that is also a huge inducement for the PD [117]. Mohammadi and Nikkhah evaluated the fibril formation of α-synuclein on the effect of different metal oxide NPs (NPs), i.e. TiO_2, silicon oxide (SiO_2), and tin oxide (SnO_2). The results show that even at low concentrations, TiO_2 NPs can promote the formation of α-synuclein fibrils, while the other two metal oxide NPs have no significant effect on mechanical fiber fibrillation. The possible mechanism was the interaction of TiO_2 NPs and α-synuclein that can enhance the α-synuclein nucleation and facilitate the fibril formation. Hence, to make PD be away from human, especially the potential of NPs, hazards of TiO_2 NPs should be carefully taken into account and be eliminated.

7.8 Conclusion

With the increase demand of early diagnosis and treatment for NDs, TiO_2 and its derivatives are expected to play an exceptional role in diagnosis and treatment for NDs, which have been widely used in biomedical applications. However, considering the particularity and hardness of NDs, there are still only a few reports on related research, and many researchers still hold different views on their application in ND. Considering the aforementioned issues that must be addressed and overcome, we hope that it can play an exceptional role in the diagnosis and therapy of NDs with the in-depth study of TiO_2 in biomedical-related fields.

Acknowledgments

This work was supported by National Key R&D Program of China (2018YFC 0910601, 2019YFA0405603), Natural Science Foundation of China (31971292, U1432114, and Grant No. 81871411), Youth Innovation Promotion Association Foundation of CAS (2017340), Zhejiang Province Financial Supporting (2017C03042, LY18H180011 and 2020C03110), the Science & Technology Bureau of Ningbo City (2015B11002, 2017C110022). Furthermore, the authors also acknowledge Shanghai Synchrotron Radiation Facility at Line BL15U (No. h15sr0021) for X-ray fluorescence imaging and National Synchrotron Radiation Laboratory in Hefei for soft X-ray imaging (No. 2016-HLS-PT-002193).

References

1 Uttara, B., Singh, A.V., Zamboni, P., and Mahajan, R.T. (2009). Oxidative stress and neurodegenerative diseases: a review of upstream and downstream antioxidant therapeutic options. *Current Neuropharmacology* 7 (1): 65–74.

2 Chen, X., Guo, C., and Kong, J. (2012). Oxidative stress in neurodegenerative diseases. *Neural Regeneration Research* 7 (5): 376–385.
3 Kim, G.H., Kim, J.E., Rhie, S.J., and Yoon, S. (2015). The role of oxidative stress in neurodegenerative diseases. *Experimental Neurobiology* 24 (4): 325–340.
4 Gilgun-Sherki, Y., Melamed, E., and Offen, D. (2004). The role of oxidative stress in the pathogenesis of multiple sclerosis: the need for effective antioxidant therapy. *Journal of Neurology* 251 (3): 261–268.
5 Barnham, K.J., Masters, C.L., and Bush, A.I. (2004). Neurodegenerative diseases and oxidative stress. *Nature Reviews Drug Discovery* 3 (3): 205.
6 Emerit, J., Edeas, M., and Bricaire, F. (2004). Neurodegenerative diseases and oxidative stress. *Biomedicine & Pharmacotherapy* 58 (1): 39–46.
7 Johri, A. and Beal, M.F. (2012). Mitochondrial dysfunction in neurodegenerative diseases. *The Journal of Pharmacology and Experimental Therapeutics* 342 (3): 619–630.
8 Reddy, P.H. (2009). Role of mitochondria in neurodegenerative diseases: mitochondria as a therapeutic target in Alzheimer's disease. *CNS Spectrums* 14 (8 Suppl 7): 8–18.
9 Lin, M.T. and Beal, M.F. (2006). Mitochondrial dysfunction and oxidative stress in neurodegenerative diseases. *Nature* 443 (7113): 787–795.
10 Golpich, M., Amini, E., Mohamed, Z. et al. (2017). Mitochondrial dysfunction and biogenesis in neurodegenerative diseases: pathogenesis and treatment. *CNS Neuroscience & Therapeutics* 23 (1): 5–22.
11 Dong, X.-X., Wang, Y., and Qin, Z.-H. (2009). Molecular mechanisms of excitotoxicity and their relevance to pathogenesis of neurodegenerative diseases. *Acta Pharmacologica Sinica* 30 (4): 379–387.
12 Silva, J., Monge-Fuentes, V., Gomes, F. et al. (2015). Pharmacological alternatives for the treatment of neurodegenerative disorders: wasp and bee venoms and their components as new neuroactive tools. *Toxins (Basel)* 7 (8): 3179–3209.
13 Meldrum, B. and Garthwaite, J. (1990). Excitatory amino acid neurotoxicity and neurodegenerative disease. *Trends in Pharmacological Sciences* 11 (9): 379–387.
14 Lipton, S.A. and Rosenberg, P.A. (1994). Excitatory amino acids as a final common pathway for neurologic disorders. *New England Journal of Medicine* 330 (9): 613–622.
15 Cappellano, G., Carecchio, M., Fleetwood, T. et al. (2013). Immunity and inflammation in neurodegenerative diseases. *American Journal of Neurodegenerative Disease* 2 (2): 89–107.
16 Amor, S., Puentes, F., Baker, D., and Van Der Valk, P. (2010). Inflammation in neurodegenerative diseases. *Immunology* 129 (2): 154–169.
17 Heppner, F.L., Ransohoff, R.M., and Becher, B. (2015). Immune attack: the role of inflammation in Alzheimer disease. *Nature Reviews Neuroscience* 16 (6): 358.
18 Neuwelt, E.A., Bauer, B., Fahlke, C. et al. (2011). Engaging neuroscience to advance translational research in brain barrier biology. *Nature Reviews Neuroscience* 12 (3): 169.

19 Kaur, I.P., Bhandari, R., Bhandari, S., and Kakkar, V. (2008). Potential of solid lipid nanoparticles in brain targeting. *Journal of Controlled Release* 127 (2): 97–109.

20 Kreuter, J., Ramge, P., Petrov, V. et al. (2003). Direct evidence that polysorbate-80-coated poly(butylcyanoacrylate) nanoparticles deliver drugs to the CNS *via* specific mechanisms requiring prior binding of drug to the nanoparticles. *Pharmaceutical Research* 20 (3): 409–416.

21 Volicer, L. (2001). Management of severe Alzheimer's disease and end-of-life issues. *Clinics in Geriatric Medicine* 17 (2): 377–391.

22 Begley, D.J. (2004). Delivery of therapeutic agents to the central nervous system: the problems and the possibilities. *Pharmacology & Therapeutics* 104 (1): 29–45.

23 Yang, X., Qin, J., Jiang, Y. et al. (2015). Fabrication of P25/Ag_3PO_4/graphene oxide heterostructures for enhanced solar photocatalytic degradation of organic pollutants and bacteria. *Applied Catalysis B* 166–167: 231–240.

24 Yang, X., Qin, J., Jiang, Y. et al. (2014). Bifunctional TiO_2/Ag_3PO_4/graphene composites with superior visible light photocatalytic performance and synergistic inactivation of bacteria. *RSC Advances* 4 (36): 18627–18636.

25 Larsen, S.T., Roursgaard, M., Jensen, K.A., and Nielsen, G.D. (2010). Nano titanium dioxide particles promote allergic sensitization and lung inflammation in mice. *Basic & Clinical Pharmacology & Toxicology* 106 (2): 114–117.

26 Song, B., Liu, J., Feng, X. et al. (2015). A review on potential neurotoxicity of titanium dioxide nanoparticles. *Nanoscale Research Letters* 10 (1): 1042.

27 Nazıroğlu, M., Muhamad, S., and Pecze, L. (2017). Nanoparticles as potential clinical therapeutic agents in Alzheimer's disease: focus on selenium nanoparticles. *Expert Review of Clinical Pharmacology* 10 (7): 773–782.

28 Gitler, A.D., Dhillon, P., and Shorter, J. (2017). Neurodegenerative disease: models, mechanisms, and a new hope. *Disease Models & Mechanisms* 10 (5): 499–502.

29 Levenson, R.W., Sturm, V.E., and Haase, C.M. (2014). Emotional and behavioral symptoms in neurodegenerative disease: a model for studying the neural bases of psychopathology. *The Annual Review of Clinical Psychology* 10: 581–606.

30 Ross, C.A. and Poirier, M.A. (2004). Protein aggregation and neurodegenerative disease. *Nature Medicine* 10: S10.

31 Forno, L.S. (1996). Neuropathology of Parkinson's disease. *Journal of Neuropathology and Experimental Neurology* 55 (3): 259–272.

32 Valente, E.M., Abou-Sleiman, P.M., Caputo, V. et al. (2004). Hereditary early-onset Parkinson's disease caused by mutations in *PINK1*. *Science* 304 (5674): 1158–1160.

33 Cleveland, D.W. and Rothstein, J.D. (2001). From charcot to lou gehrig: deciphering selective motor neuron death in als. *Nature Reviews Neuroscience* 2: 806.

34 Lee, B.I., Chung, Y.J., and Park, C.B. (2019). Photosensitizing materials and platforms for light-triggered modulation of Alzheimer's β-amyloid self-assembly. *Biomaterials* 190–191: 121–132.

35 Chen, S.W., Drakulic, S., Deas, E. et al. (2015). Structural characterization of toxic oligomers that are kinetically trapped during α-synuclein fibril formation. *Proceedings of the National Academy of Sciences of the United States of America* https://doi.org/10.1073/pnas.1421204112.

36 Taylor, J.P., Hardy, J., and Fischbeck, K.H. (2002). Toxic proteins in neurodegenerative disease. *Science* 296 (5575): 1991–1995.

37 Ceccon, A., Tugarinov, V., and Clore, G.M. (2019). TiO_2 nanoparticles catalyze oxidation of huntingtin exon 1-derived peptides impeding aggregation: a quantitative NMR study of binding and kinetics. *Journal of the American Chemical Society* 141 (1): 94–97.

38 Alexander, E.J., Ghanbari Niaki, A., Zhang, T. et al. (2018). Ubiquilin 2 modulates ALS/FTD-linked FUS–RNA complex dynamics and stress granule formation. *Proceedings of the National Academy of Sciences of the United States of America* 115 (49): E11485–E11494.

39 Feldman, H.H., Pirttila, T., Dartigues, J.F. et al. (2009). Treatment with galantamine and time to nursing home placement in Alzheimer's disease patients with and without cerebrovascular disease. *International Journal of Geriatric PsychiatrySciences* 24 (5): 479–488.

40 Siemers, E.R., Sundell, K.L., Carlson, C. et al. (2016). Phase 3 solanezumab trials: secondary outcomes in mild Alzheimer's disease patients. *Alzheimer's & Dementia* 12 (2): 110–120.

41 Falahati, F., Westman, E., and Simmons, A. (2014). Multivariate data analysis and machine learning in Alzheimer's disease with a focus on structural magnetic resonance imaging. *Journal of Alzheimer's Disease* 41 (3): 685–708.

42 Scullin, M.K., Harrison, T.L., Factor, S.A., and Bliwise, D.L. (2014). A neurodegenerative disease sleep questionnaire: principal component analysis in Parkinson's disease. *Journal of the Neurological Sciences* 336 (1–2): 243–246.

43 Stoessl, A.J. (2012). Neuroimaging in the early diagnosis of neurodegenerative disease. *Translational Neurodegeneration* 1 (1): 5.

44 Frisoni, G.B., Fox, N.C., Jack, C.R. Jr. et al. (2010). The clinical use of structural MRI in Alzheimer disease. *Nature Reviews Neurology* 6 (2): 67.

45 Brismar, J., Brismar, G., Gascon, G., and Ozand, P. (1990). Canavan disease: CT and MR imaging of the brain. *American Journal of Neuroradiology* 11 (4): 805–810.

46 Ohshima, Y., Taguchi, K., Mizuta, I. et al. (2018). Mutations in the β-amyloid precursor protein in familial Alzheimer's disease increase Aβ oligomer production in cellular models. *Heliyon* 4 (1): e00511.

47 Kumar, S., Henning-Knechtel, A., Chehade, I. et al. (2017). Foldamer-mediated structural rearrangement attenuates Aβ oligomerization and cytotoxicity. *Journal of the American Chemical Society* 139 (47): 17098–17108.

48 Li, C., Lutz, E.A., Slade, K.M. et al. (2009). ^{19}F NMR studies of α-synuclein conformation and fibrillation. *Biochemistry* 48 (36): 8578–8584.

49 Rushworth, J.V., Ahmed, A., Griffiths, H.H. et al. (2014). A label-free electrical impedimetric biosensor for the specific detection of Alzheimer's amyloid-beta oligomers. *Biosensors and Bioelectronics* 56: 83–90.

50 Li, H., Cao, Y., Wu, X. et al. (2012). Peptide-based electrochemical biosensor for amyloid β 1–42 soluble oligomer assay. *Talanta* 93: 358–363.

51 An, Y., Tang, L., Jiang, X. et al. (2010). A photoelectrochemical immunosensor based on Au-doped TiO_2 nanotube arrays for the detection of α-synuclein. *Chemistry A European Journal* 16 (48): 14439–14446.

52 Guerrini, L., Arenal, R., Mannini, B. et al. (2015). SERS detection of amyloid oligomers on metallorganic-decorated plasmonic beads. *ACS Applied Materials & Interfaces* 7 (18): 9420–9428.

53 Chandra, B., Maity, B.K., Das, A., and Maiti, S. (2018). Fluorescence quenching by lipid encased nanoparticles shows that amyloid-β has a preferred orientation in the membrane. *Chemical Communications* 54 (56): 7750–7753.

54 Zhu, L., Zhang, J., Wang, F. et al. (2016). Selective amyloid β oligomer assay based on abasic site-containing molecular beacon and enzyme-free amplification. *Biosensors and Bioelectronics* 78: 206–212.

55 Volkova, K.D., Kovalska, V.B., Segers-Nolten, G.M. et al. (2009). Explorations of the application of cyanine dyes for quantitative α-synuclein detection. *Biotechnic and Histochemistry* 84 (2): 55–61.

56 Lee, Y. and Basaran, C. (2014). Effect of Ni solute on grain boundary diffusivity and structure of βSn. *Computational Materials Science* 92: 1–7.

57 Floyd, R., Hensley, K., Jaffery, F. et al. (1999). Increased oxidative stress brought on by pro-inflammatory cytokines in neurodegenerative processes and the protective role of nitrone-based free radical traps. *Life Sciences* 65 (18–19): 1893–1899.

58 Morales, I., Guzmán-Martínez, L., Cerda-Troncoso, C. et al. (2014). Neuroinflammation in the pathogenesis of Alzheimer's disease. A rational framework for the search of novel therapeutic approaches. *Frontiers in Cellular Neuroscience* 8: 112.

59 Chen, Q., Kang, J., and Fu, C. (2018). The independence of and associations among apoptosis, autophagy, and necrosis. *Signal Transduction and Targeted Therapy* 3 (1): 18.

60 Yu, Z., Liu, N., Liu, J. et al. (2012). Neuroglobin, a novel target for endogenous neuroprotection against stroke and neurodegenerative disorders. *International Journal of Molecular Sciences* 13 (6): 6995–7014.

61 Alberch, J., Perez-Navarro, E., and Canals, J. (2002). Neuroprotection by neurotrophins and GDNF family members in the excitotoxic model of Huntington's disease. *Brain Research Bulletin* 57 (6): 817–822.

62 Mattson, M.P. and Scheff, S.W. (1994). Endogenous neuroprotection factors and traumatic brain injury: mechanisms of action and implications for therapy. *Journal of Neurotrauma* 11 (1): 3–33.

63 Marco-Contelles, J., León, R., de los Ríos, C. et al. (2006). Novel multipotent tacrine-dihydropyridine hybrids with improved acetylcholinesterase inhibitory and neuroprotective activities as potential drugs for the treatment of Alzheimer's disease. *Journal of Medicinal Chemistry* 49 (26): 7607–7610.

64 Sonkusare, S.K., Kaul, C., and Ramarao, P. (2005). Dementia of Alzheimer's disease and other neurodegenerative disorders—memantine, a new hope. *Pharmacological Research* 51 (1): 1–17.

65 Kelsey, N.A., Wilkins, H.M., and Linseman, D.A. (2010). Nutraceutical antioxidants as novel neuroprotective agents. *Molecules* 15 (11): 7792–7814.

66 Dugan, L., Lovett, E., Quick, K. et al. (2001). Fullerene-based antioxidants and neurodegenerative disorders. *Parkinsonism & Related Disorders* 7 (3): 243–246.

67 Ikonomidou, C. and Turski, L. (2002). Why did NMDA receptor antagonists fail clinical trials for stroke and traumatic brain injury? *The Lancet Neurology* 1 (6): 383–386.

68 Danysz, W. and Parsons, C.G. (2003). The NMDA receptor antagonist memantine as a symptomatological and neuroprotective treatment for Alzheimer's disease: preclinical evidence. *International Journal of Geriatric Psychiatry* 18 (S1): S23–S32.

69 Gao, H.-M., Liu, B., Zhang, W., and Hong, J.-S. (2003). Novel anti-inflammatory therapy for Parkinson's disease. *Trends in Pharmacological Sciences* 24 (8): 395–401.

70 Klegeris, A. and McGeer, P.L. (2005). Non-steroidal anti-inflammatory drugs (NSAIDs) and other anti-inflammatory agents in the treatment of neurodegenerative disease. *Current Alzheimer Research* 2 (3): 355–365.

71 Waldmeier, P.C. (2003). Prospects for antiapoptotic drug therapy of neurodegenerative diseases. *Progress in Neuro-Psychopharmacology & Biological Psychiatry* 27 (2): 303–321.

72 Wang, X. (2009). The antiapoptotic activity of melatonin in neurodegenerative diseases. *CNS Neuroscience & Therapeutics* 15 (4): 345–357.

73 Zuccato, C. and Cattaneo, E. (2009). Brain-derived neurotrophic factor in neurodegenerative diseases. *Nature Reviews Neurology* 5 (6): 311.

74 Hefti, F., Hartikka, J., and Knusel, B. (1989). Function of neurotrophic factors in the adult and aging brain and their possible use in the treatment of neurodegenerative diseases. *Neurobiology of Aging* 10 (5): 515–533.

75 Lang, A.E., Gill, S., Patel, N.K. et al. (2006). Randomized controlled trial of intraputamenal glial cell line–derived neurotrophic factor infusion in Parkinson disease. *Annals of Neurology* 59 (3): 459–466.

76 Lindvall, O., Kokaia, Z., and Martinez-Serrano, A. (2004). Stem cell therapy for human neurodegenerative disorders–how to make it work. *Nature Medicine* 10 (7s): S42.

77 Joyce, N., Annett, G., Wirthlin, L. et al. (2010). Mesenchymal stem cells for the treatment of neurodegenerative disease. *Regenerative Medicine* 5 (6): 933–946.

78 Harper, S.Q., Staber, P.D., He, X. et al. (2005). RNA interference improves motor and neuropathological abnormalities in a Huntington's disease mouse model. *Proceedings of the National Academy of Sciences of the United States of America* 102 (16): 5820–5825.

79 Davidson, B., Xia, H., Mao, Q. et al. (2005). RNA interference suppresion of neurodegenerative diseases and methods of use thereof. Google Patents US20050042646A1.

80 McNeil, C.J., Athey, D., and Ho, W.O. (1995). Direct electron transfer bioelectronic interfaces: application to clinical analysis. *Biosensors and Bioelectronics* 10 (1): 75–83.

81 Bauer, C.G., Eremenko, A.V., Ehrentreich-Förster, E. et al. (1996). Zeptomole-detecting biosensor for alkaline phosphatase in an electrochemical immunoassay for 2,4-dichlorophenoxyacetic acid. *Analytical Chemistry* 68 (15): 2453–2458.

82 Georganopoulou, D.G., Chang, L., Nam, J.-M. et al. (2005). Nanoparticle-based detection in cerebral spinal fluid of a soluble pathogenic biomarker for Alzheimer's disease. *Proceedings of the National Academy of Sciences of the United States of America* 102 (7): 2273–2276.

83 Neely, A., Perry, C., Varisli, B. et al. (2009). Ultrasensitive and highly selective detection of Alzheimer's disease biomarker using two-photon Rayleigh scattering properties of gold nanoparticle. *ACS Nano* 3 (9): 2834–2840.

84 Roney, C.A., Arora, V., Kulkarni, P.V. et al. (2009; 481031). Nanoparticulate radiolabelled quinolines detect amyloid plaques in mouse models of Alzheimer's disease. *International Journal of Alzheimer's Disease* 2009: 1–8.

85 Yu, J. and Lyubchenko, Y.L. (2009). Early stages for Parkinson's development: α-synuclein misfolding and aggregation. *Journal of NeuroImmune Pharmacology* 4 (1): 10.

86 Baron, R., Zayats, M., and Willner, I. (2005). Dopamine-, L-DOPA-, adrenaline-, and noradrenaline-induced growth of Au nanoparticles: assays for the detection of neurotransmitters and of tyrosinase activity. *Analytical Chemistry* 77 (6): 1566–1571.

87 van Kasteren, S.I., Campbell, S.J., Serres, S. et al. (2009). Glyconanoparticles allow pre-symptomatic *in vivo* imaging of brain disease. *Proceedings of the National Academy of Sciences of the United States of America* 106 (1): 18–23.

88 Petry, K.G., Boiziau, C., Dousset, V., and Brochet, B. (2007). Magnetic resonance imaging of human brain macrophage infiltration. *Neurotherapeutics* 4 (3): 434–442.

89 Baratchi, S., Kanwar, R.K., Khoshmanesh, K. et al. (2009). Promises of nanotechnology for drug delivery to brain in neurodegenerative diseases. *Current Nanoscience* 5 (1): 15–25.

90 Corso, T.D., Torres, G., Goulah, C. et al. (2005). Transfection of tyrosine kinase deleted FGF receptor-1 into rat brain substantia nigra reduces the number of tyrosine hydroxylase expressing neurons and decreases concentration levels of striatal dopamine. *Molecular Brain Research* 139 (2): 361–366.

91 Machtoub, L., Bataveljic, D., and Andjus, P. (2011). Molecular imaging of brain lipid environment of lymphocytes in amyotrophic lateral sclerosis using magnetic resonance imaging and SECARS microscopy. *Physiological Research* 60: S121.

92 Calvo, P., Gouritin, B., Villarroya, H. et al. (2002). Quantification and localization of PEGylated polycyanoacrylate nanoparticles in brain and spinal cord during experimental allergic encephalomyelitis in the rat. *The European Journal of Neuroscience* 15 (8): 1317–1326.

93 Steiner, J.P., Hamilton, G.S., Ross, D.T. et al. (1997). Neurotrophic immunophilin ligands stimulate structural and functional recovery in

neurodegenerative animal models. *Proceedings of the National Academy of Sciences of the United States of America* 94 (5): 2019–2024.

94 Kanwar, J.R., Sun, X., Punj, V. et al. (2012). Nanoparticles in the treatment and diagnosis of neurological disorders: untamed dragon with fire power to heal. *Nanomedicine: Nanotechnology, Biology and Medicine* 8 (4): 399–414.

95 Modi, G., Pillay, V., Choonara, Y.E. et al. (2009). Nanotechnological applications for the treatment of neurodegenerative disorders. *Progress in Neurobiology* 88 (4): 272–285.

96 Wilson, B., Samanta, M.K., Santhi, K. et al. (2008). Poly(n-butylcyanoacrylate) nanoparticles coated with polysorbate 80 for the targeted delivery of rivastigmine into the brain to treat Alzheimer's disease. *Brain Research* 1200: 159–168.

97 Roney, C., Kulkarni, P., Arora, V. et al. (2005). Targeted nanoparticles for drug delivery through the blood–brain barrier for Alzheimer's disease. *Journal of Controlled Release* 108 (2–3): 193–214.

98 Rao, K.S., Reddy, M.K., Horning, J.L., and Labhasetwar, V. (2008). TAT-conjugated nanoparticles for the CNS delivery of anti-HIV drugs. *Biomaterials* 29 (33): 4429–4438.

99 Fischer, H., Gottschlich, R., and Seelig, A. (1998). Blood–brain barrier permeation: molecular parameters governing passive diffusion. *The Journal of Membrane Biology* 165 (3): 201–211.

100 Gobbi, M., Re, F., Canovi, M. et al. (2010). Lipid-based nanoparticles with high binding affinity for amyloid-β1–42 peptide. *Biomaterials* 31 (25): 6519–6529.

101 Canovi, M., Markoutsa, E., Lazar, A.N. et al. (2011). The binding affinity of anti-Aβ1-42 MAb-decorated nanoliposomes to Aβ1-42 peptides *in vitro* and to amyloid deposits in post-mortem tissue. *Biomaterials* 32 (23): 5489–5497.

102 Liu, G., Men, P., Kudo, W. et al. (2009). Nanoparticle–chelator conjugates as inhibitors of amyloid-β aggregation and neurotoxicity: a novel therapeutic approach for Alzheimer disease. *Neuroscience Letters* 455 (3): 187–190.

103 Trapani, A., De Giglio, E., Cafagna, D. et al. (2011). Characterization and evaluation of chitosan nanoparticles for dopamine brain delivery. *International Journal of Pharmaceutics* 419 (1–2): 296–307.

104 Tan, Y.-J., Sui, D., Wang, W.-H. et al. (2013). Phosphopeptide enrichment with TiO_2-modified membranes and investigation of tau protein phosphorylation. *Analytical Chemistry* 85 (12): 5699–5706.

105 Wang, L.-W., Liu, H.-L., Lu, Y.-J. et al. (2018). TiO_2 nanorod-based photoelectrochemical sensor for Alzheimer's disease detection. *17th International Meeting on Chemical Sensors - IMCS 2018*, 2018-07-15-2018-07-19, Vienna, Austria, pp. 184–185.

106 Curulli, A. (2009). Electrochemical direct determination of catecholamines for the early detection of neurodegenerative diseases. *Sensors* 9 (4): 2437.

107 Stefan-van Staden, R.-I., Balahura, L.-R., Oprisanu-Vulpe, A. et al. (2017). Nanostructured materials detect dopamine in biological fluids. *Journal of the Electrochemical Society* 164 (12): B561–B566.

108 Pardridge, W.M. (2005). The blood–brain barrier: bottleneck in brain drug development. *Neuro Rx* 2 (1): 3–14.

109 Carvey, P.M., Hendey, B., and Monahan, A.J. (2009). The blood–brain barrier in neurodegenerative disease: a rhetorical perspective. *Journal of Neurochemistry* 111 (2): 291–314.

110 Brun, E., Carrière, M., and Mabondzo, A. (2012). *In vitro* evidence of dysregulation of blood–brain barrier function after acute and repeated/long-term exposure to TiO_2 nanoparticles. *Biomaterials* 33 (3): 886–896.

111 Sharma, A., Menon, P.K., Patnaik, R. et al. (2017). Chapter six-novel treatment strategies using TiO_2-nanowired delivery of histaminergic drugs and antibodies to tau with cerebrolysin for superior neuroprotection in the pathophysiology of Alzheimer's disease. In: *International Review of Neurobiology*, vol. 137 (eds. H.S. Sharma and A. Sharma), 123–165. Academic Press.

112 Sharma, H.S., Muresanu, D.F., Lafuente, J.V. et al. (2018). Co-administration of TiO_2 nanowired mesenchymal stem cells with cerebrolysin potentiates neprilysin level and reduces brain pathology in Alzheimer's disease. *Molecular Neurobiology* 55 (1): 300–311.

113 Requejo, C., Ruiz-Ortega, J.A., Cepeda, H. et al. (2018). Nanodelivery of cerebrolysin and rearing in enriched environment induce neuroprotective effects in a preclinical rat model of Parkinson's disease. *Molecular Neurobiology* 55 (1): 286–299.

114 Tian, Z.R., Aruna, S., Ala, N. et al. (2012). Nanowired drug delivery to enhance neuroprotection in spinal cord injury. *CNS & Neurological Disorders-Drug Targets* 11 (1): 86–95.

115 Ahmed, M.H., Keyes, T.E., and Byrne, J.A. (2013). The photocatalytic inactivation effect of Ag–TiO_2 on β-amyloid peptide (1–42). *Journal of Photochemistry and Photobiology A* 254: 1–11.

116 Wu, W.-H., Sun, X., Yu, Y.-P. et al. (2008). TiO_2 nanoparticles promote β-amyloid fibrillation in vitro. *Biochemical and Biophysical Research Communications* 373 (2): 315–318.

117 Mohammadi, S. and Nikkhah, M. (2017). TiO_2 nanoparticles as potential promoting agents of fibrillation of α-synuclein, a Parkinson's disease-related protein. *Iranian Journal of Biotechnology* 15 (2): 87–94.

Index

a

Aβ fibrillation 226, 227
Aβ peptide (AβP) 225
Ag-TiO_2 120–122, 226
air treatment 26–29
α-synuclein 223, 224, 228
aluminum reduction method 204
Ames assays 81
AMP-activated kinase (AMPK) 76
amyloid-beta derived diffusible ligands (ADDL) 221
amyloid precursor protein (APP) 219
antiapoptotic drugs 220
antibacterial application, of titanium dioxide (TiO_2) nanoparticles
  aerobic denitrifiers 112
  Ag doped TiO_2 nanoparticles 120–122
  biofilm 111
  Cu doped TiO_2 nanoparticles 123–124
  environmental application 125
  food safety application 126
  hydroxyl radicals 106
  ion doped-TiO_2 nanoparticles 113–119
  isoelectric point (IEP) 107
  medical application 124–125
  photoactivated and antibacterial property 108
  photocatalytic performance 107
  photokilling approach 110
  prrF RNA in *Pseudomonas brassicacearum* 108
  unsaturated and saturated fatty acids 110
  Zn doped TiO_2 nanoparticles 123
antimicrobial effect 15, 16, 34, 112
apoptosis 18, 72, 74–77, 80, 83, 84, 154, 158, 166, 190, 218, 220
aqueous imidacloprid 38
atomic layer deposition (ALD) technology 138
autoimmune reactions 21
autophagy 74–77

b

base excision repair (BER) 79
Beclin 1 76, 77
bioactive nanomaterials 21
biokinetic/biodistribution patterns 72
biological oxygen demand (BOD_5) 37
black titanium dioxide (TiO_2) nanomaterials, cancer theranostics
  advantages 186
  aluminum reduction method 204
  chemical reduction method 188
  chemo-phototherapy 199–202
  hydrogenation reduction method 187
  hydrogen plasma method 187–188
  imaging guided phototherapy
    MRI 195, 196
    real-time monitoring 195
    therapeutical accuracy 195
  microwave-assisted method 193
  near infrared (NIR) light 186
  photodynamic therapy 194–195

TiO_2 Nanoparticles: Applications in Nanobiotechnology and Nanomedicine,
First Edition. Edited by Aiguo Wu and Wenzhi Ren.
© 2020 Wiley-VCH Verlag GmbH & Co. KGaA. Published 2020 by Wiley-VCH Verlag GmbH & Co. KGaA.

black titanium dioxide (TiO_2)
nanomaterials, cancer theranostics (*contd.*)
photothermal therapy 190–194
properties 188–189
sonodynamic-photothermal therapy 202–205
up-conversion luminescence efficiency 186
UV light 185
B-mode ultrasonography 202

c

cancer photodynamic therapy 9
carcinogenicity 81–83
caspase-3 19, 75, 77
caspase-9 75
central nervous system (CNS) disease 37, 70, 222
charge transfer (CT) process 23, 116, 136, 137
chemical oxygen demand (COD) 26, 37
chemical reduction method 188
chemical vapour deposition (CVD) 11
chemo-phototherapy 199–202
comet assays 80, 81
conduction bands (CBs) 4, 107, 114, 121, 122, 137, 188, 191
culture plate method 16

d

3,4-dihydroxyphenilacetic acid (DOPAC) 156
diphenylarsinic acid (DPAA) 35
dopamine acid (DA) 222
drug-resistant leukemia cells 155

e

electrochemical methods 133
electron paramagnetic resonance (EPR) spectrum 191
enzyme-linked immunosorbent assay (ELISA) 86, 220, 221
evaporation-mediated self-assembly 33

f

fibrinogen 6
flavin mononucleotide (FMN) 169, 170
flourine-doped tin oxide (FTO) substrate 7, 223
folic acid (FA) 19, 200
Fourier Transform Infrared spectroscopy 25

g

genotoxicity 74, 75, 79–81, 83, 88, 206
glioblastoma multiforme (GBM) 156, 157
glutathione S-transferase (GST) 85
graphene 23, 33, 135, 136, 166

h

herbicides 36, 39
high-intensity focused ultrasound (HIFU) 154, 166, 167, 202, 203
human acute monocytic leukemia (THP-1) cells 18, 80
human pulmonary epithelial (NCI-H292) cells 80
Huntington's protein 219
hydrogenated nanowires, colors of 187
hydrogenation process 31, 33
hydrogenation reduction method 187
hydrogen plasma method 187–188
hydrothermal synthetic method 7

i

imidaclorpid 37, 38, 188
immunotoxicity 83
incident photon-to-current conversion efficiency (IPCE) 32
inorganic photosensitizers 19, 154–161
ion doped-TiO_2 nanoparticles
F. graminearum macroconidium 117
gram-negative bacteria 114
gram-positive bacteria 114
Nd element 118
palladium additive 115
PdO nanoparticles 116
ROS generation 113

sol-gel method 113
V_2O_5-TiO_2 119

l

Langmuir–Hinshelwood kinetics model 26
linear alkyl benzene sulfonate (LAS) 37
Listeria monocytogenes bacteria 16, 111
lysosomal membrane permeabilization (LMP) 74, 77

m

magnetic resonance imaging (MRI) 2, 20, 167–168
3-mercaptopropionic acid (MPA) 223
mesenchymal stem cells (MSCS) 225
mesoporous silica ($mSiO_2$) drug carriers 200
metal ion nanoparticles 106
metal organic CVD (MOCVD) 11
metal-organic frameworks (MOF) 13, 28, 205
Methionine^7 (Met^7) oxidation 226
methylene blue (MB) target molecules 15, 22, 24, 136, 142
microwave-assisted hydrothermal method 193
mitochondrial outer membrane permeabilization (MOMP) 74
molybdenum disulphide (MoS_2) 33
mouse macrophages (MH-S) cells 86

n

N-acetylcysteine (NAC) 80
nanocatalysts 21
nanoliposomes (NL) 222
nanomedicine 2, 14, 17–21, 67, 85, 89, 167
nanoparticle-enhanced filtration 21
nanoparticle exposures 69
nanosorbents 21
neural stem cell transplantation 221
neurodegenerative diseases (NDs)
  acute NDs and chronic NDs 218
  diagnosis 221, 222–224
  free radical 217
  immune inflammation 218
  medicine for 220–221
  oxidative stress 217
  symptoms 219–220
  treatment 222, 225
Neurodegenerative Disease Sleep Questionnaire (NDSQ) 220
neurotrophic disorders 218
neurotrophic factor (NTF) 220, 221
nitrophenols 24, 35, 36
nucleotide excision repair (NER) 79

o

organic photosensitizers 154, 161
oxidative stress 68, 72, 74, 75, 76, 78, 80, 83, 84, 88, 217, 218

p

paclitaxel (PTX) 170
pancreatic cancer stem cells (PCSCs) 197
PEG coating 190
pesticides removal 36–40
photodynamic inactivation (PDI) 15
photodynamic therapy (PDT) 194, 199
  antibody-linked DOPAC-TiO_2 nanoparticles 157
  Au nanoclusters 194
  DOX-coated UCL-TiO_2 nanocomposites 172
  fluorescent imaging 168–169
  low upconversion luminescence efficiency 194
  mechanism 189
  MRI 167–168
  multifunctional Fe_3O_4–TiO_2 nanocomposites 168
  980 nm NIR-responsive nanoplatform 158, 159, 160
  principle 154–155
  ultraviolet excitation 194
photo-Fenton reaction 38
photo-induced charge-transfer (PICT) process 136

photothermal therapy (PTT) 190, 199
breast cancer model 201
H-TiO_2-PEG nanoparticles 190
mechanism 190
reactive oxygen radicals 190
physical vapor deposition (PVD) 11–12
polyacrylic acids (PAA) 155
polyethylene glycol (PEG) 88, 190
polyethyleneimine (PEI) 169
polymerase chain reaction (PCR) 217
proapoptotic protein 77
p-type semiconductors 23

r

reactive oxygen species (ROS) 14, 68, 74, 106, 154, 198, 218
real-time quantitative PCR (RT-PCR) 86
reticuloendothelial system (RES) 71, 221
retinal pigment epithelial cells (RPE-19) 79
reversed-phase high performance liquid chromatography (RP-HPLC) 88
Rheumatoid arthritis (RA) 169
Rhodamine B (RhB) 22
RNA interferenc 221

s

scanning electron microscopy 8, 12, 25, 134
Schottky barrier 23
selected area electron diffraction (SAED) pattern 148, 203
silver nanoparticles (Ag-TiO_2) 226
Si-monocrystal substrates 109
soil remediation 2, 14, 35–36, 41
sol-gel method 8–10, 25, 28, 113, 155
solvothermal synthetic strategy 10, 11
sonodynamic therapy
docetaxel (DTX) loading 166
dual-frequency US 163
hydrophilized W-TiO_2 nanoparticles 166
principle 162
sonosensitizers molecules 162
sound dynamic therapy (SDT) 203
sub-acute toxicity 86–87
sub-chronic toxicity 87–88
superoxide dismutase (SOD1) gene 220
surface enhanced Raman spectrum, of TiO_2 nanoparticles
advantages 136
biosensing 144–150
in-situ detection fields 135
light illumination and noble-metal materials 134
mechanism 137–139
non-metal platforms 135
novel strategies 139
synchrotron X-ray fluorescence microscopy 156

t

teterasuplhonatophenyl porphyrin (TSPP) 169
thermal decomposition method 6, 12–13
thiamethoxam 38
TiO_2 core-shell nanoparticles 20, 41, 122
titanium dioxide antiopal 142, 157
titanium dioxide (TiO_2) nanoparticles
air treatment 26–29
chemical and physical vapor deposition method 11–12
crystal properties 2–3
electrochemical properties 5–6
energy device 29–30
food and cosmetics 34
hydrothermal synthetic method 7
nanobiotechnology 14–17
nanomedicine 17–21
optical properties 3–5
oxidation method 13
paint and paper productions 40–41
pesticides removal 36–40
soil remediation 35–36
sol-gel synthetic method 9
solvothermal synthetic strategy 10

thermal decomposition method 12–13
wastewater treatment 21–26
water splitting for hydrogen production 30–33
titanium tetraisopropoxide (TTIP) 7
toxicity, of titanium dioxide (TiO_2) nanoparticles
apoptosis 74–75
autophagy 76
carcinogenicity 81–83
cellular and molecular interactions 67
cellular uptake 78
genotoxicity 79–81
immunotoxicity 83
nanomaterial distribution
dermal route 73
inhalation 70–71
injection 72–73
oral administration 71
necrosis 77
neurotoxicity of 83–84
oxidative stress 78
reproductive and developmental toxicity 81
SDT and PDT 68
sub-acute toxicity 86–87
sub-chronic toxicity 87–88
therapeutics and theranostics 67
vertebrates and invertebrates, effects of 69
tungstophosphoric acid (TPA) 24

u

ultrasound (US) 19, 120, 121, 154, 162, 163, 166–167, 195, 196, 202, 205
ultraviolet light responsive photodynamic therapy 155–156
upconversion nanoparticles (UCNPs) 18, 155

v

valence bands (VB) gain energy 4, 107, 137, 171, 188
volatile organic compounds (VOCs) 26

w

Western blotting 217
white titanium dioxides (W-TiO_2) nanomaterials
drug delivery and synergistic therapy 170–172
808 nm NIR-responsive PDT 158–161
fluorescent imaging 168–169
high-intensity focused ultrasound (HIFU) 166–167
MRI 167–168
multi-mode imaging 169–170
980 nm NIR-responsive PDT 156–158
organic and inorganic dual-mode PDT 161
photocatalytic performance 153
photodynamic therapy principle 154–155
sonodynamic therapy
docetaxel (DTX) loading 166
dual-frequency US 163
electron/hole pairs efficiency 166
hydrophilized W-TiO_2 nanoparticles 166
principle 162
sonosensitizers molecules 162
ultraviolet light responsive photodynamic therapy 155–156

z

ZnTPyP self-assemblednanocrystals (ZSN) 169